DETERMINATION OF FATIGUE LIFE PROBABILITY DISTRIBUTIONS

COMPUTER PREDICTION AND EXPERIMENTAL DETERMINATION OF FATIGUE LIFE PROBABILITY DISTRIBUTIONS

by

HODA ABDEL-KADER ELMARAGHY, M.ENG.

A Thesis

Submitted to the School of Graduate Studies

in Partial Fulfilment of the Requirements

for the Degree

Doctor of Philosophy

McMaster University

April 1976

DOCTOR OF PHILOSOPHY (1976) McMASTER UNIVERSITY
(Mechanical Engineering) Hamilton, Ontario.

TITLE: Computer Prediction and Experimental Determination of Fatigue Life Probability Distributions

AUTHOR: Hoda Abdel-Kader Elmaraghy,
B.Sc. (Cairo University)
M.Eng. (McMaster University)

SUPERVISOR: Professor J. N. Siddall

NUMBER OF PAGES: (xxi), 214

ABSTRACT

One of the central unsolved problems of engineering design is prediction of the probability distribution of fatigue life of structural members and machine components. Fatigue data scatter is a manifestation of the probabilistic nature of fatigue failure. A relationship is known to exist between the distributions of the number of cycles-to-failure and the applied stress through the probabilistic stress-life (S-N) curve.

A method was developed for predicting the scatter of fatigue life for structures and components subjected to constant, complex or narrow band random amplitude cyclic loading. The method provides a unique way of predicting the statistical properties of fatigue life using a Monte Carlo simulation technique. In this method the randomness of material properties as well as that of the applied loading are incorporated into a stochastic model in conjunction with appropriate fatigue failure criterion to determine the fatigue life distribution.

A modified probabilistic S-N diagram is used to reflect the variability of the endurance limit and the fatigue strength coefficient. Any damage criterion can be used with the simulated S-N diagrams. When the linear damage law is used, the analysis yields a damage criterion analogous to Miner's rule but with a random cycle ratio. The proposed

method was used to analytically predict the characteristics of the cycle ratio distribution. Good agreement with available experimental results is obtained. This result is of particular importance since no assumption regarding the fatigue failure mechanism is made. A phenomenological treatment of damage accumulation below the endurance limit is presented.

The validity of the method is demonstrated for different load histories and materials. Fatigue life data for axial and bending test specimens of SAE 1008 steel sheets subjected to constant amplitude, block and narrow band random loading were generated experimentally. The distributions of the endurance limit, ultimate strength and fatigue strength coefficient were obtained. The endurance life and cyclic stress-strain curve were also determined experimentally. The suggested method has proved successful in predicting fatigue life distributions for each case.

The effects of the randomness of loads, material properties, and the shape of load probability density function were investigated. This study indicates that the large scatter exhibited in fatigue test data is mostly explained by the scatter in the material properties. It was found that the randomness of the fatigue strength coefficient does not significantly affect the scatter of predicted life or its estimated mean value. On the other hand, the variance of the endurance limit has a pronounced effect on the variability of fatigue life. Its effect on the estimated mean is also considerable.

It was shown that the scatter in fatigue life under random loading is less than that under sinusoidal constant amplitude loading. The mean value of fatigue life decreases slightly as a result of increasing the variance of the applied load. Changes in the shape of the load probability density function affect the scatter of life more than its mean value. The predicted fatigue life distribution under random loading depends upon the accuracy of the load probability density function.

The method has the capability of simulating complex load histories of the kind that occur in service. It can also be extended to include possible correlation between peaks of the applied load.

The suggested method is believed to be an efficient tool that can be used at the design stage; it is ideal for parametric studies and provides an attractive alternative to the costly and time consuming prototype fatigue tests. Minimum experimental data is needed for the analysis.

It is concluded that implementation of this new technique will substantially improve the ability of the engineer to design reliable fatigue resistant components efficiently.

ACKNOWLEDGEMENTS

The author is deeply indebted to her supervisor Professor J. N. Siddall for his useful suggestions, guidance and encouragement during the course of this investigation.

The author is pleased to record her gratitude to Dr. J. H. T. Wade for his interest and support throughout the period of this research.

Sincere thanks are extented to Dr. D. S. Weaver for his interest and useful exchange of views during this interim.

Thanks are also due to Dr. M. L. Tiku and Dr. J. F. MacGregor for acting as members of the Ph.D supervisory committee.

The author wishes to express her appreciation to Dr. M. A. Dokainish, Dr. J. Tlusty of the Department of Mechanical Engineering and Dr. R. Kitai of the Electrical Engineering Department for their assistance in the use of some of their equipment.

The author wishes to acknowledge the assistance of Dr. G. Montgomery and Mr. T. Parker of the Steel Company of Canada Limited (STELCO) in supplying the material used in this investigation and their help in generating some of the material properties data.

Useful discussions with Professor T. H. Topper and Dr. J. Martin of the University of Waterloo, at the early stages of this research are thankfully acknowledged.

Many thanks are due to Ms. BettyAnne Bedell for her expert typing of the manuscript.

Last but not least, the understanding and continuous support of my husband, Waguih, is deeply appreciated.

TABLE OF CONTENTS

			Page
NOMENCLATURE			(xii)
LIST OF FIGURES			(xv)
LIST OF TABLES			(xx)
CHAPTER 1		INTRODUCTION AND LITERATURE SURVEY	1
	1.1	General Background	2
	1.2	The Fatigue Process	4
	1.3	Prediction of Fatigue Life	7
		1.3.1 Description of Service Loads	8
		1.3.2 Cyclic Stress-Strain Behaviour	10
		1.3.3 Treatment of Fatigue Damage	11
	1.4	The Probabilistic Character of Fatigue Failure	16
		1.4.1 Statistical Interpretation of Fatigue Data	19
		1.4.2 Probabilistic Fatigue Models	22
	1.5	Purpose and Scope of Present Investigation	26
CHAPTER 2		THEORETICAL FATIGUE LIFE PREDICTION MODEL AND ITS APPLICATION	31
	2.1	Introduction	31
	2.2	Simulation of the Sample S-N Diagrams	35
	2.3	Simulation of Fatigue Life	38
	2.4	Comparison of Predictions Using Suggested Model and Previously Published Experimental Results	41

		Page
CHAPTER 3	EXPERIMENTAL MATERIAL CHARACTERIZATION	53
3.1	Choice of Material and Sampling Scheme	53
	3.1.1 Selection of Material	53
	3.1.2 Sampling Scheme	54
	3.1.3 Tests and Specimens Required	55
3.2	Tensile Tests	58
	3.2.1 Experimental Test Set-up	58
	3.2.2 Results of Tensile Tests	59
	3.2.3 Comments on the Test Results	64
3.3	Axial Fatigue Tests	67
	3.3.1 Experimental Test Set-up	67
	3.3.2 Fatigue Strength Properties	70
	3.3.3 Cyclic Stress-Strain Curve	74
	3.3.4 Comments on the Test Results	77
3.4	Bending Fatigue Tests	83
	3.4.1 Experimental Test Set-up	84
	3.4.2 Design of Test Specimen	84
	3.4.3 Staircase Test to Determine the Distribution of the Fatigue Endurance Limit	87
	3.4.4 Comments on the Staircase-Test Results	91
CHAPTER 4	CONSTANT AMPLITUDE AND BLOCK LOAD TESTING	92
4.1	Introduction	92
4.2	Experimental Program	93
	4.2.1 Test Specimen	93
	4.2.2 Test Set-up	97
	4.2.3 Load Program	102

			Page
	4.3	Results of Constant Amplitude and Block Load Tests	105
		4.3.1 Experimentally Determined Distributions	105
		4.3.2 Theoretically Predicted Distributions	106
		4.3.3 Comparison of Theoretical and Experimental Distributions	119
CHAPTER 5		NARROW BAND RANDOM FATIGUE TESTS	121
	5.1	Introduction	121
	5.2	Experiment	124
		5.2.1 Test Set-up and Specimens	124
		5.2.2 Measurements of Load Parameters and Definition of its PDF	125
	5.3	Results of Narrow Band Random Tests	133
		5.3.1 Comparison of Theoretical and Experimental Distributions	134
	5.4	Effect of Load Variability on Fatigue Life	140
		5.4.1 Effect on Mean Life	140
		5.4.2 Effect on the Standard Deviation of the Life Distribution	141
	5.5	Effect of Scatter of Fatigue Strength Coefficient and Endurance Limit on Fatigue Life	143
		5.5.1 Effect of the Standard Deviation of the Fatigue Strength Coefficient	143
		5.5.2 Effect of the Variance of Fatigue Endurance Limit	145
	5.6	Effect of Shape of the Load Probability Density Function on Fatigue Life Distribution	150
CHAPTER 6		CONCLUSIONS AND RECOMMENDATIONS FOR FURTHER RESEARCH	157

		Page
6.1	Concluding Remarks	157
6.2	Scope for Future Investigations	163
REFERENCES		165
APPENDIX A	EVALUATION OF FATIGUE ENDURANCE LIMIT DISTRIBUTION USING THE STAIRCASE METHOD	173
APPENDIX B	NUMERICAL CONTROL PROGRAM FOR CUTTING BENDING FATIGUE SPECIMENS	179
APPENDIX C	TABLES OF EXPERIMENTAL DATA, ANALYTICAL PREDICTIONS, AND COMPUTER OUTPUTS	185

NOMENCLATURE

A	Cross-sectional area
b	Fatigue strength exponent
c	Fatigue ductility exponent
C	Cycle ratio, ratio of number of cycles at a given stress to the number of cycles to failure corresponding to the same stress
C_i	The i^{th} central moment of a probability distribution
CNC	Computer numerical control
d	Inverse slope of log S-log N diagram
E	Young's modulus
E_i	Expected frequency in the i^{th} class interval
e_u	Uniform strain, strain corresponding to the maximum load in tension tests
$F( )$	Cumulative distribution function
$f( )$	Probability distribution function
N	Number of cycles
N_f	Number of cycles to failure
$2N_f$	Number of reversals to failure
N_e	Fatigue endurance life
N_t	Transition fatigue life
N_m	Life calculated using the mean S-N diagram and Miner's rule
O_i	Observed frequency in the i^{th} class interval
PDF	Probability density function
PSD	Power spectral density
P-S-N	Probability-Stress-Number of cycles (diagram)
R_x	Autocorrelation function of random variable X

r	Number of distribution parameters
r_s	Stress ratio, ratio of the alternating stress to the mean stress
RMS	Root mean square
S	Stress amplitude
S_m	Mean stress
S_y	Yield stress
S'_y	Cyclic yield stress
S_f	Engineering fracture stress
S_{ft}	True fracture stress
S_u	Ultimate tensile strength
S_{ut}	True ultimate stress
S_e	Fatigue endurance stress
S'_f	Fatigue strength coefficient
t	Time
α_i	Fraction of all cycles at stress S_i
β_1	Coefficient of skewness
β_2	Coefficient of peakedness
ϵ	True strain
$\Delta\epsilon_e$	True elastic strain range
$\Delta\epsilon_p$	True plastic strain range
$\Delta\epsilon_t$	True total strain range
ϵ'_f	Fatigue ductility coefficient
σ	Standard deviation of a stress distribution
σ_ℓ	Standard deviation of the predicted life distribution when the applied load is Gaussian
σ_e	Standard deviation of the endurance limit (experimentally determined)
σ_f	Standard deviation of the fatigue strength coefficient (experimentally determined)

σ'	Standard deviation of the predicted life distribution when the applied load is deterministic
σ_e^*	Assumed value of the standard deviation of the endurance stress distribution
σ^*	Predicted value of the standard deviation of the life distributions when $\sigma_e = \sigma_e^*$
μ	Mean value of a stress distribution
μ_ℓ	Mean value of the predicted life distribution when the applied load is Gaussian
μ'	Mean value of the predicted life distribution when the applied load is deterministic
μ^*	Predicted mean value of the fatigue life distributions when $\sigma_e = \sigma_e^*$
τ	Time delay

LIST OF FIGURES

Figure		Page
1.1	Classification of Service Load Data.	9
1.2	Monotonic and Cyclic Stress-Strain Curves for Two Conditions of SAE 1045 Steel.	12
1.3	Strain-Life Plots in Cyclic Loading.	13
1.4	Schematic Representation of P-S-N Diagram.	18
1.5	Determination of Strength Distributions from Life Distributions.	21
1.6	Statistical Log S-Log N Diagram.	23
1.7	Distributional Goodman Fatigue Diagram for 10^6 Cycles of Life for SAE 4340 Steel.	24
1.8	General Outline of the Theoretical and Experimental Aspects of the Present Investigation.	30
2.1	Conventional Log S-Log N Diagram.	33
2.2	Determination of the Number of Cycles at the Knee (Endurance).	37
2.3	Monte Carlo Simulation of Probabilistic S-N Diagram.	39
2.4	Comparison Between Observed and Predicted Mean Life and Scatter Band (Life $\pm$ 3σ) for SAE 4340 Steel.	46
2.5	Predicted and Experimental Normal Fatigue Life Distribution at Stress 101,000 psi (696,370 K Pa) of SAE 4340 Steel.	47
2.6	Predicted and Experimental Normal Fatigue Life Distribution at Stress 89,000 psi (613,633 K Pa) of SAE 4340 Steel.	48
2.7	Predicted and Experimental Normal Fatigue Life Distribution at Stress 80,800 psi (557,696 K Pa) of SAE 4340 Steel.	49
2.8	Predicted and Experimental Normal Fatigue Life Distribution at Stress 68,000 psi (468,843 K Pa) of SAE 4340 Steel.	50

Figure		Page
2.9	Predicted and Experimental Distributions of Logarithm the Fatigue Life of SAE 4340 Steel at Four Stress Levels.	51
3.1	Spatial Orientation of Sample Coil.	56
3.2	Position of Specimens and Legend Used.	57
3.3	Configuration and Dimensions of the Tensile Test Specimen.	60
3.4	Photograph Showing Tensile Test Specimens, Before and After Fracture.	61
3.5	Typical Load-Extension Diagram for SAE-1008 Sheet Steel.	62
3.6	Comparison of Engineering and True Stress-Strain Curves for SAE 1008 Sheet Steel.	66
3.7	Configuration and Dimensions of the Axial Fatigue Specimen.	68
3.8	Photograph Showing Axial Fatigue Specimens Before and After Fracture.	69
3.9	Strain-Reversals to Failure Data for SAE 1008 Sheet Steel Subjected to Reversed (Controlled) Strain.	72
3.10	Axial Stress Amplitude-Reversals to Failure Diagram for SAE 1008 Sheet Steel Subjected to Axial Reversed Strain.	73
3.11	Schematic Representation of Cyclic and Monotonic Stress-Strain Curves [74].	76
3.12	Strain-Time History Used in the Incremental Step Test.	78
3.13	Hysteresis Loops After One Strain Block of the Incremental Step Test.	79
3.14	Stabilized Hysteresis Loops After 30, 32, and 34 Blocks of Load.	80
3.15	Experimental Cyclic and Monotonic Stress-Strain Curves of SAE 1008 Sheet Steel.	81
3.16	Cyclic Softening and Stabilization Exhibited by SAE 1008 Sheet Steel Subjected to Incremental Step Test Loading.	82

Figure		Page
3.17	Block Diagram of Bending Fatigue Test Set-Up.	85
3.18	Configuration and Dimensions of the Bending Fatigue Test Specimen.	88
4.1	Photograph Showing a General View of the CNC Milling Machine and Hewlett Packard Minicomputer Used to Manufacture the Bending Fatigue Test Specimens.	95
4.2	Photograph Showing Closeups of the Bending Fatigue Specimens and Cutting Tool.	95
4.3	Photograph Showing the Strain Gauges Applied to the Bending Fatigue Specimens.	96
4.4	Photograph Showing Bending Fatigue Test Specimens, Before and After Fracture.	96
4.5	Photograph Showing General View of the Bending Fatigue Test Set-Up.	99
4.6	Photograph Showing a Closeup of the Specimen-Shaker Assembly.	100
4.7	Photograph Showing the Strain (Upper Trace) and Displacement (Lower Trace) Signals of a Sinusoidal Constant Amplitude Test.	100
4.8	Schematic Diagram of the Triggering Circuit.	103
4.9	Schematic Representation of the Three Sinusoidal Load Programs Used in the Tests.	104
4.10	Predicted and Experimental Fatigue Life Distribution of SAE 1008 Steel Subjected to Sinusoidal Constant Amplitude Loading.	107
4.11	Predicted and Experimental Distribution of Logarithm the Fatigue Life of SAE 1008 Steel Subjected to Sinusoidal Constant Amplitude Loading.	108
4.12	The Predicted Cycle Ratio Distribution of SAE-1008 Steel Subjected to Sinusoidal Constant Amplitude Loading.	109
4.13	Predicted and Experimental Fatigue Life Distribution of SAE 1008 Steel Subjected to Hi-Lo Sinusoidal Block Loading.	111

Figure		Page
4.14	Predicted and Experimental Distribution of Logarithm the Fatigue Life of SAE 1008 Steel Subjected to Hi-Lo Sinusoidal Block Loading.	112
4.15	The Predicted Cycle Ratio Distribution of SAE 1008 Steel Subjected to Hi-Lo Sinusoidal Block Loading.	113
4.16	Predicted and Experimental Fatigue Life Distribution of SAE 1008 Steel Subjected to Lo-Hi-Lo Sinusoidal Block Loading.	115
4.17	Predicted and Experimental Distribution of Logarithm the Fatigue Life of SAE 1008 Steel Subjected to Lo-Hi-Lo Sinusoidal Block Loading.	116
4.18	The Predicted Cycle Ratio Distribution of SAE 1008 Steel Subjected to Lo-Hi-Lo Sinusoidal Block Loading.	117
5.1	Methods of Random Load Testing.	123
5.2	Photograph Showing the Ruscom Logics Graph Digitizer.	127
5.3	Photograph Showing the Auto-correlation Function of the Displacement Plotted Versus Time Delay (τ). Time Scale 1μs/mm.	127
5.4	Photograph Showing a Time Record of Narrow Band Random Displacement Signal. Time Scale 50 m sec/div.	129
5.5	Photograph Showing the Force (Upper Trace) and Strain (Lower Trace) Random Signals. Time Scale 0.1 sec/division.	129
5.6	Photograph Showing the Instantaneous Value Probability Density Distribution of the Strain Narrow Band Signal.	130
5.7	Photograph Showing the Cumulative Distribution of the Instantaneous Value of the Strain Signal.	130
5.8	Experimental Histogram of the Random Peak Stress and Fitted Distributions.	132
5.9	Predicted and Experimental Fatigue Life Distributions of SAE 1008 Steel Subjected to Narrow Band Random Loading.	137

Figure		Page
5.10	Predicted and Experimental Distributions of Logarithm the Fatigue Life of SAE 1008 Steel Subjected to Narrow Band Random Loading.	138
5.11	The Predicted Cycle Ratio Distributions of SAE 1008 Steel Subjected to Narrow Band Random Loading.	139
5.12	Effect of the Applied Stress Variance on Predicted Mean Value of Life and its Logarithm.	142
5.13	Effect of the Applied Stress Variance on the Variance of the Predicted Fatigue Life and its Logarithm at a Stress Level 101,000 psi.	144
5.14	Effect of the Variance of the Fatigue Strength Coefficient on the Variance of the Predicted Fatigue Life at Stress Level 101,000 psi.	146
5.15	Effect of the Endurance Limit Variance on the Randomness of the Predicted Fatigue Life, at Stress Level 101,000 psi.	148
5.16	Effect of the Variance of the Endurance Limit on the Mean Predicted Fatigue Life at Stress Level 101,000 psi.	149
5.17	Schematic Representation of the Stress Distributions Used to Test the Shape Effect of the Load PDF.	153
5.18	Effect of the Coefficient of Skewness of the Input PDF on the Fatigue Life and Its Standard Deviation.	154
5.19	Plots of Both the Mode and Median Stresses vs. the Fatigue Life and its Standard Deviation.	155
A.1	Experimental Results of the Staircase Test to Determine the Distribution of the Endurance Limit of SAE 1008 Steel.	177

LIST OF TABLES

Table		Page
2.1	Wire Fatigue Machine Results for .0625 in (1.5878 mm) Diameter SAE 4340 Steel Wire in Rotating Bending, Taken from [48].	42
2.2	Comparison between Experiment and Prediction of Fatigue Life for SAE 4340 Steel.	44
2.3	Comparison between Experiment and Prediction of Logarithm the Fatigue Life for SAE 4340 Steel.	45
3.1	Material Chemical Analysis (SAE 1008 Steel).	54
3.2	SAE 1008 Steel Static Material Properties.	65
3.3	Staircase Test Results and Data Reduction to Determine the Mean and Standard Deviation of the Endurance Stress Distribution for SAE-1008 Steel.	90
4.1	Instruments Used in Bending Fatigue Experiments (Legend for Fig. 3.17).	98
4.2	Comparison of Experimental and Predicted Fatigue Life Distributions of Constant Amplitude Sinusoidal Loading for SAE 1008 Steel.	110
4.3	Comparison of Experimental and Predicted Fatigue Life Distributions of HI-LO Block Form Loading for SAE 1008 Steel.	114
4.4	Comparison of Experimental and Predicted Fatigue Life Distributions of LO-HI-LO Block Form Loading for SAE 1008 Steel.	118
5.1	Comparison of Experimental and Predicted Fatigue Life Distributions of Narrow Band Random Tests for SAE 1008 Steel.	136
B.1	N/C Data Program Used to Manufacture the Bending Fatigue Specimens.	180
C.1	Results of Tensile Tests of SAE 1008 Steel.	185
C.2	Results of Axial Fatigue Tests of SAE 1008 Steel (Loading Parallel to Direction of Rolling).	188

C.3	Results of the Staircase Test to Determine the Distribution of the Fatigue Endurance Limit.	189
C.4	Experimental Data of the Constant Amplitude Sinusoidal Bending Fatigue Tests for SAE-1008 Steel.	191
C.5	Statistical Characteristics of the Experimental and Predicted Life Distributions of SAE 1008 Steel Under Constant Amplitude Sinusoidal Loading.	192
C.6	Experimental Data of the HI-LO Bending Fatigue Tests for SAE 1008 Steel.	195
C.7	Statistical Characteristics of the Experimental and Predicted Life Distributions of SAE 1008 Steel Under HI-LO Block Loading.	196
C.8	Experimental Data of the LO-HI-LO Bending Fatigue Tests for SAE 1008 Steel.	199
C.9	Statistical Characteristics of the Experimental and Predicted Life Distributions of SAE 1008 Steel Under LO-HI-LO Block Loading.	200
C.10	Experimental Data of the Narrow Band Random Bending Fatigue Tests.	203
C.11	Statistical Characteristics of the Input Peak Stress Distributions and Results of χ^2 Goodness-of-Fit Tests.	204
C.12	Statistical Characteristics of the Experimental and Predicted Life Distributions of SAE 1008 Steel Under Narrow Band Random Loading.	206
C.13	Effect of Changing the Standard Deviation of the Endurance Limit (σ_e) at Stress Level of 89,000 psi, on the Predicted Life Distribution of SAE 4340 Steel.	210
C.14	Effect of Changing the Standard Deviation of the Fatigue Strength Coefficient (σ_f) at Stress Level of 89,000 psi, on the Predicted Life Distribution of SAE 4340 Steel.	211
C.15	Effect of Changing the Variance of a Random Stress S ~ N (101,000, σ) for SAE 4340 Steel.	212
C.16	Effect of Changing the Variance of a Random Stress S ~ N (68,000, σ) for SAE 4340 Steel.	213

CHAPTER 1

INTRODUCTION AND LITERATURE SURVEY

One of the central unsolved problems of engineering design is prediction of the probability distribution of fatigue life of structural members and machine components. It is a central problem because fatigue is a major failure mode in mechanical devices, and because the stochastic variability of fatigue life is characteristically high -- much higher than most design characteristics.

It can be said that all stress analyses are basically fatigue analyses, the differences lying in the number of cycles of applied stress. The portion of the entire design process known as fatigue design can only follow the loads and stress analyses. A stress analysis is required to define the stress history at any critical point in the structure; the application of a theory of fatigue damage defines the amount of damage accumulated, at the same location, as a function of that stress history.

At the start of any effort on life prediction it should be fully recognized that the development of fatigue cracks in metals is a statistically random process. The stresses in any structure subjected to natural loads, and the properties and conditions of the materials in these structures, will also vary in a random manner. The integrated influence

of all these variables yields wide scatter in the results.

The objective of this dissertation is to propose and evaluate a Monte Carlo technique for predicting the random nature of fatigue life for use in design. The use, accuracy and applicability of the suggested model for predicting fatigue life and its scatter are the subject of this thesis.

1.1 General Background

The history of fatigue research is inextricably bound up with the history of railways. Ever since Poncelet [1]* first used the term fatigue in 1839, it has been recognized as a potentially catastrophic mode of failure. Careful analyses revealed that the nominal maximum stresses in parts that failed in fatigue were below the ultimate strength of the material and quite frequently even below the yield strength. The most distinguishing characteristic of these failures has been that the stresses have been repeated a very large number of times. Hence the failure is called "fatigue" failure. The earliest reports [2, 3] were all concerned with failures in railway axles. In 1870 Wöhler [4] published the results of the first experiments on fatigue. His work laid the foundation for the fatigue research of the following 80 years.

* Number in square brackets designate Reference number

Bauschinger [5] and Foppl [6] continued the work on stress concentration and Gerber [7] and, later, Goodman [8] modified the Wöhler stress life curves to allow for the effect of mean stress. The stress-life curve in its present form was established by Basquin [9] in 1910.

The last 20 years have seen a resurgence of interest in fatigue research. Just as in the case of the initial interest, the impetus was provided by a new means of transport, in this case aircraft and spacecraft. The nuclear power industry and ground vehicle industry have also played a part. In all these applications, fatigue is the most prevalent mode of failure. The extent of this interest is shown by the 7000 or so papers published on the subject in the last two decades, less than 200 of which dealt with random fatigue. But, in spite of this work, too many problems are still unsolved and fatigue failure will challenge many researchers for years to come.

This chapter presents a brief description of the basic process of fatigue. This is followed by a discussion of some of the available methods of fatigue analysis and the probabilistic character of fatigue failure. While many exhaustive and critical reviews on these topics are available in the literature [10 - 17], the main purpose of this presentation is to provide basic information for the illustrative fatigue damage evaluation and the life prediction model to be presented in Chapter 4.

1.2 The Fatigue Process

Unlike most other structural failure mechanisms in which failure is the result of a large scale deformation process, fatigue is a highly localized phenomenon. Fatigue failure gives no warning, it is sudden and potentially dangerous.

While the title of this section might imply that the fundamental process or mechanism by which the fatigue damage occurs is well known; actually this is not the case. Despite all the efforts made the fatigue mechanisms have yet to be described mathematically. Correlation of existing data provides a fairly adequate picture of the process.

The fatigue process has been broadly divided into two stages, namely a crack initiation stage and a crack propagation stage. These stages are governed by somewhat different criteria. Earlier studies either did not differentiate between the two stages or arbitrarily defined initiation as corresponding to the development of a crack to a given small size. Recently, the advent of electron microscopic techniques has facilitated more fundamental studies of the basic process of fatigue which have resulted in more rational definitions for initiation and propagation. It is now generally accepted that the deformation of crystals under a cyclic load occurs by slip or shear displacement of one atom plane past an adjacent plane. The location of initial slip on a plane and the choice of a plane are generally determined by the type of crystal and by the presence of a

discontinuity in the form of a dislocation, inclusion, or a void. Such a break in the regular atomic pattern is a stress concentration that acts to increase the local stress beyond the shear limit. Cyclic input of strain energy alters the thermal and internal surface energies such that dislocations tend to collect on planes already containing one or more of them. Small quanta of strain energy are required to slip one plane one atomic distance past the other plane; separation normal to the planes does not usually occur.

Theories of crack nucleation can be grouped into three categories:

(i) The first group postulates that the individual slip lines will join to form a cluster of slip lines (slip band) generally on a free surface at the critical locations. As the stress cycling continues there will be continual sliding along the surfaces which is accompanied by friction. As a result of this friction, according to this theory, the material gradually wears along the surfaces of sliding and a crack results.

(ii) The second group postulates that the crystalline structure in the deformation zone progressively deteriorates leaving a crack in the material. It suggests that the cracks responsible for fatigue fracture are initiated by the integrated effect of stress concentration resulting from the piling-up of dislocations at defects.

(iii) The third group assumes that a pre-existent surface

crack, blemish or void is always present in the material and the fatigue mechanism is one of crack propagation only.

Both the first and second-postulates necessarily imply a probabilistic behaviour at this stage owing to random distribution of grain size, orientation, presence of inclusions with different sizes and shapes, differences in spacing of hardening particles, micro residual stresses, and so on. In other words this means that the severity of the weak points or "nucleation points" is random. This crack nucleation stage does not exceed ten percent of the life for low cycle fatigue, while it can extend to 30-40% of the life for high-cycle fatigue. The percentage of fatigue life spent in nucleating a crack depends also upon the geometry, size and loading of the component.

Continued cycling or input of strain energy causes the crack to grow within the crystal until the crystal separates into two or more fragments, with interference and distortion of the adjacent crystals. Further cycling would eventually cause the crack to cross the grain boundary into an adjacent grain. This change-over from intercrystalline to transcrystalline crack growth is influenced by random material parameters such as grain size, impurities and slip mode in addition to the maximum principal stress. The crack continues to grow along a plane normal to the direction of the maximum principal stress. In addition to cyclic slip, a tensile maximum stress is necessary for fatigue crack growth. Further

cycling would eventually cause the cracks to grow and coalesce into an open area, resulting finally in insufficient area to support the load, and fracture.

Investigations into the physical aspects of fatigue have revealed four salient points which appear common to many, if not all, metals and alloys:

(i) Slip on an atomic lattice plane starts at a common value of critical resolved shear stress, approximately 200 psi, and a common strain of 10^{-4}.

(ii) The slope of the plastic strain versus the number of reversals to failure curve (ϵ_p vs. 2 N_f) is common for most materials at $-\frac{1}{2}$.

(iii) A value of 1% plastic strain causes failure in about 1000 cycles.

(iv) The slope of the stress intensity factor vs. the fatigue crack growth rate curve (k vs. d2a/dN) is common at +4.

1.3 Prediction of Fatigue Life

The prediction activity, or designing against fatigue failure includes several tasks:

(i) Definition of the load-time history the structure has to withstand, based on data collected from similar existing structures. Possible future changes in the use, service environment of the structure or alterations of design details should be taken into consideration.

(ii) Stress and strain analysis of the critical locations in the structure, to establish the design stress-time or strain-time history.

(iii) Both (i) and (ii) are prerequisites to the application of a damage rule, which is used to compare the design stresses with standard stress or strain-life data in order to estimate life.

1.3.1 Description of Service Loads

Description of service loads is, in many cases, the source of the greatest error and it is partly a problem of analysis. In very few cases can the loading be easily described; examples are eccentric masses rotating at constant speed or components which experience a periodic force. Almost all other cases cause a complex stress history. In general, any observed data representing a physical phenomena can be broadly classified as being either deterministic or random, as shown in Figure 1.1. For periodic loads; the mean load, the amplitude and the frequency constitute a complete description of the load as a function of time. Even for a set of discrete-amplitude periodic loads, the definition of a cycle is still fairly evident. The event to be counted, however, is not universally agreed upon; it may be the peaks, level crossings, ranges, range-pairs, and so forth. For the random response the definition of a cycle is not at all evident; thus the counting becomes even more complex. A large number of counting methods have been proposed [18, 21, 90].

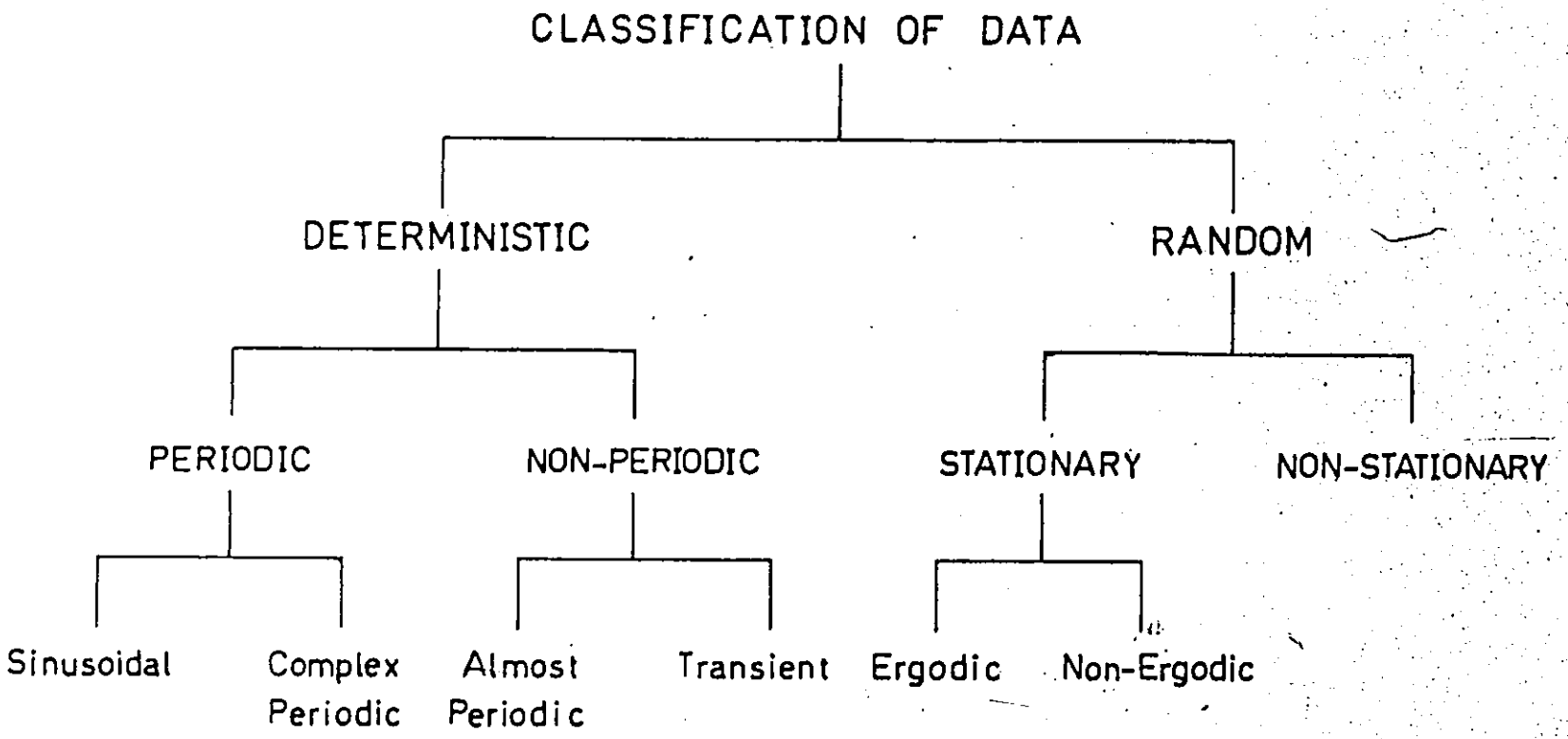

Figure 1.1 Classification of Service Load Data.

Using a cycle counting technique, a variable amplitude history can be reduced to a series of cycles or half-cycles whose maximum and minimum values are defined. Mean values can then be calculated and hence the cycles or half-cycles are completely determined. Fatigue life can then be calculated from constant amplitude data using a cumulative damage law.

Cycle counting methods use records of finite length and assume that they are identically repeated until failure. A powerful new technique of continuous load analysis, referred to loosely as Power Spectral Density analysis, is quickly becoming recognized as a valid approach to the delineation of fatigue loads. The use of this approach results in the determination of a statistically-defined load spectrum for the component under consideration. This spectrum is usually presented as a relative frequency plot of load level versus number of cycles of loading at that level. An envelope spectrum will encompass several load spectra to yield a design capable of withstanding any of the component load spectra.

Knowing the characteristic of the load-time history, a cumulative damage rule can be used, with constant amplitude stress-life, strain-life or the more relevant RMS-life plots to predict the fatigue life.

1.3.2 Cyclic Stress-Strain Behaviour

Fatigue damage will occur at locations where the conditions are sufficient to cause local reversed plasticity. Without this plastic strain cycling, there can be no fatigue

failure [89-92]. Because it is plasticity which leads to damage, it is unrealistic to calculate stress concentration at the critical locations using the elasticity theory. The establishment of the relationship between plastic strain and fatigue, the development of the cyclic stress-strain behaviour, and the application of Neuber's rule to fatigue stress concentrations were among the most important developments in fatigue research in the past twenty years. The work of Coffin, Manson, Jo Dean Morrow, Topper and others [10, 19-28, 72-74] is of particular significance in this respect. A typical cyclic stress-strain curve and the strain-life plots are shown in Figures 1.2 and 1.3 respectively. A detailed discussion of these plots is given in Chapter 3. It is a well agreed upon fact that using the local stress-strain behaviour to predict fatigue life yields better results than the conventional nominal stress approach.

1.3.3 Treatment of Fatigue Damage

There are several methods for the prediction of fatigue life; fundamentally, they all involve the concept of gradual accumulation of damage during the process of loading. The differences between the methods is in the emphasis placed on particular aspects of formulae for the representation of either or both the applied loading spectra and the allowable S-N data. The methods fall into two categories according to the type of damage accumulation law used.

a) Linear Cumulative Damage

The earliest cumulative damage summation rule proposed

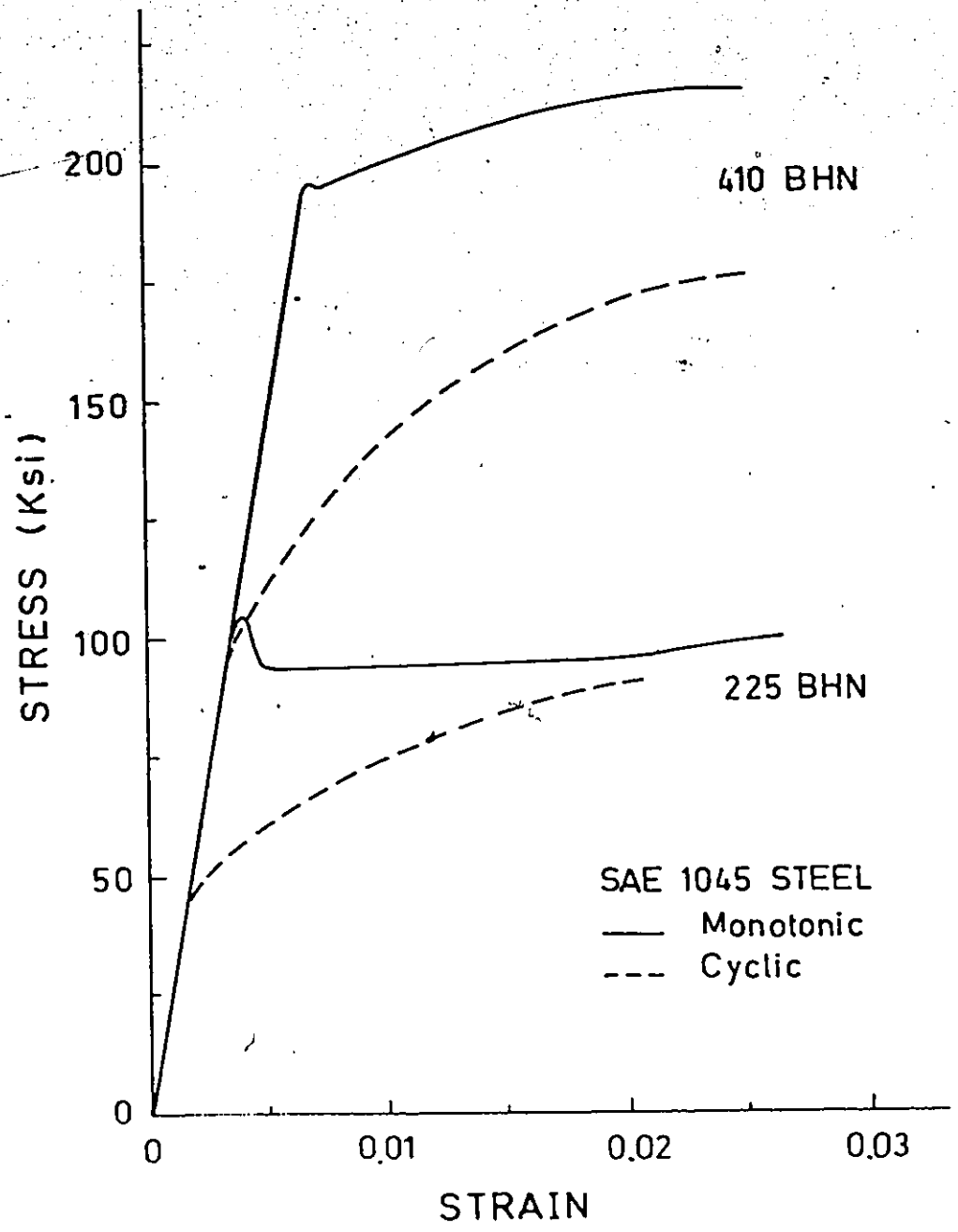

Figure 1.2 Monotonic and Cyclic Stress-Strain Curves for Two Conditions of SAE 1045 Steel [27].

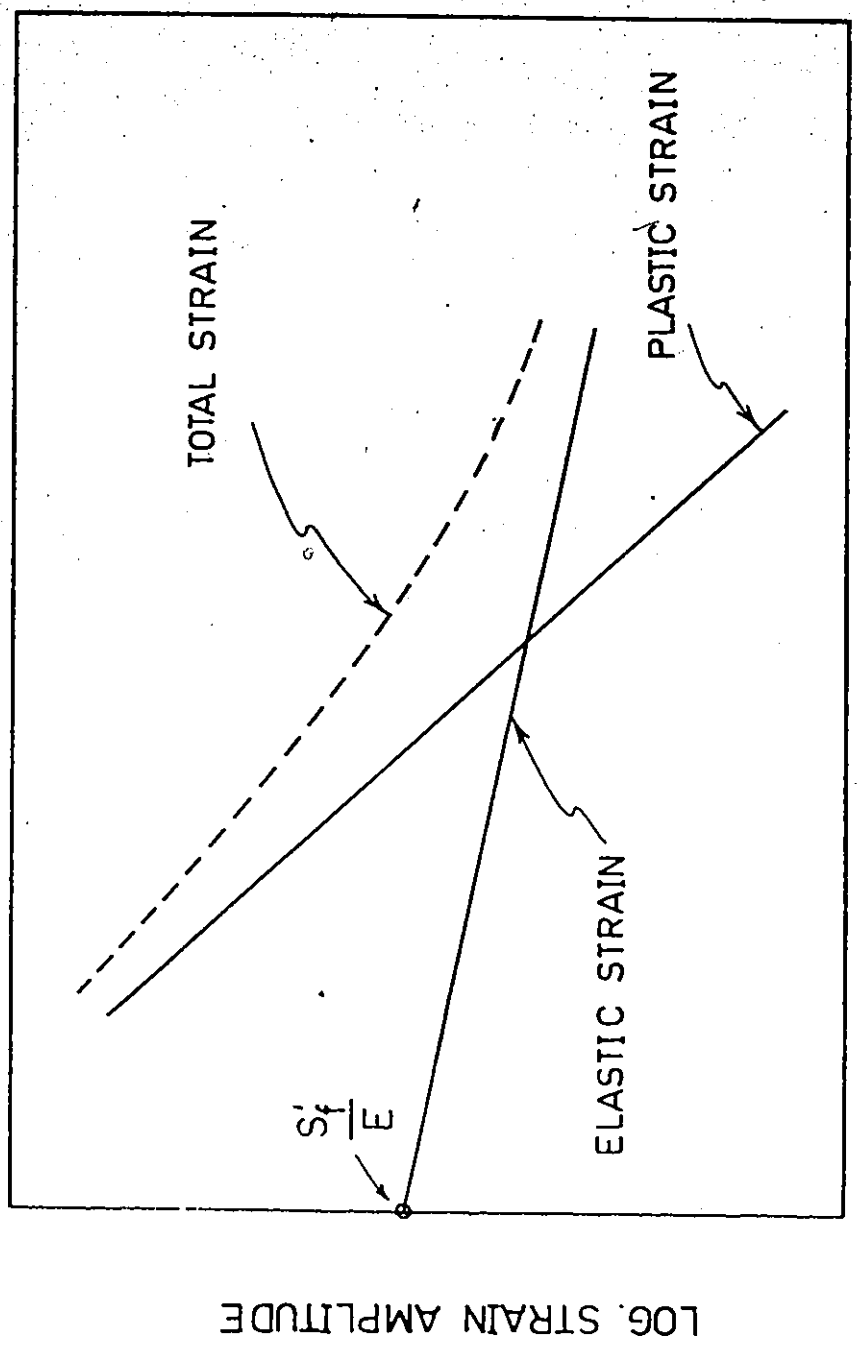

Figure 1.3 Strain-Life Plots in Cyclic Loading.

by Palmgren [30] and later extended by Miner [31], defined damage per cycle as the inverse of the number of cycles to failure at any given stress amplitude and used the conventional S-N diagram as the fatigue damage criterion. When the total damage, as defined by this concept, reaches unity, failure should occur. This rule can be represented in the following form:

$$\sum_i \frac{n_i}{N_i} = 1 \qquad (1.1)$$

where

n_i = number of cycles at a given level (i) of the applied load.

N_i = number of cycles to failure corresponding to the applied load at level (i).

This rule has received widespread use and gained considerable prominence since its inception, because of its simplicity. In spite of its simplicity and usefulness, Miner's rule is open to some criticism. Namely, it fails to include in the treatment the effect of mean stress and loading sequence. Many researchers have had varying degrees of success with this rule. Average values of damage ranging between 0.1 to 10, depending on the loading conditions, have been reported [33, 86, 87, 90].

b) Non Linear Cumulative Damage

The shortcomings of the linear damage accumulation

rule have prompted many efforts to formulate a more comprehensive rule. Such efforts have generally yielded expressions of considerable complexity as compared to Miner's summation, occasionally requiring data that is not available. In general these methods provided improvement in accuracy for some load programs at the expense of added complexity. Corten and Dolan [32] were among the earliest to propose that the fatigue process could be represented as a crack growth process. A non-linear expression for the damage accumulation law, including the altered response of the material caused by prior cycling, expresses fatigue life as:

$$N = \frac{N_1}{\Sigma\ \alpha_i (S_i/S_1)^d} \tag{1.2}$$

where

N_1 = the nominal fatigue life at the highest stress S_1

α_i = the fraction of all cycles that occur at the corresponding stress S_i

d = a material constant, roughly equal to the inverse of slope of the log S-log N curve, influenced somewhat by the stress concentration factors.

To derive the expression given by equation (1.2), the authors used an idealized crack propagation model which ignored the effect of load sequence on the rate of crack propagation. Their analysis did not include other factors such as residual

stresses, metallurgical changes, the number of cracks present and their state of coalescence. Evaluations of this non-linear law yielded results very close to those of the linear law.

Many other useful methods of damage accumulation, which are basically variations of the two previously discussed, have been proposed [17]. The linear law still retains its popularity because a theory which is distinctly superior to the Palmgren-Miner rule simply does not exist.

1.4 The Probabilistic Character of Fatigue Failure

With the continued growth of the stockpile of experimental evidence gathered by fatigue investigators it has become increasingly apparent that the basic problems of failure by fatigue are inherently statistical in nature. The existence of scatter in test results is not peculiar to fatigue tests. Some variation can usually be found in repeated observations of any measurable quantity, but there are particular observations that may be noted in connection with the scatter in fatigue data. Firstly, the amount of scatter observed in fatigue data is much more than that found in other strength test data. Secondly, the scatter of fatigue test results, formerly attributed to incorrect testing procedures, is now recognized to be due mostly to material behaviour [15, 34, 35, 96] The fatigue resistance of one small elemental volume of the material will differ from the resistance of another owing to the presence of such random factors as inclusions, differen

in grain size or orientation, spacing of hardening particles, presence of micro-residual stresses, and so forth. Excellent studies of the effect of these factors on fatigue life and strength is found elsewhere [34-46]. Thirdly, there are many parameters which affect the scatter in fatigue life. Some of these parameters are the stress amplitude, the stress ratio (ratio of alternating to mean stress), and the sequence with which the amplitudes are applied. In general, the data from programmed block or spectrum tests show less scatter than that from constant amplitude tests [17].

The number of repetitions to failure of any fixed load is not a physical constant, identically the same for each metallic specimen which can be measured exactly with a single test. It is, rather, a stochastic variable for which knowledge of the distribution function is essential in the prediction of time to failure and reliability analysis. Therefore, one cannot legitimately speak of the fatigue life in terms of a single value but must regard the S N curve more as a family of curves, each of which indicates a definite probability of failure, as shown in Figure 1.4

Researchers have always been concerned with the statistical interpretation of fatigue data and the physical explanation of scatter. Many attempts have been made to understand the mechanism by which the material produces scatter, and several theories have been proposed to this end. Details of such studies can be found in references [15, 41, 42, 43, 46]. The investigations reported in the

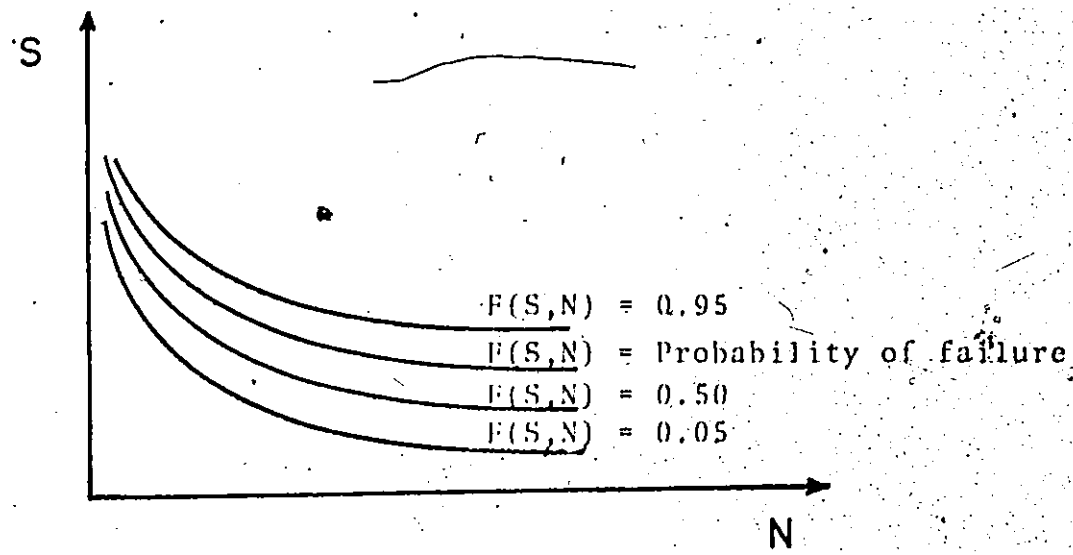

Figure 1.4 Schematic Representation of P-S-N Diagram.

literature can be divided into two main categories:

(i) Interpretation of the experimental results. This includes the different ways of data plotting, curve fitting, determination of the distribution functions and estimating their parameters and the confidence limits associated with them.

(ii) Probabilistic analysis of the fatigue process. This category includes the probabilistic cumulative damage concepts and simulation of the crack propagation process using probabilistic mathematical models.

1.4.1 Statistical Interpretation of Fatigue Data

Because interpolation and extrapolation based on limited experimental evidence has been the aim of most tests, attention was initially focused on various suitable methods of data plotting, curve fitting, and determination of distribution functions for fatigue life. Today, regression analysis and mathematical techniques of curve fitting, aided by computers, have replaced the previous less sophisticated methods of data analysis. The statistical distributions of fatigue life are characteristically unsymmetrical (skewed to the right), and have been found to be well represented by a log-normal [46] or Weibull [35] distributions. If the fatigue life distributions are defined for several stress levels, it is possible to construct the P-S-N reliability curves shown in Figure 1.4. The use of normal and log-normal distributions has been supplemented with Extremal distributions which

either fit the data better or are based on an underlying physical process. To date proponents of various theories are not in complete agreement on the most suitable distribution functions for the description of the statistical variations of fatigue life.

It was found that the fatigue strength of a material, for a specified life, is also a stochastic variable defined by a Normal distribution function. A method of converting life distributions into strength distributions is given in [50] and shown schematically in Figure 1.5. The method presumes the knowledge of the median S-N curve. It was also observed that the scatter of fatigue life is much larger than the scatter of fatigue strength. Probit analysis and Staircase method were also proposed for the determination of fatigue endurance limit distribution. These methods are discussed in Appendix A.

Recently, a large amount of experimental data was generated and statistically analyzed for different materials and stress ratios [47-49]. Normal and log-normal distributions were fitted to fatigue life using the Chi-square goodness-of-fit test. Finite life distributional Goodman diagrams, which present allowable combinations of alternating stress and mean stress, have also been developed. These diagrams were created from strength distributions obtained from P-S-N diagrams at various ratios of alternating to mean stress for different cycle life values. It was found that the Von-Mises Hencky ellipse, for cycle life values above 10^4 cycles, is

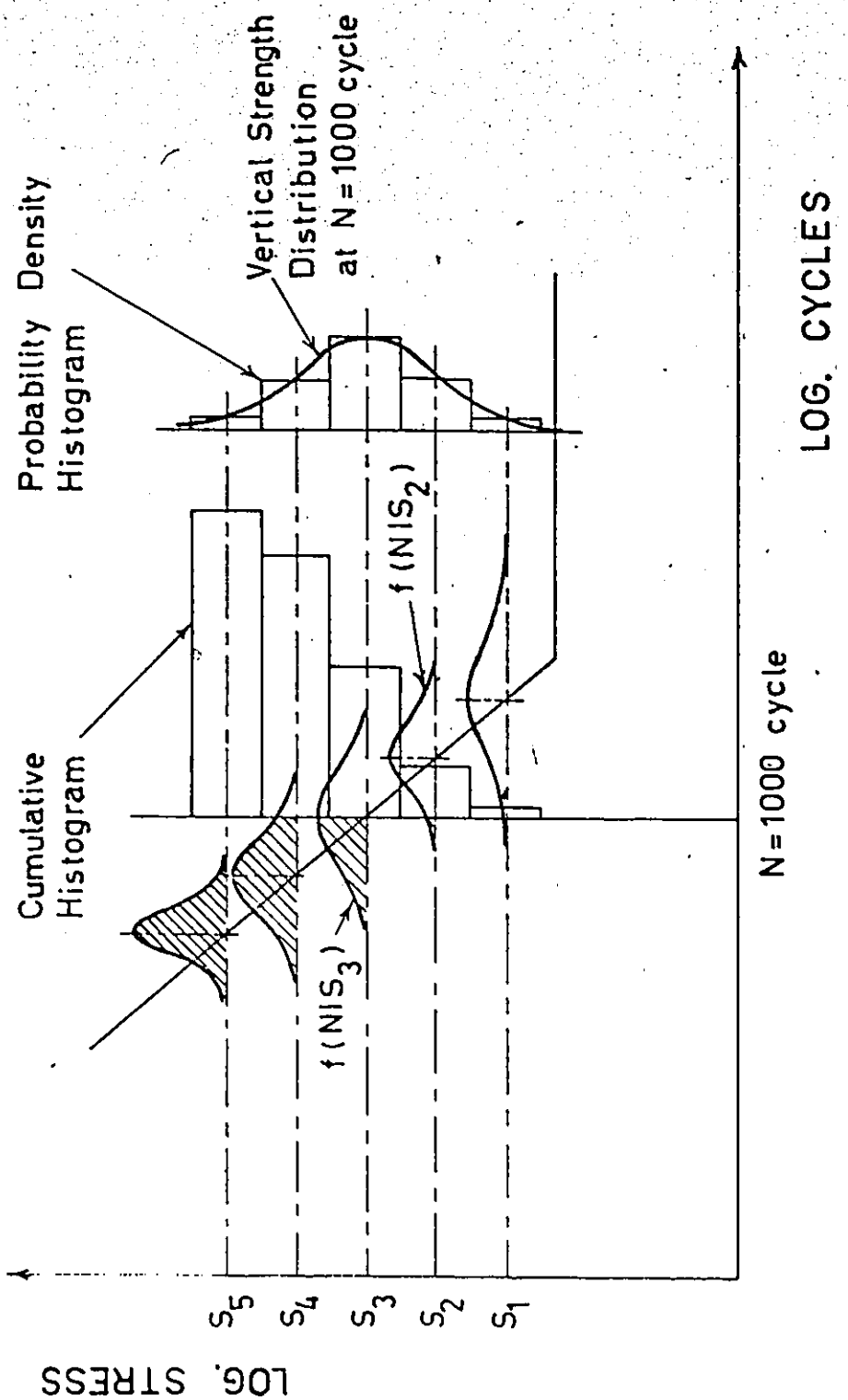

Figure 1.5 Determination of Strength Distributions from Life Distributions [50].

an adequate model for the finite-life probabilistic Goodman diagram. Probabilistic life distributions and distributional Goodman diagram are shown in Figures 1.6 and 1.7 respectively.

The response curves and confidence bands for fatigue strength and life distributions have received considerable attention in the past. Methods are still being sought to determine justifiable fatigue lives based on a minimum number of test results. Although statistical design of experiments and decision theory are well known to statisticians, the use of these techniques in the planning of fatigue tests and interpretation of results has received wide recognition only during the last few years. These methods point the way towards the most efficient utilization of available specimens.

1.4.2 Probabilistic Fatigue Models

The principal purpose of fatigue analysis is not only the descriptive representation of the data, but also their use for inductive prediction of fatigue life and fatigue strength at extreme probability levels. These levels could never be reached in actual tests because of the prohibitive number of experiments needed. Several probabilistic models and statistical theoretical interpretations have been proposed to achieve this. Details of such studies can be found in references [15] and [51]. Some of these models will be briefly summarized here.

a) The Weakest Link Theory

The weakest link theory treats each component as a

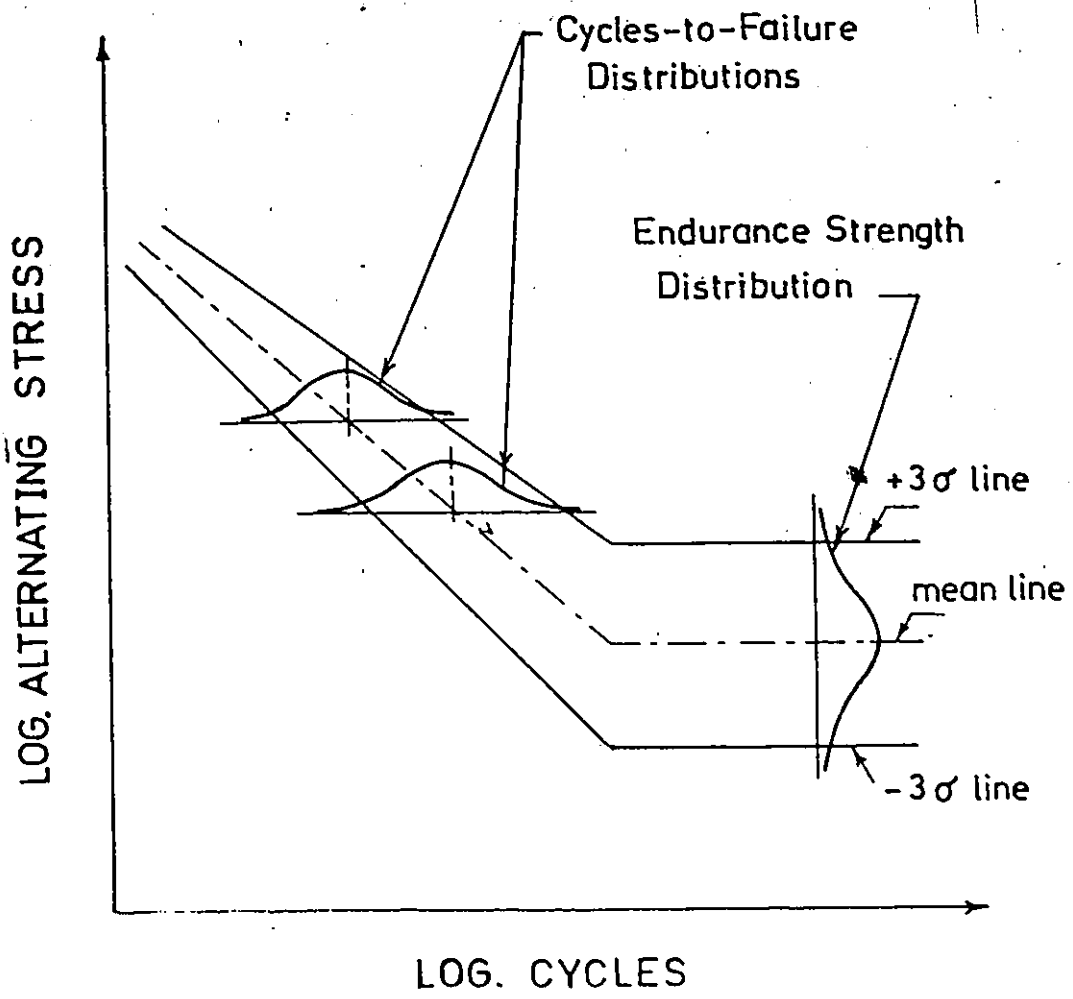

Figure 1.6 Statistical Log S-Log N Diagram.

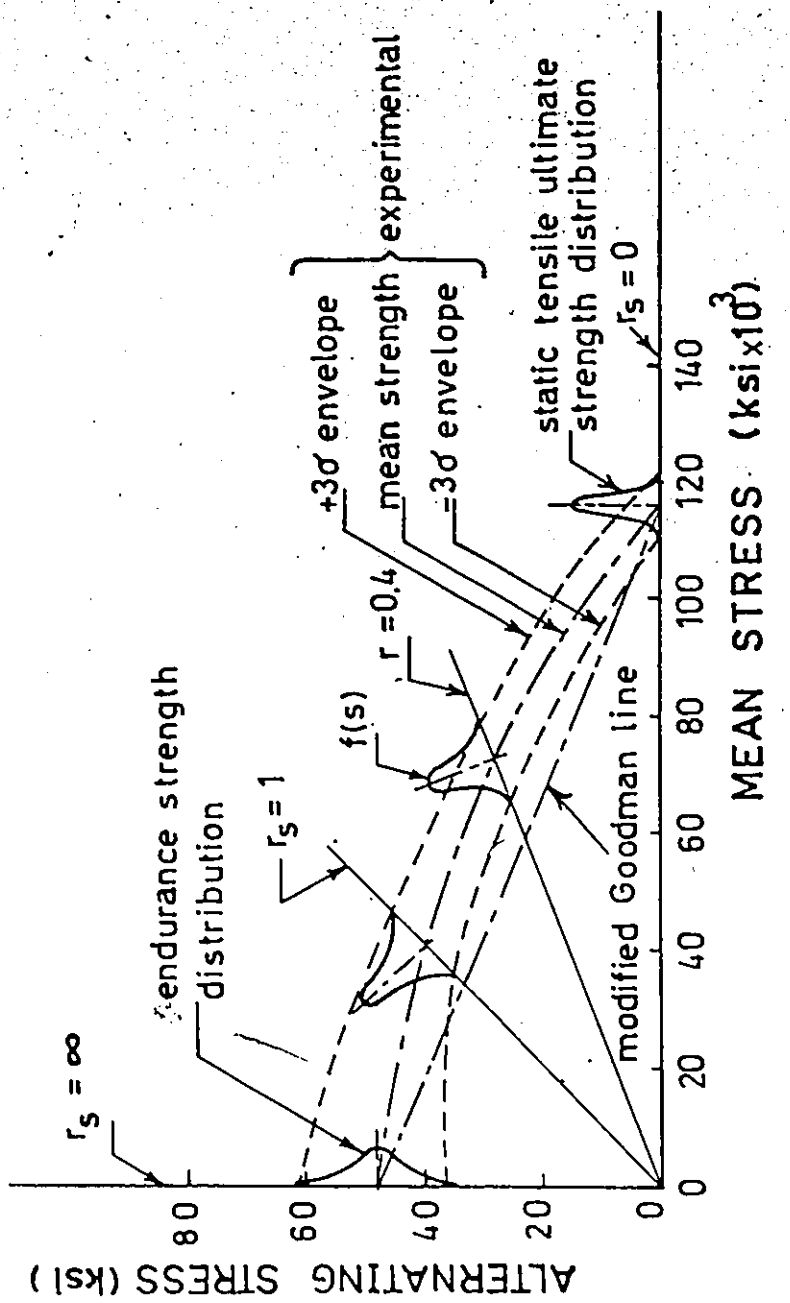

Figure 1.7 Distributional Goodman Fatigue Diagram for 10^6 Cycles of Life for SAE 4340 Steel [50].

series of many subcomponents. It interprets the strength of the component in terms of the minimum values of the strength of the subcomponents. Each link will have cracks with a certain assumed distribution, and the component will fail when the weakest link fails. The derived fatigue life distribution obviously depends on the assumed life distribution of the subcomponents.

b) The Parallel Strand Theory

To understand this theory it is convenient to consider the strands of a multistranded rope. The component is made up of subcomponents such as the strands of a rope and cannot fail until every strand has failed. Life lengths of the subcomponents determine the life pattern of the component. The subcomponent lives are assumed to be independent and identically distributed. The life for the component is then a function of the subcomponent distributions. When the life of the parallel strands is assumed exponentially distributed, the component life becomes a Gamma distribution. If the number of strands approaches infinity, as it would for a metal specimen, the life distributions of both subcomponents and components approach the normal distribution.

c) Crack Nucleation and Propagation Models

Several models have been suggested to simulate the crack nucleation, propagation and the accumulation of damage phenomenon [15, 53-56]. Since all these models attempt to

describe the mechanisms of fatigue failure, the least understood aspect of fatigue, they naturally resort to many assumptions. Most of these assumptions are experimentally unjustifiable, need refinements, or use parameters which are practically unmeasurable. Examples of these assumptions are:

- the distribution of minute flaws, inclusions or voids is known.
- rate of crack growth is constant.
- rate of crack growth is proportional to crack size.
- the distribution of the critical crack length is known.
- failure is caused by single or multiple cracks.
- assumptions regarding the damage rate per cycle.

Comparisons between various theories and experimental results together with physical considerations have shown that no theory is really satisfactory. If this approach is to be successful greater efforts will be required in the development of a complete picture of fatigue crack nucleation and propagation, and the association of this with the microscopic characteristics and behaviour of the material structure. No theory or procedure is presently available which permits a designer to predict the probability distribution of fatigue life, using relatively simple and conveniently available loading and material data.

1.5 Purpose and Scope of Present Investigation

A major conclusion to be drawn from the literature review is that there is a considerable lack of information

concerning the probabilistic fatigue behaviour of structural steels. Directly related to this is the incomplete knowledge regarding the mechanisms of fatigue failure. The literature has shown that material properties are important variables which largely determine the fatigue life and its scatter.

It is evident that the problem of the large scatter exhibited in fatigue testing results has so far been a subject of study in a large number of papers, however, little research has been reported in the literature considering the probability distribution of the material strength parameters. Therefore, this investigation attempts to study the randomness of fatigue life under constant and random load amplitudes considering the randomness of two fatigue properties, the endurance limit (S_e) and the fatigue strength coefficient (S_f').

Since reliability is the best available quantitative measure of the performance integrity of the designed component, it is the purpose of this study to provide the basic data required to meet today's needs of designing specified reliabilities into components under fatigue loading conditions. For performance of reliability analysis for structures subjected to sinusoidal or irregularly varying service loads, the characteristics of the cycle life distribution should be known. Estimates of these characteristics can be derived using the digital simulation technique described in this thesis.

The growing interest in probability and statistics,

and the recognition of its relevance to engineering design, underlines the importance of this kind of study. The deterministic approach to design of structures and components has shortcomings that are well recognized. It does not allow for the fact that most of the design variables are stochastic and have statistical variations. Moreover, the safety factor concept completely ignores the facts of variability that result in different reliabilities for the same safety factor [57]. To implement the probabilistic approach to design, the statistical distributions of the different design variables and factors must be known and synthesized as mathematical functions amenable to further manipulations.

To carry out a design by reliability, the generation of supporting data in distributional form, reflecting inherent variability, is of prime importance. In this investigation, the emphasis is being placed on developing a model for fatigue failure, which considers the variability of the material properties as well as the variability of the applied load. The effect of the shape of the load probability density function is to be investigated using the suggested model and results compared with the published literature which suggests the importance of this factor. This study is based on the belief that a phenomenological approach should be used in developing the model, thus avoiding any assumptions regarding the mechanisms of fatigue failure.

This dissertation will concentrate on establishing a stochastic model capable of simulating the observed probabilistic nature of fatigue life of components subjected to different

load histories. An experimental program has been carried out to generate data needed to check the applicability of this model. The limited experimental data available in the literature will also be compared with results obtained using the new model.

Chapter 2 describes the suggested model and its applications. Chapter 3 outlines the experimental material characterization carried out to provide the basic distributional data needed for prediction. Chapters 4 and 5 demonstrate experimentally that this new technique adequately predicts fatigue life distributions under various load-time histories. The second half of Chapter 5 is devoted to investigating the effect of some factors on fatigue life distributions using the model. Conclusions and suggestions for further research are given in Chapter 6.

An outline of the present investigation is shown in Figure 1.8.

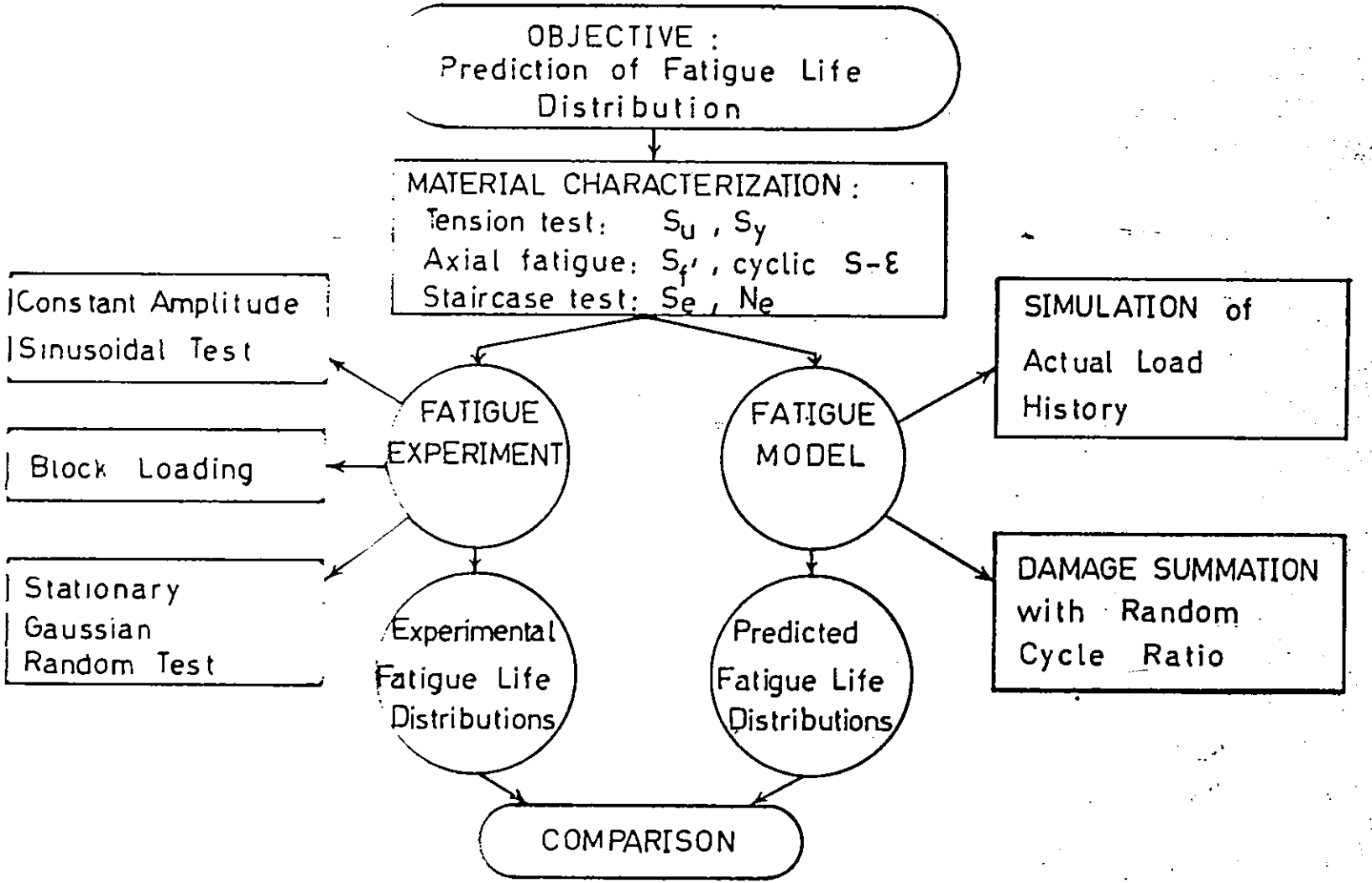

Figure ..3 General Outline of the Theoretical and Experimental Aspects of the Present Investigation.

CHAPTER 2

THEORETICAL FATIGUE LIFE PREDICTION MODEL AND ITS APPLICATIONS

2.1 Introduction

Following the literature survey, it is useful to discuss some basic ideas regarding the establishment of a new model for fatigue life prediction.

(i) It has been well established that the observed scatter in fatigue failures is an inherent characteristic of the material and the fatigue fracture phenomenon. The growing need for more reliable designs has necessitated considering scatter in fatigue as a fundamental problem. The statistical nature of design variables should not be ignored. It is therefore important to acquire adequate knowledge about material properties and their distribution.

(ii) Fundamental studies in the area of material properties made on an atomic basis have not reached a stage at which they would be capable of predicting the macroscopic behaviour. The immediate requirement of quantitative data for analysis, has created a need for phenomenological studies. Such studies need a vast amount of experimental observations before truly general conclusions can be reached.

(iii) A phenomenological study to simulate the scatter of fatigue data appears to be a promising approach. However, care must be taken to ensure that any assumptions used for simulation are rational and well founded and supported by experimental evidence.

(iv) The S-N diagram is a plot of the stress amplitude versus the number of cycles to failure on a log-log scale as shown in Figure 2.1. To construct the conventional S-N diagram, designers have always used mean values of material properties such as the ultimate strength and endurance limit. Recognition of inherent differences in cycles-to-failure at fixed stress resulted in the development of the P-S-N diagram, shown in Figure 1.4, to reflect the scatter of life in terms of distribution parameters. Since a fatigue test is a destructive one, the endurance limit and the ultimate strength cannot be determined using the same specimen. Therefore, the actual properties of each single specimen cannot be determined. The experiments carried out by Ransom et al. [61, 62] shed some light on this problem. They used one hundred specimens, from a single large pipe, made from SAE 4340 forged steel. The S-N diagrams obtained for sets each consisting of 10 specimens show that the S-N lines do intersect. Based on these observations, it is reasonable to assume that, for each specimen, the material properties used to construct the S-N lines are independent, and that

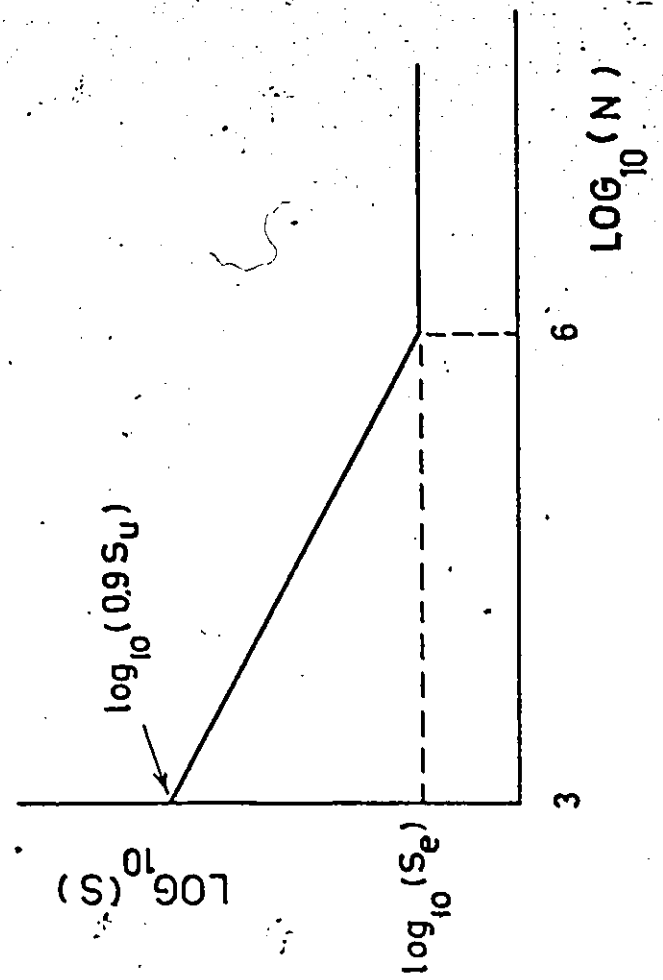

Figure 2.1 Conventional Log S-Log N Diagram.

correlation applies only to the mean values. This assumption is used in the proposed model to simulate the S-N diagrams of the different specimens. It should be noted that the use of statistically dependent properties in the simulation yields predictions which do not agree with the published experimental results.

(v) It is desirable that the simulation technique can be programmed for the digital computers.

It is believed that the following strategy meets the above requirements for predicting a probabilistic fatigue life. In this strategy, a theoretical sample of specimens or members is generated, each member having a hypothetical S-N curve. Each curve is generated by sampling from the distributions of the quantities that define it -- the endurance limit (S_e), and the fatigue strength coefficient (S_f'). These are the only material properties required by this method.

Each hypothetical member is then subjected to a hypothetical loading. For constant amplitude loading, the life of each member is obtained directly from its curve, thus giving a theoretical sample of lives which defines the probability distribution of fatigue life. If the loading is random or in block form, a linear damage law is used, again for each individual theoretical member; thus giving a theoretical sample defining fatigue life.

2.2 Simulation of the Sample S-2N Diagram

The following assumptions are made in simulating individual S-2N diagrams where N and 2N represent the cycles-to-failure and reversals-to-failure respectively.

(i) The curve is assumed to be a straight line on a log-log plot up to $2N_e$ at which the knee occurs. This is defined by the following equation, valid for $10^3 \leq N \leq N_e$

$$\log_{10} 2N = \frac{\log_{10} 2N_e}{\log_{10} S'_f - \log_{10} S_e} (\log_{10} S'_f - \log_{10} S) \qquad (2.1)$$

where S is the applied stress amplitud

Beyond $2N_e$ the curve is horizontal at a stress level of S_e.

(ii) The number of cycles at which the knee of the curves occurs, is assumed to be constant. This simplifying assumption was also made by other researchers (see for example [50] and [63]). In the present simulation model this assumption will have very little effect on the predicted life distributions. The value of N_e is assumed to be defined by the intersection of the mean S-N sloping line, and a horizontal line representing the experimentally determined mean endurance limit, $\bar{S}_e$. In the present investigation experimental values are used to define the number of cycles at which the knee occurs, instead of arbitrarily assuming it to be 10^6 cycles, as is often done [50].

(iii) The mean S-N curve can be established experimentally by testing several specimens at different stress levels. A minimum of 25-30 specimens should be tested at each level in order to determine the mean fatigue life. A log-log plot of stress amplitudes and the corresponding mean life defines the mean S-N line. In the absence of such information an alternative approach can be used to define the mean S-N line. In this approach a straight line joining the experimentally determined $\bar{S}'_f$ plotted at one reversal and 0.9 $\bar{S}_u$ plotted at 2×10^3 reversal is assumed to represent the mean S-2N line. The intersection of this line and the horizontal line representing the mean endurance limit defines the number of reversals at which the knee occurs, $2N_e$, as illustrated in Figure 2.2. The assumption that the mean S-N curve for steel passes through a stress value of ninety percent of the engineering ultimate tensile stress, S_u, at 10^3 cycles is a valid generalization justified by experimental evidence given by Shigley [64], Osgood [17], the American Society for Testing of Materials [63] and others.

(iv) The distributions of the fatigue strength coefficient, S'_f, the ultimate stress, S_u, and the endurance limit, S_e, are determined experimentally as part of the material characterization discussed in Chapter 3. The fatigue strength coefficient is the true stress

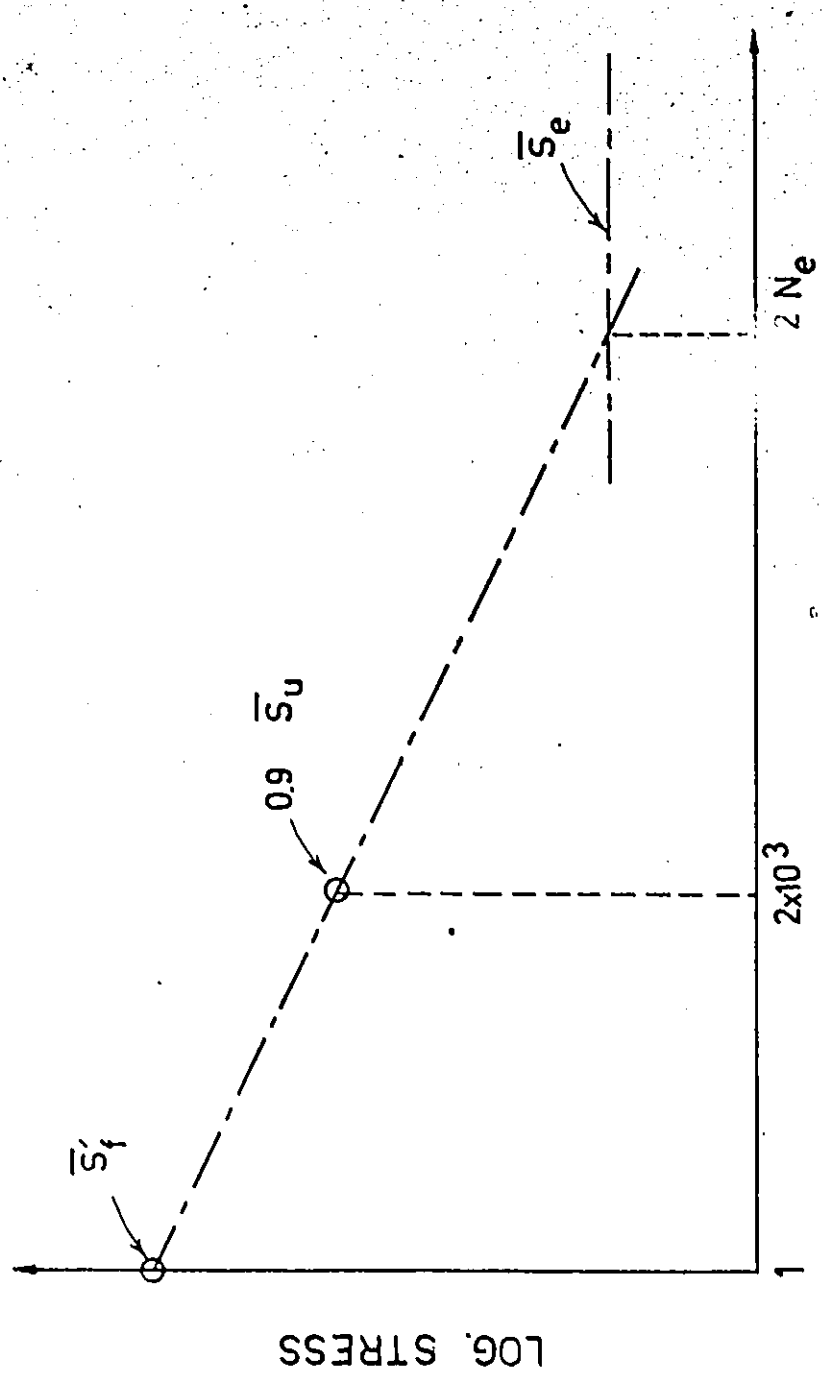

Figure 2.2 Determination of the Number of Cycles at the Knee (Endurance).

required to cause fracture on first reversal [60]. In this study it is assumed that the scatter of S_f' is equal to that of the ultimate tensile strength of the same material. It will be shown in Chapter 5 that the scatter of S_f' has little effect on the predicted fatigue life distributions.

2.3 Simulation of Fatigue Life

Examples of S-2N lines used in the simulation process are illustrated in Figure 2.3. Lines (1) and (2) represent the stress-reversals diagrams for two different hypothetical specimens. In analogy to Miner's rule, the cycle ratio of these two specimens can be calculated as follows:

$$C_1 = \frac{N_1}{N_m} > 1$$

and

$$C_2 = \frac{N_2}{N_m} < 1$$

where N_m is the fatigue life predicted for a specimen subjected to a load S, using the mean S-2N diagram. The load S can be sinusoidal, complex or random. In all these cases the nominal life, N_m, is calculated by applying the load to the mean S-2N line. The cycle ratio for any hypothetical specimen is the ratio of the predicted life of that particular specimen, N_i, to the calculated nominal life.

This, in essence, is equivalent to assuming that the cycle ratio in Miner's rule is not a fixed number, but rather, a random variable. The variability of the cycle ratio

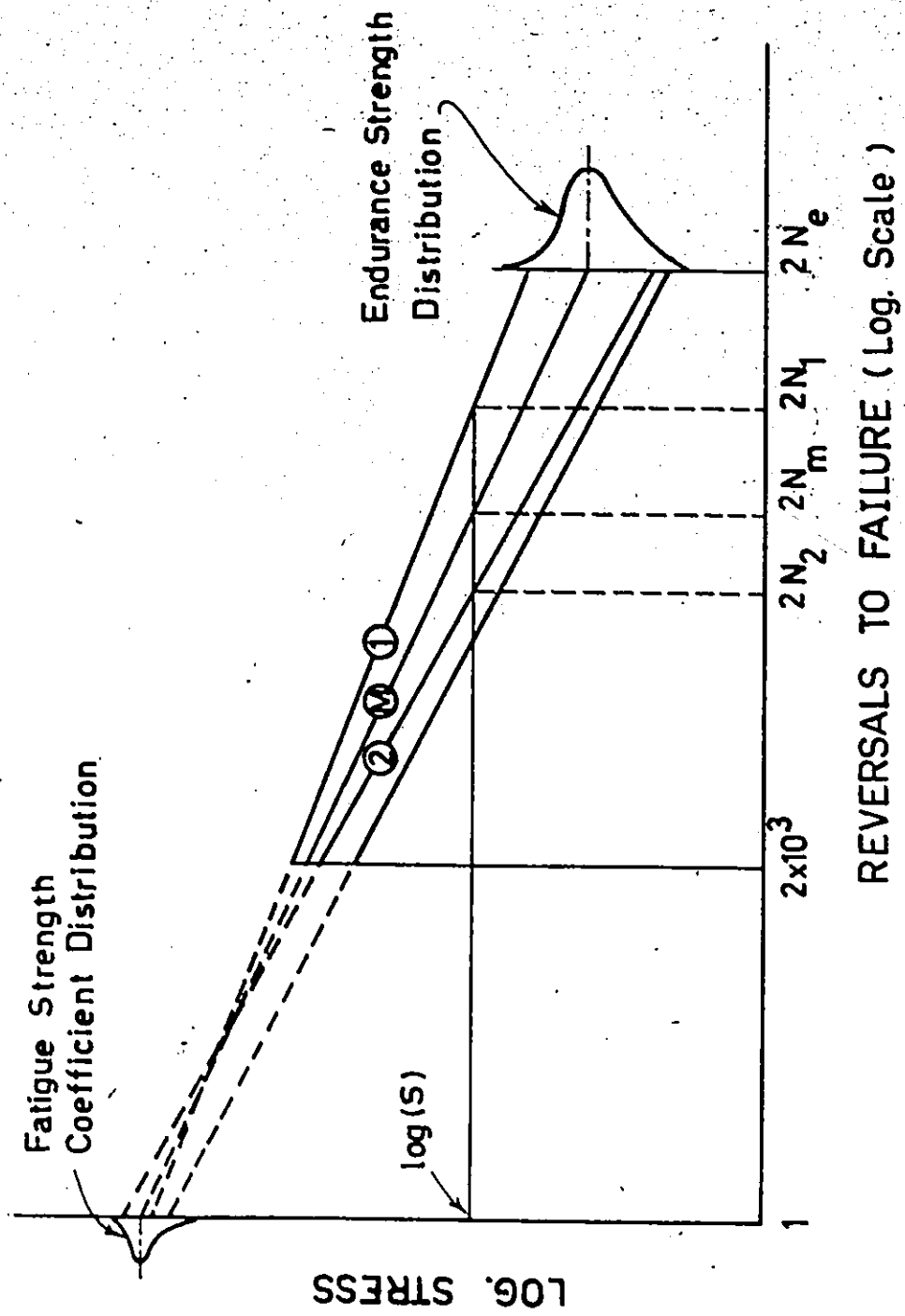

Figure 2.3 Monte Carlo Simulation of Probabilistic S-N Diagram.

in this model stems from the fact that both the endurance limit and fatigue strength coefficient are random variables, reflecting the variability of fatigue life. No assumption is made regarding any characteristic of the cycle ratio distribution. This distribution is defined, using the suggested model, by calculating the value of C for a large number of hypothetical specimens. It is evident that the suggested simulation method succeeds, where Miner's rule fails, to account for the variability of the cycle ratio without introducing any assumption regarding its distribution.

For constant amplitude loading, the life of each specimen is obtained directly from its curve, thus forming a theoretical sample of lives which defines the probability density function of fatigue life. If the loading is random or in block form, a linear damage law is used for each individual theoretical specimen to define fatigue life. For random loading each hypothetical specimen is subjected to a large number of load amplitudes samples from the load probability distribution. The specimen is assumed to have failed when $\Sigma\ n/N = 1$ for that particular specimen. This process is repeated for each generated hypothetical specimen.

The damage below the mean endurance limit is assumed to accumulate at the same rate as above it. No damage, however, is accumulated below the lower bound of the endurance limit ($\bar{S}_e - 4\ \hat{\sigma}_e$). While there is no theoretical or physical basis for this approach to damage accumulation below $\bar{S}_e$, it seems appropriate due to the probabilistic nature of the fatigue endurance limit. It should be noted that Miner's rule

assumes no damage accumulation below the endurance limit.

Although the method described above relates constant amplitude life to spectrum or random life by assuming $\Sigma\ n/N = 1$ for each hypothetical specimen, the crux of the method does not assign any value to the mean cycle ratio. Rather it is a means of estimating the distribution of the cycle ratio ($\Sigma\ n/N$). The suggested simulation of the fatigue properties of each individual specimen using Monte Carlo technique is general enough to be used with any failure criterion. Linear as well as non-linear damage criteria can be used together with the proposed simulation method to predict fatigue failures. The new method can be used with different types of load histories including random and spectrum loading, utilizing any suitable cycle counting technique. The method is easily programmed for digital computers.

2.4 Comparison of Predictions Using Suggested Model and Previously Published Experimental Results

At this point it is useful to investigate the capability of the suggested model to reproduce the distributions of fatigue life reported in [48]. In this reference the material properties, needed for the present method, were given in distributional form. The experimental results shown in Table 2.1 for 0.0625 in. diameter SAE 4340 smooth steel wire in rotating bending will be used in this study. Sufficient experimental data, at four stress levels was available to define the mean S-N curve, S_f' and N_e. It was found

TABLE 2.1 WIRE FATIGUE MACHINE RESULTS FOR 1.5878 mm (.0625 in.) DIAMETER SAE 4340 STEEL WIRE IN ROTATING BENDING [48]

Maximum Alternating Stress Level (K Pa)	Cycles to Failure			
	Normal Distribution		Log normal* Distribution	
	Mean	Standard Deviation	Mean	Standard Deviation
468,843 (68,000 Psi)	356,900	193,400	5.4979	0.2185
557,096 (80,000 Psi)	84,900	34,000	4.8953	0.1746
613,633 (89,000 Psi)	43,900	13,100	4.6233	0.1303
696,370 (101,000 Psi)	21,100	3,700	4.3177	0.0768
Endurance Strength Distribution (Normal) Parameters Estimated at 2×10^6 Cycles				
Mean 420,580 K Pa (61,000 Psi)		Standard Deviation 27,579 K Pa (4,000 Psi)		

* $\log_{10}$ of cycles to failure

that

$$N_e = 7.278 \times 10^5 \text{ cycles}$$

and $$S_f' = 393.4113 \times 10^3 \text{ psi}$$

The distributions of fatigue life have been determined using the proposed simulation. The number of cycles to failure corresponding to the applied stress amplitude has been predicted for 9,000 hypothetical specimens. The mean and standard deviation values were calculated for both the fatigue life and its logarithm. This procedure was repeated at the four stress levels for the sake of comparison with the experimental results. The data obtained at these stress levels is given in Tables 2.2 and 2.3 and Figure 2.4. Plots of the predicted life distributions and the corresponding experimental data are shown in Figures 2.5 to 2.9. Fatigue life and its common logarithm are plotted against cumulative frequency on normal probability paper for both the predicted and the experimental results. The distributions cover a relative frequency range from approximately 0.1% to 99.98%. It is evident that the model always predicts life distributions which are continuous, unimodal and slightly skewed to the right. It is also clearly observed that the predicted distributions, represented by dotted lines, compare favourably with those experimentally found shown by solid lines.

Though phenomenological and restricted to certain metals and alloys exhibiting an endurance limit, the suggested model is a useful tool for design analysts and

TABLE 2.2 COMPARISON BETWEEN EXPERIMENT AND PREDICTION OF FATIGUE LIFE FOR SAE 4340 STEEL

Maximum Alternating Stress Level (psi)	Cycles-to-Failure				% Error	
	Experiment *		Prediction			
	Mean	Standard Deviation	Mean	Standard Deviation	Mean	Standard Deviation
68,000	356,900	193,400	353,800	169,570	-.868	-12.32
80,800	84,900	34,000	93,318	40,016	9.910	17.69
89,000	43,900	13,100	44,255	17,748	.809	35.48
101,000	21,100	3,700	17,687	5,093	-16.175	37.65

* Taken from reference [48]

TABLE 2.3 COMPARISON BETWEEN EXPERIMENT AND PREDICTION OF LOGARITHM THE FATIGUE LIFE OF SAE 4340 STEEL

Maximum Alternating Stress Level (psi)	Logarithm the Cycles-to-Failure				% Error	
	Experiment *		Prediction			
	Mean	Standard Deviation	Mean	Standard Deviation	Mean	Standard Deviation
68,000	5.4979	0.2185	5.503	0.1997	0.091	-8.595
80,800	4.8953	0.1746	4.9327	0.1801	0.764	3.161
89,000	4.6233	0.1303	4.6131	0.1691	-0.221	29.800
101,000	4.3177	0.0768	4.2849	0.1025	-0.759	33.464

* Taken from reference [48]

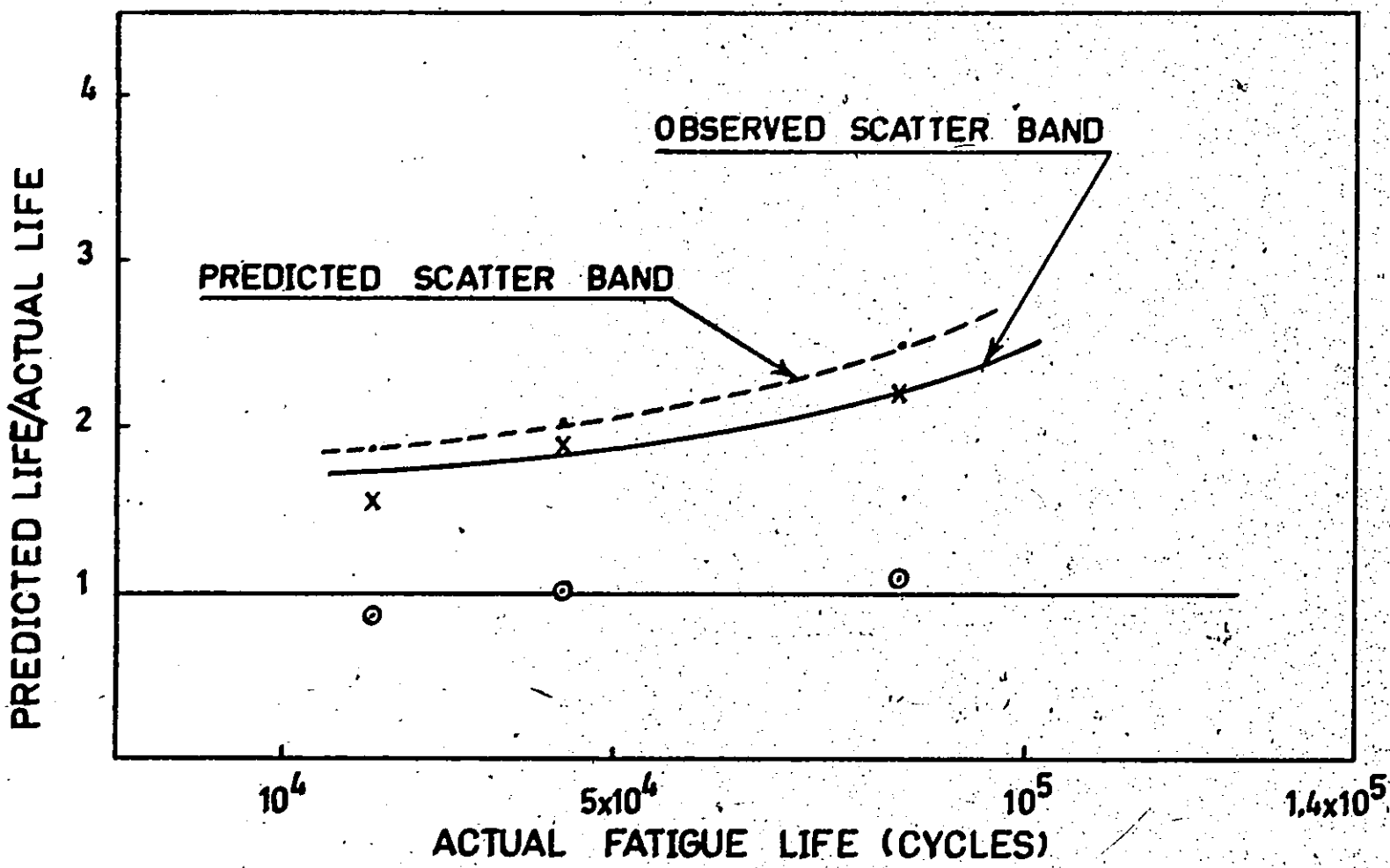

Figure 2.4 Comparison Between Observed and Predicted Mean Life and Scatter Band (Life ± 3σ) for SAE 4340 Steel.

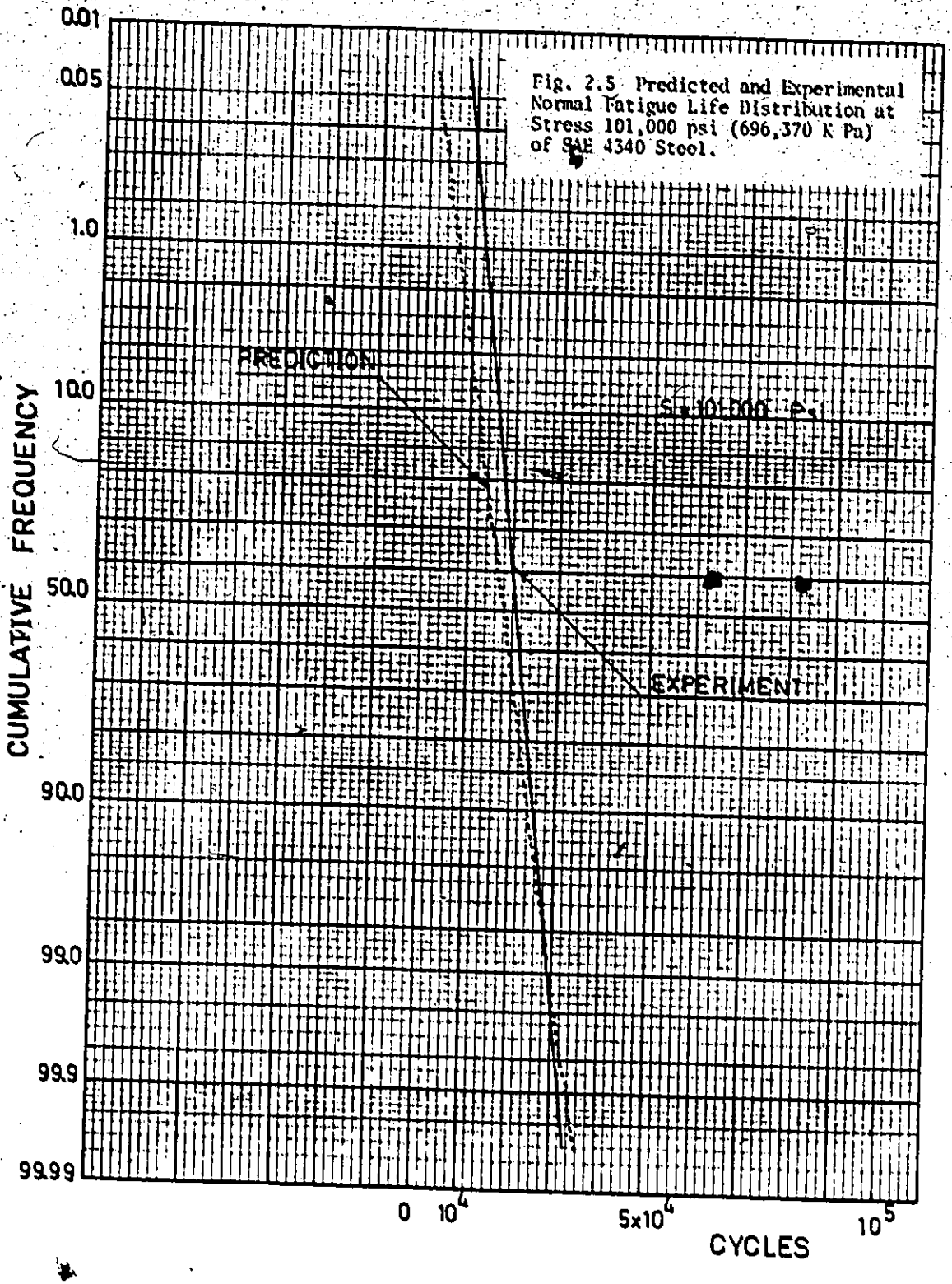

Fig. 2.5 Predicted and Experimental Normal Fatigue Life Distribution at Stress 101,000 psi (696,370 K Pa) of SAE 4340 Steel.

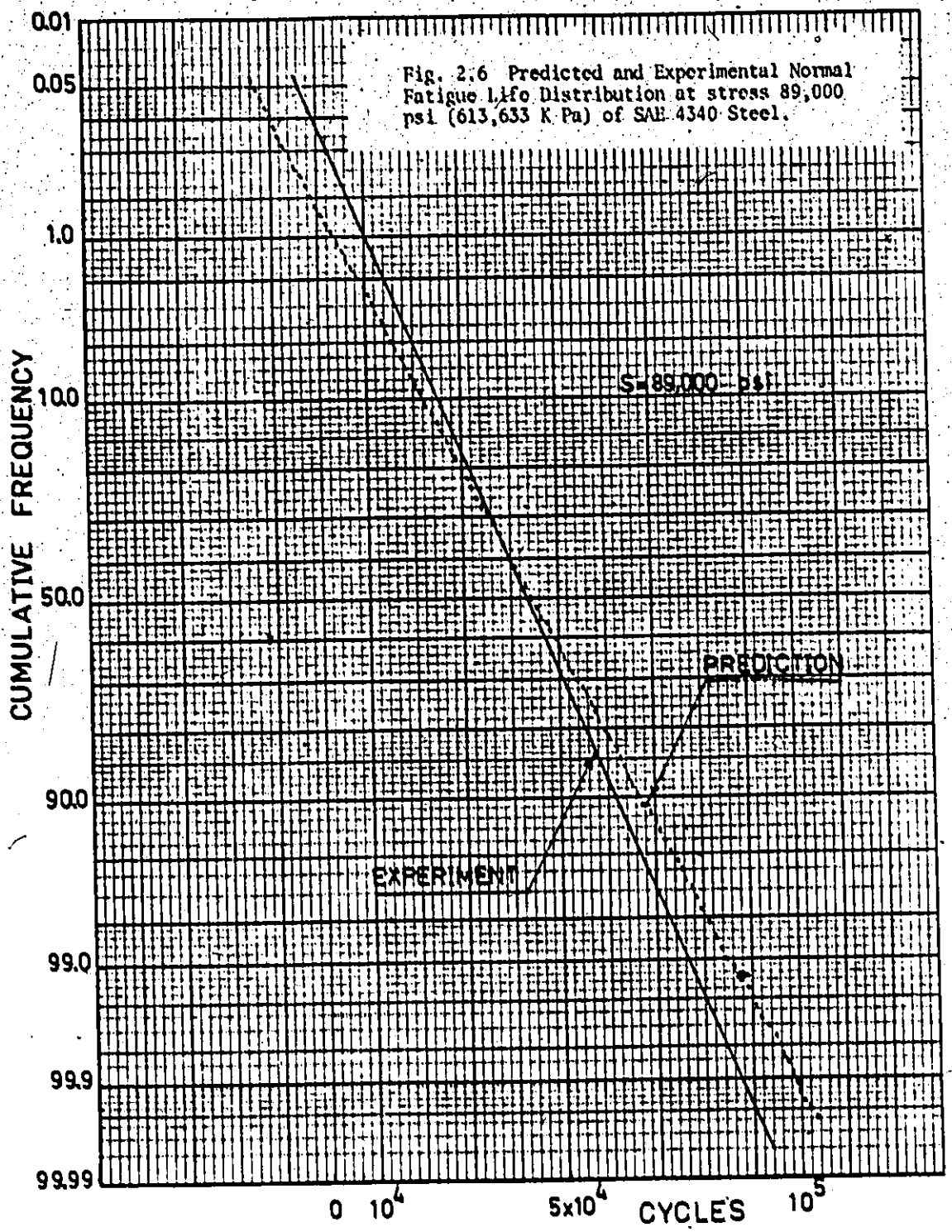

Fig. 2.6 Predicted and Experimental Normal Fatigue Life Distribution at stress 89,000 psi (613,633 K Pa) of SAE 4340 Steel.

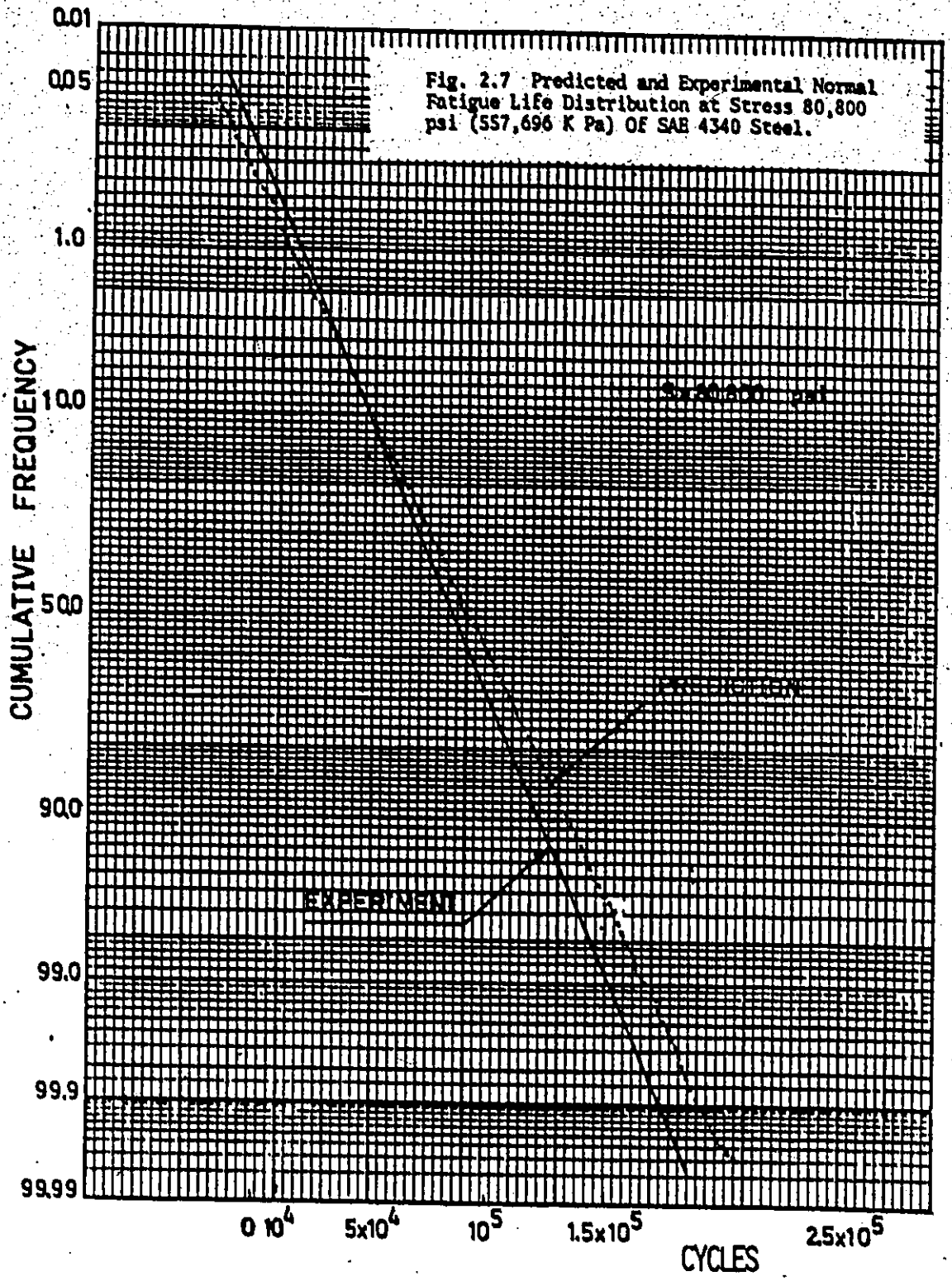

Fig. 2.7 Predicted and Experimental Normal Fatigue Life Distribution at Stress 80,800 psi (557,696 K Pa) Of SAE 4340 Steel.

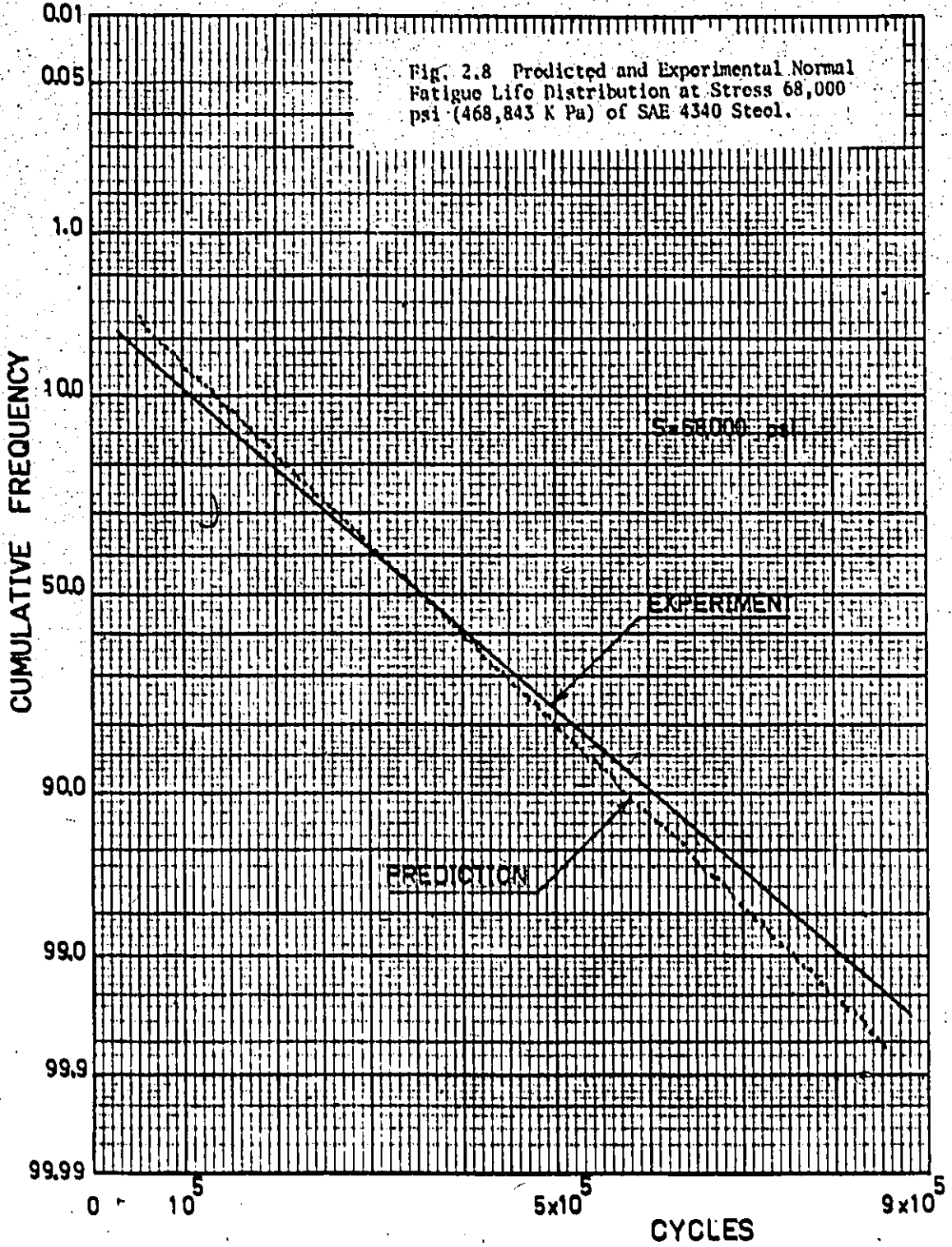

Fig. 2.8 Predicted and Experimental Normal Fatigue Life Distribution at Stress 68,000 psi (468,843 K Pa) of SAE 4340 Steel.

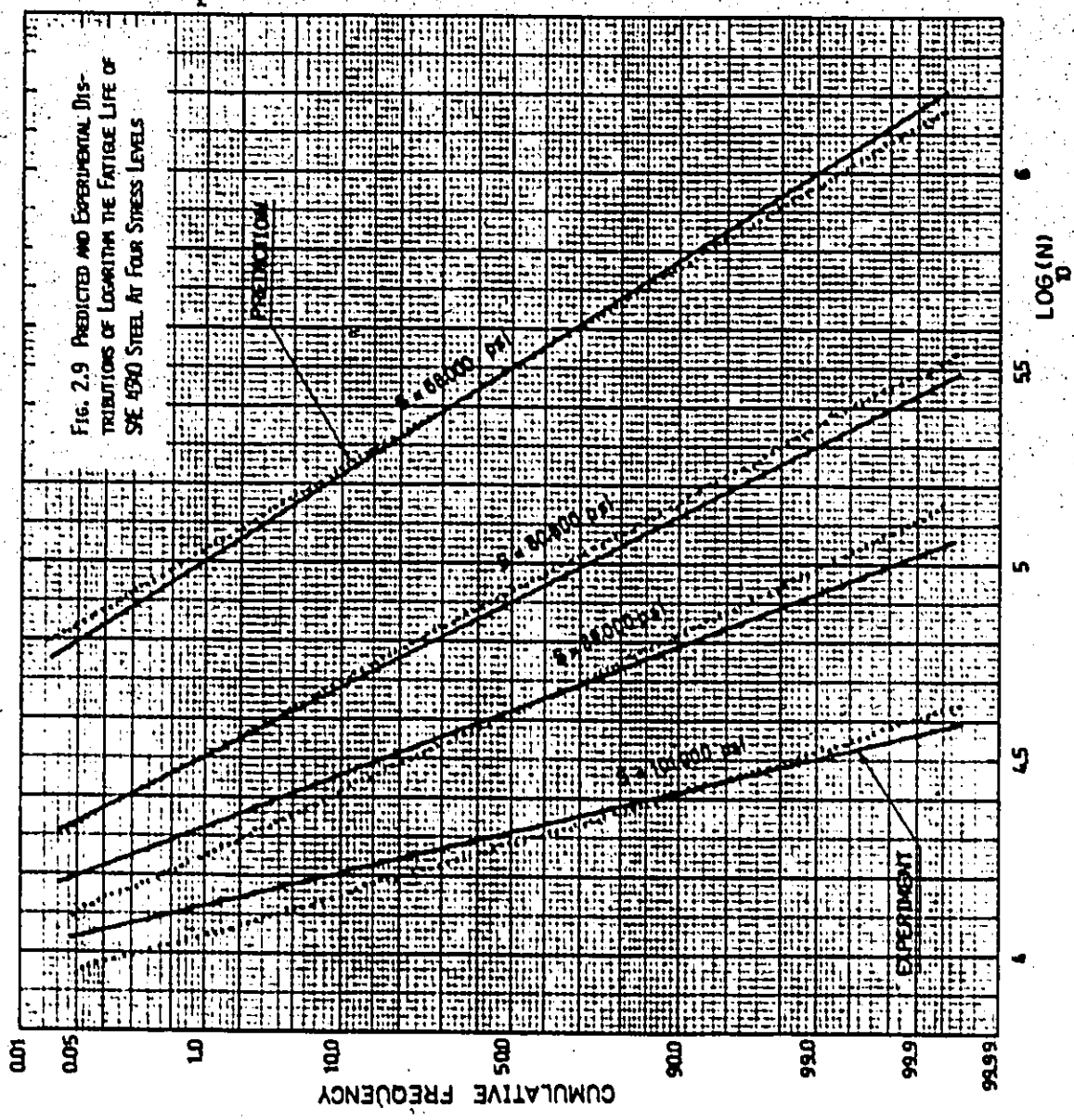

Fig. 2.9 Predicted and Experimental Distributions of Logarithm the Fatigue Life of SAE 4340 Steel At Four Stress Levels

provides a basis for generalization. The encouraging results presented in this chapter suggest that it was worthwile carrying out an experimental program aimed at evaluating the applicability of the new model to the different loading conditions. These experiments and their results compared to the predictions using the proposed model are the subject of the following chapters.

CHAPTER 3

EXPERIMENTAL MATERIAL CHARACTERIZATION

The experimental part of this study is concerned mainly with the verification of the validity of the suggested simulation technique for predicting the distribution of fatigue life under different load histories. Much experimental work has been done, to determine the properties of different materials assuming that they are deterministic. Little effort has been devoted to establishing the distribution of such properties. The validity of utilizing published material properties is questionable because materials, though nominally the same, may differ in some aspects. Properties provided by the manufacturers can be used when carefully collected to reflect the variations of properties. This experimental program was designed so as to be complete in itself. It encompasses not only determination of the fatigue life distributions, but also determination of the distributional design data of the material properties used in the analysis.

3.1 Choice of Material and Sampling Scheme

3.1.1 Selection of Material

There are usually many factors governing the choice of the materials used in tests. These factors include the availability, machinability characteristics of the material,

its fields of application and how well the intended test program represent the loading conditions in these applications.

A general purpose grade hot-rolled SAE 1008 sheet steel was selected. This grade of steel is used in: automobile structural parts, highway trailer, aircraft and railcar structural components and airframe sections. Since many of the structural parts of an automobile body and chassis are made of this grade of steel, it was felt that tests on this material would be most useful. The typical chemical analysis of this material is given in Table 3.1.

TABLE 3.1

Chemical Analysis of SAE 1008 Steel

Alloying Element	Percent
Carbon	.06-.07
Manganese	.35
Phosphorous	.025
Sulphur	.02

3.1.2 Sampling Scheme

Adequate sampling procedures are important when designing an experiment. A sample which reflects all possible variations in the population under consideration is always sought. The results of previous investigations on different steel grades [65, 66] indicate a statistically insignificant variation between the ingots within a given heat, and a

statistically significant variation within an ingot between the high and low rim areas. Five to ten percent variation in static ultimate strength, yield strength, area reduction, elongation and in the endurance limit, within a given ingot, was reported.

The material used in this investigation was supplied by STELCO* in the form of 12 x 12 x .085 in. sheet samples. Twelve of these samples were collected so as to represent the variation of properties within the ingots, i.e., cross-coil variations, as shown in Figure 3.1. Specimens needed for the different tests were cut out of these sheets in such a way that the specimens for each test were taken from all possible locations as shown in Figure 3.2. After machining and surface preparation, the specimens were kept in a dessicator and assigned to the different test programs (i.e. endurance limit, constant amplitude, block and random loading) at random.

3.1.3 Tests and Specimens Required

The following properties will be determined experimentally:

(i) Distribution of the fatigue endurance limit.

(ii) Distribution of the ultimate tensile strength.

(iii) Distribution of the fatigue strength coefficient.

(iv) Cyclic stress-strain behaviour of SAE 1008 steel.

---

* The Steel Company of Canada Limited, Hamilton, Ontario.

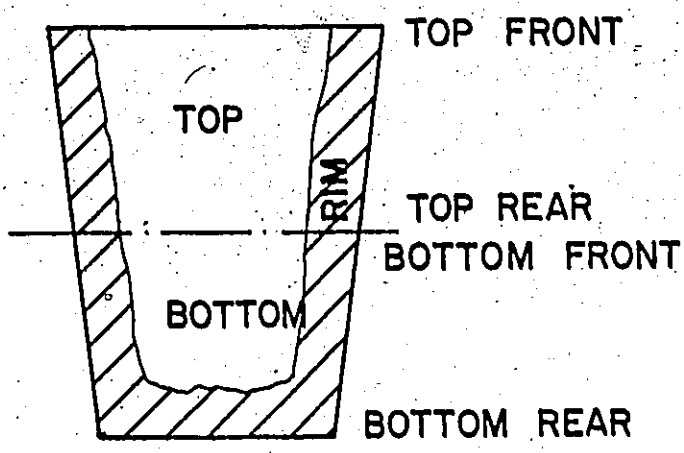

Vertical Section Through Ingot

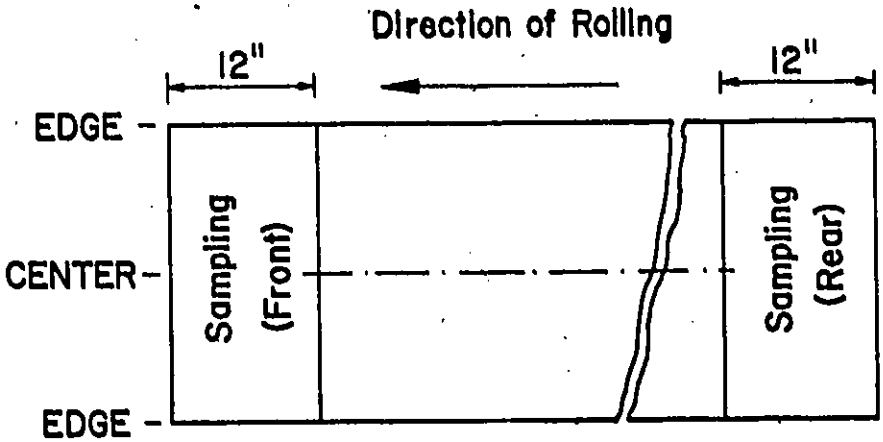

Steel Strip Rolled From Half of Ingot

Figure 3.1 Spatial Orientation of Sample Coil.

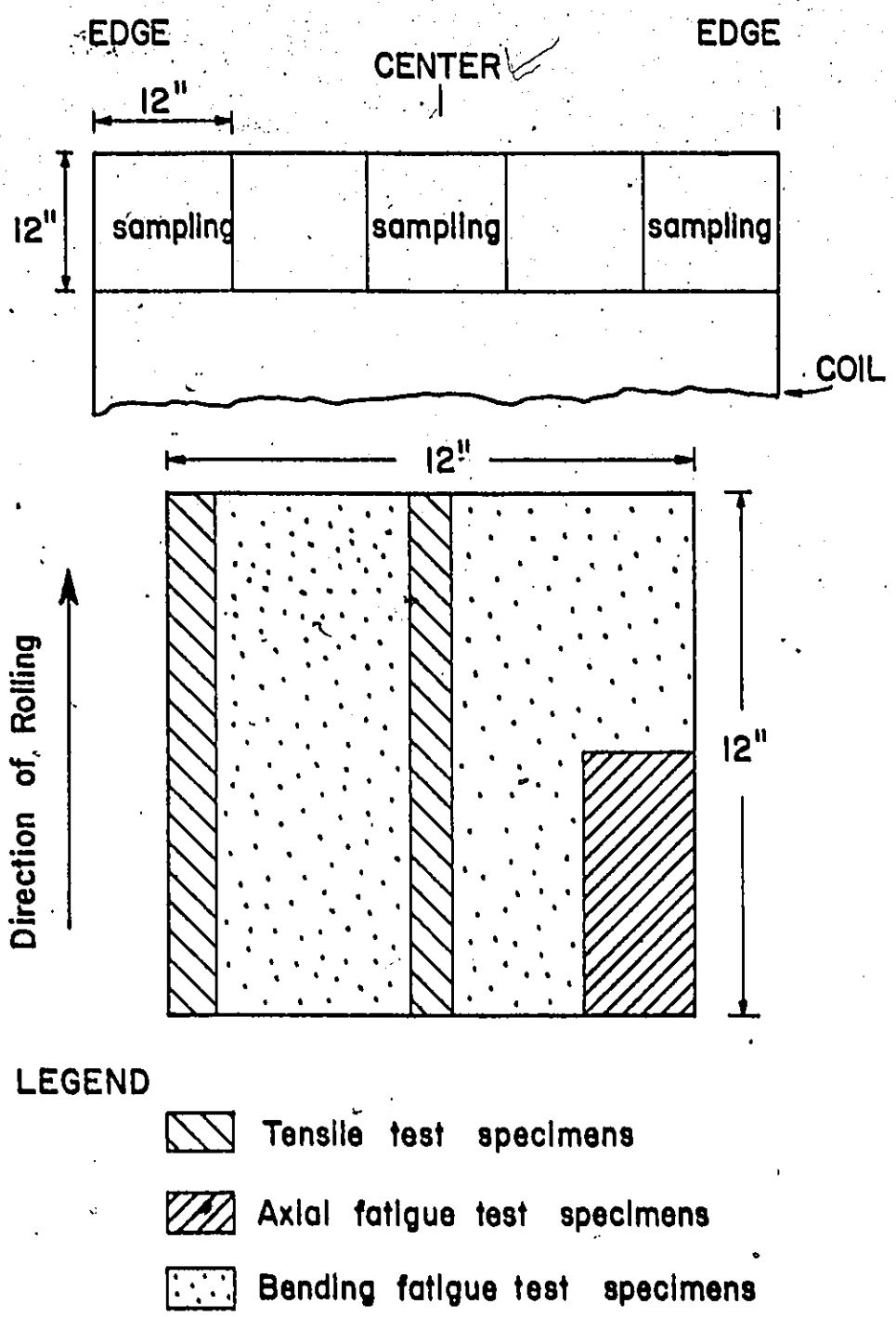

Figure 3.2 Position of Specimens and Legend Used.

The data we need to collect to obtain values for these properties are:

(i) Monotonic properties.

(ii) Cyclic stress-strain curve and hysteresis loops.

(iii) Strain-life plots.

The fatigue life distributions for the loading conditions of interest in this study for comparison with the analytical predictions are also obtained.

Three types of specimens are used, each being designed for a different purpose, namely the tension test specimen, axial, and bending fatigue test specimens. All specimens are tested in the "as rolled" condition for the unmachined surfaces. No attempt was made to provide a uniform surface finish on the specimens since the "as rolled" surface was most typical of actual conditions and moreover, no surface observations were to be made. In the final machining, progressively lighter passes were used to minimize the residual stresses induced. The machined surfaces were hand-polished using emery paper. All specimens were oriented so that the longitudinal axis was always parallel to the longitudinal direction of the grain (i.e., the direction of rolling). Each type of specimen was "sized" and "shaped" to the load capacity of the testing equipment used.

3.2 Tensile Tests

3.2.1 Experimental Test Set-up

Since the material properties and their distributions

are important; uniaxial tensile tests were performed on fifty two tension specimens made from SAE 1008 steel and sampled as described above. The tensile specimen shown in Figure 3.3, was designed to be tested on an "Instron" testing machine. Each specimen was subjected to a continually increasing uniaxial tensile force while simultaneous observations were made of the elongation of the specimen. Figure 3.4 shows the tensile specimen before and after testing. A clip gauge extensometer, which uses strain gauges as sensing elements was used to measure the longitudinal strain. After the specimen was clamped in the vice grips, it was pulled at a rate of 0.5 inches per minute. The output from the extensometer and the load cell were both recorded on an Instron chart recorder. A typical load-displacement plot is shown in Figure 3.5. The engineering as well as the true stress-strain properties were determined from the tension tests. Measuring true stress-strain behaviour actually reduce to simultaneous determinations of the load and area of the tensile specimen.

3.2.2 Results of Tensile Tests

The tensile properties of interest are the yield stress (S_y), the engineering and true ultimate tensile strength (S_u, S_{tu}), engineering and true fracture stress (S_f, S_{ft}) and the uniform strain (e_u). These properties are defined as follows:

$$S_y = \frac{\text{Yield load}}{A_o} \qquad (3.1)$$

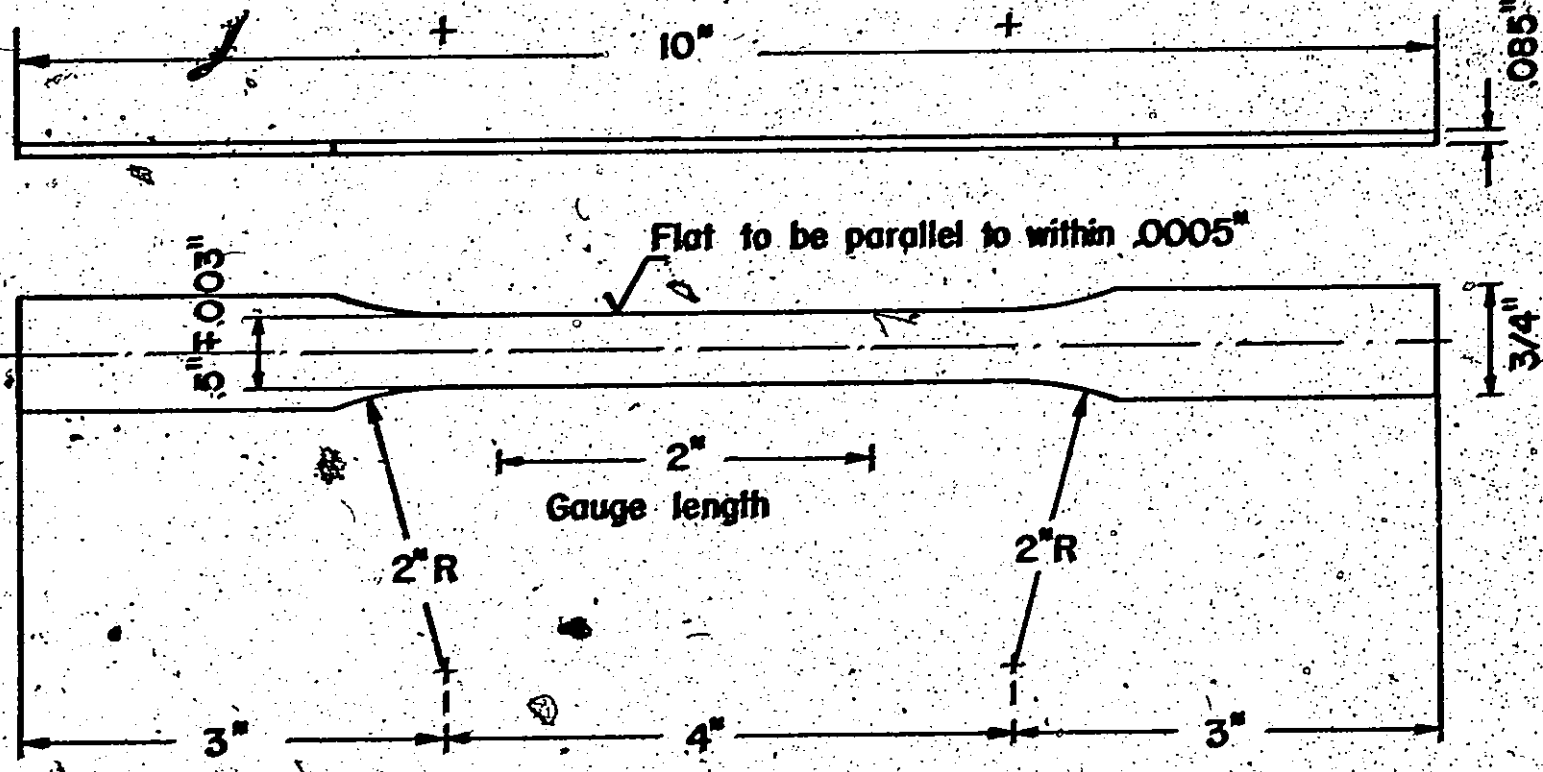

Notes: Symmetric about centerline Material: SAE-1008 Steel sheets

Scale= 3:4

Figure 3.3 Configuration and Dimensions of the Tensile Test Specimen.

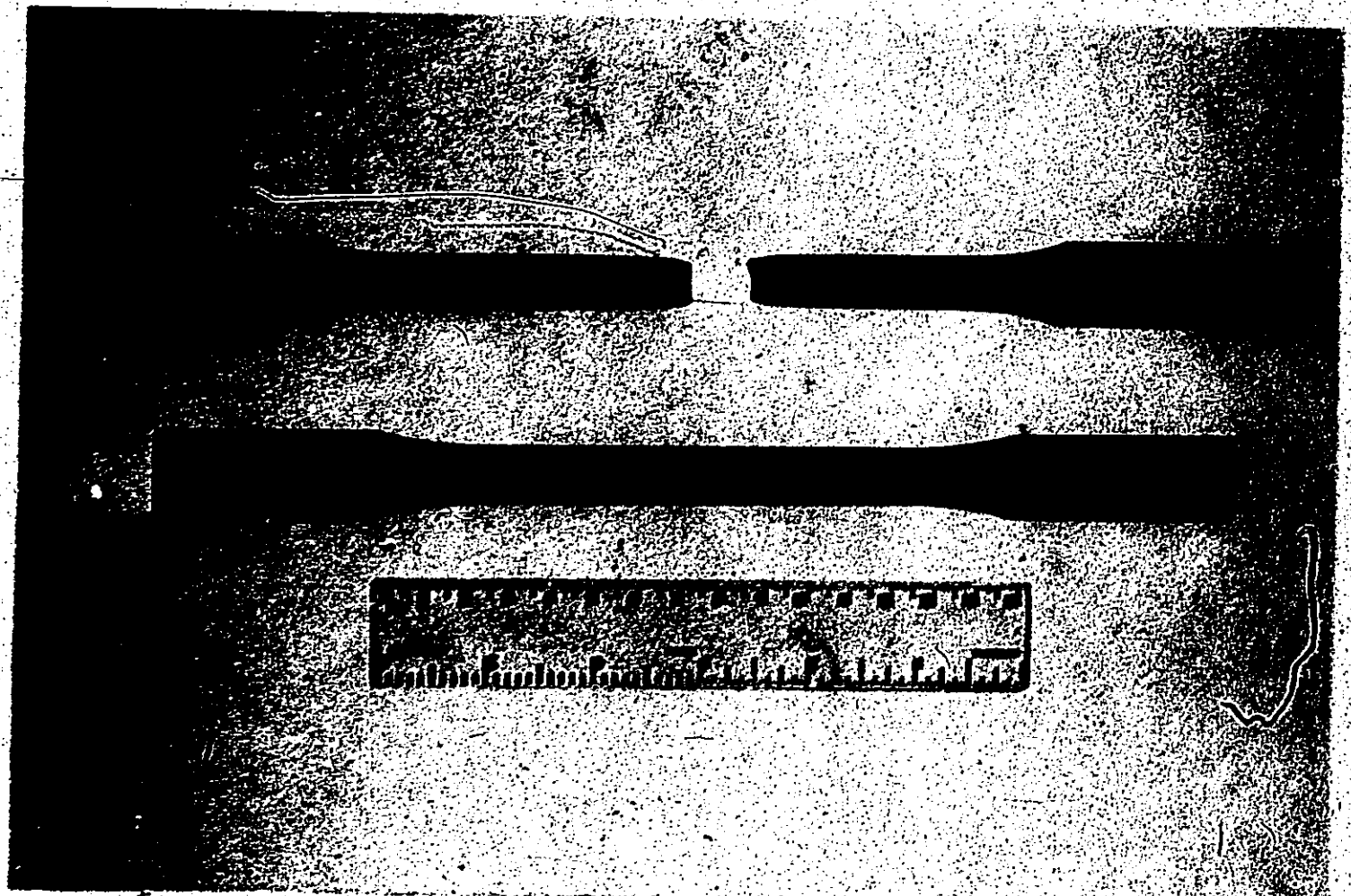

Figure 3.4 Photograph Showing Tensile Test Specimens, Before and After Fracture.

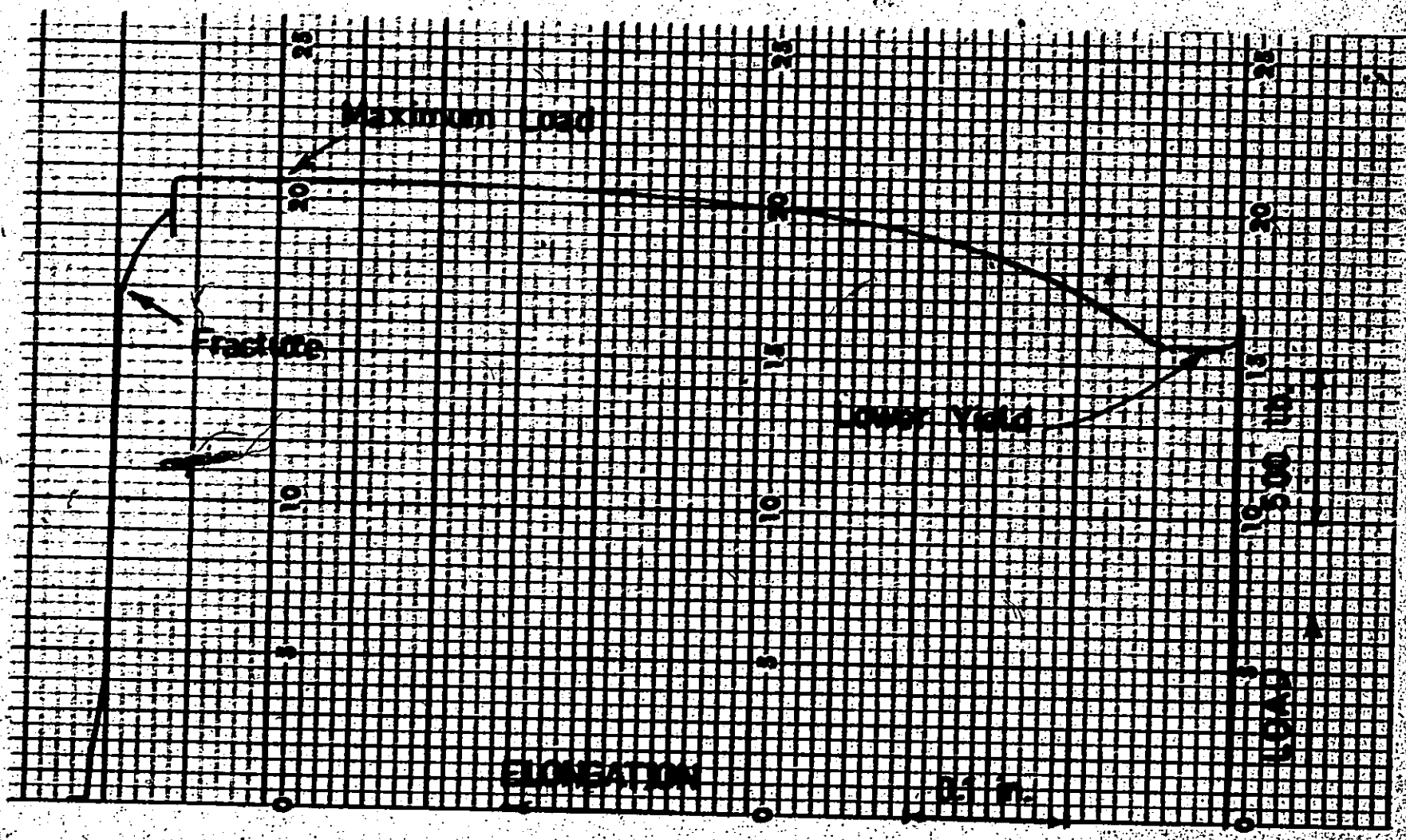

Figure 3.5 Typical Load-Extension Diagram for SAE 1008 Sheet Steel.

$$S_u = \frac{\text{Maximum load}}{A_o} \tag{3.2}$$

$$S_f = \frac{\text{Fracture load}}{A_o} \tag{3.3}$$

$$S_{ft} = \frac{\text{Fracture load}}{A_f} \tag{3.4}$$

where A_o is the initial cross-sectional area.

A_f is the cross-sectional area at fracture.

Measurement of the final fracture area for SAE 1008 specimens was complicated by the irregularity caused by the extensive amount of necking which takes place after the maximum load is reached. The approximate calculation of the cross-sectional area at fracture, induces some uncertainty in the computed values of the true fracture stress.

The uniform strain is defined as the strain up to the maximum load

$$e_u = \frac{\Delta \ell_m}{\ell_o} \tag{3.5}$$

where ℓ_o is the initial gauge length

$\Delta \ell_m$ is the change of the gauge length at the maximum load.

If we let

ℓ_m be the gauge length at maximum load,

A_m be the cross-sectional area at maximum load,

then by the constancy-of-volume relationship,

$$A_o \ell_o = A_m \ell_m$$

and

$$A_o = A_m \left(\frac{\ell_o + \Delta\ell_m}{\ell_o}\right)$$

$$= A_m (1 + e_u) \qquad (3.6)$$

The true ultimate stress is defined as:

$$S_{ut} = \frac{\text{Maximum load}}{A_m} = \frac{\text{Maximum load}}{A_o} (1 + e_u)$$

$$= S_u (1 + e_u) \qquad (3.7)$$

The results of the fifty two tests were compiled and analysed. Mean values and the distribution of parameters of interest were determined. These results are presented in Table 3.2 and Figure 3.6. Young's modulus of SAE 1008 steel was experimentally determined and provided by STELCO. E = Young's Modulus = 32×10^6 psi.

3.2.3 Comments on the Test Results

Study of results of the monotonic tests leads to the following remarks:

(i) The monotonic tests were useful in establishing the material properties of interest in distributional form.

(ii) It was found that some of the properties such as the ultimate and true fracture stress are normally distributed, as suggested in the literature, while other properties are not.

(iii) The coefficient of variation of the true fracture stress is relatively high, which reflects the effect of

TABLE 3.2 SAE 1008 STEEL STATIC MATERIAL PROPERTIES

PROPERTY	MEAN VALUE	STANDARD DEVIATION	COEFFICIENT OF VARIATION
Engineering Lower Yield Stress [psi]	37691.47	1608.97	.0427
Engineering Ultimate Stress [psi]	49119.05	866.22	.0176
Uniform Strain [in./in.]	0.18293	0.01756	.096
True Ultimate Stress [psi]	58105.13	1364.06	.0235
True Fracture Stress [psi]	105743.39	93763.39	.8867

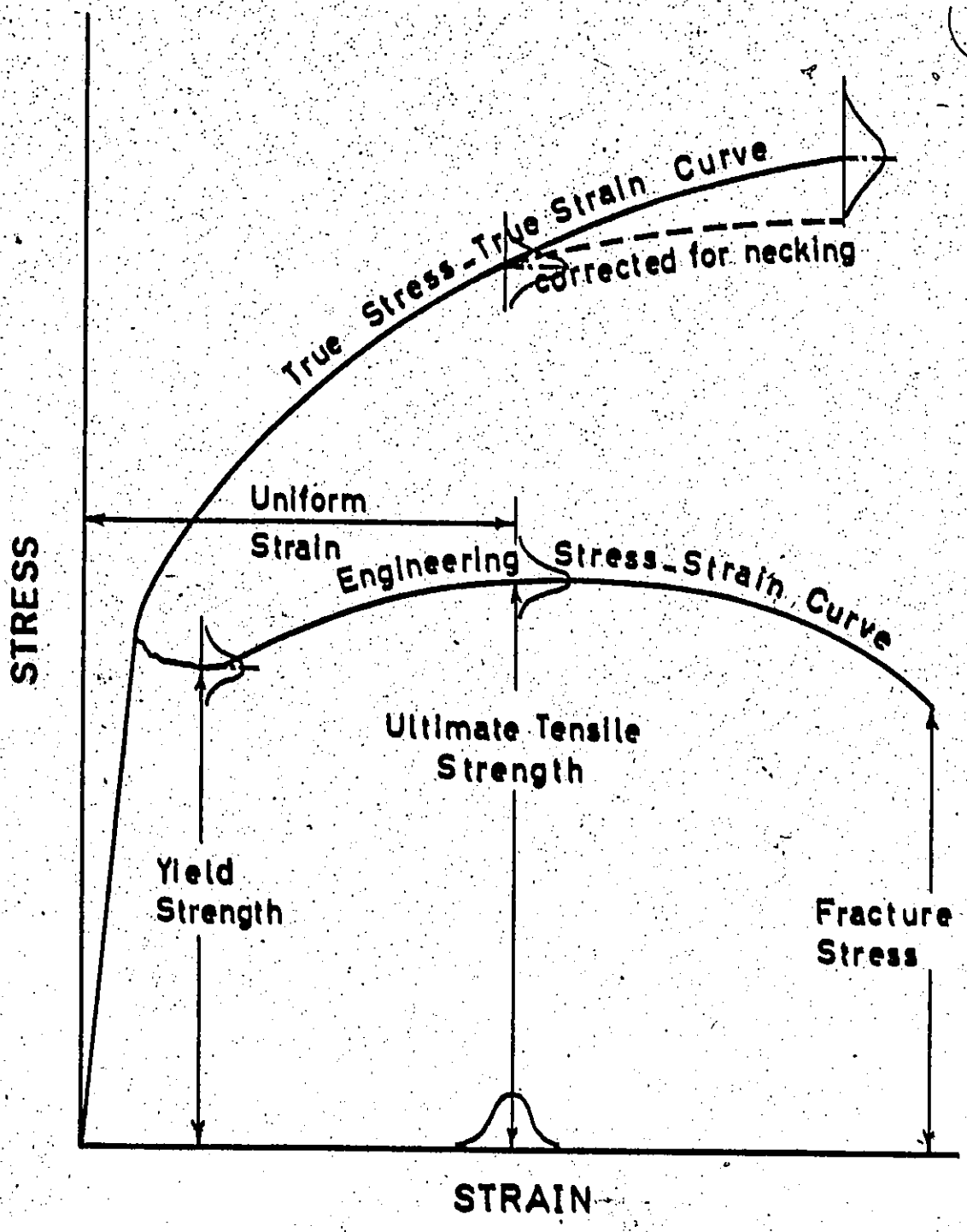

Figure 3.6 Comparison of Engineering and True Stress-Strain Curves for SAE 1008 Sheet Steel.

the necking phenomenon and the irregularity of the final area on the measurements.

3.3 Axial Fatigue Tests

Material stress-strain characteristics, based on monotonic tests, are not applicable to cyclic loading conditions because stress-strain response varies with cyclic history. The purpose of this part of the experimental program is to:

(i) Define the cyclic stress-strain behaviour of SAE 1008 steel sheets using the incremental-step test.

(ii) Determine a mean value of the fatigue strength coefficient, S'_f, from plots of the elastic strain component versus fatigue life.

(iii) Establish the stress-life diagram of the material under axial push-pull loading conditions.

(iv) Study the axial fatigue characteristics of SAE 1008. The analysis based on axial deformation and fatigue data provides a close approximation of flexural fatigue behaviour when applied to the state of stress and strain at the extreme fiber of a flexural section [68-70].

3.3.1 Experimental Test Set-up

The shape and dimensions of the axial fatigue specimen is shown in Figure 3.7. Figure 3.8 shows a photograph of the specimen before testing and after failure. It was necessary for the gauge section of this specimen to be

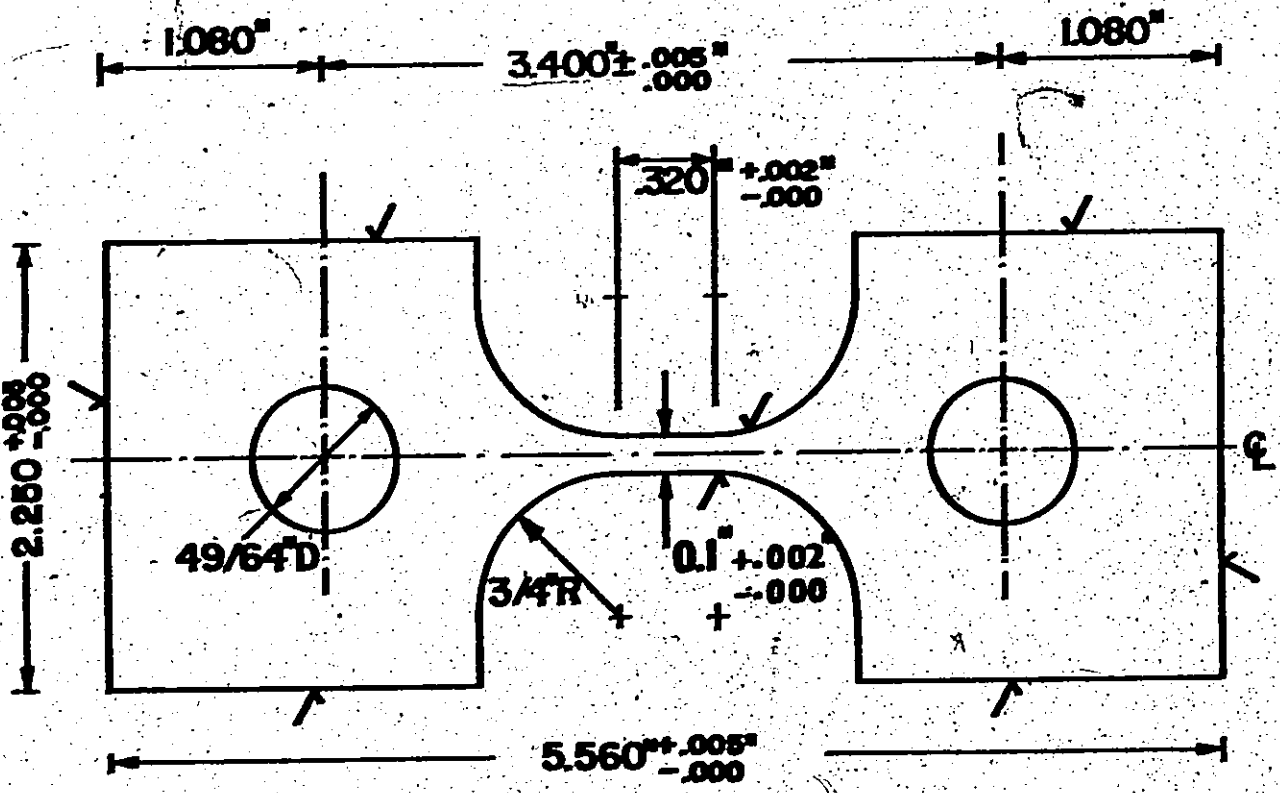

Figure 3.7 Configuration and Dimensions of the Axial Fatigue Specimen.

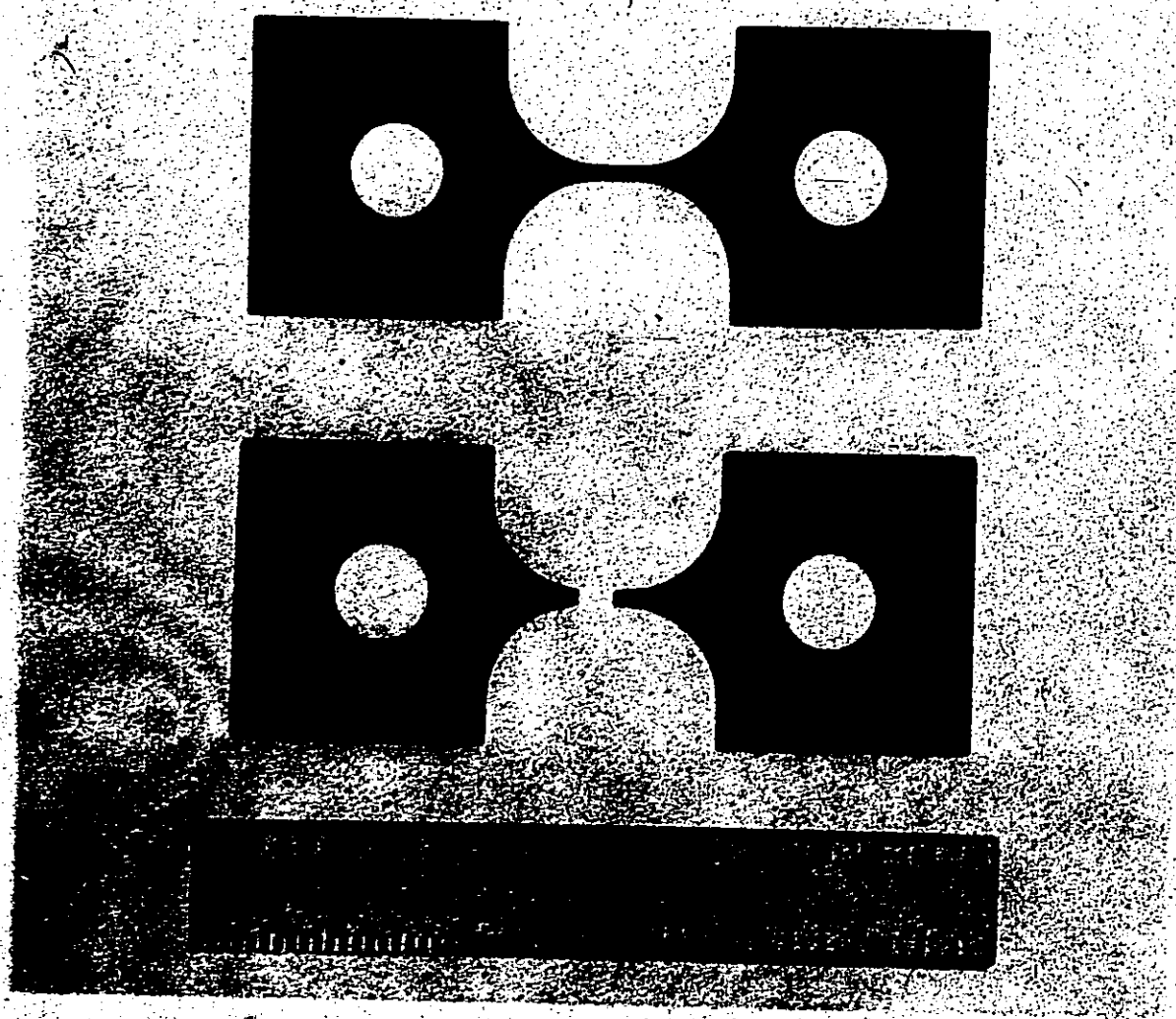

Figure 3.8 Photograph Showing Axial Fatigue Specimens Before and After Fracture.

straight because the longitudinal strain was measured using an Instron clip gauge which was also used to control the strain. Twelve of these specimens were tested using a "closed loop" servo-hydraulic axial fatigue testing machine, set up for positive control of the load into the specimen. The load and strain were continuously recorded on strip chart recorder and hysteresis loops were plotted on an X-Y recorder at suitable intervals.

The specimen was considered to have failed when complete fracture occurs. In order to prevent hammer damage to the fracture surfaces and obtain the proper number of cycles to failure, provisions were made for first stopping the specimen prior to its complete separation. The shut off device which was used is a load peak counter which requires that a predetermined load be reached on each successive cycle for the test to continue. This load is usually set at about 50 percent of the steady state stress response of the specimen. This allows the operator to run the final few cycles while carefully observing the specimen. The indication of a crack can also be noted by the development of an inflection point in the compressive half of the hysteresis loop.

3.3.2 Fatigue Strength Properties

Low-cycle fatigue properties are known to be associated with the components of elastic and plastic strain. Eight specimens were cycled to failure to establish the strain-reversals to failure and stress-reversals to failure data. The sinusoidal total strain amplitude was between 0.08 and

0.5 percent and the plastic strain amplitude ranged between 0.016 and 0.382 percent. The results of these tests are shown in Figures 3.9 and 3.10. Figure 3.9 is representative of the strain-reversals to failure data for many engineering metals; a log-log linear least squares fit approximates the data reasonably well. The following equations describe the two straight lines shown in Figure 3.9.

For elastic strain,

$$\frac{\Delta\varepsilon_e}{2} = \frac{S_f'}{E} (2N_f)^b \qquad (3.8)$$

or in terms of stress,

$$\frac{\Delta S}{2} = S_f' (2N_f)^b \qquad (3.9)$$

For plastic strain,

$$\frac{\Delta\varepsilon_p}{2} = \varepsilon_f' (2N_f)^c \qquad (3.10)$$

where

S_f' is the fatigue strength coefficient

ε_f' is the fatigue ductility coefficient

b is the fatigue strength exponent

c is the fatigue ductility exponent

and $2N_f$ is the number of reversals to failure

At long lives the elastic line is dominant and at short lives the plastic line dominates. The transition fatigue life, $2N_t$, is the number of reversals for which the

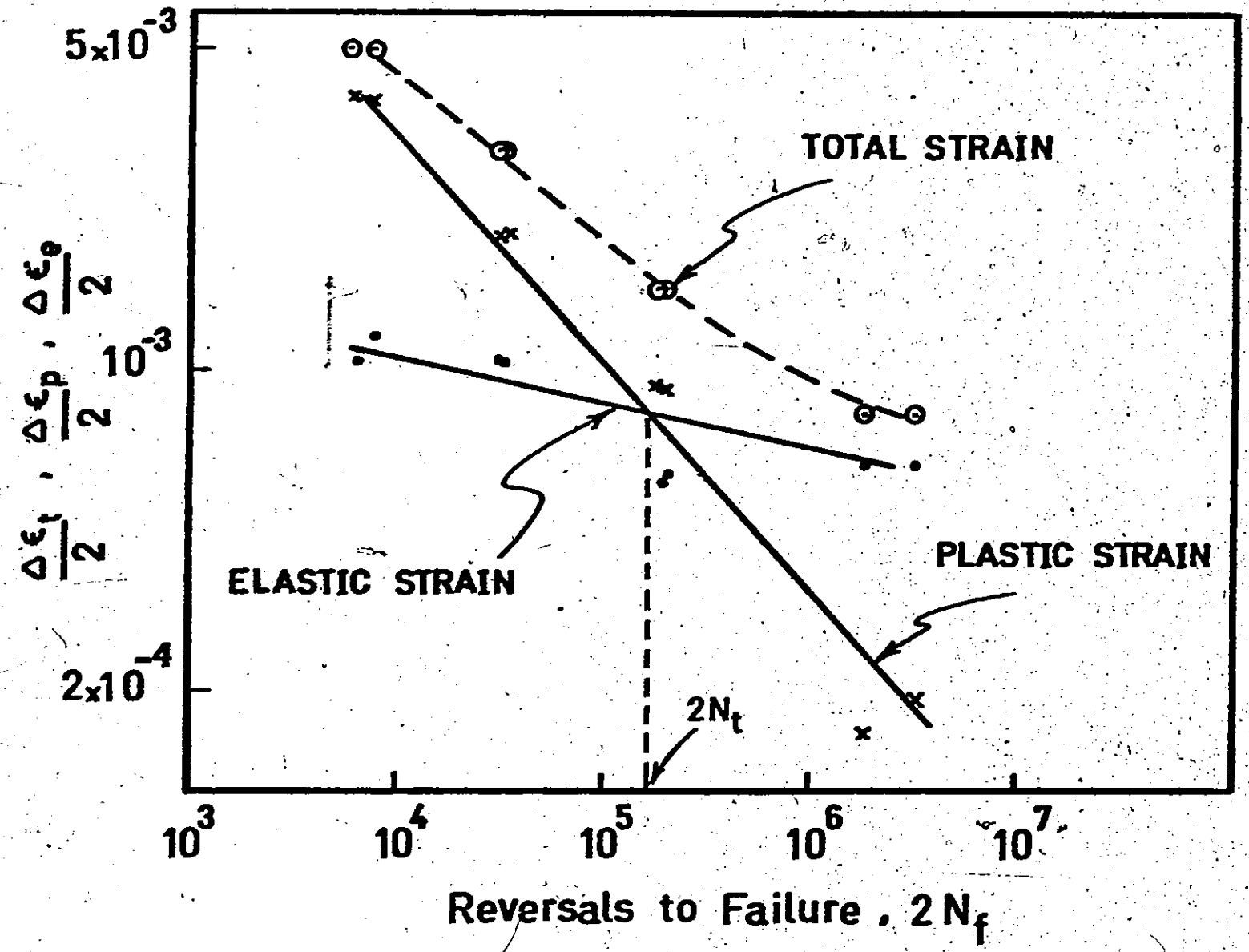

Figure 3.9 Strain-Reversals to Failure Data for SAE 1008 Sheet Steel Subjected to Reversed (Controlled) Strain.

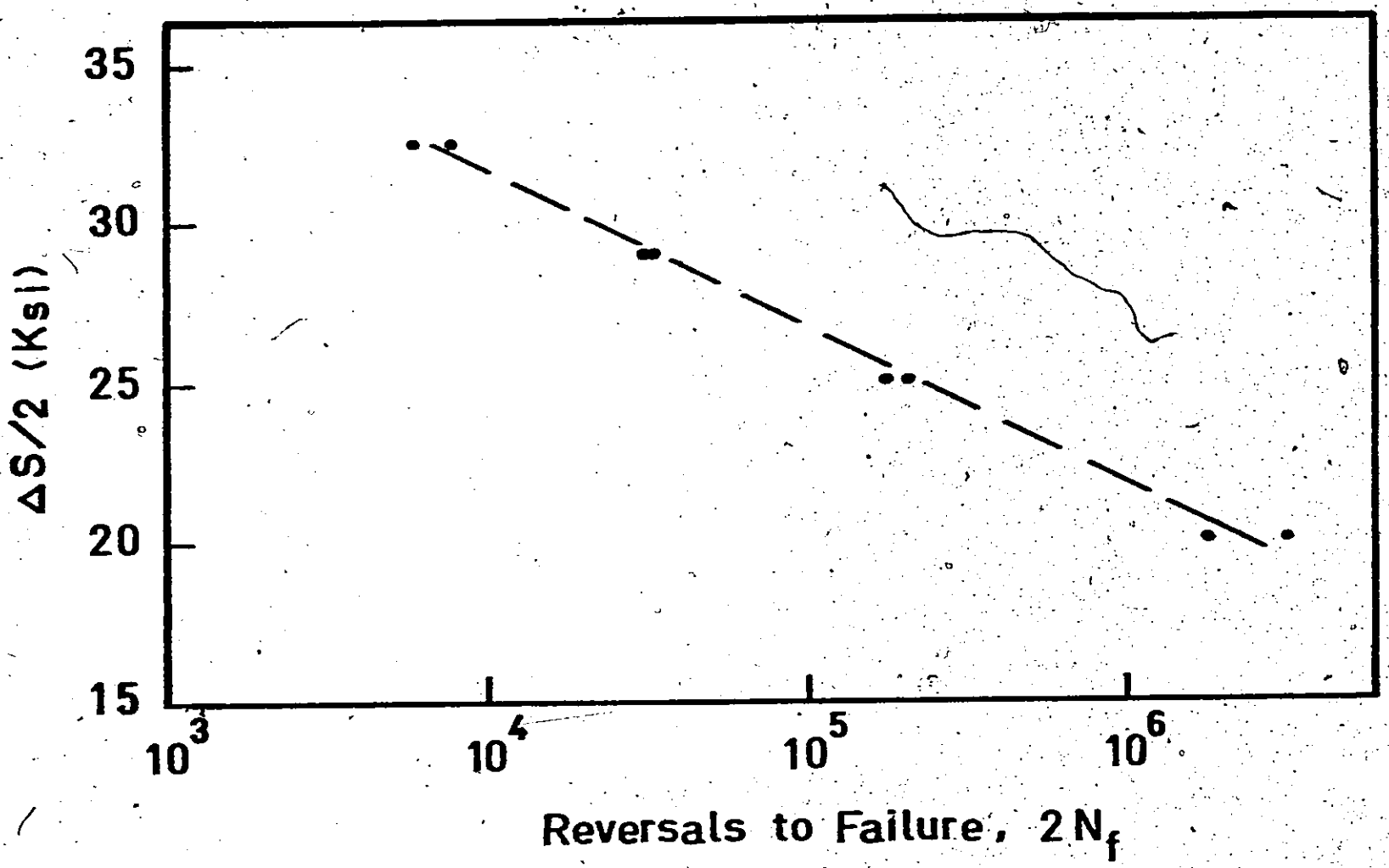

Figure 3.10 Axial Stress Amplitude-Reversals to Failure Diagram for SAE 1008 Sheet Steel Subjected to Axial Reversed Strain.

elastic and plastic strain components are equal. Equations (3.8) and (3.10) can be combined into a single equation for total strain:

$$\frac{\Delta\varepsilon}{2} = \frac{\Delta\varepsilon_e}{2} + \frac{\Delta\varepsilon_p}{2} = \frac{S_f'}{E}(2N_f)^b + \varepsilon_f'(2N_f)^c \qquad (3.11)$$

The elastic strain-life line is used to determine the mean value of the fatigue strength coefficient, S_f'.

The quantity S_f'/E is, by definition [72], the elastic strain amplitude when $2N_f = 1$, or in other words, it is the intercept point for the log $\Delta\varepsilon_e/2$ versus log $2N_f$ plot. Using the results of the least squares fit and the previous definition, S_f' is determined as follows.

$$\frac{\Delta\varepsilon_e}{2} = 2.775 \times 10^{-3} (2N_f)^{-.105}$$

hence,

$$\frac{S_f'}{E} = 2.775 \times 10^{-3}$$

and for Young's modulus $E = 32 \times 10^6$ psi,

$$S_f' = 88.8 \times 10^3 \text{ psi}$$

and as discussed in Chapter 2, the standard deviation of S_f' is approximated by the standard deviation of the ultimate tensile strength.

3.3.3 Cyclic Stress-Strain Curve

While the static stress-strain curve is obtained from

monotonic tests, the cyclic stress-strain curve can be obtained by one of the various methods suggested in Reference [72]. Since most metals stabilize rather quickly after transient changes in the cyclic stress-strain amplitude, it is possible to determine the cyclic stress-strain curve from one specimen using one of the following techniques:

(i) Multiple step test.

(ii) Incremental step test.

(iii) Monotonic tension after spectrum straining.

The steady state deformation and cyclic stress-strain curve which describes the hysteresis loop, have been studied quite extensively by Morrow [73]. A definite distinction is made between the monotonic stress-strain curve from tensile tests, and the cyclic stress-strain curve as shown in Figure 3.11.

In the case of multiple specimen tests, several identical specimens are strain cycled, each one at a different constant strain amplitude. The locus of stress, strain amplitude values corresponding to the stable state defines the cyclic stress-strain curve. On the other hand in the incremental step test, a single specimen is subjected to blocks of gradually increasing and then decreasing strain amplitudes until the material stabilizes. A continuous plot of the hysteresis loops throughout a block will result in a clearly defined locus of loop tips, which defines the cyclic stress-strain curve. This method is simple and requires only a single specimen to obtain the cyclic stress

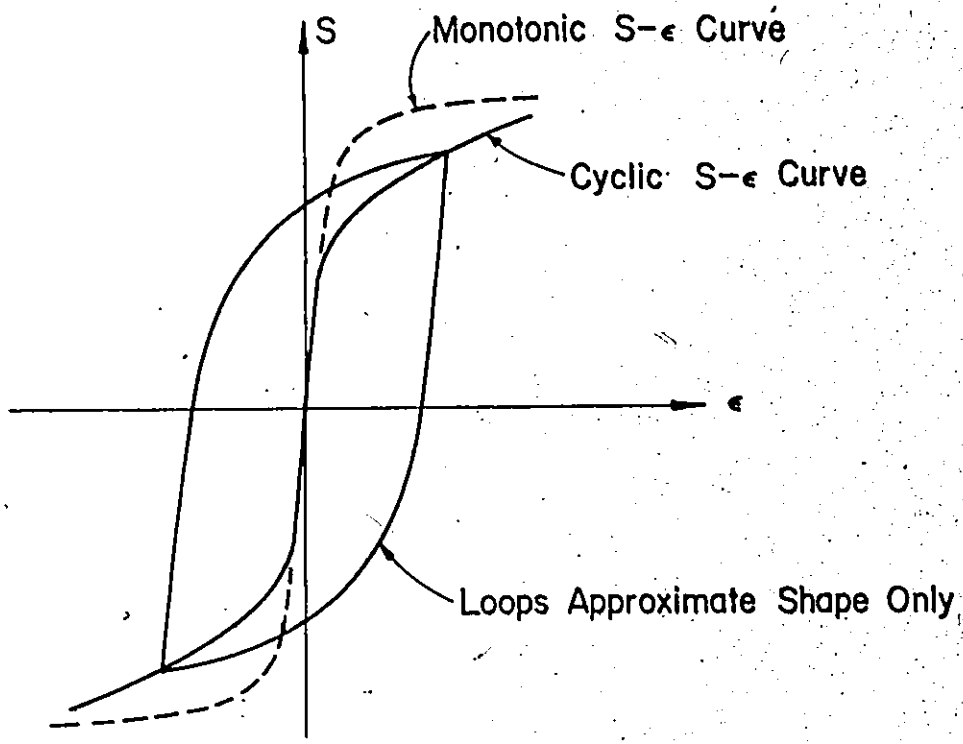

Figure 3.11 Schematic Representation of Cyclic and Monotonic Stress-Strain Curves [74].

strain curve. The different methods for obtaining the cyclic stress-strain curve have been found to be in reasonable agreement [72].

The incremental step test was used in this investigation. It incorporates a modulated strain-time program in which the strain signal is a sine wave, the amplitude of which increases and decreases linearly to form the blocks shown in Figure 3.12. Comparison between the monotonic and cyclic stress-strain curves after one block of loading is shown in Figure 3.13. After the application of several blocks of this increasing-decreasing strain-time history, a stabilized stress-strain response develops. The curve connecting the tips of these stabilized hysteresis loops represents the cyclic stress-strain curve and is shown in Figures 3.14 and 3.15. The cyclic softening and stabilization phenomenon exhibited by SAE 1008 steel when subjected to the previously described incremental-step test with a maximum strain amplitude of .5 percent is presented in Figure 3.16.

3.3.4 Comments on the Test Results

(i) This series of tests was useful in characterizing the axial fatigue behaviour of the material used. It also helped determine many parameters that were valuable during the course of this investigation for constructing the prediction model, designing the different experiments and for many calculations.

(ii) Morrow [74] found that the fatigue strength coefficient, S'_f, can be approximated by the monotonic true fracture

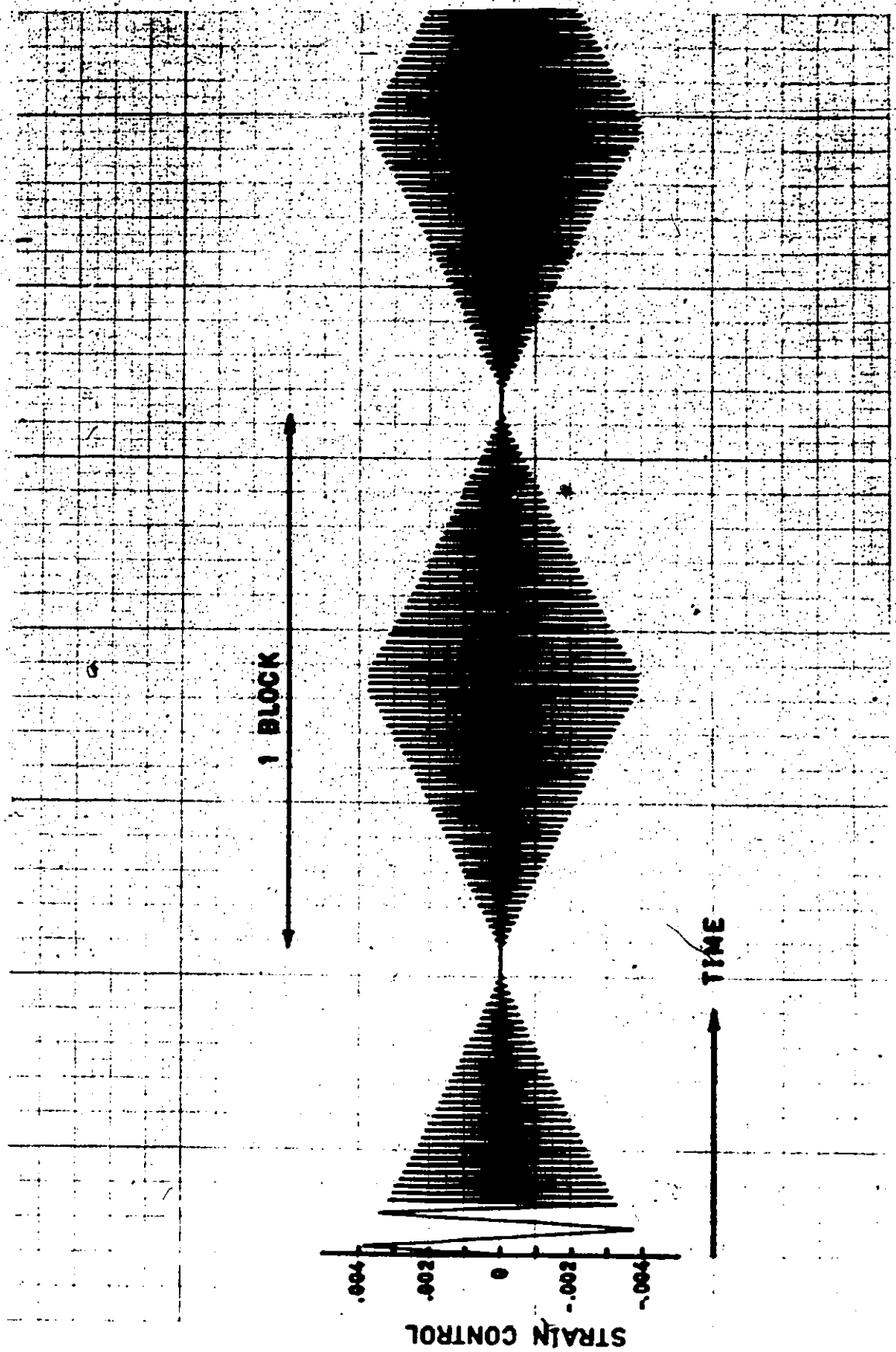

Figure 3.12 Strain-time History Used in the Incremental Step Test.

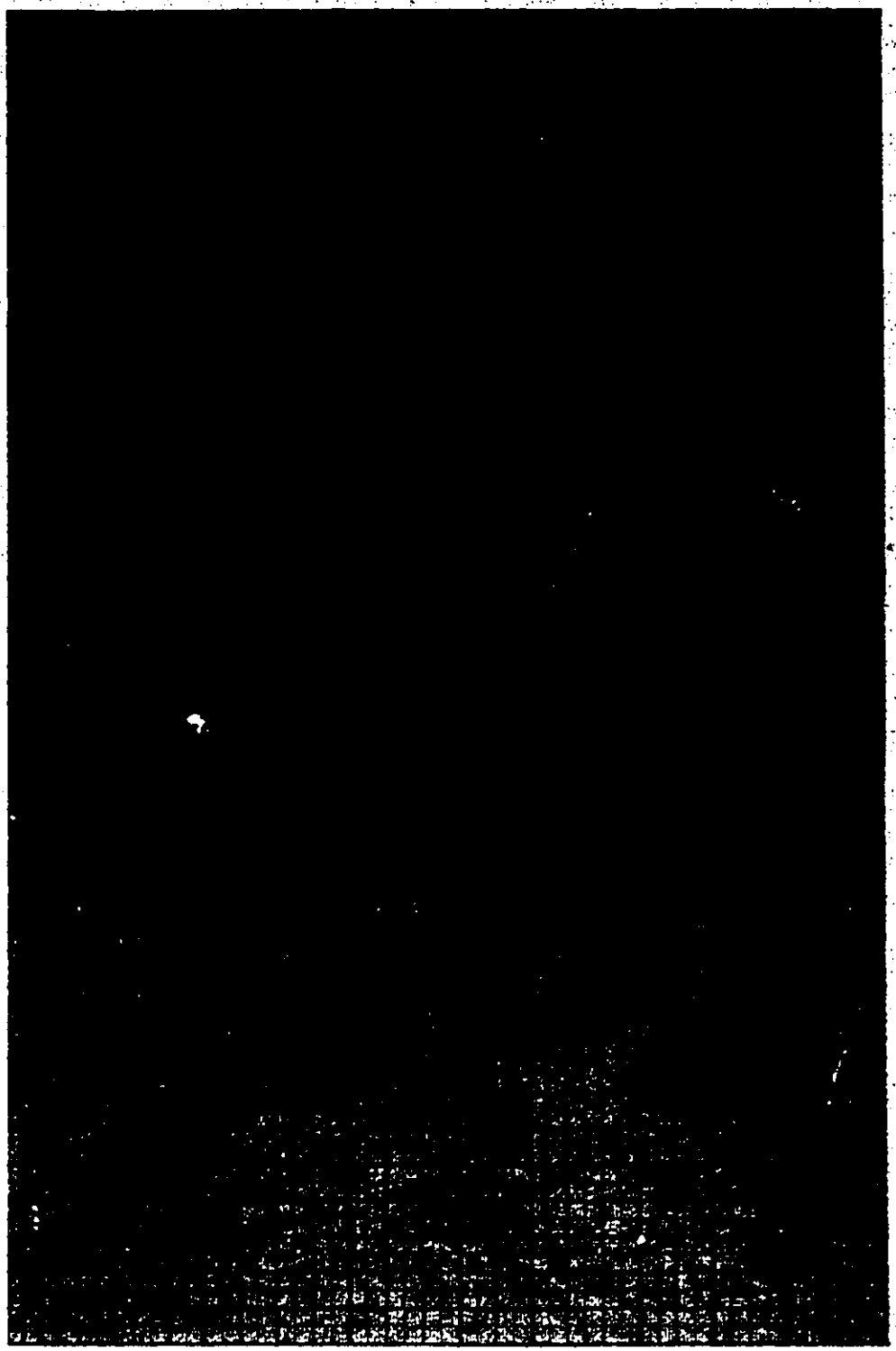

Figure 3.13 Hysteresis Loops After One Strain Block of the Incremental Step Test.

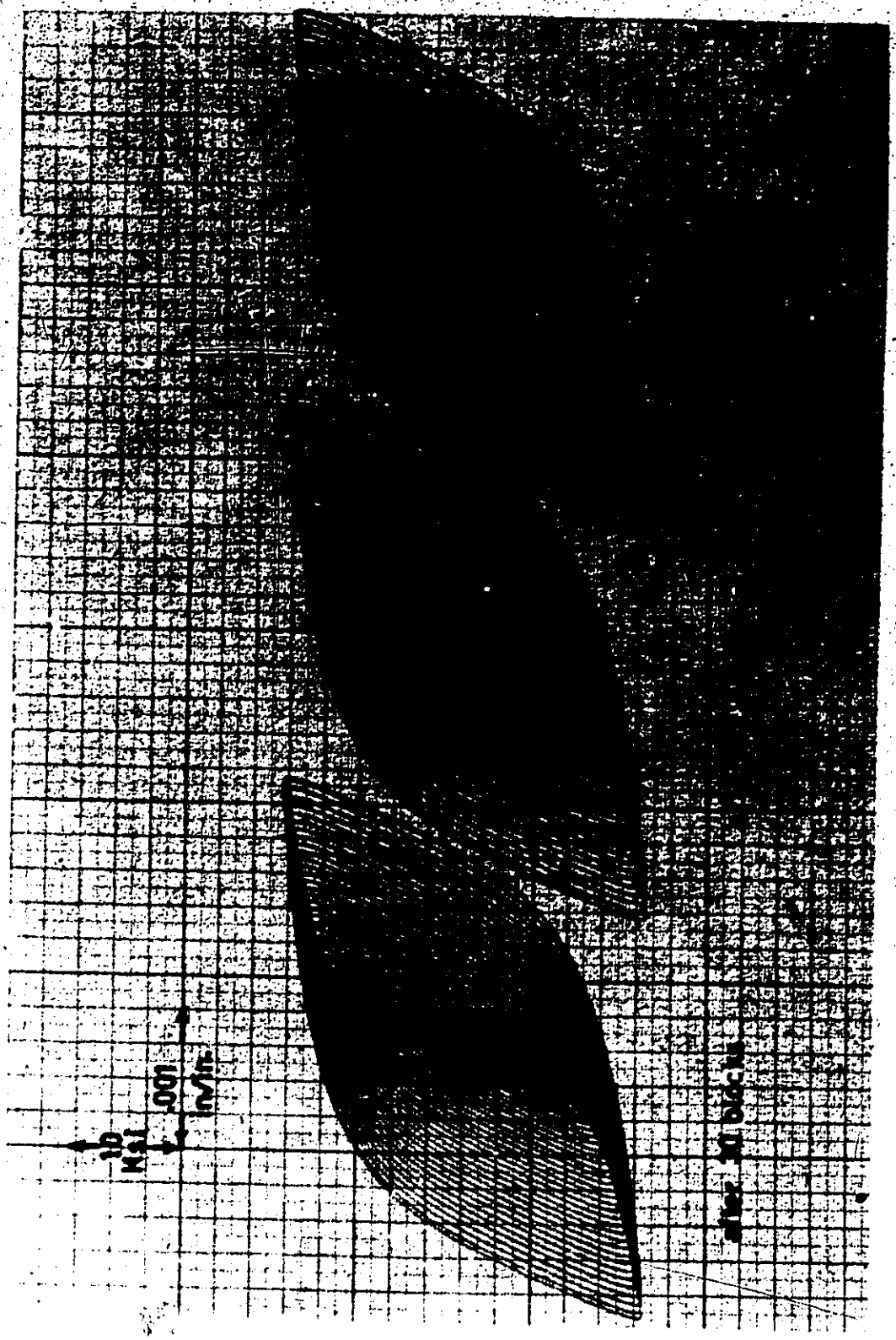

Figure 3.14 Stabilized Hysteresis Loops After 30, 32, 34 Blocks of Load.

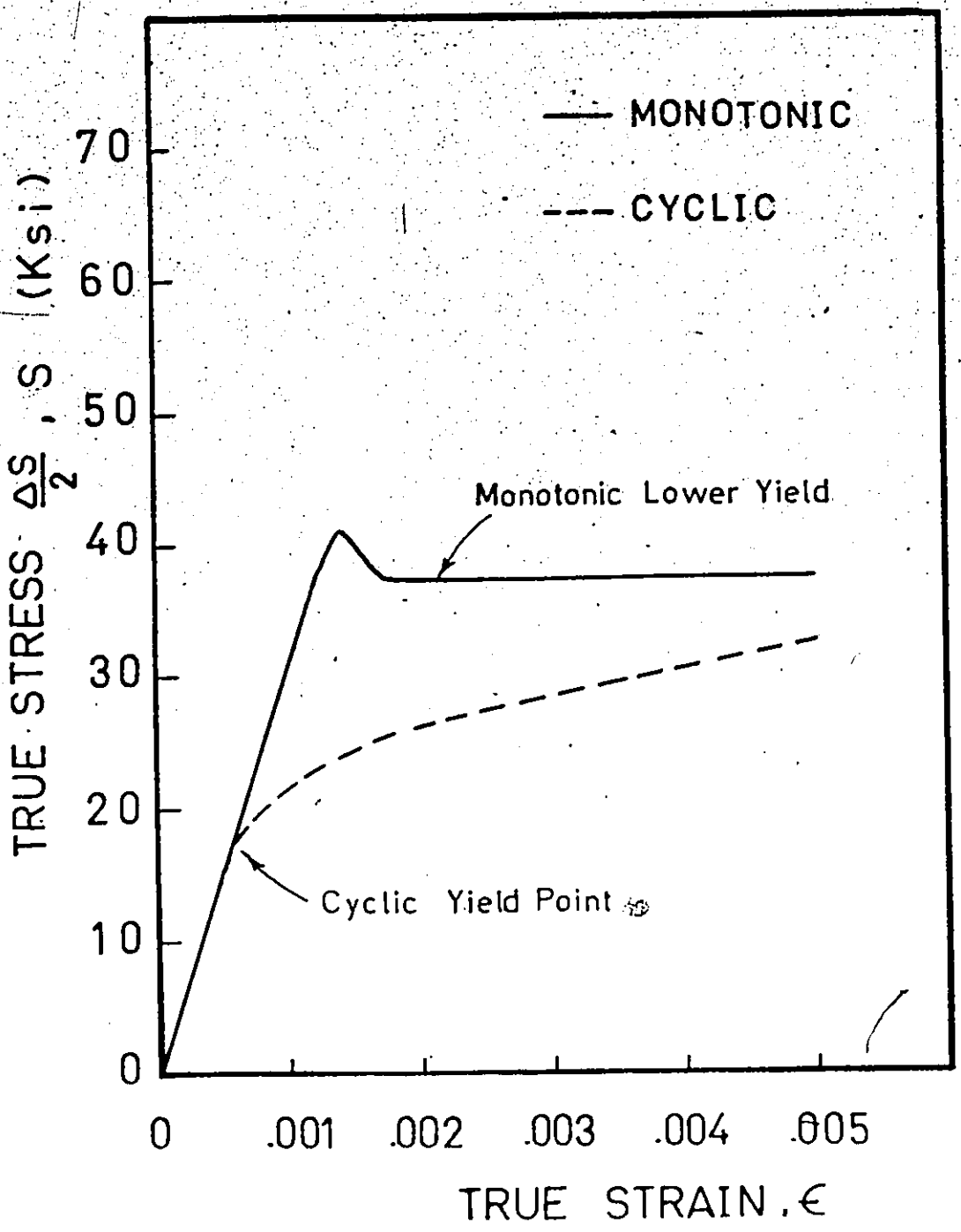

Figure 3.15 Experimental Cyclic and Monotonic Stress-Strain Curves of SAE 1008 Sheet Steel.

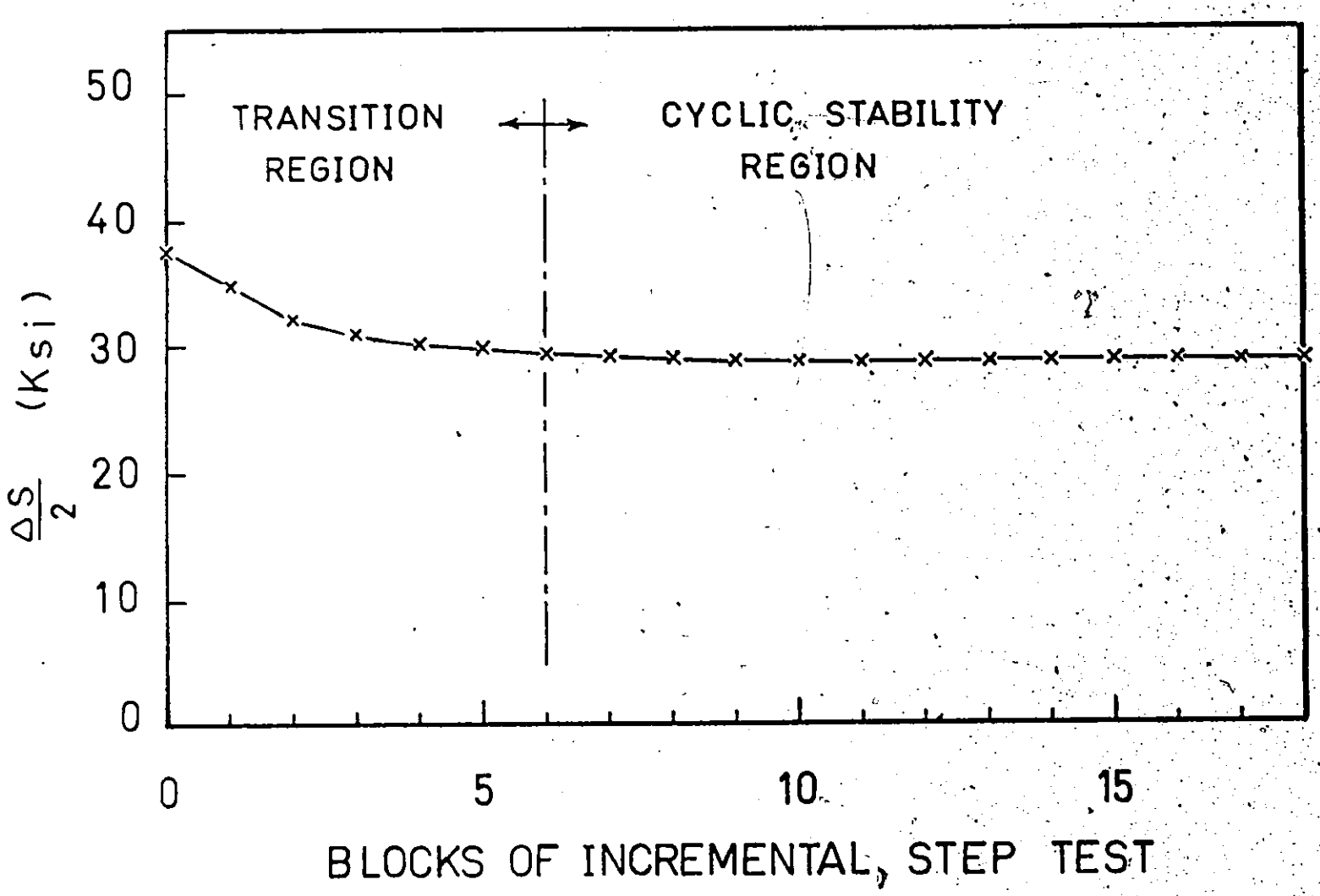

Figure 3.16 Cyclic Softening and Stabilization Exhibited by SAE 1008 Sheet Steel Subjected to Incremental Step Test Loading.

strength corrected for necking. Calculation of the true fracture strength corrected for necking was not possible since a necking correction factor for specimens having rectangular cross-section does not exist. It should be noted, however, that the fatigue strength coefficient estimated experimentally from $\frac{\varepsilon_e}{2}$ - $2N_f$ plots is less than the true fracture strength without correction for necking which was determined in Section 3.2.2. Morrow also showed that the value of stress amplitude at one reversal in log S-log 2N plots is equal to the fatigue strength coefficient.

(iii) The cyclic yield strength, S'_y, after which the cyclic strain is no longer linearly related to the cyclic stress; is also determined from these tests and was found to be

$$S'_y = 18.5 \times 10^3 \text{ psi}$$

Comparison of this value with the monotonic yield strength (37.69×10^3 psi) indicates the degree of softening exhibited by SAE 1008 steel.

The tension and axial fatigue tests were carried out in STELCO research laboratories.

3.4 Bending Fatigue Tests

Most of the data in this dissertation are for reversed bending fatigue with different load-time histories. Flexure is a common mode of structural loading, and the

results obtained from these tests can provide useful information for design.

3.4.1 Experimental Test Set-up

It is desirable to have an experimental set-up capable of applying both sinusoidal and random loads, with easily adjustable load levels and which provides an accurate means of counting the cycles-to-failure. A block diagram for the experimental set-up is shown in Figure 3.17. A detailed description of its operation and characteristics can be found in Chapter 4. This set-up was used to establish experimentally the distributions of fatigue life under different loading conditions as well as the distribution of the fatigue endurance stress.

3.4.2 Design of Test Specimen

Before bending fatigue tests could be performed, it was necessary to design the test specimen. Some basic considerations had to be taken into account in designing it. The following is a summary of some of these considerations and how they were met in the design.

(i) Constant stress distribution over the test section. This was achieved using a tapered test section along the length of the test specimen as shown in Figure 3.18.

(ii) The maximum bending stress to occur away from the clamping fixture. This was done by contouring the ends of the test section.

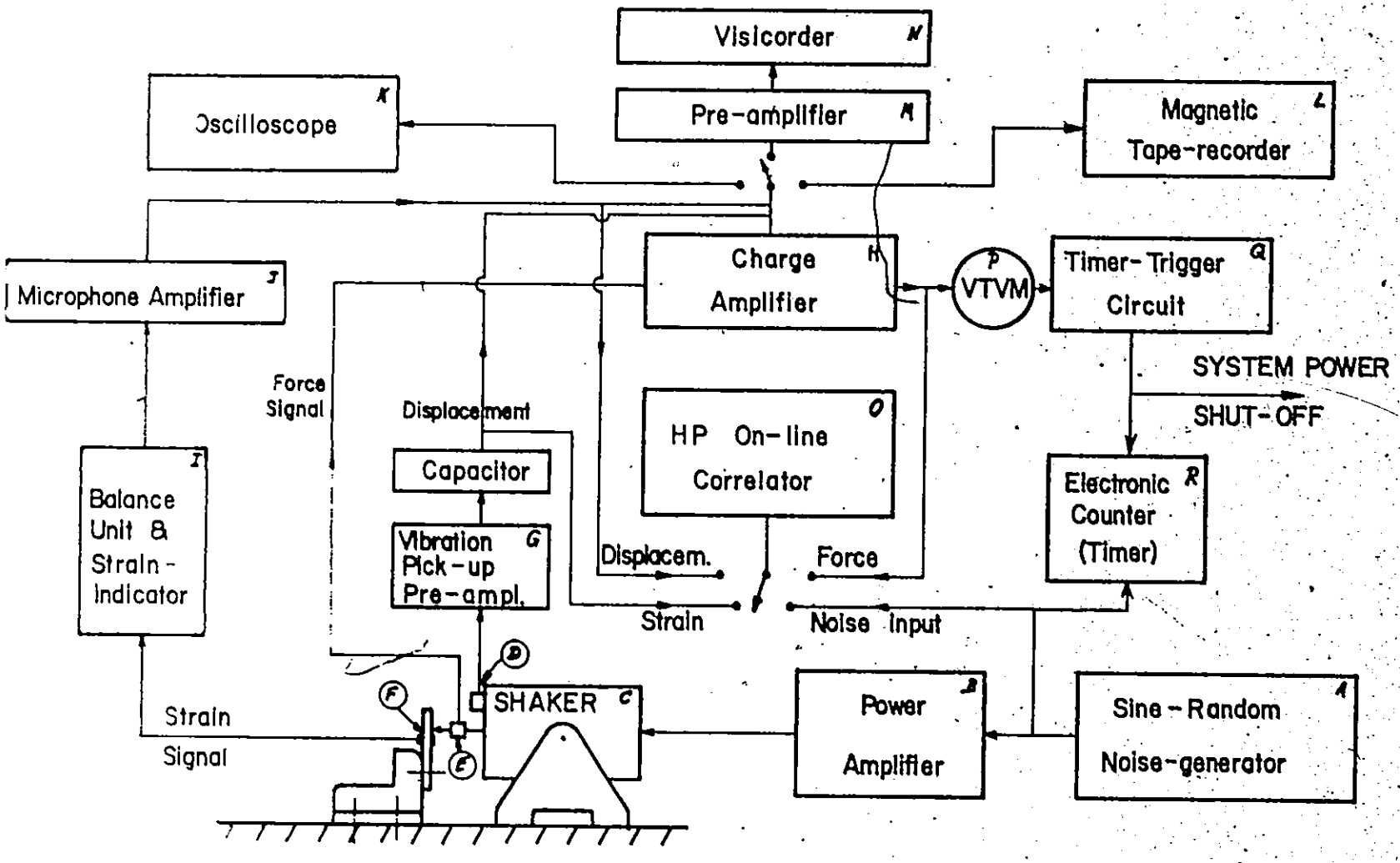

Figure 3.17 Block Diagram of Bending Fatigue Test Set-Up.

(iii) The specimen had to be sized to meet the capacity of the shaker, the available material thickness and at the same time produce the desired stress levels.

(iv) Flat transfer function over the frequency range of interest. This was met by maximizing the first natural frequency of the system, that is the specimen and the moving parts of the shaker. The transfer matrix technique [96] was used to obtain the dynamic response of the system.

To optimize the non-uniform shape of the test specimen subjected to forced vibration loading conditions, some simplifying assumptions were made. The system is assumed to be linear, the material damping is neglected, and the continuous specimen-shaker system is reduced to a ten-station lumped-parameter model.

The optimization objective was to maximize the first natural frequency of the system, to allow a wide frequency range below the first natural frequency where the system transfer function is flat. The design parameters to be optimized are dimensions of the specimen testing section, and the external force given the material thickness and properties. The optimum parameters have to maximize the objective function, satisfy the equations which describe the behaviour of the system and at the same time satisfy certain design constraints. These design constraints can be classified as follows:

(i) Geometrical

lower bounds on the dimensions arising from particular space or design considerations (e.g., all dimensions should be greater than or equal to zero).

(ii) Force constraint; which requires that the external force be less than the maximum capacity of the available shaker.

(iii) Stress constraint; which insures that the maximum required stress level is, at least, achieved without exceeding the yield point of the material.

(iv) Deflection constraint, which places an upper limit on the specimen deflection dictated by the allowable displacement of the shaker moving parts.

A direct search method was utilized for optimization. Different starting points were used to achieve a global optimum. The optimum shape of the test specimen is shown in Figure 3.18. The first natural frequency was estimated to be 130 Hertz. Preliminary tests have shown that the design was adequate and that the actual first natural frequency was close to the predicted one. The optimization approach proved to be successful in designing the test specimen which satisfies the previously discussed requirements.

3.4 Staircase Test to Determine the Distribution of the Fatigue Endurance Limit

It is well established in the literature that the fatigue endurance limit is normally distributed [48]. The

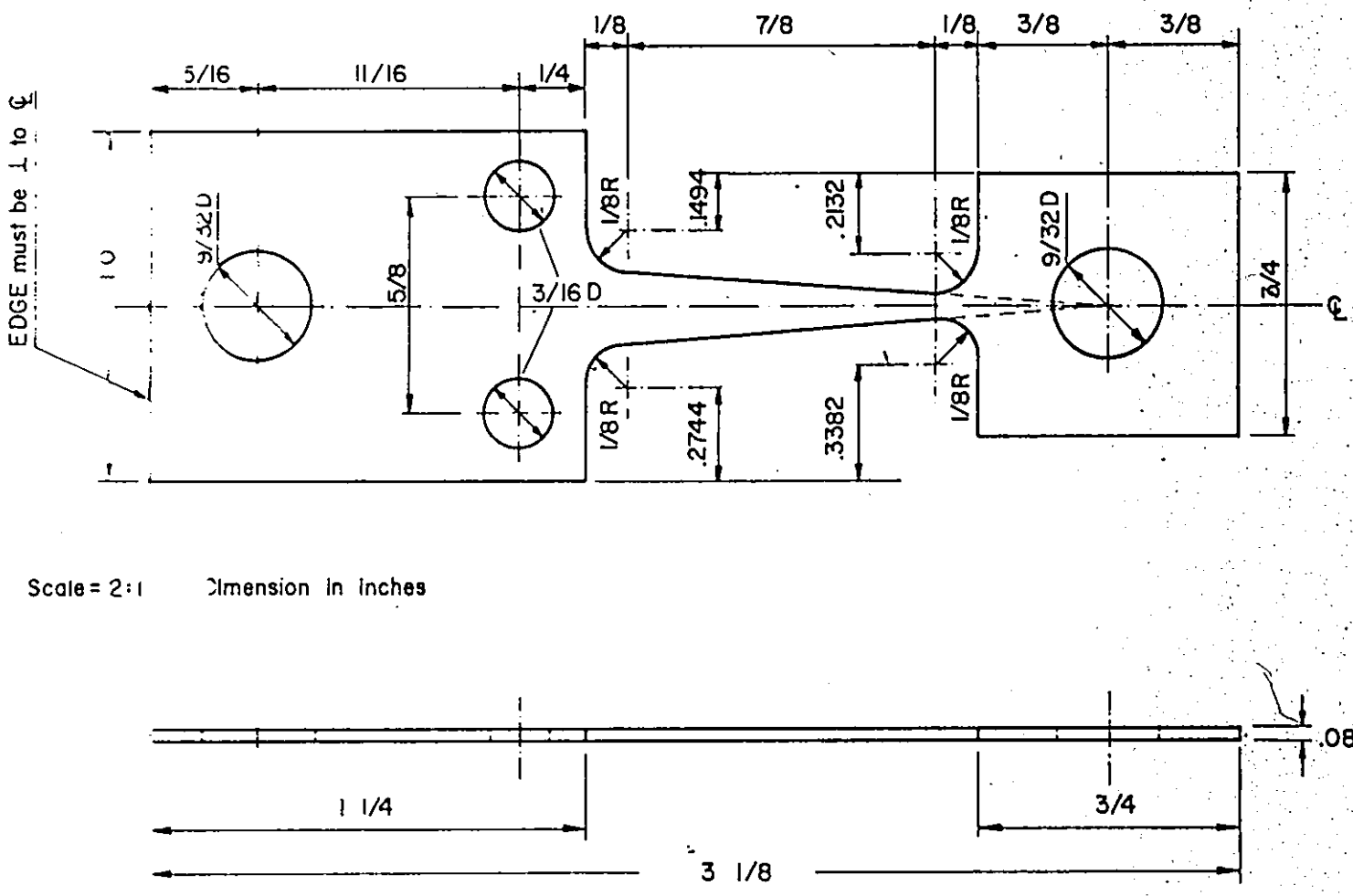

Figure 3.18 Configuration and Dimensions of the Bending Fatigue Test Specimen.

standard staircase fatigue testing and data reduction procedure was used (see Appendix A). Thirty seven specimens were cycled for 6×10^6 cycles or to failure whichever occurred first. The applied stress was sinusoidal fully reversed bending stress at a frequency of 50 Hertz. If the specimen reached 6×10^6 cycles without failure, the testing of that particular specimen was terminated and a fresh specimen was tested at one stress increment higher. If the test specimen failed before accumulating 6×10^6 cycles, a fresh specimen was tested at a load level one increment lower than the previous level. This procedure was followed for all subsequent specimens until 35 good specimens were run. The first two specimens in this test are not included in the calculation, since no change of mode (from failure to success or vice versa) occurred. The test is considered to have started with the specimen prior to the one where the first change of mode occurs. The test results are shown in Table 3.3 Calculation of the mean endurance limit and its standard deviation is given in Appendix A. The obtained results are summarized as follows:

$$\bar{S}_e = 21,621.6 \text{ psi}$$

$$\hat{\sigma}_e = 1,038.9 \text{ psi}$$

Using the experimentally determined values of $\bar{S}_e$, $\hat{\sigma}_e$, $\hat{\sigma}_n$ together with the method outlined in Chapter 2, the mean S 2N line and the number of cycles at the knee, N_e, are defined. It was found that,

TABLE 3.3 Staircase Test Results and Data Reduction to Determine the Mean and Standard Deviation of the Endurance Strength for SAE 1008 Steel Specimens.

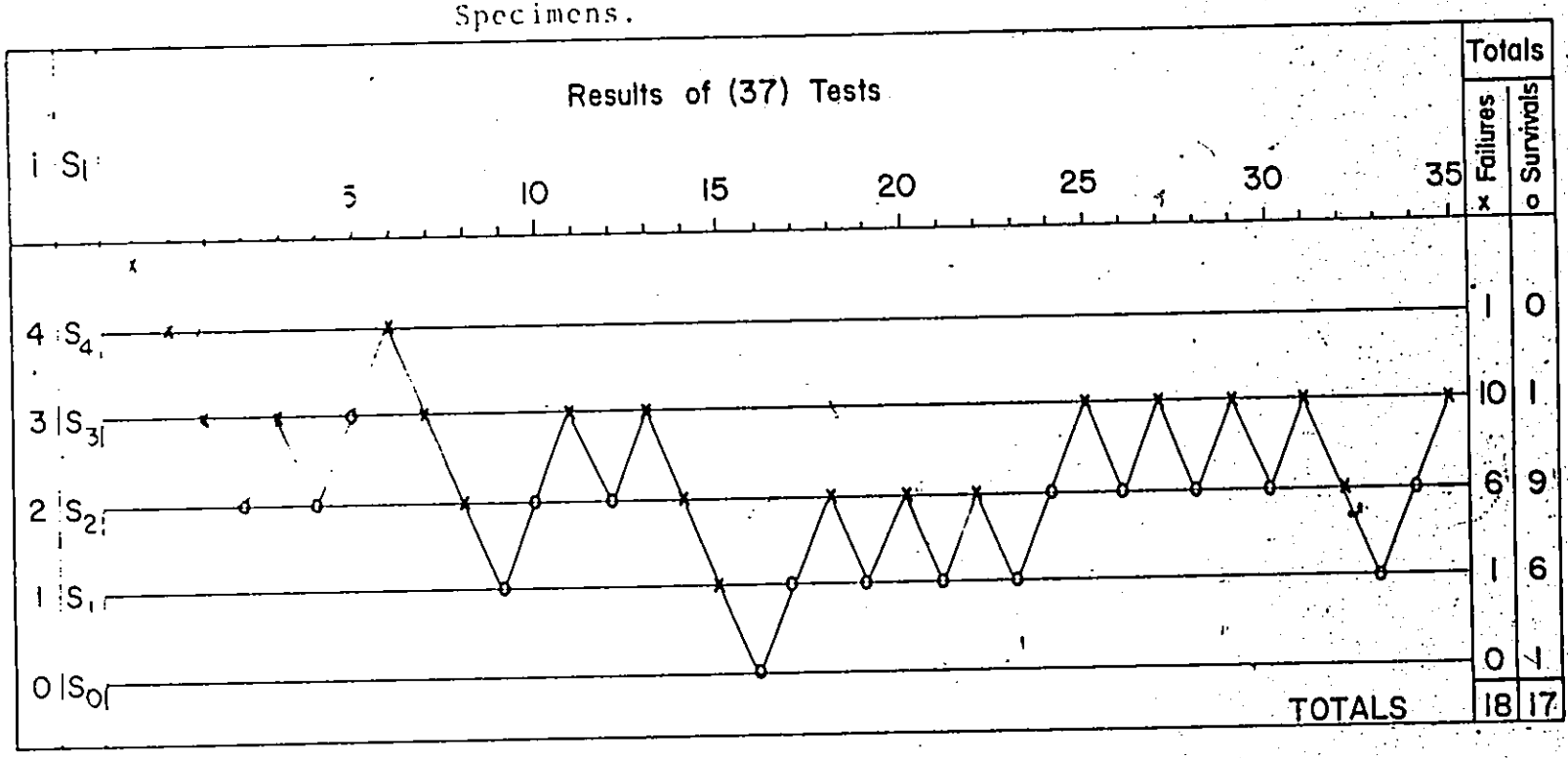

$$N_e = 2.424837 \times 10^6 \text{ cycles}$$

for SAE 1008 steel subjected to bending fatigue loading.

3.4.4 Comments on the Staircase Test Results

(i) The staircase method proved to be an effective method for determining the distribution of the fatigue endurance limit.

(ii) The coefficient of variation of the endurance stress, which is the ratio of the standard deviation to the mean, equals 4.8 percent. It is higher than the coefficient of variation of either the engineering ultimate stress (1.76 percent) or the true ultimate stress (2.35 percent). This result was expected and is borne out by the published data [48].

(iii) The actual cyclic stress-strain relation and the actual measurements of strain were used in these calculations rather than the nominal values since the latter do not reflect the actual behaviour of the material.

(iv) Many precautions in testing, machining and calibration were taken to minimize non random errors in the tests which can add to the scatter of the results. These precautions will be discussed in the subsequent chapter.

CHAPTER 4

CONSTANT AMPLITUDE AND BLOCK LOAD TESTING

4.1 Introduction

As a prerequisite to fatigue design, the working loads, their modes and frequencies of application and the resultant stress fields must be known to the required degree of completeness and accuracy. The fact that fatigue is inherently a dynamic phenomenon makes it imperative that the dynamic loads be known and that any "equivalent static" analysis be handled with the proper degree of conservatism.

A variety of load-time histories exist in actual service conditions. The constant amplitude test (Wöhler test) is often used as a fatigue criterion. In the Wöhler test the load is reduced to a sine wave with constant amplitude, often equal to the highest amplitudes in the service loading. The mean load, the amplitude and the frequency constitute a complete description of the load as a function of time.

The interpretation of a fatigue load-time function as a sine wave is acceptable only if the structural parts are subjected to loads which approach this type of wave form such as in the case of railway carriage axles, components for which Wöhler derived his well known testing method. But in more modern applications for land, sea, air and space vehicles, the nature of load occurences is random, especially

for moving bodies not tied to a ground frame. For such vehicles, the most acceptable approach is now well recognized to be the probabilistic one. Random loading will be discussed in more detail in Chapter 5. However, the constant amplitude test remains an important fatigue design tool as it is often used together with an adequate damage accumulation rule to predict fatigue life of components subjected to complex load histories. Therefore, an experimental verification of the suggested model using constant amplitude tests is attempted in this chapter.

4.2 Experimental Program

4.2.1 Test Specimen

The final design of the bending fatigue specimen shown in Figure 3.18 satisfied all the basic criteria previously mentioned in Section 3.4.2. Since in this study we are mainly concerned with the scatter due to the material behaviour, it was desirable to produce specimens as identical as possible. A TOS-FA4V knee type milling machine controlled via a HP-2100 minicomputer with 16K of memory, was used to machine the test specimens. The Computer Numerical Control (CNC) milling technique was chosen for the accuracy of the numerical control operation and the repeatability of positioning characteristics. Numerical input from a paper tape was used to control the cutter path, feed rate and indicate the change of tool or spindle speed during the cutting process. All of the required numerical information was preselected

and stored on the paper tape. A copy of the N/C data program is included in Appendix B. The N/C data tape is entered only once via a high speed reader for each manufacturing series and stored in computer memory. The specimens were machined in batches of five held down to the table using specially designed clamps. A good lubricant was used liberally during the machining process to minimize the workpiece deformations caused by the thermal effects. Figure 4.1 shows a general view of the milling machine, HP-2100 minicomputer, controller and teletype used to machine the test specimens. Figure 4.2 shows closeups of the specimens, clamps and cutting tool. The dimensions of the test section of the used specimens were checked using a "Wilder" microprojector to examine their scatter. It was found that the variation of the different dimensions was negligible. Only the machined surfaces were hand-polished. The rolled surfaces received no preparation except for those specimens on which strain gauges were placed for calibration purposes. Strain gauges WD-DY-050AR-350 by Inter-Technology were used to establish the static and dynamic load strain relation and also the strain deflection and strain force calibration curves. One strain gauge on each side of the testing section were placed longitudinally, to compensate for the thermal effects and increase the bridge sensitivity. Figure 4.3 shows specimens with and without strain gauges. The fact that the stress is uniformly distributed over the testing section made the strain gauge placement less critical

FIGURE 4.1 PHOTOGRAPH SHOWING A GENERAL VIEW OF THE CNC MILLING MACHINE AND HEWLET PACKARD MINICOMPUTER USED TO MANUFACTURE THE BENDING FATIGUE TEST SPECIMENS.

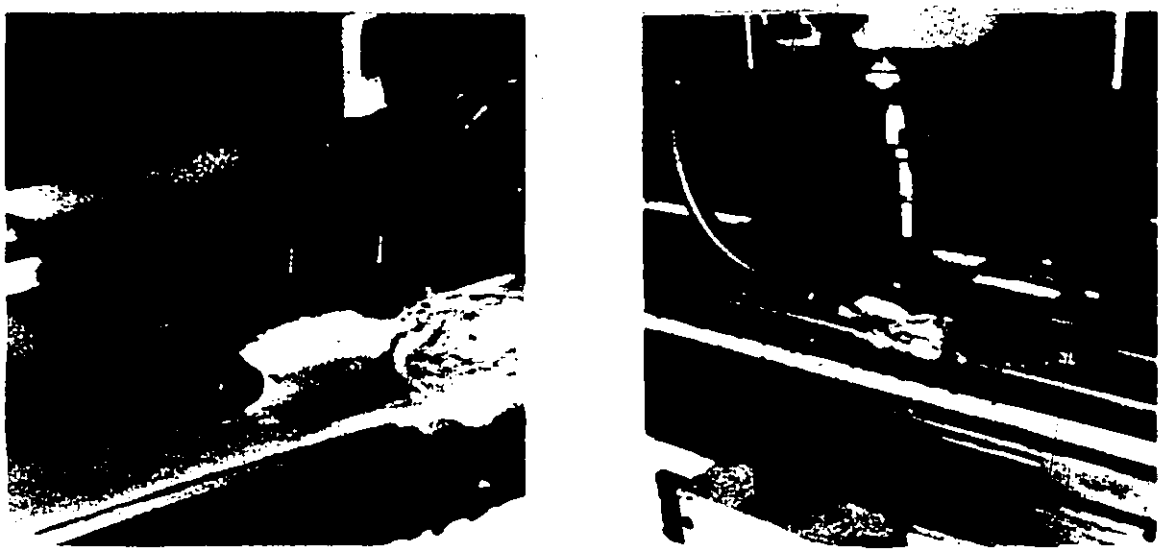

FIGURE 4.2 PHOTOGRAPHS SHOWING CLOSEUPS OF THE BENDING FATIGUE SPECIMENS AND CUTTING TOOL.

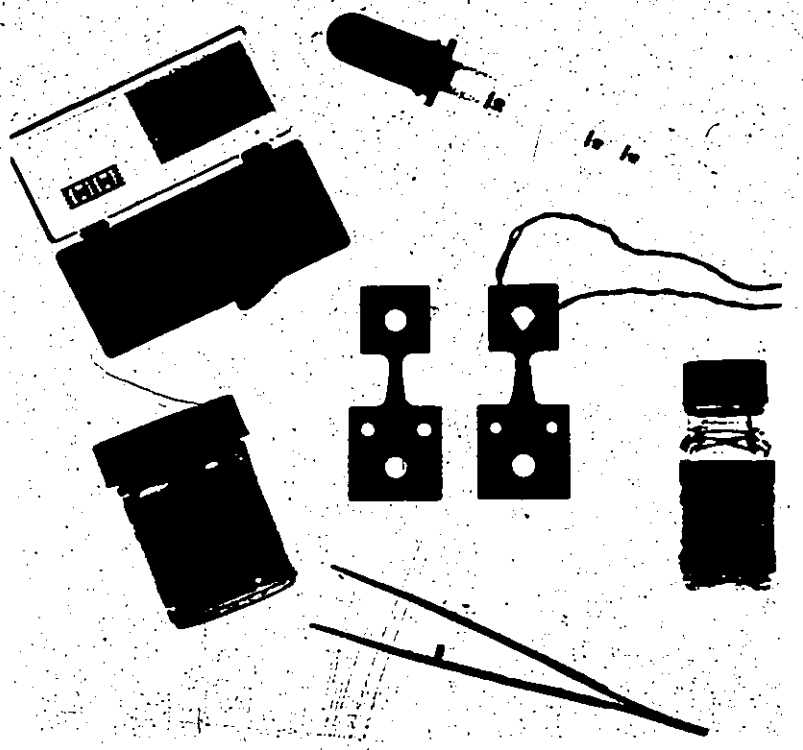

FIGURE 4.3 PHOTOGRAPH SHOWING THE STRAIN GAUGES APPLIED TO THE BENDING FATIGUE SPECIMENS.

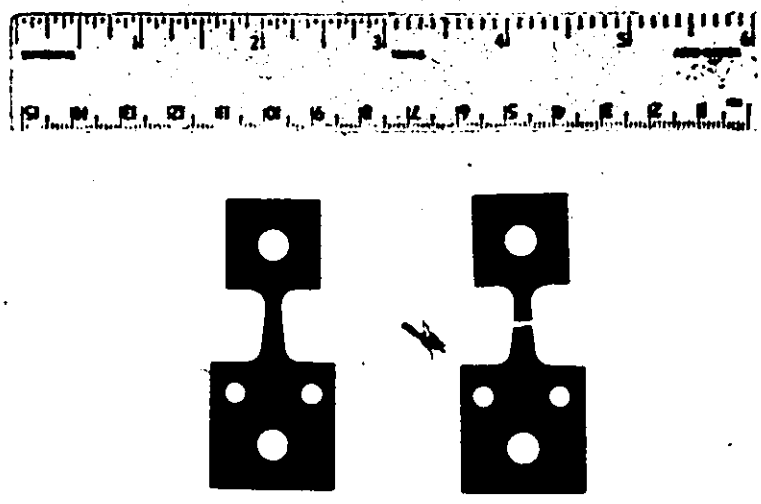

FIGURE 4.4 PHOTOGRAPH SHOWING BENDING FATIGUE TEST SPECIMENS, BEFORE AND AFTER FRACTURE.

Figure 4.4 shows test specimens before and after fracture.

4.2.2 Test Set-up

The main objective was to design a test set-up which is capable of applying both sinusoidal and random loads and provides an accurate means of counting the cycles-to-failure. Figure 3.17 shows the instrumentation block diagram with the legend of the actual equipment specifications presented in Table 4.1. The input signal was generated using a B & K Sine Random Generator. This signal was amplified before using it to excite the shaker. The shaker was connected to the test specimen using a ball joint which allows the upper end of the specimen to rotate and thus simulate a cantilever beam loading condition. The shaker and clamping fixture were leveled and positioned relative to each other in such a way that the mounted specimen is practically free of stresses at the beginning of the test. This was checked using the strain gauges, strain indicator and the digital readout with one microstrain (1 με) resolution. Both the shaker and the fixture were fixed to the table for the rest of the tests. This set up was rechecked before each series of tests. Constant tightening pressure was used every time a new specimen is mounted using a torque wrench. Two stops were machined in the clamping fixture to ensure identical positioning for all specimens. A general view of the test set up and a closeup of the shaker specimen assembly are shown in Figures 4.5 and 4.6 respectively.

TABLE 4.1 INSTRUMENTS USED IN BENDING FATIGUE EXPERIMENTS (Legend for Fig. 3.17)

No.	Instrument	Make	Type
A	Sine Random Generator	B & K	1024
B	Power Amplifier	MB	2250
C	Electro-dynamic Shaker	MB	PM-50
D	Accelerometer	B & K	4332
E	Piezoelectric Force Transducer	Kistler	931A
F	Electrical Strain Gauge	Inter-Technology	WD-DY-050AR-350
G	Vibration Pick-up Preamplifier	B & K	2625
H	Charge Amplifier	Kistler	504A
I	Portable Strain Indicator	Vishay	1011
	Digital Indicator	Vishay	V/E-13
J	Microphone Amplifier	B & K	2603
K	Oscilloscope	Tektronix	561A
L	Closed loop FM Magnetic Rocorder/Reproducer	Philips	EL 1070
M	Preamplifier Visicorder	Honeywell	117 DC
N	Visicorder	Honeywell	2106
O	Correlator	H.P	3721A
P	Vacuum Tube Voltmeter	RCA	[illegible]
Q	[illegible]	Designed and built for [illegible] experiment	
R	Electronic Counter	H.P	[illegible]
(Not Shown)	[illegible]	[illegible]	

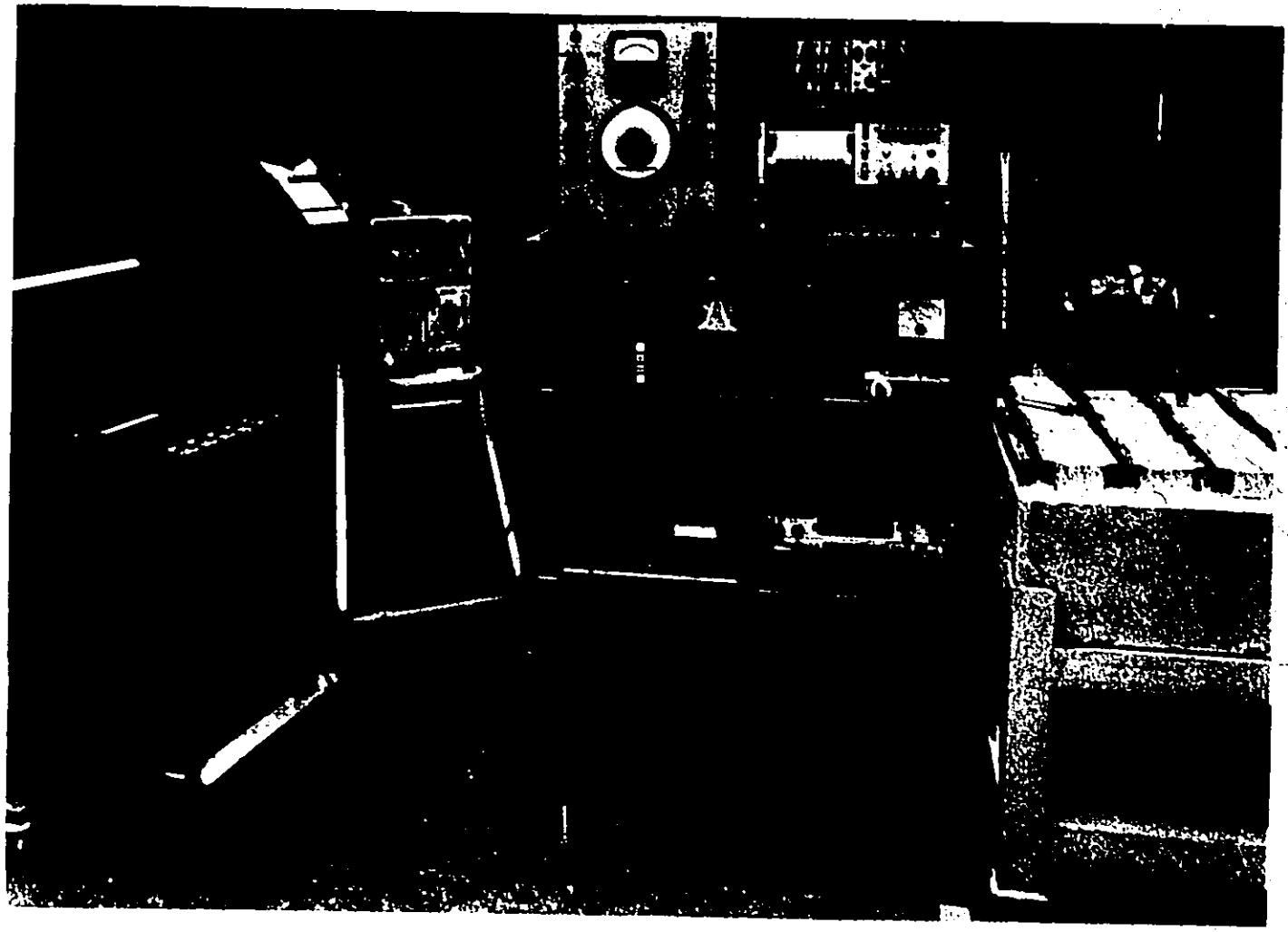

FIGURE 4.5 PHOTOGRAPH SHOWING GENERAL VIEW OF THE BENDING FATIGUE TEST SET-UP.

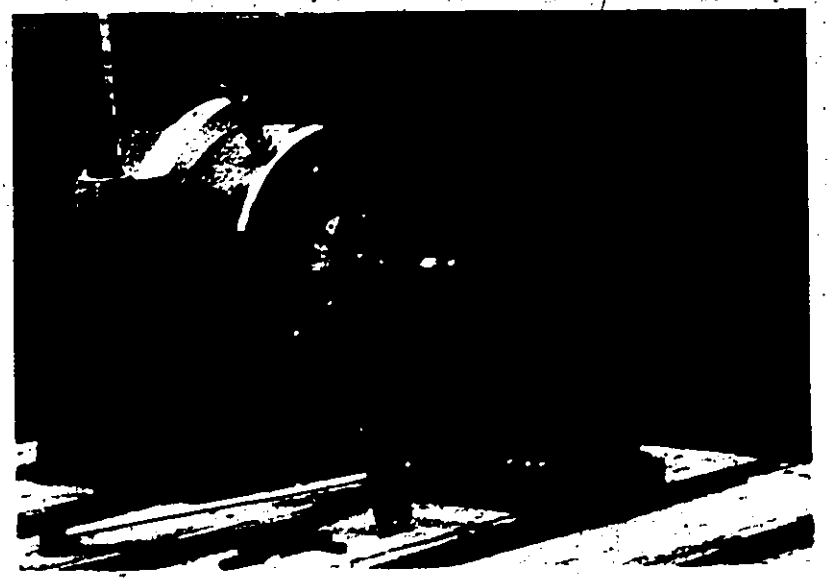

Figure 4.6 Photograph Showing a Closeup of the Specimen-Shaker Assembly.

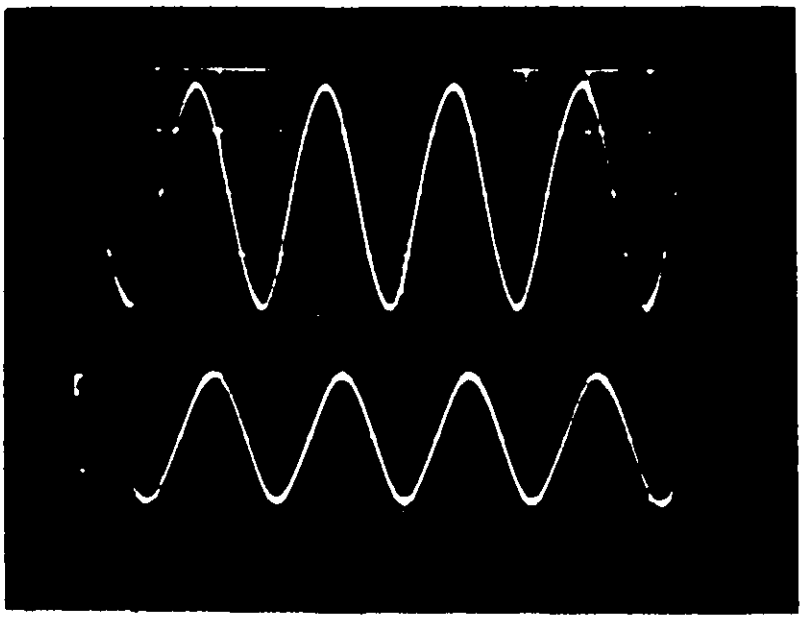

Figure 4.7 Photograph Showing the Strain (Upper Trace) and Displacement (Lower Trace) Signals of a Sinusoidal Constant Amplitude Test.

A - Measurement Devices

Two signals were used in each test. First, the force acting on the specimen measured using a piezoelectric force link mounted between the specimen and the shaker.

The force signal drops very rapidly at fracture. It was used together with the triggering circuit described later to determine the number of cycles-to-failure. Second, the specimen tip displacement was measured using a piezoelectric accelerometer. The displacement signal was calibrated with the actual true strain measured using two strain gauges placed on the test-section of the specimen. The fatigue life of the strain gauges is generally less than the fatigue life of the specimen. Moreover, since thirty specimens or more were to be tested for each load program, it was economically prohibitive to place two strain gauges on each specimen. The accelerometer mounted on the moving face of the shaker provided a response signal which lasted until failure. Therefore, the calibrated tip displacement signal was used to adjust the applied loads. The different signals were measured and monitored using an Oscilloscope. The signals were recorded using a Visicorder or an FM Tape Recorder for subsequent analysis. A photograph of deflection and strain signals is shown in Figure 4.7

B Cycle Counting and Definition of Failure

When fracture occurs the specimen is considered to have failed and provisions were made for stopping the test as soon as this happens. A triggering circuit was designed

to act as a shutoff device. It is essentially a load peak counter which rectifies and averages the input signal, and requires that a predetermined load be reached on each successive cycle for the test to continue. The timer was started automatically using the input signal to the system. The force signal was used to trigger a relay which deactivated the timer when the signal dropped below 20% of its steady state value. A schematic representation of the triggering circuit is shown in Figure 4.8.

4.2.3 Load Program

Three sinusoidal load programs were used. In the first program the amplitude was kept constant throughout the test. The second program consisted of two blocks of sinusoidal loading with the load being higher in the first portion of the program (Hi-Lo). The third program is also a block loading with a Low-High-Low (Lo-Hi-Lo) sequence of amplitudes. The switch-over of amplitudes was manual and almost instantaneous. The signal frequency was 50 Hertz in the three load programs. The frequency counter was used to accurately determine and adjust the excitation frequency at the beginning of each test. The three programs are illustrated in Figure 4.9. The true stress amplitudes in all the tests were below the monotonic lower yield strength of the material but greater than the cyclic yield strength determined in Chapter 3. Thirty specimens were tested in each program which increases the confidence in statistical

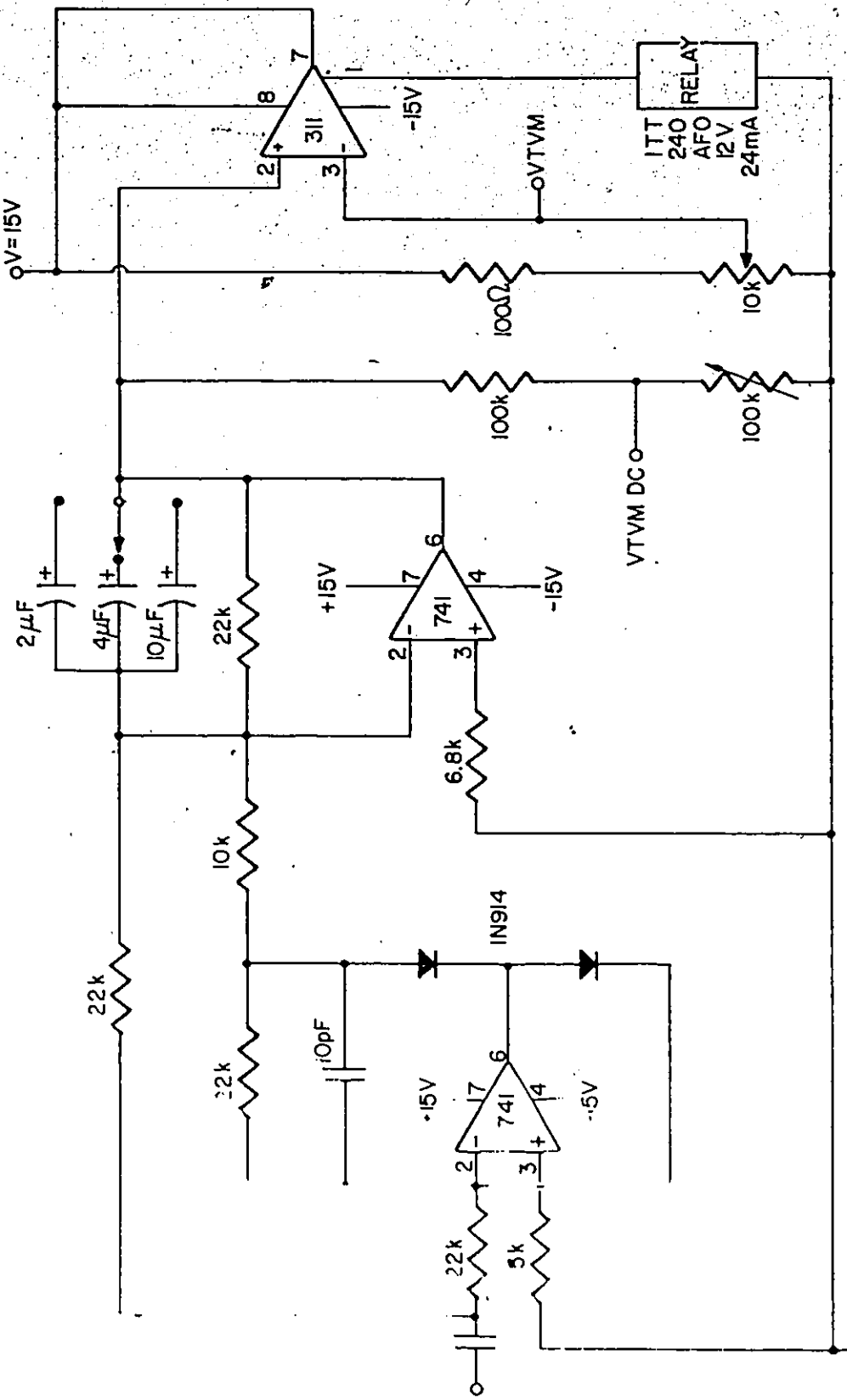

Figure 4.8 Schematic Diagram of the Triggering Circuit.

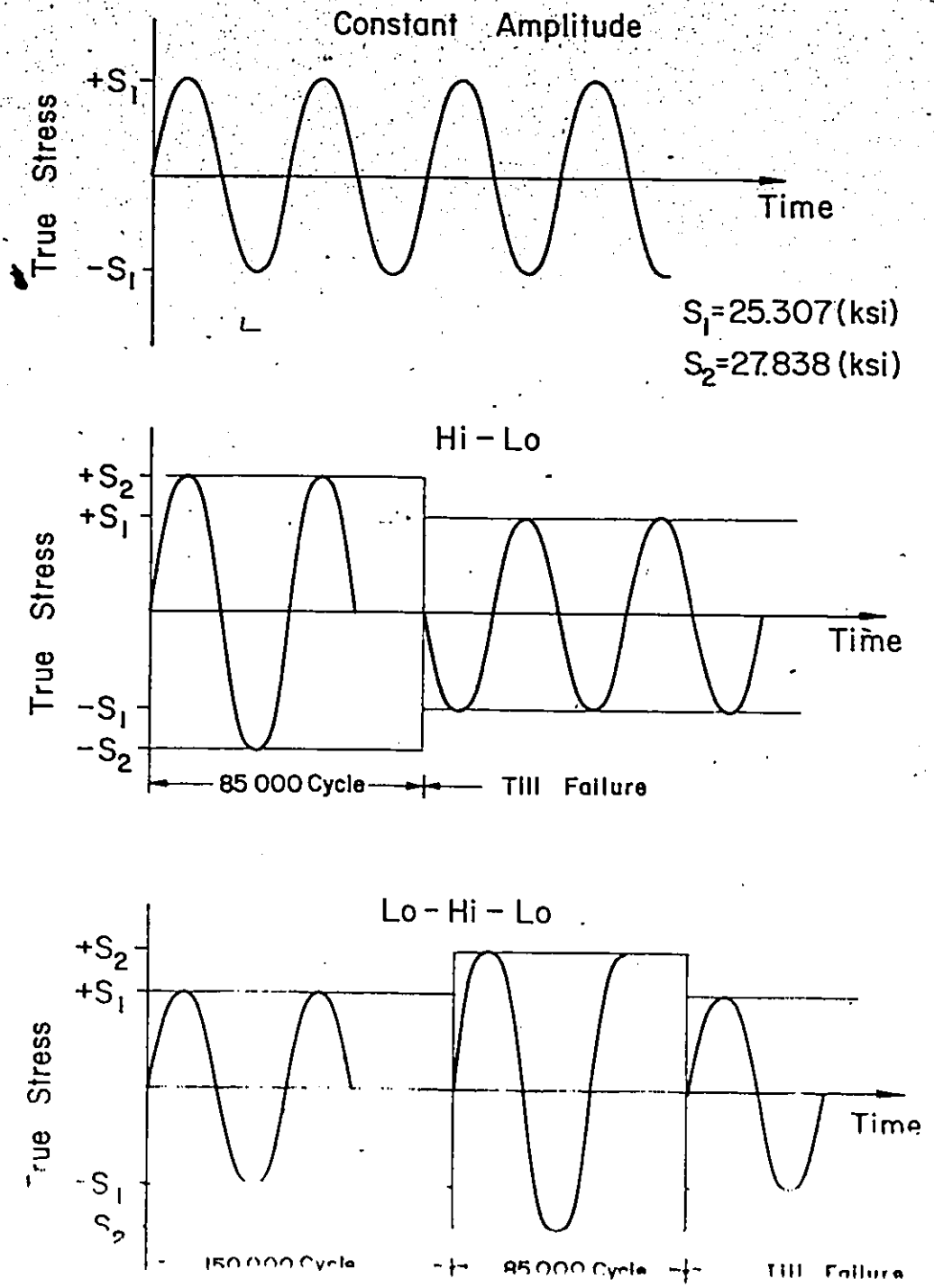

Figure 4.9 Schematic Representation of the Three Sinusoidal Load Programs Used in the Tests.

conclusions drawn from this investigation, compared to other studies where usually much less number of specimens are tested.

4.3 Results of Constant Amplitude and Block Load Tests

4.3.1 Experimentally Determined Distributions

The time to failure registered by the timer was recorded for each specimen. For the previously described cases of loading the definition of a cycle is fairly evident and the number of cycles is determined by simple counting. The fatigue life is equal to the time-to-failure in seconds multiplied by the signal frequency in Hertz. The first four central moments of the fatigue life and its common logarithm are calculated for each loading program. These moments were used to define the different probability density functions using the Maximum Entropy method [79]. It is known that any distribution is completely defined by all of its moments, but it has been shown by Siddall et al. [80] that using the Maximum Entropy Function constrained by the first few moments to define the distribution yields very good results. No attempt was made to assume a certain distribution for fatigue life data. The exponential which fits the PDF was obtained using the Maximum Entropy function approach. The problem of deciding which statistical law is the "true one" in fatigue studies has occupied investigators for many years. It is now being realized that this is a fruitless pursuit and can never be actually decided, since

no single distribution can describe fatigue data obtained for different loading conditions. Plots of the experimentally determined distributions are shown in Figures 4.10 to 4.18. Time-to-failure and cycles-to-failure data as well as the detailed characteristics of the life distributions are given in Appendix C.

4.3.2 Theoretically Predicted Distributions

The material characteristics (S_f', S_e, S_u) obtained in Chapter 3 were used to define the parameters needed for the fatigue life prediction model proposed in Chapter 2. This model was used to predict the fatigue life distributions under the described loading conditions. The stress amplitudes used in the model were obtained by converting the true strain amplitude of each block to true stress amplitude using the experimentally determined cyclic stress-strain curve. This method of defining the applied stress amplitudes uses the actual behaviour of the material, thus avoiding any linear elastic assumptions.

Probability density functions of the predicted life and its common logarithm were also determined using the Maximum Entropy Function method. The prediction technique is described in Sections 2.4 and 2.5. The obtained plots are shown in Figures 4.10 to 4.18. A summary of the predicted and experimentally found characteristics of the different distributions is given in Tables 4.2 to 4.4.

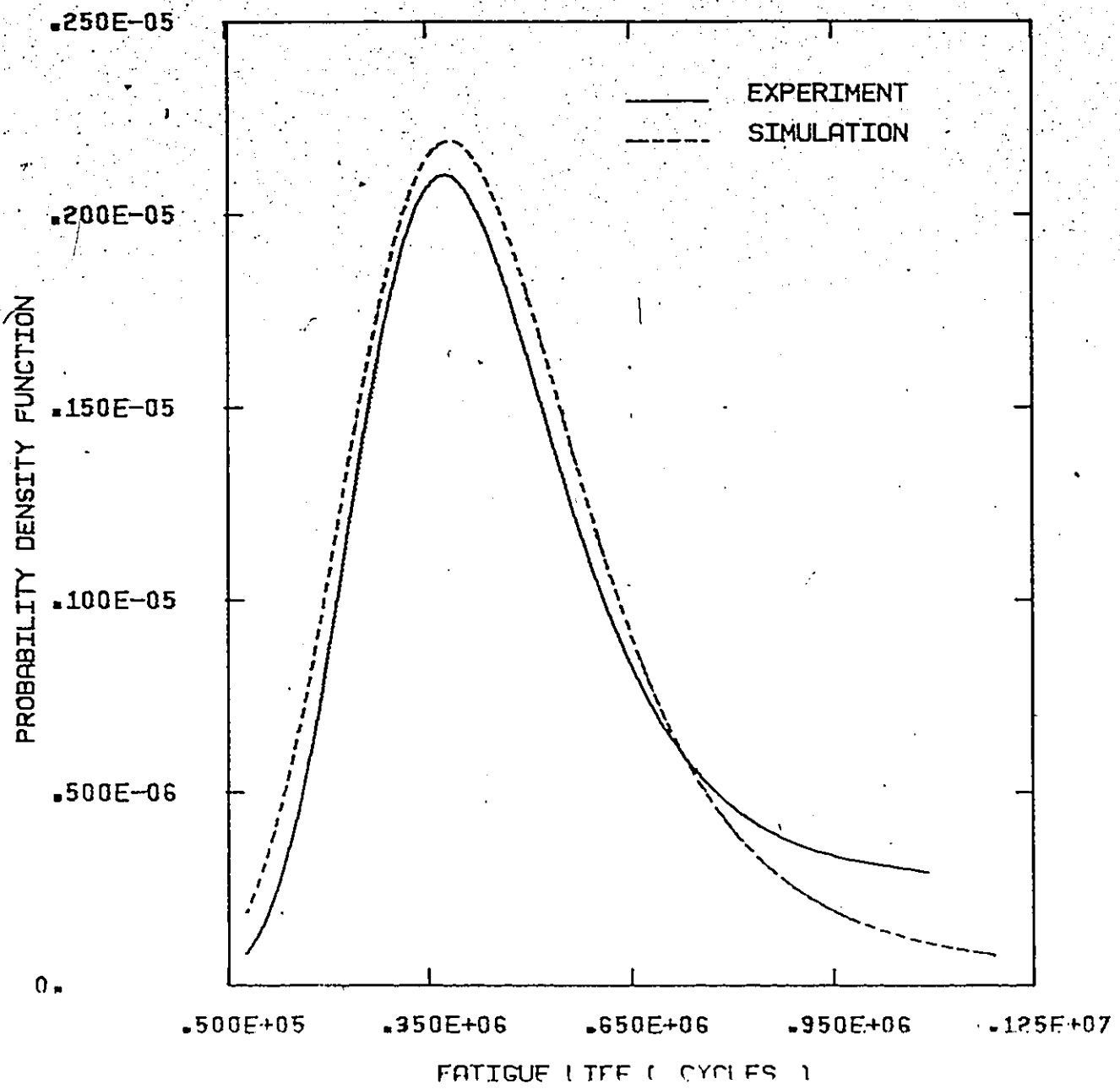

Figure 4.10 Predicted and Experimental Fatigue Life Distribution of SAE 1008 Steel Subjected to Sinusoidal Constant Amplitude Loading.

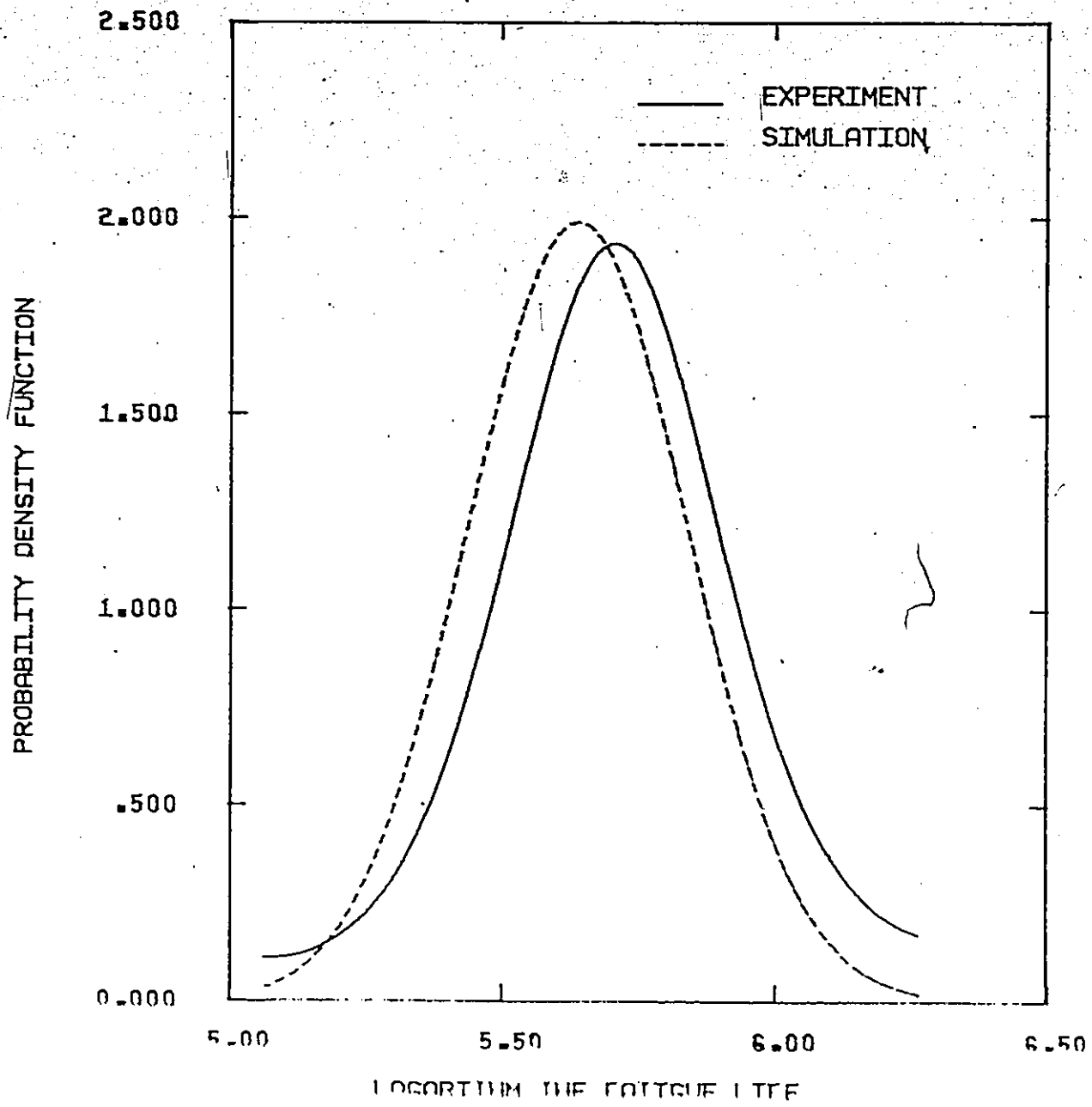

Figure 4.11 Predicted and Experimental Distribution of logarithm the Fatigue Life of SAE 1008 Steel Subjected to Sinusoidal Constant Amplitude Loading.

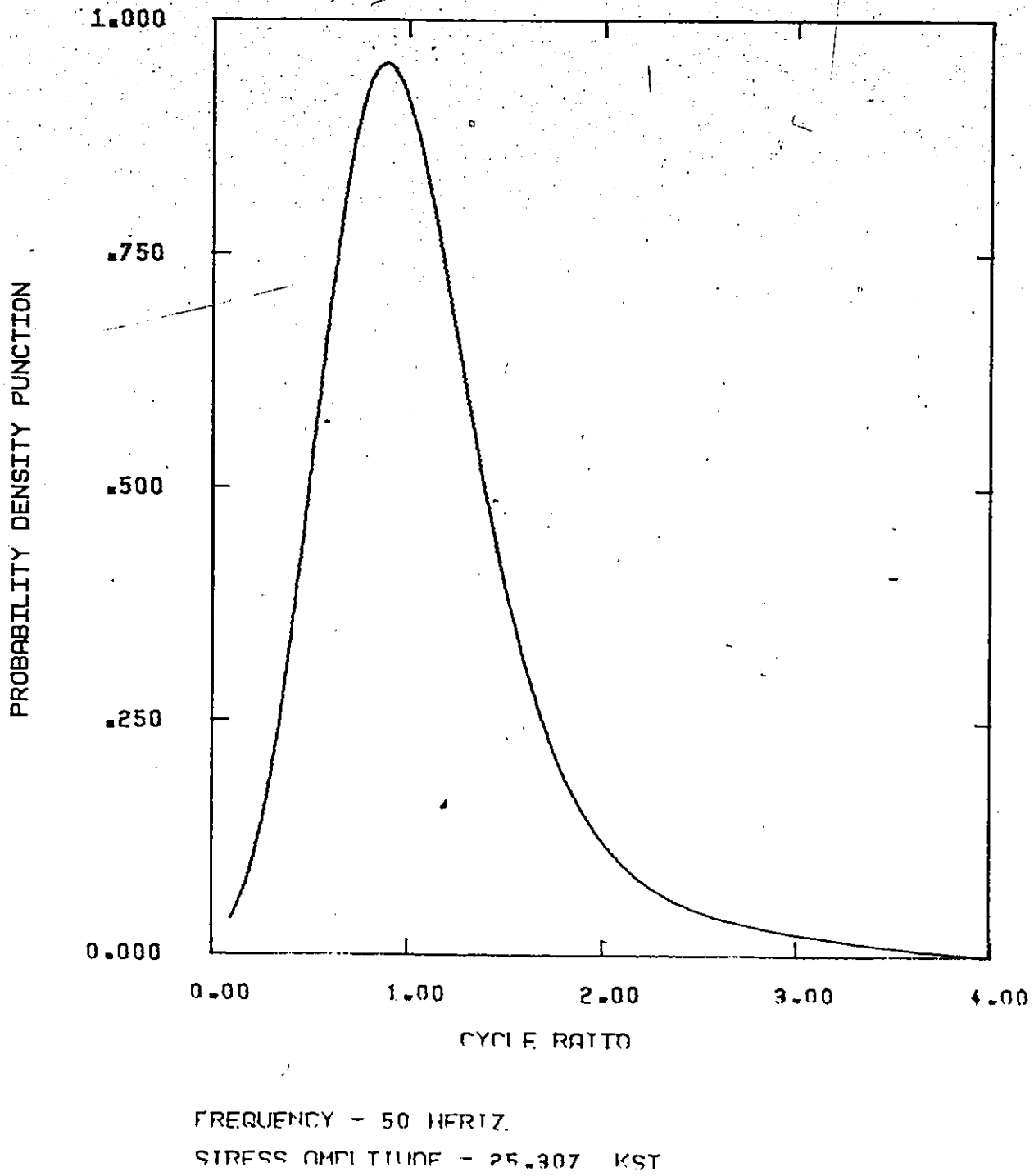

Figure 4.12 The Predicted Cycle Ratio Distribution of SAE 1008 Steel Subjected to Sinusoidal Constant Amplitude Loading.

TABLE 4.2 COMPARISON OF EXPERIMENTAL AND PREDICTED FATIGUE LIFE DISTRIBUTIONS OF CONSTANT AMPLITUDE SINUSOIDAL LOADING FOR SAE 1008 STEEL

	MEAN VALUE			STANDARD DEVIATION $\hat{S}$			COEFFICIENT OF VARIATION $\hat{S}/\mu$	
	Experiment E	Prediction P	Error % $\frac{P-E}{E}$x100	Experiment E	Prediction P	Error % $\frac{P-E}{E}$x100	Experiment	Prediction
Fatigue Life (Cycles	5.354435x10^{5}	4.360756x10^{5}	-9.22	2.619038x10^{5}	2.324452x10^{5}	-11.25	0.489	0.478
Logarithm The Fatigue Lif	5.673879	5.641644	-0.57	0.2320677	0.1976277	-14.84	0.041	0.035
Cycle Ratio n/		1.113402			0.532438			0.478

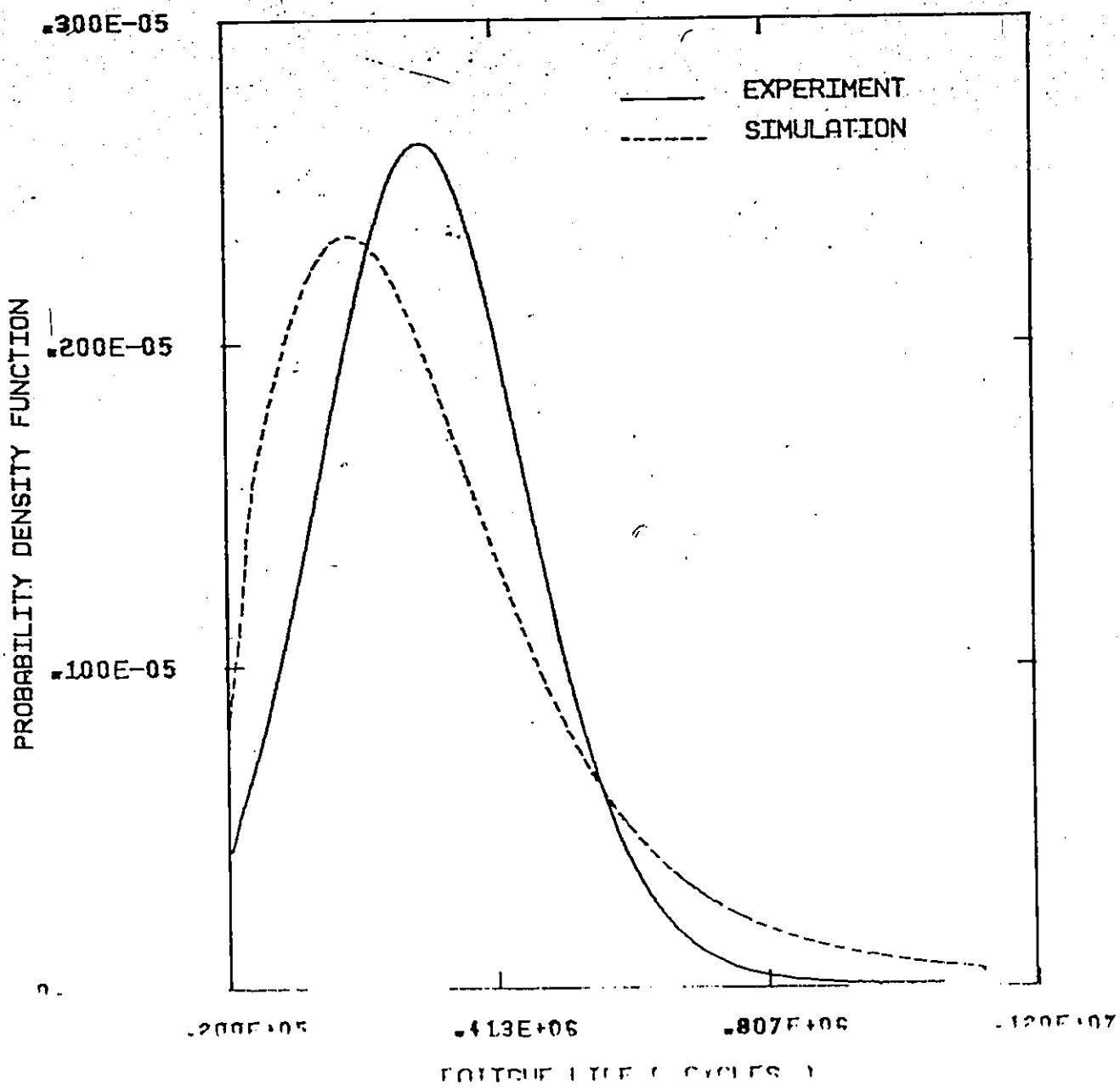

Figure 4.19 Predicted and Experimental Fatigue Life Distribution of SAE 1008 Steel Subjected to Hi Lo Sinusoidal Block Loading

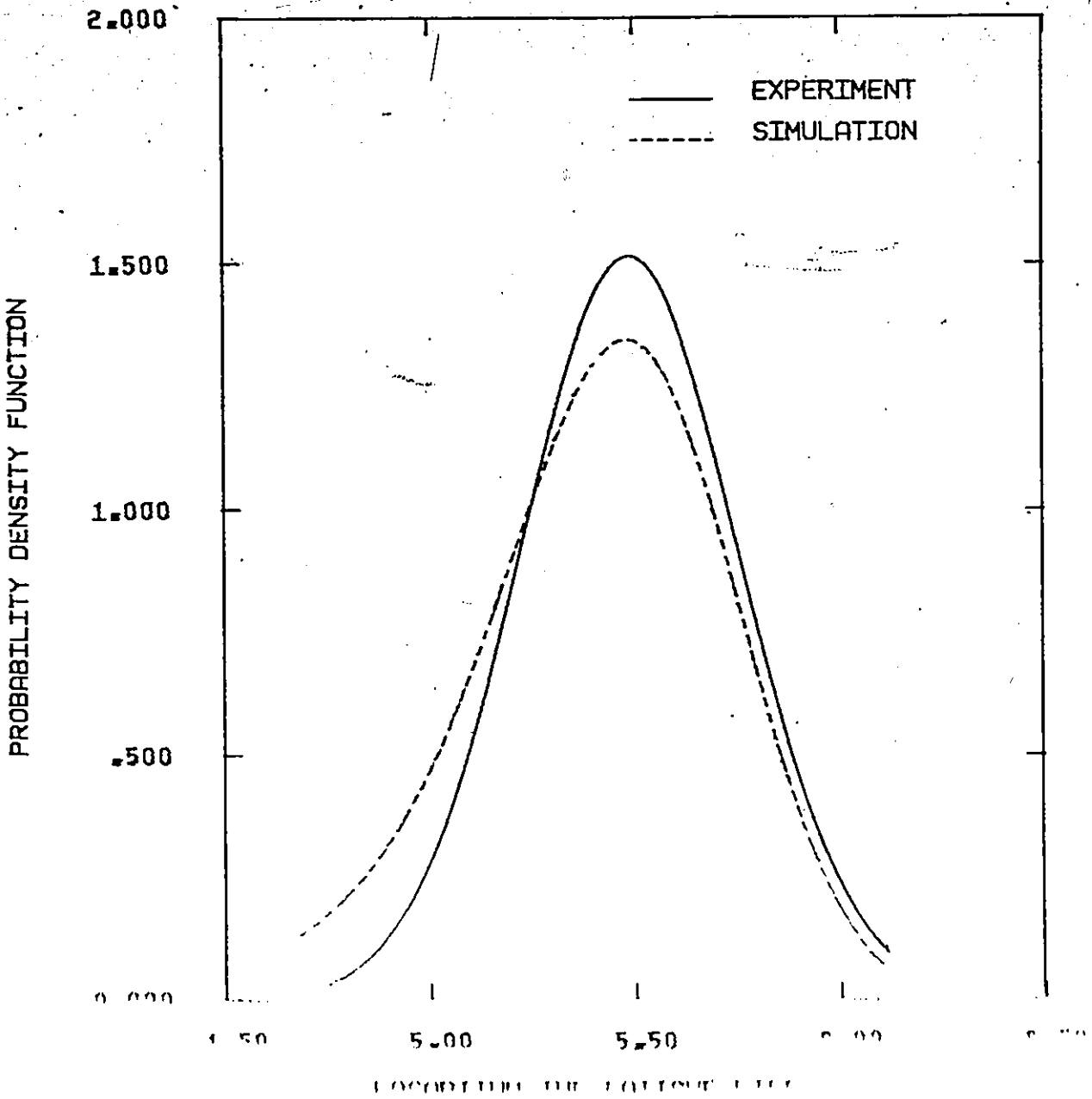

Figure 4.11 Theoretical and Experimental Distribution of Logarithm the Fatigue Life of SAE 1008 Steel Subjected to Two Level Sinusoidal Block Loading

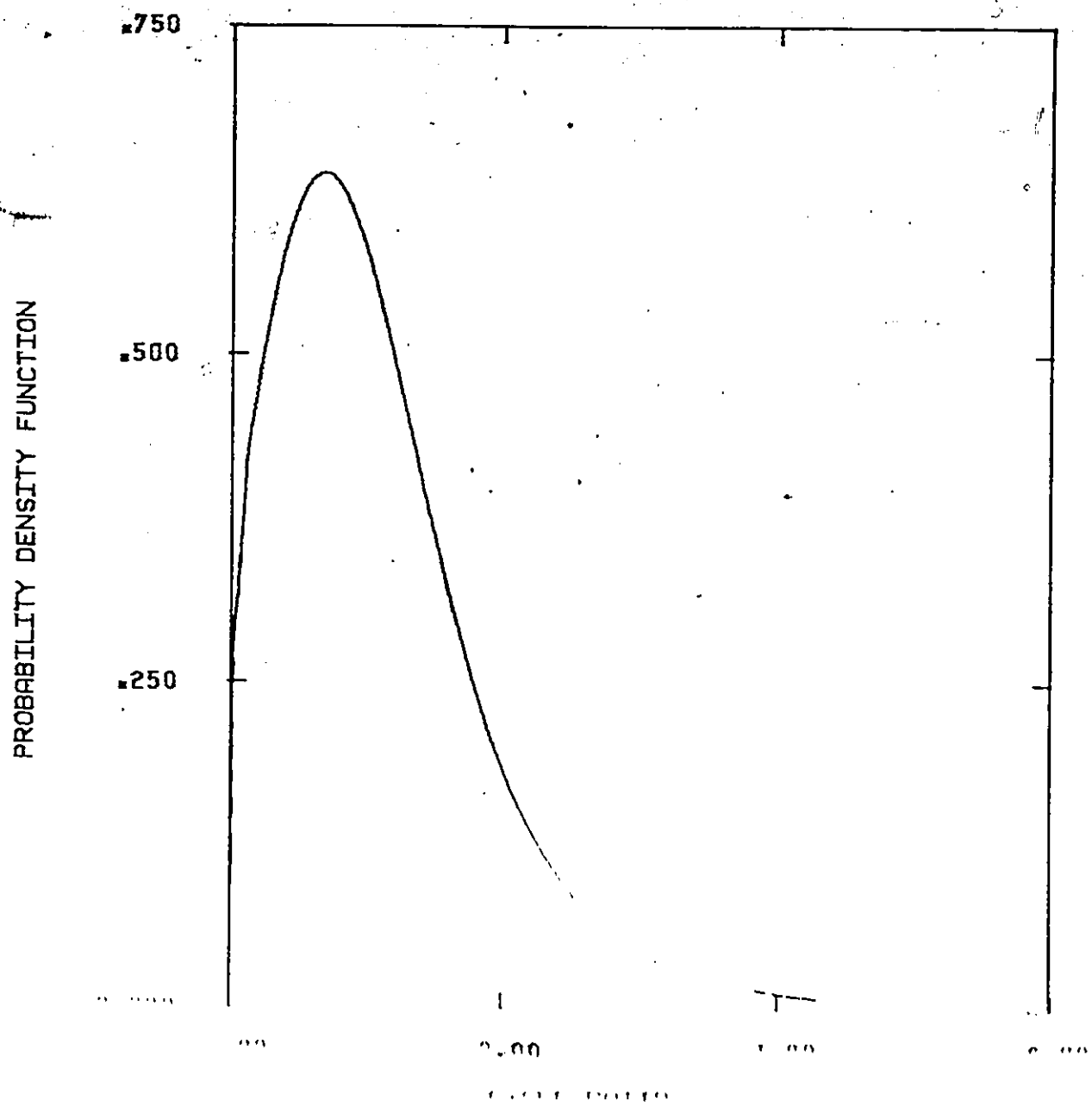

FREQUENCY = 50 HERTZ
FIRST STRESS LEVEL = 27.838 KSI 85000 CYCLE
SECOND STRESS LEVEL = 25.307 KSI L. FAILURE

[illegible] of 4L 1008 Steel Subjected to [illegible] Sinusoidal Block Loading

TABLE 4.3 COMPARISON OF EXPERIMENTAL AND PREDICTED FATIGUE LIFE DISTRIBUTIONS OF HI-LO BLOCK FORM LOADING FOR SAE-1008 STEEL

	MEAN VALUE			STANDARD DEVIATION $\hat{S}$			COEFFICIENT OF VARIATION $\hat{S}/\mu$	
	Experiment E	Prediction P	Error % $\frac{P-E}{E}x100$	Experiment E	Prediction P	Error % $\frac{P-E}{E}x100$	Experiment	Prediction
Fatigue Life (Cycles)	3.637443x10^5	3.323059x10^5	-8.64	$2.325332x10^5$	$2.223921x10^5$	-4.36	0.639	0.674
Logarithm The Fatigue Life	5.486266	5.427454	-1.07	0.2654115	0.295354	+11.28	0.048	0.054
Cycles Ratio n		1.18099			0.790365			0.669

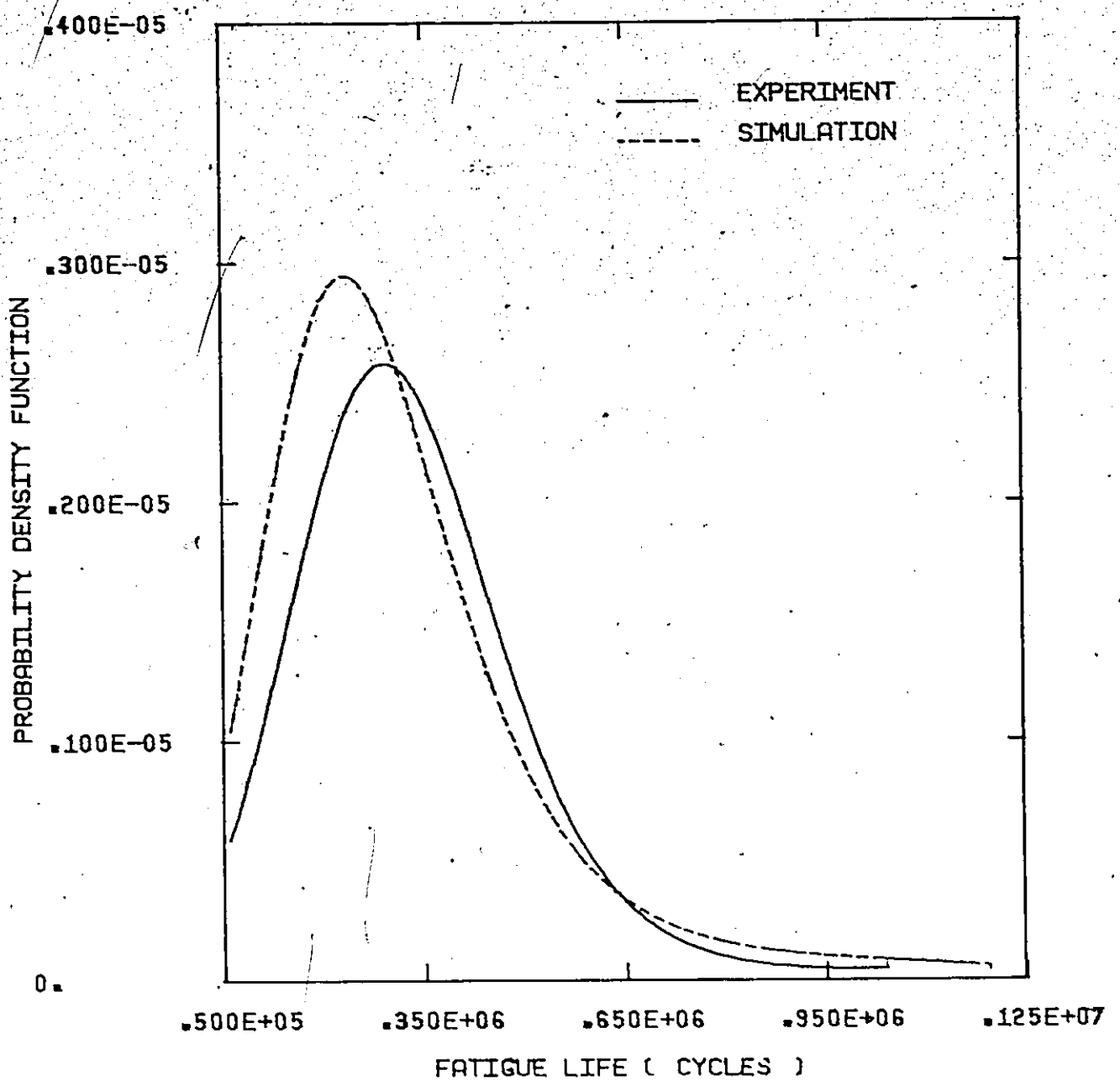

FREQUENCY = 50 HERTZ

FIRST STRESS LEVEL	= 25.307 KSI	150000 CYCLE
SECOND STRESS LEVEL	= 27.838 KSI	85000 CYCLE
THIRD STRESS LEVEL	= 25.307 KSI	TILL FAILURE

Figure 4.16 Predicted and Experimental Fatigue Life Distribution of SAE 1008 Steel Subjected to Lo-Hi-Lo Sinusoidal Block Loading.

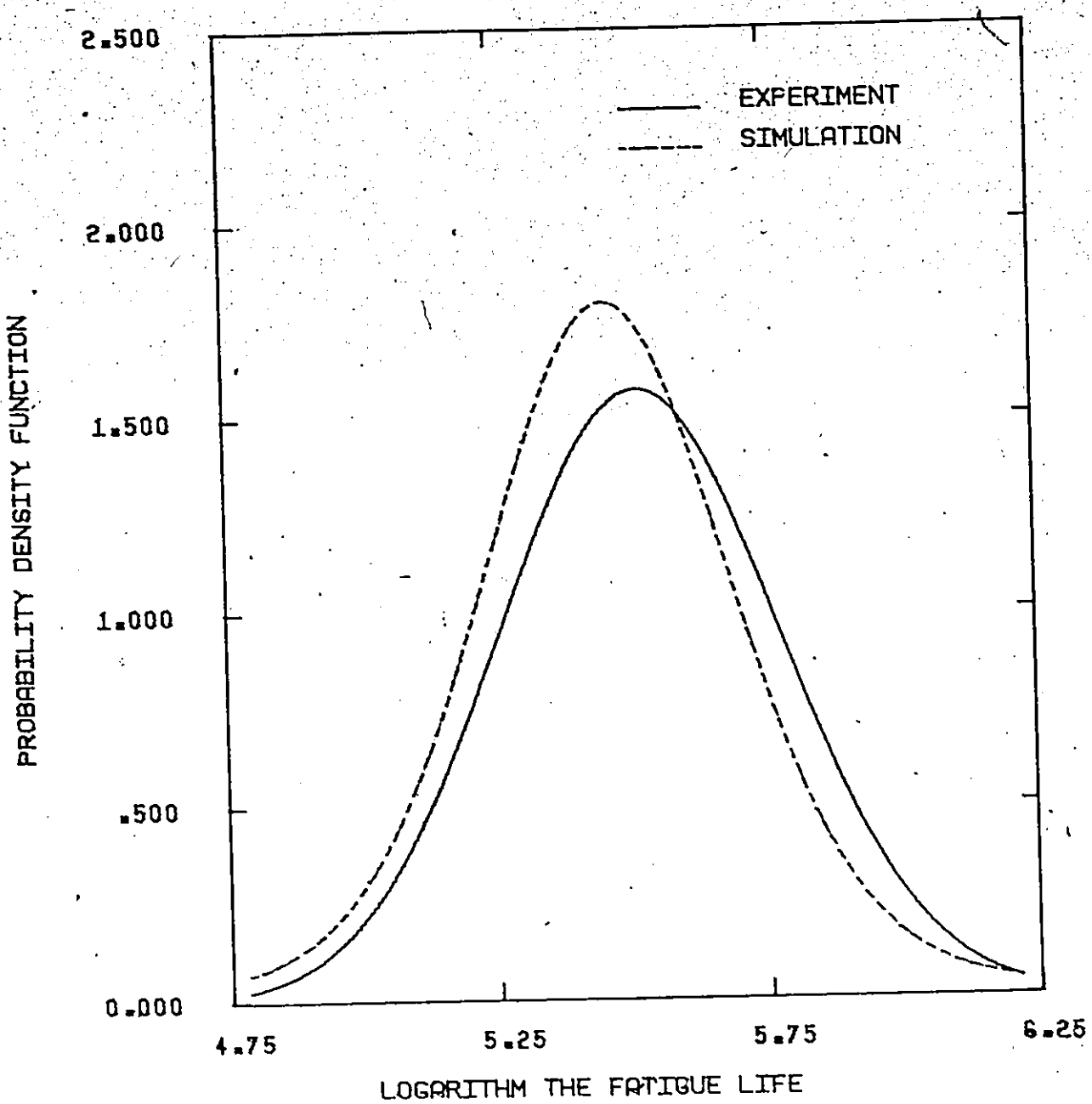

FREQUENCY = 50 HERTZ

FIRST STRESS LEVEL	= 25.307 KSI	150000 CYCLE
SECOND STRESS LEVEL	= 27.838 KSI	85000 CYCLE
THIRD STRESS LEVEL	= 25.307 KSI	TILL FAILURE

Figure 4.17 Predicted and Experimental Distribution of Logarithm the Fatigue Life of SAE 1008 Steel Subjected to Lo-Hi-Lo Sinusoidal Block Loading.

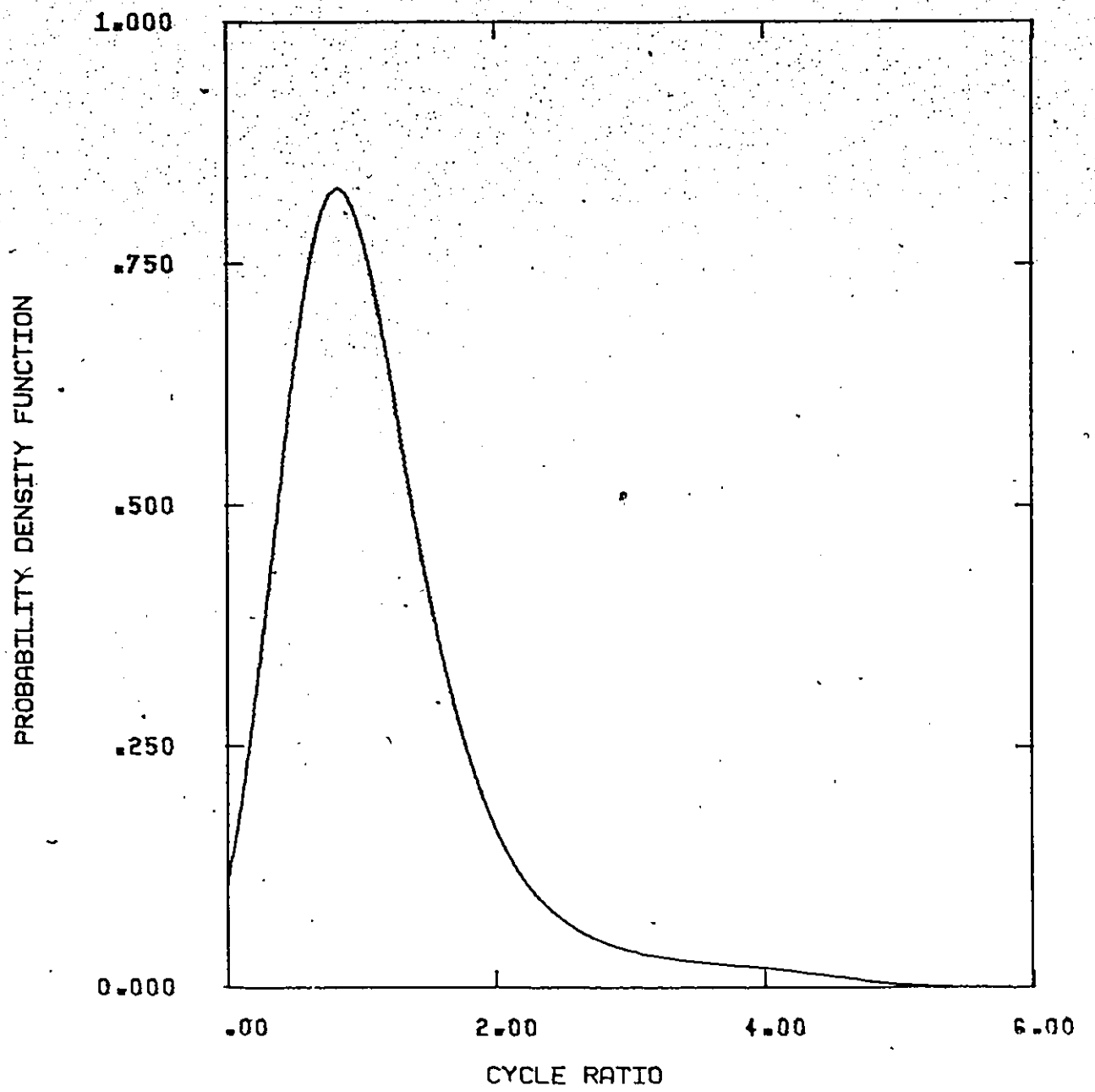

FREQUENCY = 50 HERTZ .

FIRST STRESS LEVEL	= 25.307 KSI	150000 CYCLE
SECOND STRESS LEVEL	= 27.838 KSI	85000 CYCLE
THIRD STRESS LEVEL	= 25.307 KSI	TILL FAILURE

Figure 4.18 The Predicted Cycle Ratio Distribution of SAE 1008 Steel Subjected to Lo-Hi-Lo Sinusoidal Block Loading.

TABLE 4.4 COMPARISON OF EXPERIMENTAL AND PREDICTED FATIGUE LIFE DISTRIBUTIONS OF LO-HI-LO BLOCK FORM LOADING FOR SAE 1008 STEEL

	MEAN VALUE μ			STANDARD DEVIATION $\hat{S}$			COEFFICIENT OF VARIATION $\hat{S}/\mu$	
	Experiment E	Prediction P	Error % $\frac{P-E}{E}x100$	Experiment E	Prediction P	Error % $\frac{P-E}{E}x100$	Experiment	Prediction
Fatigue Life (Cycles)	$3.808086x10^5$	$3.538003x10^5$	-7.09	$2.41849x10^5$	$2.031625x10^5$	-15.99	0.635	0.574
Logarithm The Fatigue Life	5.50737	5.493584	-0.25	0.2558204	0.208654	-18.44	0.046	0.038
Cycle Ratio n/N		1.25738			0.722044			0.547

4.3.3 Comparison of Theoretical and Experimental Distributions

Some comments can be made based on examining the experimental results and the theoretical predictions.

(i) It is evident that the model always predicts life distributions which are continuous, unimodal, and slightly skewed to the right.

(ii) It is clearly observed that the predicted distributions compare favorably well with those experimentally found. The predictions tend to slightly underestimate both the mean life and the standard deviation in most of the cases.

(iii) The cycle ratio distribution is defined for the different cases. The mean values varied between 1.18 and 1.11. The minimum cycle ratio ranged between .16 and .414 while maximum cycle ratios between 5.18 and 5.84 were obtained. These results are borne out by the observations of many researchers and agree well with their published results (e.g., [82]). The predicted cycle ratio distribution is not normal but rather skewed to the right. The first four central moments and the exponential which fits its probability density function are given in Appendix C.

(iv) Linear cumulative damage rule combined with simulated probabilistic stress life curves accurately predicted failure of specimens used in these test series.

(v) Monte Carlo simulation technique using the endurance stress and fatigue strength coefficient distributions,

which reflect the statistical variations of material properties, proved successful.

(vi) It is to be noticed that the proposed model predicted shorter life for the Hi-Lo load program compared with that predicted for the Lo-Hi-Lo program. This indicates that the suggested model is sensitive to the load sequence effects.

(vii) The computer simulation is efficient. A single run which includes theoretical prediction, analysis of experimental and theoretical results, definition and plotting of five probability density functions uses about 70 CP seconds, at a cost of less than $10.

CHAPTER 5

NARROW BAND RANDOM FATIGUE TESTS

5.1 Introduction

The powerful new technique of probabilistic analysis is rapidly becoming recognized as a valid approach to the evaluation of fatigue life for metal structures. The use of this approach requires the determination of a statistically defined load spectrum for the component in question. It is now generally agreed upon that the source of loads, such as atmospheric turbulence, road shock, and propellant combustion, is properly represented by a continuous, random process.

Swanson in his survey of random load fatigue testing [11], reviewed and discussed the different techniques. He showed that information concerning the highest load amplitude is, in itself, no longer sufficient. In principle, the complete load-time history should be known. This is generally impossible to achieve, therefore methods must be developed which describe the loading by means of statistical parameters. These parameters should, of course, be relevant to the process of fatigue damage accumulation. Knowledge of the load time function can be obtained through direct measurements on structures in service. These measurements, together with the function for which a new structure is intended and expected

future developments, are used to predict the load-time history to which the structure will be subjected during its planned service life. Figure 5.1 illustrates the three basic methods of using the measured load-time data in testing. These methods can be summarized as follows:

(i) The exact reproduction of the registered load-time data in a testing machine. This method, however, excludes the possibility of adjustments arising from future developments. Therefore, it is justified only if the expected usage of the component is identical to that of the instrumented one.

(ii) Reduction of the load-time function to a load-spectrum by means of the different counting methods. This load spectrum is used to construct a program loading. Adjustments for future changes are possible. However, the counting methods do have an influence on fatigue test results. Tests have shown that none of the counting methods lead to a program loading representative of the original random loading [87]. All program load tests overestimate the actual fatigue life.

(iii) Analogous random load testing by means of statistical parameters derived from the measured load time histories. It was found that the Root Mean Square (RMS), Power Spectral Density (PSD) function, and Probability Density Function (PDF) are important for the description of stationary random loads used in

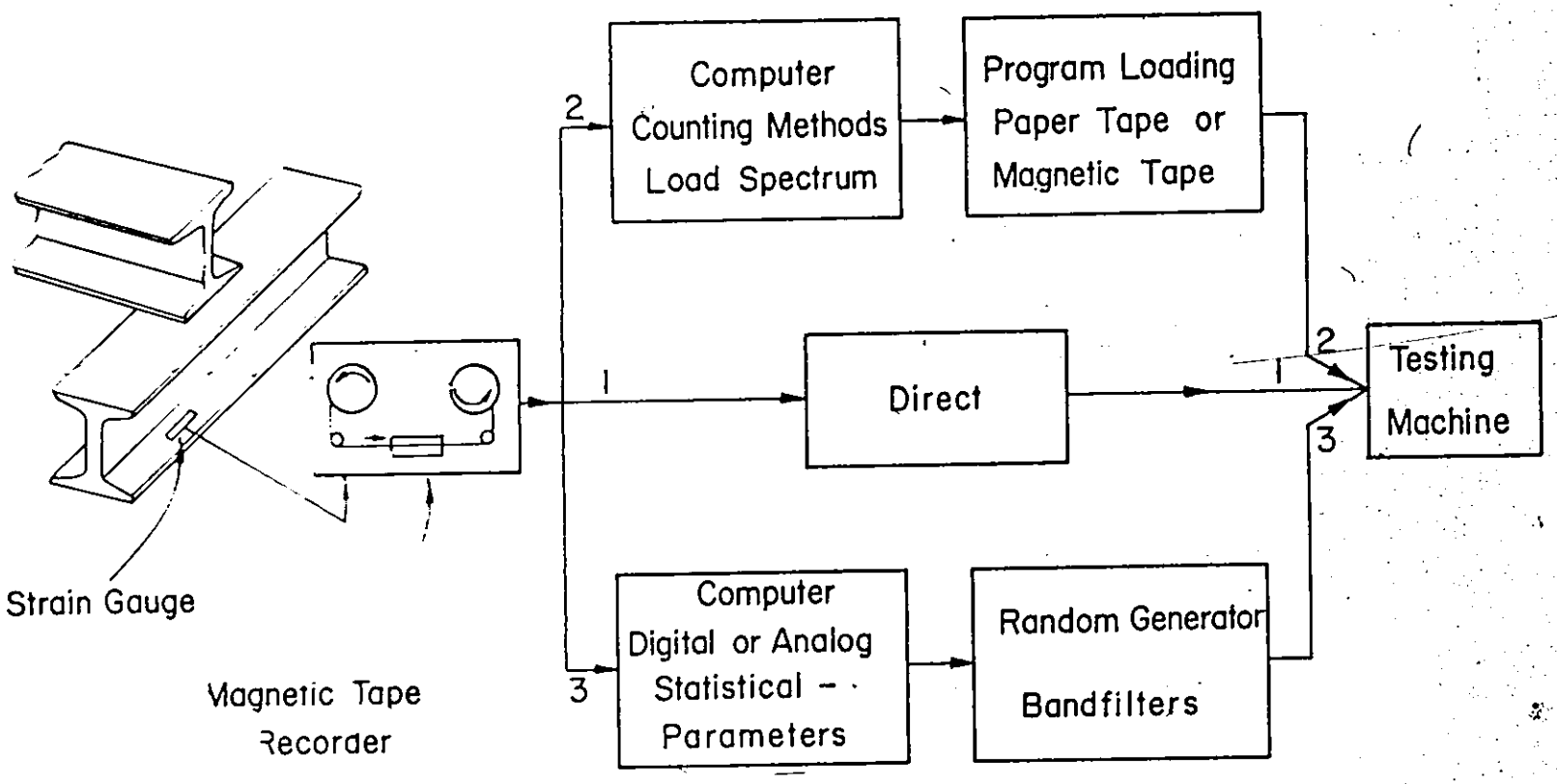

Figure 5.1 Methods of Random Load Testing.

fatigue analysis [11, 83-87].

In this part of the investigation, analogous laboratory narrow band random signal is used to load the specimens. Examples of vital structures which are broad band in response to fatigue loading are comparatively rare. Even when the input loading is a broad band random process, the stress response in practical structures is usually much more "peaked" than the input due to the effect of resonance. Also, the definition of a cycle in a narrow band process is fairly evident. As such, narrow band loading is used more frequently in fatigue analysis than broad band loading.

In this chapter the random fatigue tests are described. The experimental results are analysed and compared with theoretical predictions obtained using the proposed model. The effect of load variability (i.e., standard deviation and shape of PDF) is also studied.

5.2 Experiment

5.2.1 Test Set-up and Specimens

The same test set up shown in Figure 3.17 was used. However, the random test required more measurements than the constant amplitude test. The Bruel and Kjaer noise generator which provided the sine wave for the constant amplitude testing, also provided the narrow band random signal. The noise generator supplies a signal with a Gaussian probability density function and constant power spectrum. The central frequency and RMS values were tuned

manually. The band width can be selected on the noise generator in discrete steps: 10, 30, 100 and 300 Hertz, by further filtering within the generator. The characteristics of the narrow band signal used in this test are as follows:

Central frequency	:	48 Hz
Band width	:	10 Hz

Before each random test was started the center frequency of the noise generator was checked using the frequency counter. The Hewlett Packard correlator is an additional feature of the random test set-up. It was used for on-line analysis of the different random signals and to double check the input RMS value, as will be explained later.

5.2.2 Measurements of Load Parameters and Definition of the Probability Density Function

RMS Strain Level

Since many tests were performed and the digitization process is time consuming, the fastest possible method of adjusting the RMS strain level, without loss in accuracy was desired. An AC vibration meter with a time constant of 30 seconds was found to be very fast and reasonably accurate.

After the output signal stabilized, usually in 30 to 40 seconds, the displacement and force signals were recorded on the tape loop or using the Visicorder for further analysis. The peaks of the displacement signal were digitized using

a Ruscom Logics graph digitizer shown in Figure 5.2. The resulting digitized data spanned about 30 seconds of real time data for each test. The displacement values were converted to strain using the displacement-strain calibration. Use was made of the cyclic stress-strain curve to convert the strain amplitude to stress amplitudes. A statistical analysis was done to calculate the mean value, the mean square value, the RMS and the variance of the displacement, strain, and stress values. The Correlator was also used to sample the random displacement signal on-line, calculate its autocorrelation function and display it. This process usually takes only a few seconds. The value of the autocorrelation function at zero time delay (τ) is equal to the mean square value of the signal, and was used to check the displacement RMS level. Definitions of the parameters used in the statistical analysis of the different signals are as follows:

$$\text{Mean} = \bar{x} = \frac{1}{n}\sum_{i=1}^{n} x_i \qquad (5.3)$$

$$\text{Variance} = \sigma^2 = \overline{x^2} - (\bar{x})^2 \qquad (5.3)$$

$$\text{RMS value} = \sqrt{\overline{x^2}} \qquad (5.3)$$

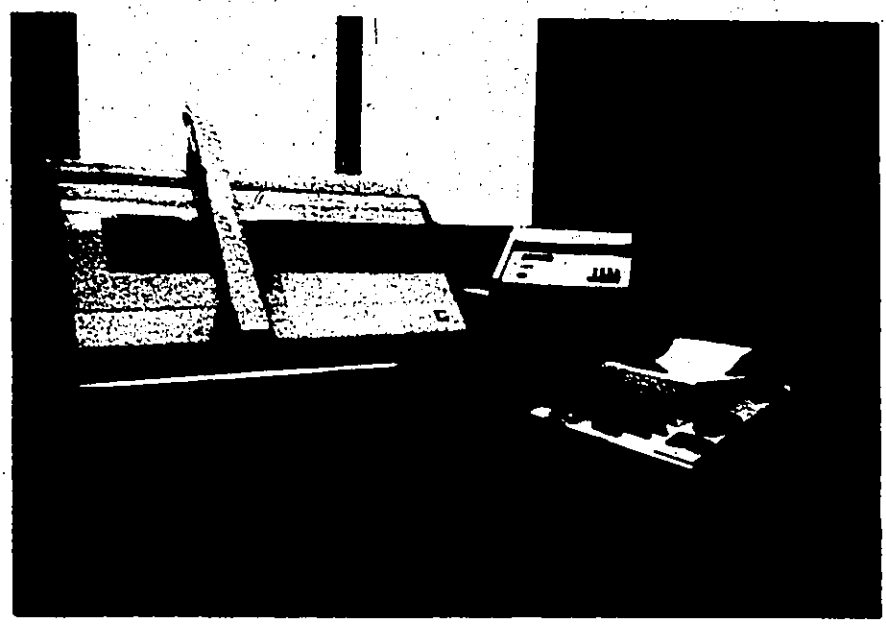

Figure 5.2 Photograph Showing the Ruscom Logics Graph Digitizer.

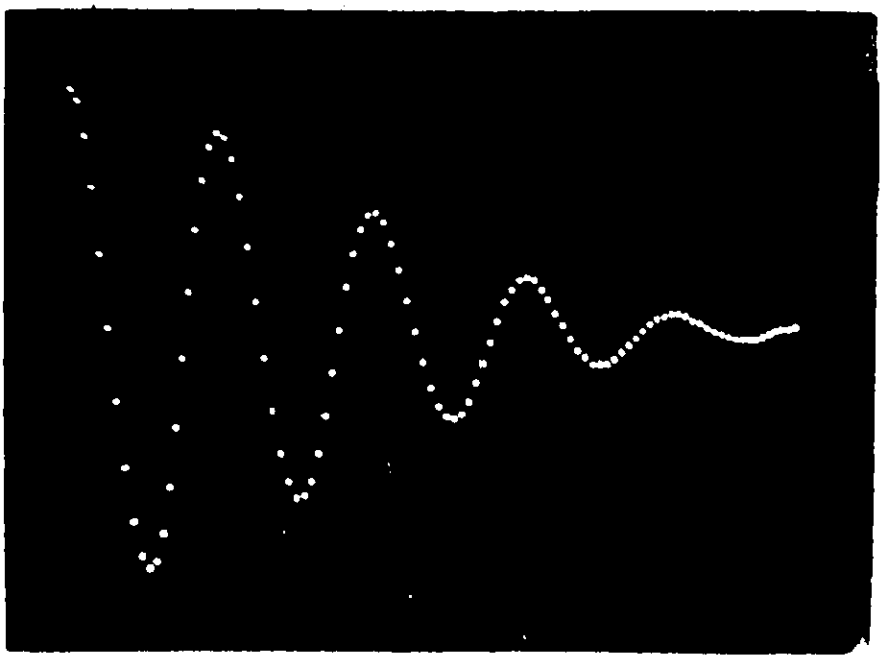

Figure 5.3 Photograph Showing the Auto-Correlation Function of the Displacement.

where σ is the standard deviation.

When the mean value is zero the RMS value of the signal is equal to its standard deviation. The auto-correlation function is given by

$$R_X(\tau) = \lim_{T\to\infty} \frac{1}{T} \int_0^T X(t)\, X(t+\tau)\, dt \qquad (5.5)$$

where

$$\overline{X^2} = R_X(0)$$

$$\overline{X} = \sqrt{R_X(\infty)}$$

Figure 5.3 shows the shape of the displacement autocorrelation function.

Probability Density Functions

Prediction of fatigue life distribution under stationary random loads, as explained in Chapter 2, is based upon knowing the peak probability density function of the applied strain and consequently the stress. The probability distribution of the strain and stress peaks were determined from the recorded displacement signal.

The displacement signal is shown in Figure 5.4. The signal is zero crossing type, the number of positive peaks is equal to the number of negative peaks and the irregularity factor is equal to 1. Figure 5.5 represents the force and strain signals. The Correlator was used to determine the instantaneous ratio distribution of the strain signal. A photograph of this is shown in Figure 5.6. The ratio was recorded in the peak counter, distribution of the strain from the peaks of the displacement signal.

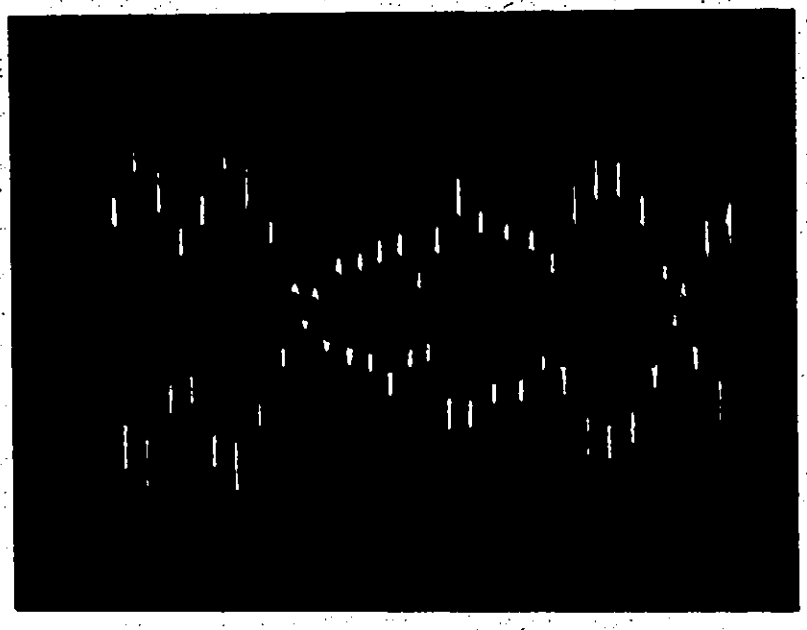

Figure 5.4 Photograph Showing a Time Record of Narrow Band Random Displacement Signal.

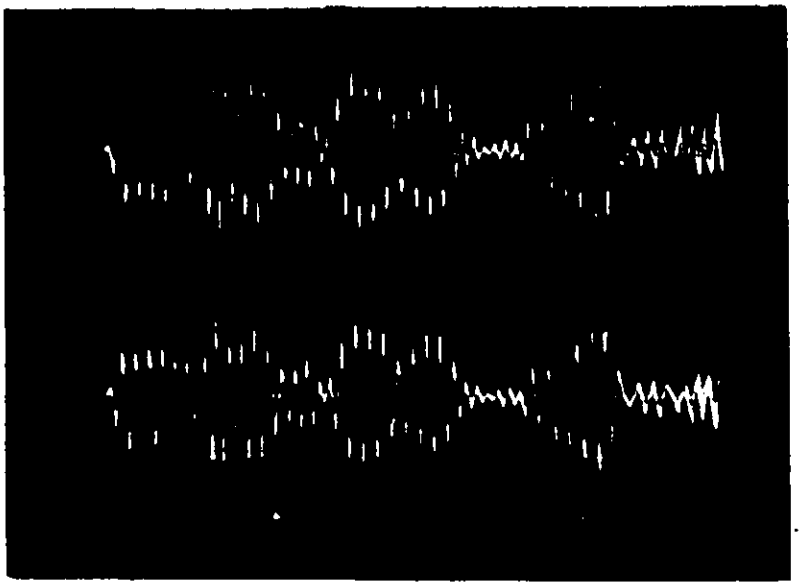

Figure 5.5 Photograph Showing the Force (Upper Trace) and Strain (Lower Trace) Random Signals. Time Scale 0.1 Sec./Division.

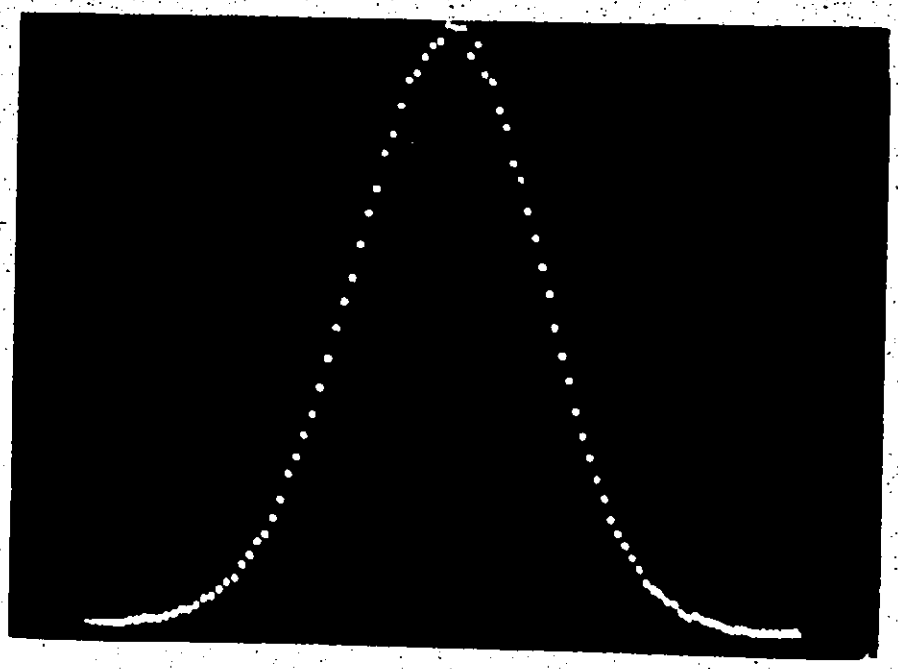

Figure 5.6 Photograph Showing the Instantaneous Value Probability Density Distribution of the Strain Narrow Band Signal.

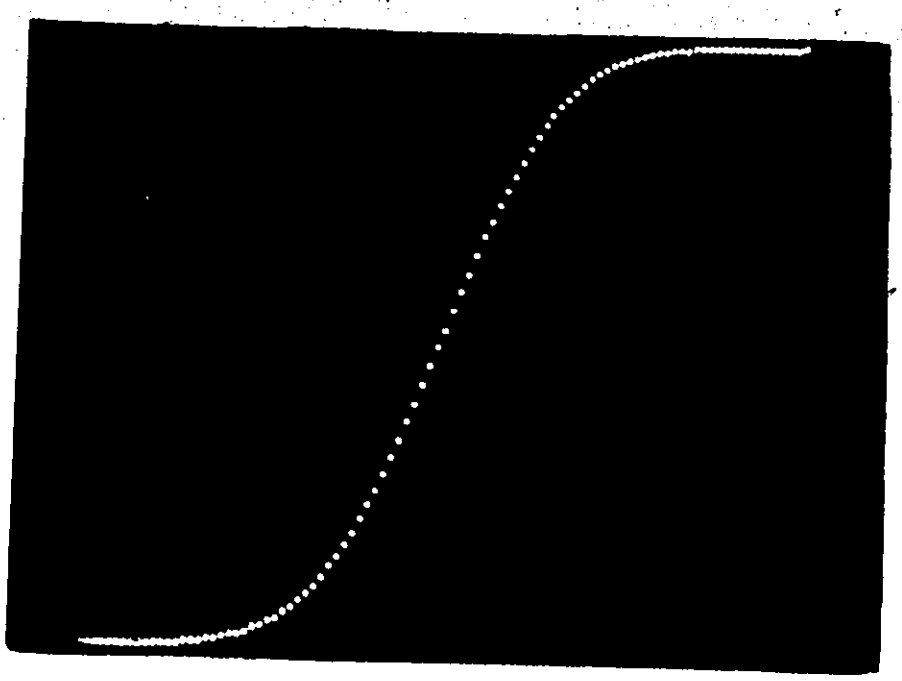

Figure 5.7 Photograph Showing the Cumulative Distribution of the Instantaneous Value of the Strain Signal.

were digitized and converted to stress as explained before.

A statistical analysis was performed to determine the peak stress probability density function. The procedure of calculating the PDF consists of determining a histogram, fitting different theoretical distributions to it and checking the goodness-of-fit of each distribution. The governing equation for the Chi-Squared goodness-of-fit test is,

$$\chi^2_{N-r-1} = \sum_{i=1}^{N} \left[\frac{(O_i - E_i)^2}{E_i}\right] \qquad (5.6)$$

where χ^2_{N-r-1} the calculated Chi-Squared value for (N-r-1) degrees of freedom estimated.

r number of distribution parameters being estimated.

N number of class intervals.

O_i the observed sample frequency in the i^{th} class interval.

E_i expected frequency of the fitted distribution in the i^{th} class interval.

Large χ^2 values indicate a poor fit. If the calculated χ^2 value is less than the tabulated one, the hypothesis that the data represents the fitted distribution is accepted. This hypothesis is rejected if the probability of the tabulated χ^2 value being greater than the calculated value of χ^2 is five percent or less.

The experimental data of the applied peak stress as well as the fitted distributions are shown in Figure 5.8.

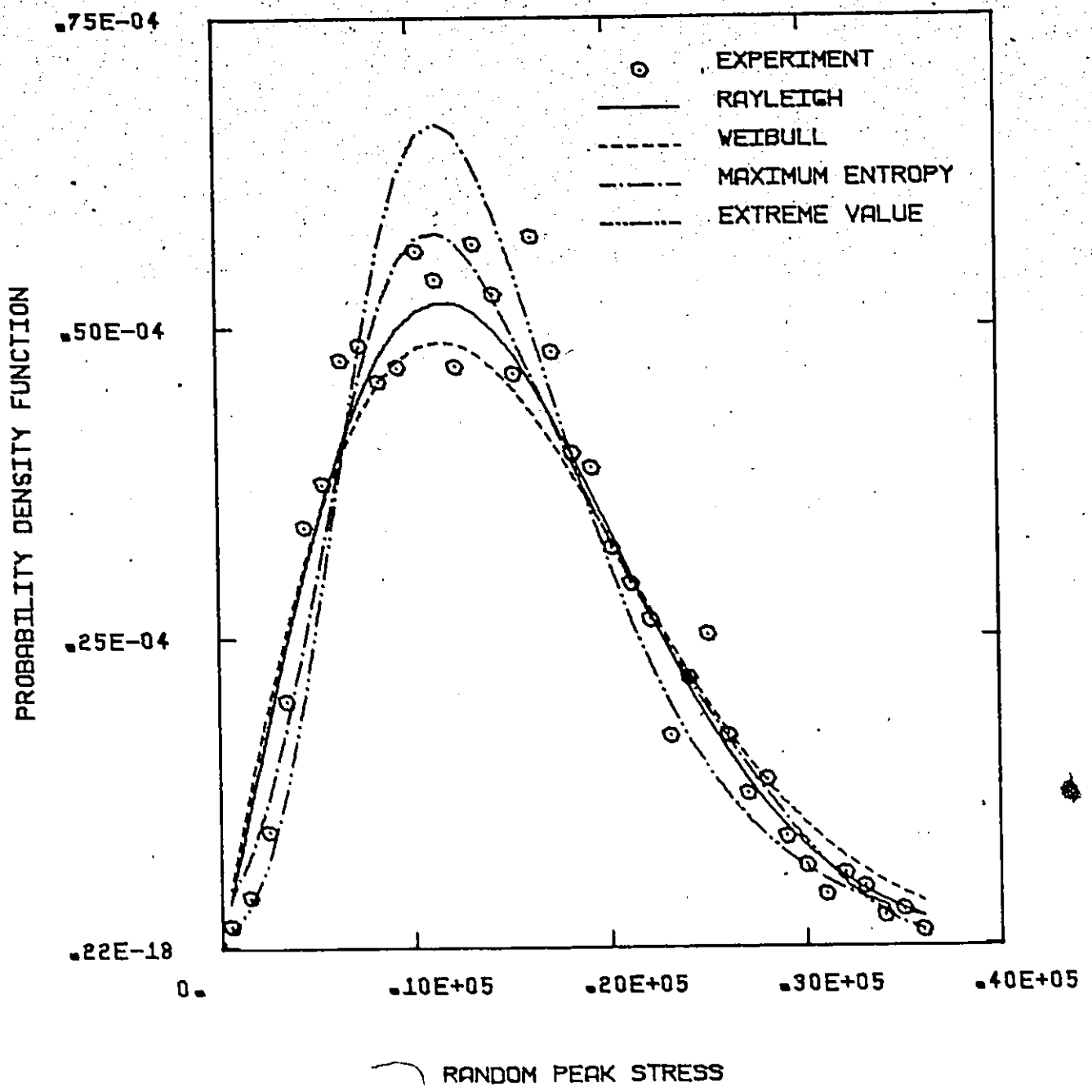

Figure 5.8 Experimental Histogram of the Random Peak Stress and Fitted Distributions.

The data points represent the height of the histogram for each class interval of the peak stress values. Values of the estimated parameters for each fitted distribution and results of χ^2 tests of goodness-of-fit are given in Appendix C. A Rayleigh distribution fitted the data very well. The Maximum Entropy Distribution fit was also accepted but with a calculated χ^2 greater than Rayleigh's. The extreme value and Weibull's fit were poor according to the χ^2 test.

The probability density function of the Rayleigh distribution fitted to the peak stress distribution is given by

$$P(X) = \frac{X}{\sigma^2} e^{-\frac{1}{2}(\frac{X}{\sigma})^2} \tag{5.7}$$

where

X is the peak stress

σ is the standard deviation (σ = 11.65 Ksi)

The distribution has a maximum peak stress of 36.446 Ksi and a zero minimum.

5.3 Results of Narrow Band Random Tests

Forty five specimens were tested in this series. The time-to-failure was recorded for each specimen. For the random signals the definition of a cycle is not generally obvious; thus the counting problem becomes complex. While the evaluations of event-counting methods are voluminous and varied (for example [87] and [88]), there seems to be a growing body of opinion that the most appropriate counting

method is a matter of convenience and experience. It further appears that the validity of this point of view is directly related to the degree of symmetry of the statistical properties of the load-time curve about the mean load. In view of the fact that the positive and negative peaks of the load time history in these tests are symmetric about the zero mean and that the irregularity factor of the signal is one; using the central frequency as an average frequency appears to be a valid assumption. Thus, the cycles-to-failure were calculated by multiplying the time-to-failure in seconds by the value of the central frequency in Hertz. The time-to-failure and cycle-to-failure data is presented in Appendix C.

The experimental data was analysed and fatigue life distributions were established using the Maximum Entropy Function approach. Simulated distributions were obtained using three representations of the random load namely Rayleigh, Maximum Entropy and Weibull. Experimental and predicted life distributions are shown in Figures 5.9 to 5.11.

5.3.1 Comparison of Theoretical and Experimental Distributions

Although the Rayleigh distribution was found to fit the data best, the Maximum Entropy distribution and the Wiebull distribution (which was rejected according to χ^2 test) were also used to predict fatigue life distributions using the proposed model. This was done to show the

importance of determining the load PDF accurately. A summary of the predicted and experimentally found characteristics of the different distributions is presented in Table 5.1. Detailed description of the characteristics of these distributions can be found in Appendix C. Plots of the theoretical and experimental fatigue life distributions are shown in Figures 5.9 to 5.11 The following conclusions can be drawn from these results:

(ii) The experimental results agree reasonably well with the suggested model prediction using a linear cumulative damage rule.

(ii) The shape of the cycle ratio distribution for random loading is similar to that obtained for the sinusoidal loading. The mean value ranged between 1.17 and 1.92. Cycle ratios as low as 0.379 and as high as 5.8 were also obtained. These values of the cycle ratio confirm previous findings by many researchers [87, 98-100].

(iii) The results of the predictions suggest that the probability density function of the load has an appreciable influence on fatigue life. This agrees with experimental findings by Strating [87] who concluded that this function deserves more attention than the exact shape of the power spectrum. Special care should be given, therefore, to field measurements of this function.

(iv) In predicting the fatigue life, the assumption that there is no damage contributed by stress amplitude

TABLE 5.1 COMPARISON OF EXPERIMENTAL AND PREDICTED FATIGUE LIFE DISTRIBUTIONS OF NARROW BAND RANDOM TEST FOR SAE 1008 STEEL

Experimental Results:	Mean	Standard Deviation	Coefficient of Variation
Fatigue Life (Cycles)	6.915836×10^5	2.601878×10^5	0.376
Logarithm Fatigue Life	5.811345	0.1559434	0.027

		RAYLEIGH		MAXIMUM ENTROPY		WEIBULL	
		Prediction	Error %	Prediction	Error %	Prediction	Error %
Fatigue Life (Cycles)	Mean	6.475546×10^5	-6.37	7.915827×10^5	14.46	4.865848×10^5	-29.64
	Standard Deviation	2.512325×10^5	-3.44	3.153478×10^5	21.2	1.861418×10^5	-28.46
	Coefficient of Variation	0.388		0.398		0.383	
Logarithm Fatigue Life	Mean	5.780597	-.53	5.866253	0.94	5.657293	-2.65
	Standard Deviation	0.1631662	4.63	0.1672687	7.26	0.1609758	3.22
	Coefficient of Variation	0.028		0.029		0.028	
Cycle Ratio Σ n/N	Mean	1.566888		1.915392		1.177389	
	Standard Deviation	0.6079071		0.763047		0.4504073	
	Coefficient of Variation	0.388		0.398		0.383	

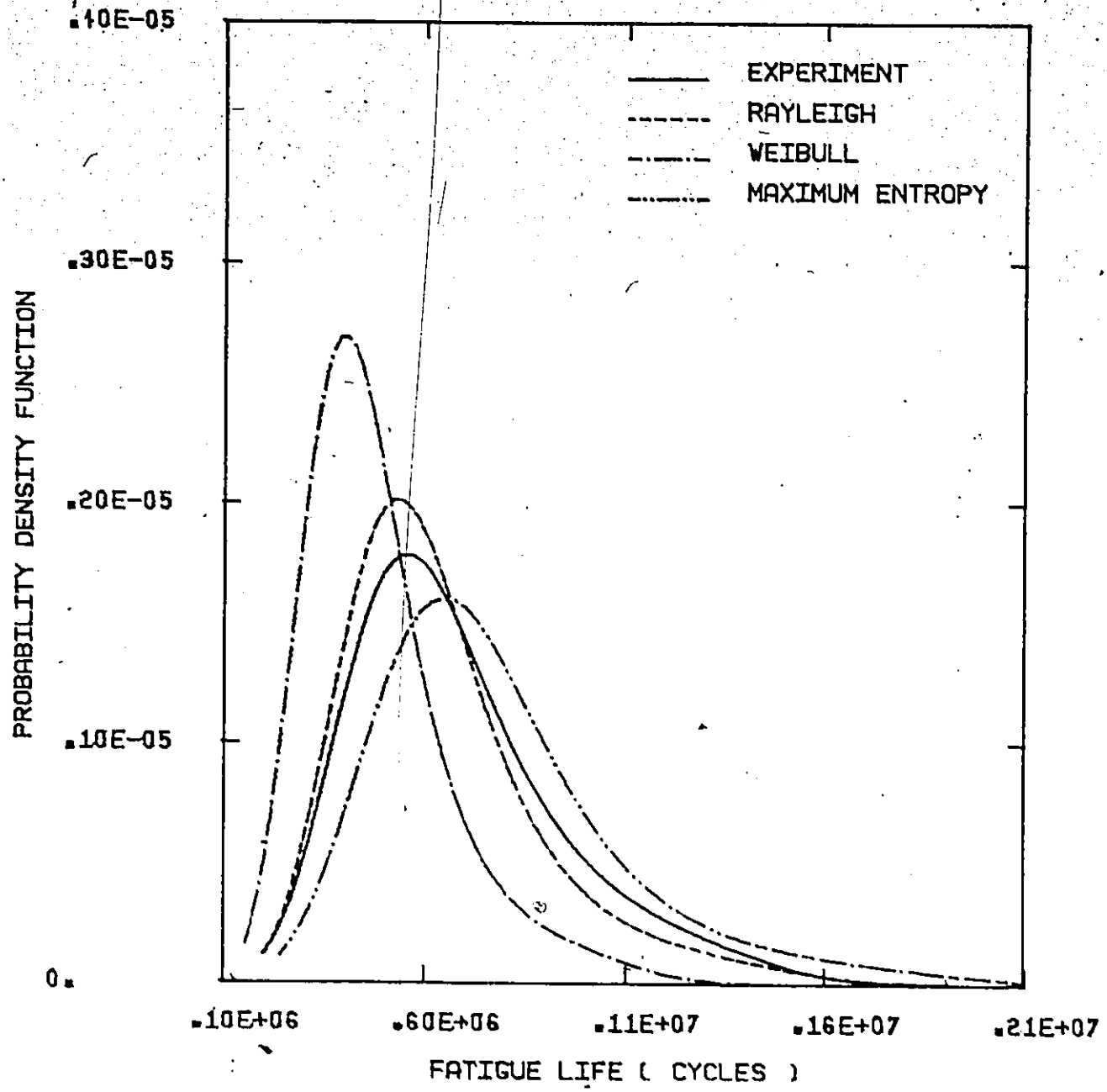

Figure 5.9 Predicted and Experimental Fatigue Life Distributions of SAE 1008 Steel Subjected to Narrow Band Random Loading.

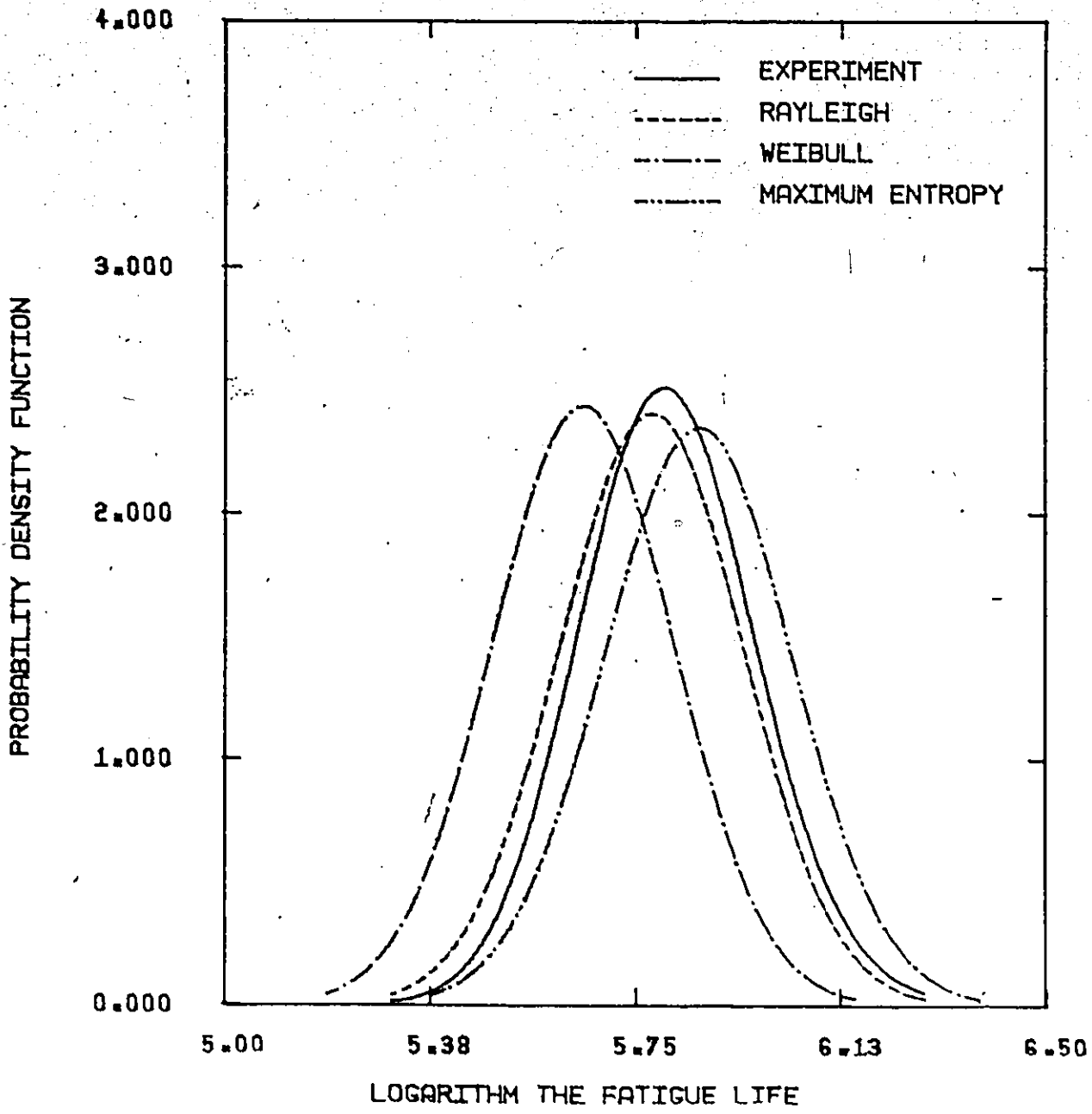

Figure 5.10 Predicted and Experimental Distributions of Logarithm the Fatigue Life of SAE 1008 Steel Subjected to Narrow Band Random Loading.

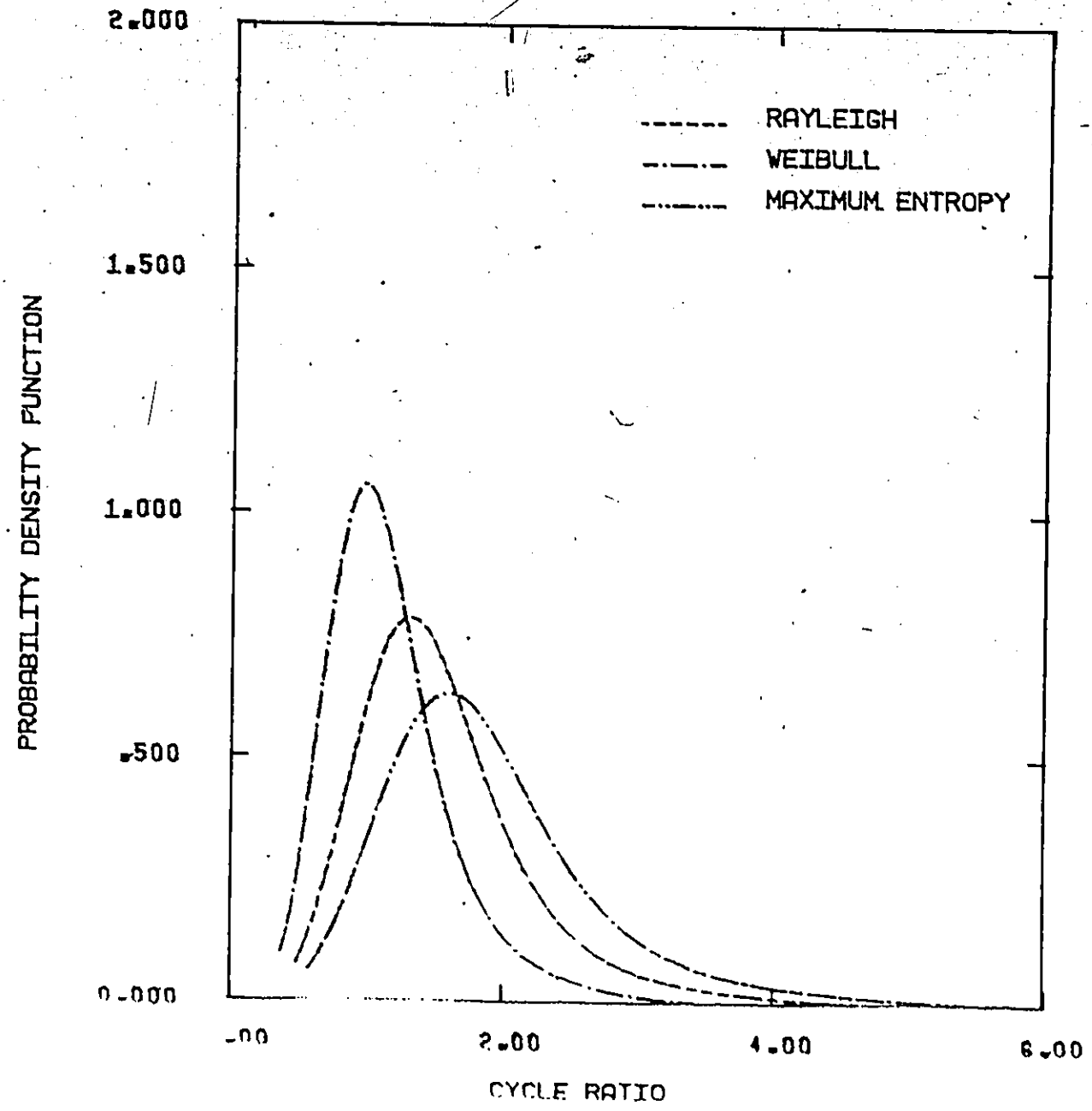

NARROW BAND RANDOM NOISE
CENTRAL FREQUENCY = 48 HERTZ
BAND WIDTH = 10 HERTZ

Figure 5.11 The Predicted Cycle Ratio Distributions of SAE 1008 Steel Subjected to Narrow Band Random Loading.

less than the lower limit of the endurance stress distribution is reasonable because of the relationship between this lower limit and the cyclic yield stress. It is assumed that the lower limit is the mean endurance stress minus four times the standard deviation. Using the values obtained in Chapter 3 the lower limit of endurance stress is 17.47 ksi, a value which is very close to the cyclic yield stress found in Chapter 3 as 18.5 ksi. The cyclic yield stress is the strain below which no hysteretic behaviour is exhibited by the material (i.e., no plastic strain component is present). This fact justifies the damage limit assumption since plastic strain energy associated with the hysteresis loops is directly related to fatigue damage [89-92].

This concludes the presentation of experimental data and theoretical predictions. The following sections present the application of the suggested prediction model to study the effect of load variability on fatigue life.

5.4 Effect of Load Variability on Fatigue Life

5.4.1 Effect on the Mean Life

Digital simulation experiments were performed on SAE-4340 steel the properties of which are listed in Table 2.1. The random loads are normally distributed having known means and standard deviations. Two mean stress values of 68,000 and 101,000 psi were used. The standard deviation

was varied from zero to 10% of the mean stress, that is to say, the maximum coefficient of variation is 0.1. The mean and standard deviation values of both fatigue life and its common logarithm were calculated.

The predicted mean life for different values of the standard deviation of the applied load was always compared with the predicted mean life using an applied load having the same mean value and zero standard deviation (i.e., a constant amplitude load the value of which is equal to the mean value of the random load). The result of this comparison is presented in Figure 5.12. From these results it was found that a standard deviation of up to 1% of the mean applied stress does not significantly alter the mean fatigue life. Increasing the standard deviation beyond this value causes the mean life to slightly drop in a non-linear fashion. This effect was consistent for the two stress levels tested. The amount of reduction in the mean fatigue life with increasing percentage of standard deviation is also shown in Table 5.12.

5.4.3 Effect on the Standard Deviation of the Life Distribution

The analysis performed in this study indicates that the fatigue life variance under random loading is different from that for constant amplitude cyclic loading. The standard deviation of the fatigue life distribution decreases as the scatter of the applied load increases. The reduction is up to 44% for a standard deviation of about 10% of the

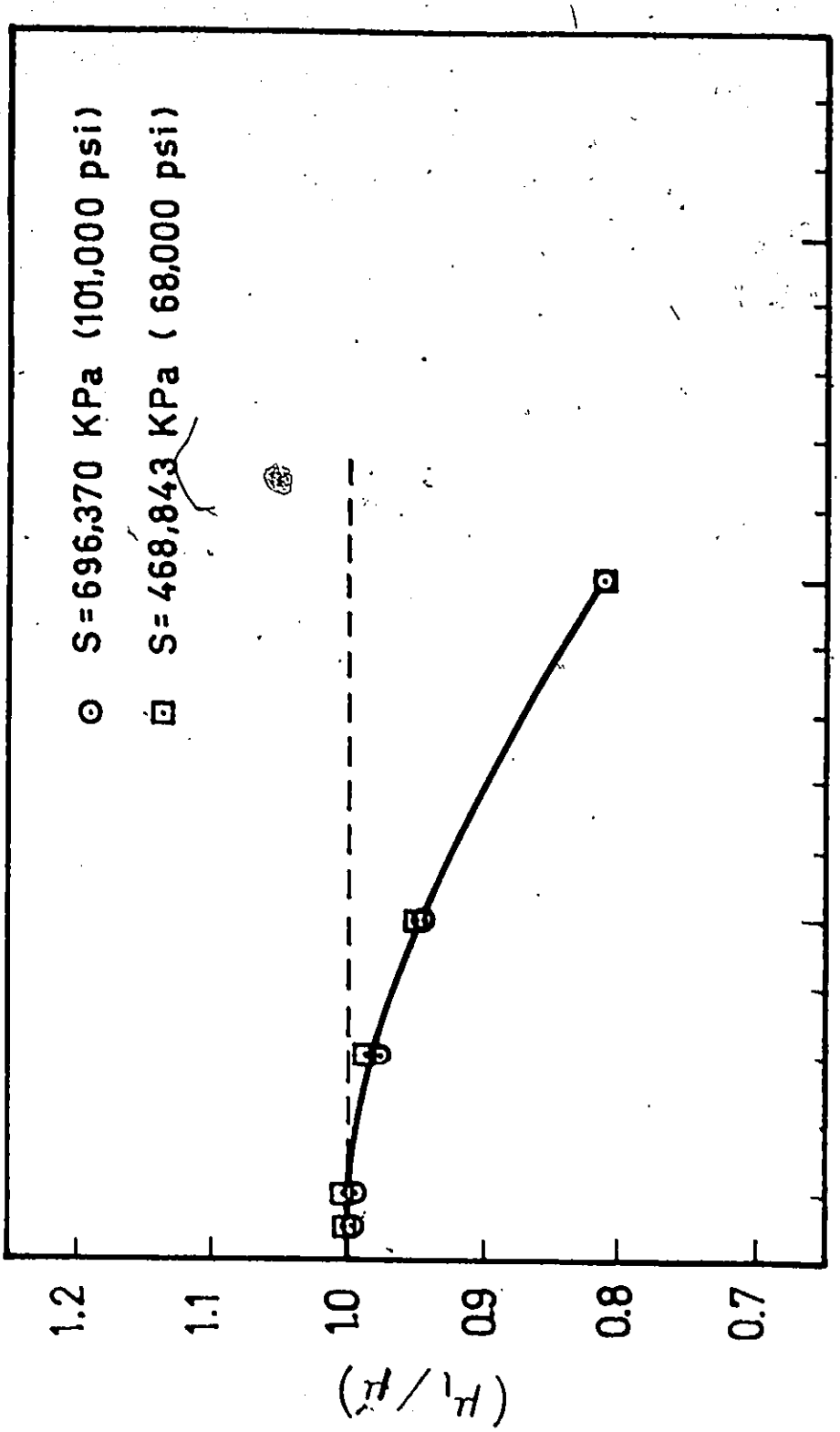

Figure 5.12 Effect of the Applied Stress Variance on Predicted Mean Value of Life at Different Stresses.

mean applied stress. This is an observed fact in random fatigue tests. The results obtained in this study are illustrated in Figure 5.13. These results confirm the conclusions reached by other researchers [93, 94, 101].

Itagaki and Shinozuka [95] found that the randomness in stress history alone cannot reproduce the wide dispersion of fatigue lives as observed in the experiments. This indicates also that the large scatter exhibited in fatigue tests is mostly explained by the scatter in the material properties itself. Only a small amount of this scatter can be explained by the scatter in the applied load.

5.5 Effect of Scatter of Fatigue Strength Coefficient and Endurance Limit on Fatigue Life

The next stage in the present study was directed towards utilizing the developed simulation model to investigate the effect of the randomness of both the endurance limit and the fatigue strength coefficient on the scatter of fatigue life. The effect of the standard deviation of the endurance limit (σ_e) was studied by keeping the value of the standard deviation of the fatigue strength coefficient (σ_f) constantly set at its experimental value while changing σ_e in steps. The same procedure was followed to study the effect of the variance of the fatigue strength coefficient.

5.5.1 Effect of the Standard Deviation of the Fatigue Strength Coefficient

Eight simulation experiments with decreasing values of σ_f and sinusoidal loading were performed on SAE 4340 steel.

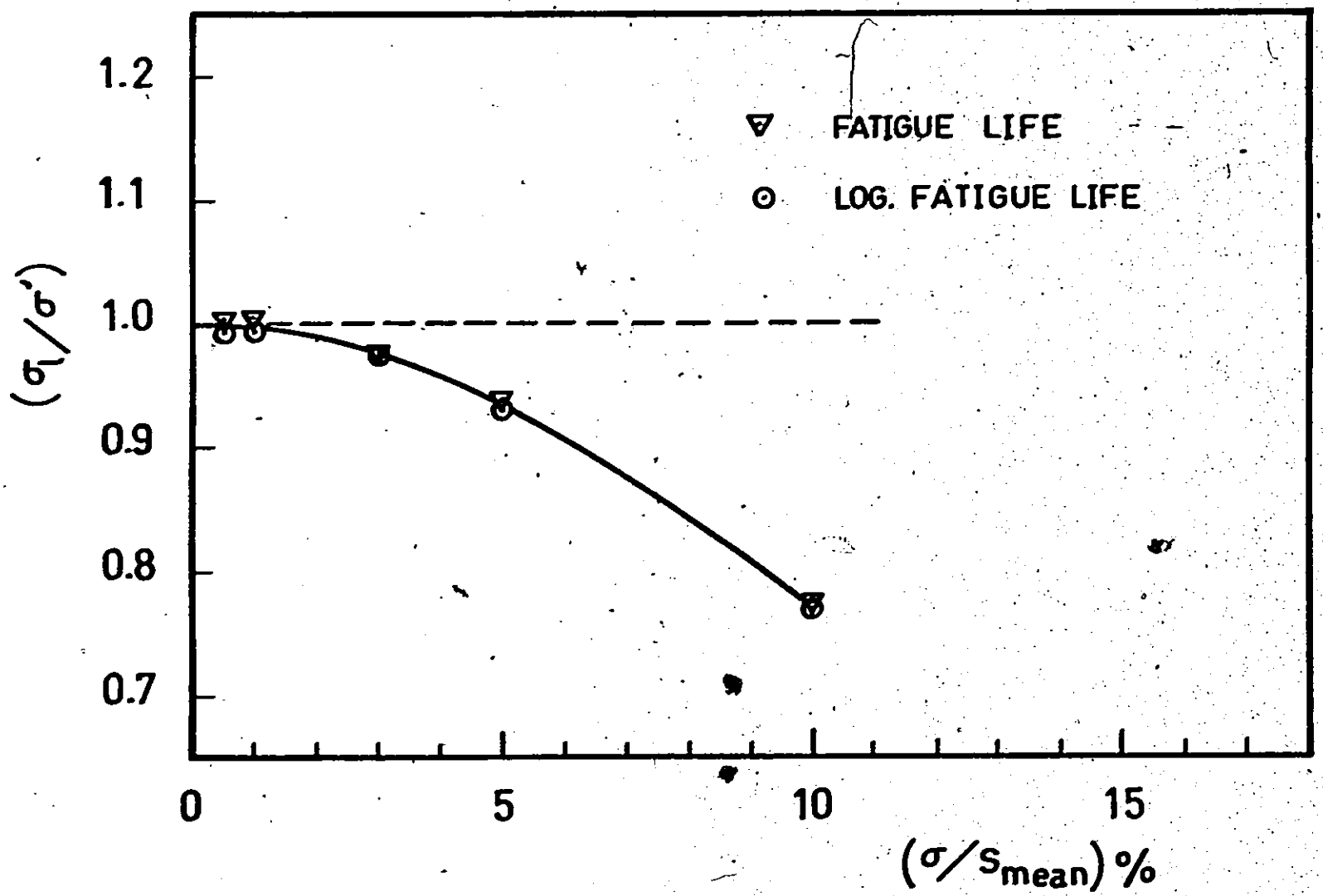

Figure 5.13 Effect of the Applied Stress Variance on the Variance of the Predicted Fatigue Life and its Logarithm at a Stress Level 101,000 psi.

In the last simulation the standard deviation was zero, that is to say, the fatigue strength coefficient S_f' was considered deterministic. The mean and standard deviation of the predicted life distributions for different values of σ_f were compared with those of the predicted life distribution using the experimental value of σ_f. The results of this comparison are examined for distributions of fatigue life and its logarithm.

Examining these results indicates that the errors in determining the mean life resulting from changing σ_f are negligibly small. The maximum error introduced when S_f' is considered deterministic does not exceed + .25% of the mean life predicted using the experimental value of σ_f. The contribution of the randomness of the fatigue strength coefficient to the randomness of the predicted fatigue life variability using the suggested model is shown to be small. The variability of S_f' explains only 2.74% of the variability of the fatigue life. This conclusion shows that any approximation introduced by assuming that the scatter of the fatigue strength coefficient S_f, is equal to the scatter of the ultimate tensile strength or the true fracture stress will not significantly affect the obtained results as shown in Figure 5.14. It also shows that for preliminary design purposes S_f' can safely be considered deterministic.

5.5.2 Effect of the Variance of the Fatigue Endurance Limit

To study this effect five simulation experiments

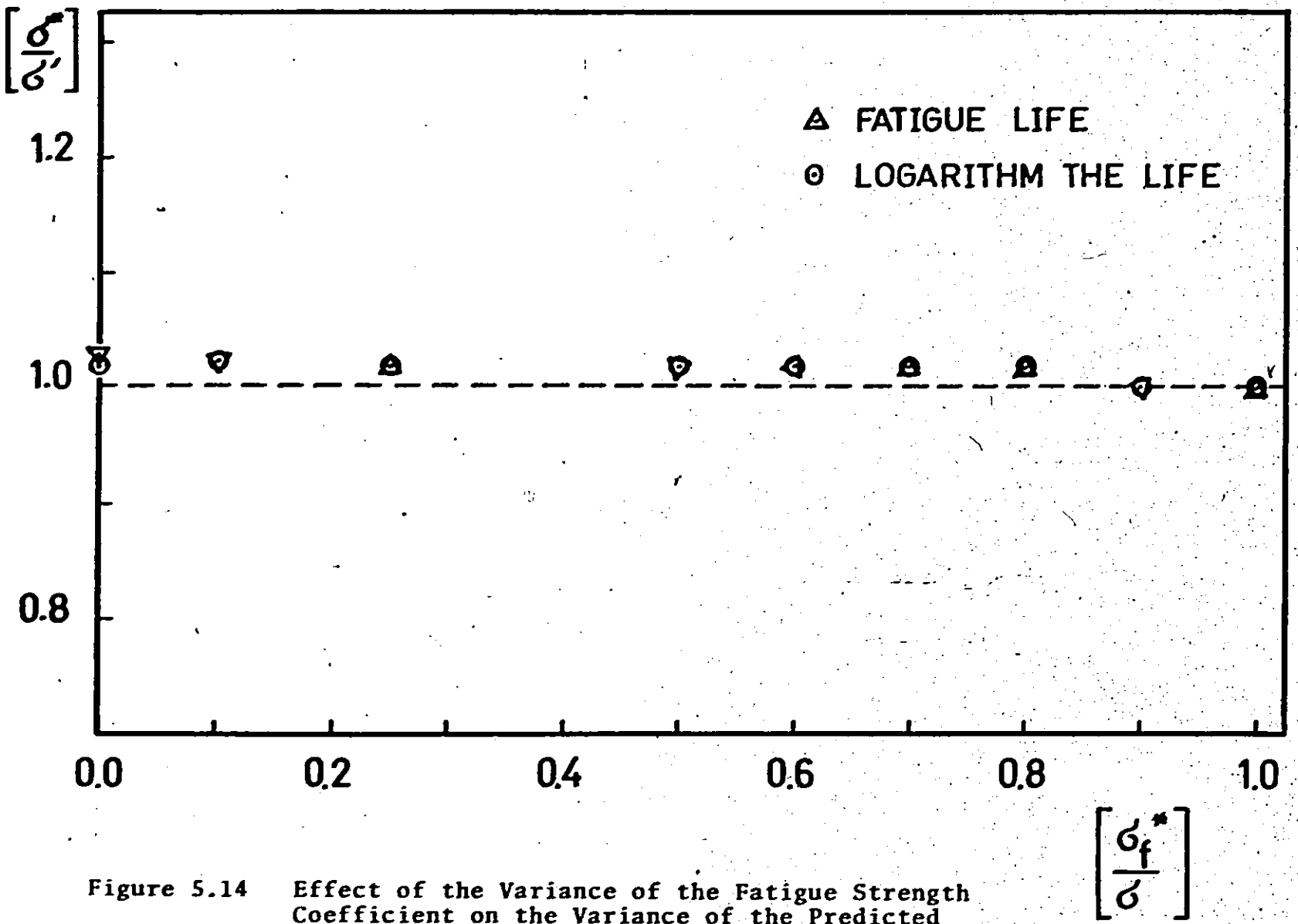

Figure 5.14 Effect of the Variance of the Fatigue Strength Coefficient on the Variance of the Predicted Fatigue Life at Stress Level 101,000 psi.

using sinusoidal loading were performed on the same grade of steel with up to 50% reduction in the value of the standard deviation of the endurance limit, σ_e, keeping the standard deviation of the fatigue strength coefficient, σ_f, constant. The mean and standard deviation of the predicted life distributions for different values of σ_e were also compared with those of the predicted life distribution using the experimental value of σ_e. The resulting fatigue life and its logarithm are examined. The effect of changing σ_e on the predicted mean and standard deviation of the fatigue life is plotted in Figures 5.15 and 5.16.

It is noticed that the change in the standard deviation of the predicted life is almost the same for both distributions of fatigue life and its logarithm. It is also observed that decreasing σ_e decreases the estimated mean life. This decrease is negligibly small in the case of the fatigue life logarithm. When the fatigue life is analysed, the error in estimating the life due to changes of σ_e is up to 5.04% of the originally predicted life for a reduction of 50% of σ_e.

The results clearly indicate the significant effect the endurance limit variability has on the variability of the fatigue life. The analysis shows that the scatter of the endurance limit explains most of the scatter observed in the predicted life. This conclusion emphasizes the importance of accurate estimation of the endurance limit distribution parameters.

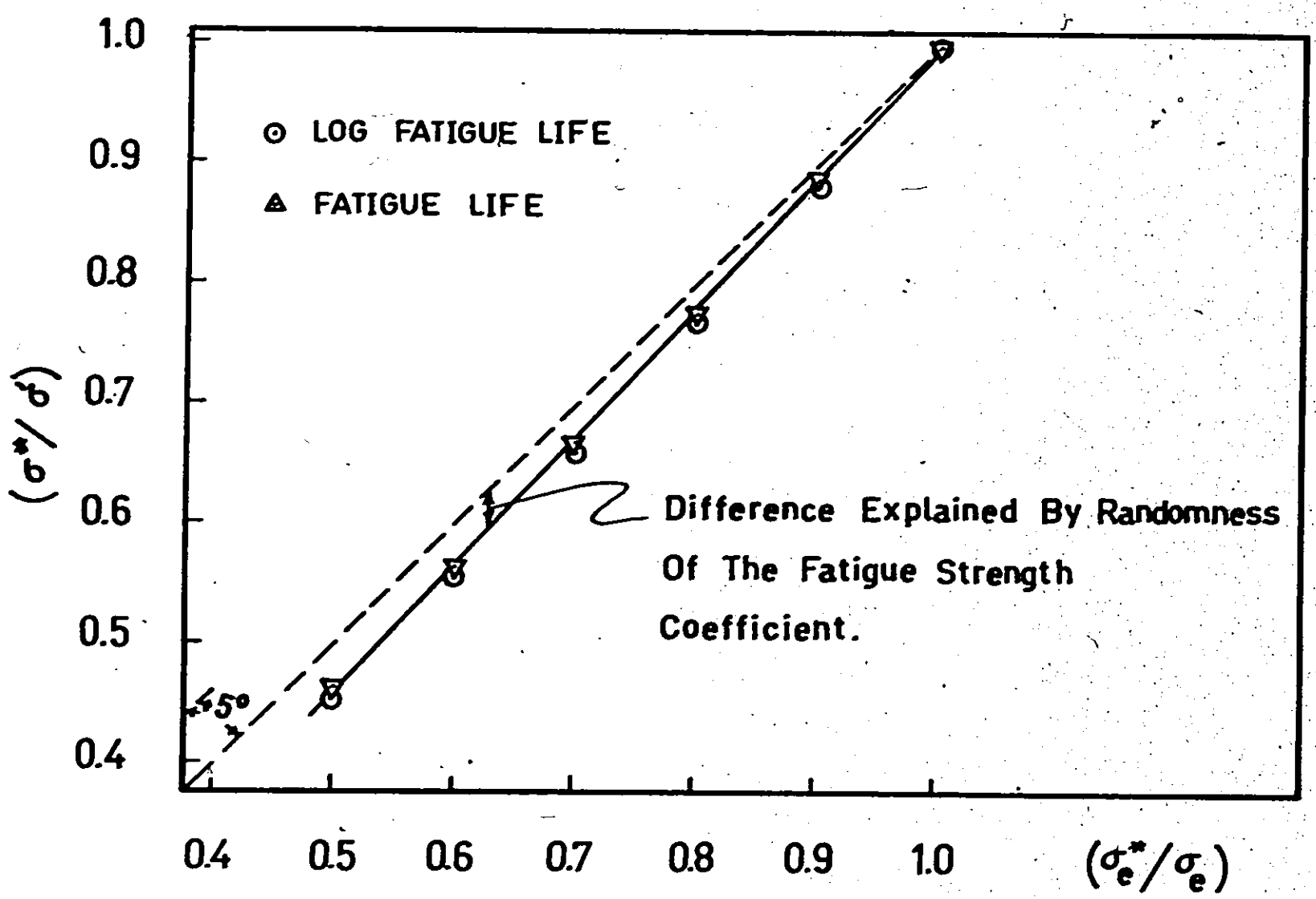

Figure 5.15 Effect of the Endurance Limit Variance on the Randomness of the Predicted Fatigue Life, at Stress Level 101,000 psi.

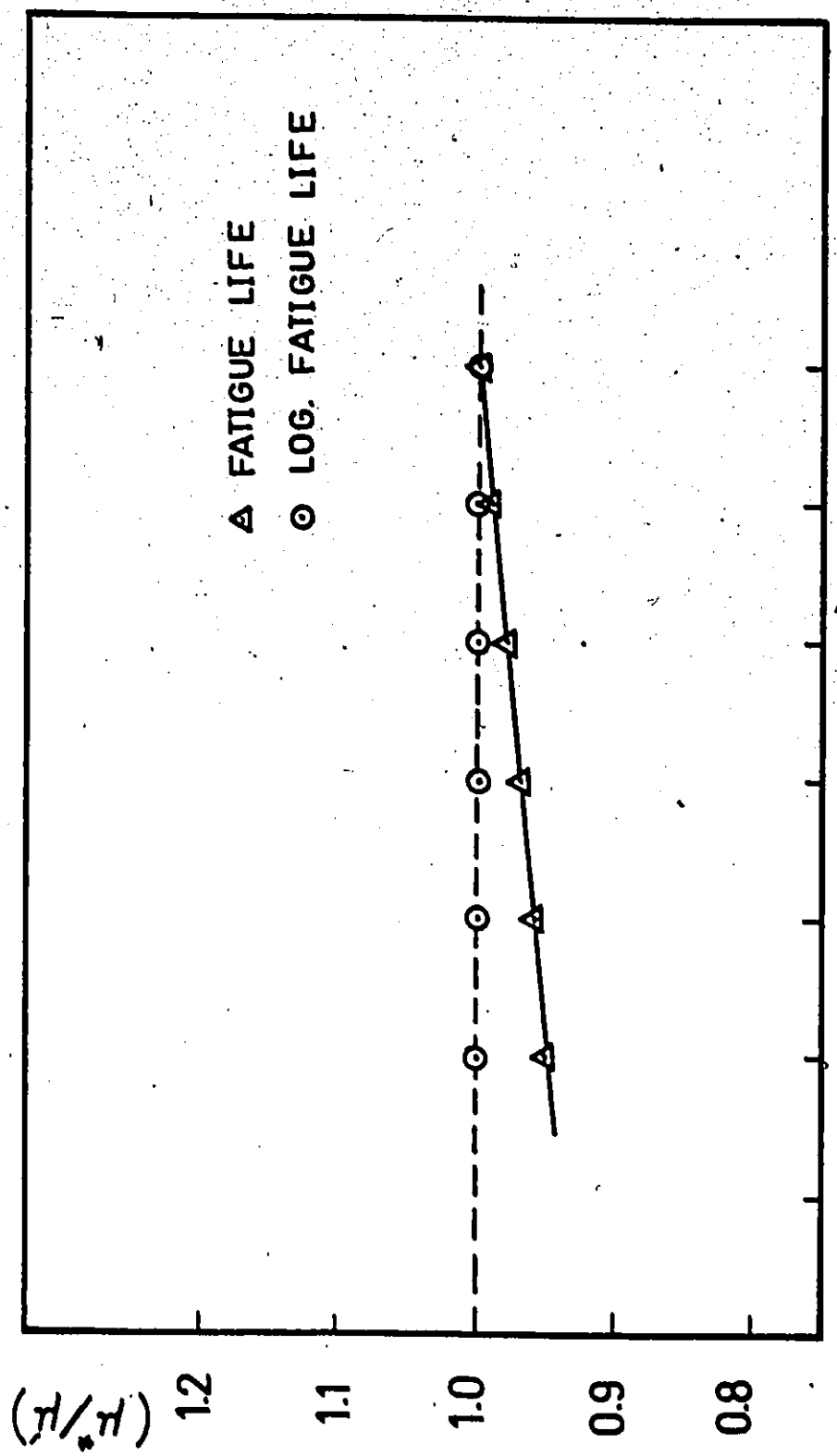

Figure 5.16 Effect of the Variance of the Endurance Limit on the Mean Predicted Fatigue Life at Stress Level 101,000 psi.

5.6 Effect of Shape of the Load Probability Density Function on Fatigue Life Distribution

It has been noted in the literature that the load probability density function merits more attention in future studies. Although many PDF shapes are possible, many actual load-time histories have density functions with a shape not far from the normal.

The next step in the present study was directed towards utilizing the developed simulation model to investigate the effect of the shape of the load probability density function on the fatigue life distribution. The analysis required a distribution of the density function which can easily be altered. It was also necessary to isolate the effect of the shape of the probability density function by keeping the other variables constant. It is especially important to keep the RMS value as well as the upper and lower limits of the load distribution constant for all the distributions tested. In this study the first four central moments of the load distribution were used to define its probability density function using the Maximum Entropy method. These moments are defined as follows:

$$
\begin{aligned}
C_1 &= \sum_{i=1}^{s} X_i/s = \mu \\
C_2 &= \sum_{i=1}^{s} (X_i - \mu)^2(s - 1) = \sigma^2 \\
C_3 &= \sum_{i=1}^{s} (X_i - \mu)^3/s \\
C_4 &= \sum_{i=1}^{s} (X_i - \mu)^4/s
\end{aligned}
\qquad (5.8)
$$

where

X_i = the i^{th} value of load amplitude

s = the sample size

μ = the mean value

σ^2 = the variance

An estimate of the probability density function is obtained in the following form:

$$f(X) = \text{Exp}\,(\lambda_1 + \lambda_2 X + \lambda_3 X^2 + \ldots + \lambda_{n+1} X^n) \qquad (5.9)$$

where the λ_i's are the Lagrange's multipliers used to maximize Shannon's Logarithmic Entropy Function, with the given four moments as constraints [80]. This approach proved to be very useful and convenient for studying the effects of the shape of the probability density function on the predicted fatigue life distribution. It allowed keeping the values of the first, second and fourth central moment of the applied load distribution constant while varying the third central moment, which indicates skewness or asymmetry of the load distribution. A negative value for C_3 means that probability density curve is skewed left, while a positive one indicates right skewness.

The standardized measure of skewness, β_1, is given by

$$\beta_1 = \left(\frac{C_3}{\sigma^3}\right)^2 \qquad (5.9)$$

Digital experiments were performed on SAE 4340 steel where the applied load in each of them was simulated by

one of the distributions shown in Figure 5.17. All the distributions have the following common characteristics:

Mean value	= 80.8 ksi
Standard deviation	= 5.0 ksi
Coefficient of variation	= 0.062
Lower limit	= 6.4 ksi
Upper limit	= 98. ksi
Coefficient of peakedness	= 3.

Three positive and three negative values of β_1 were used. The mean and standard deviation of the predicted life distributions for the different cases shown in Appendix C were compared with the predicted life distribution for a normal load distribution ($\beta_1 = 0$).

The results indicate that as the shape of the load probability density function is changed, the predicted mean life and standard deviation are also changed. This observation motivated a search for some sort of correlation between a shape characteristic of the load distribution and the fatigue life distribution parameters. The first four central moments except the third, are identical for all load distributions. Since the mode and median stresses change according to C_3, correlating the mode and median stress as well as β_1 with the predicted mean and standard deviation of the fatigue life was attempted as shown in Figures 5.18 and 5.19. It is clear that the standardized measure of

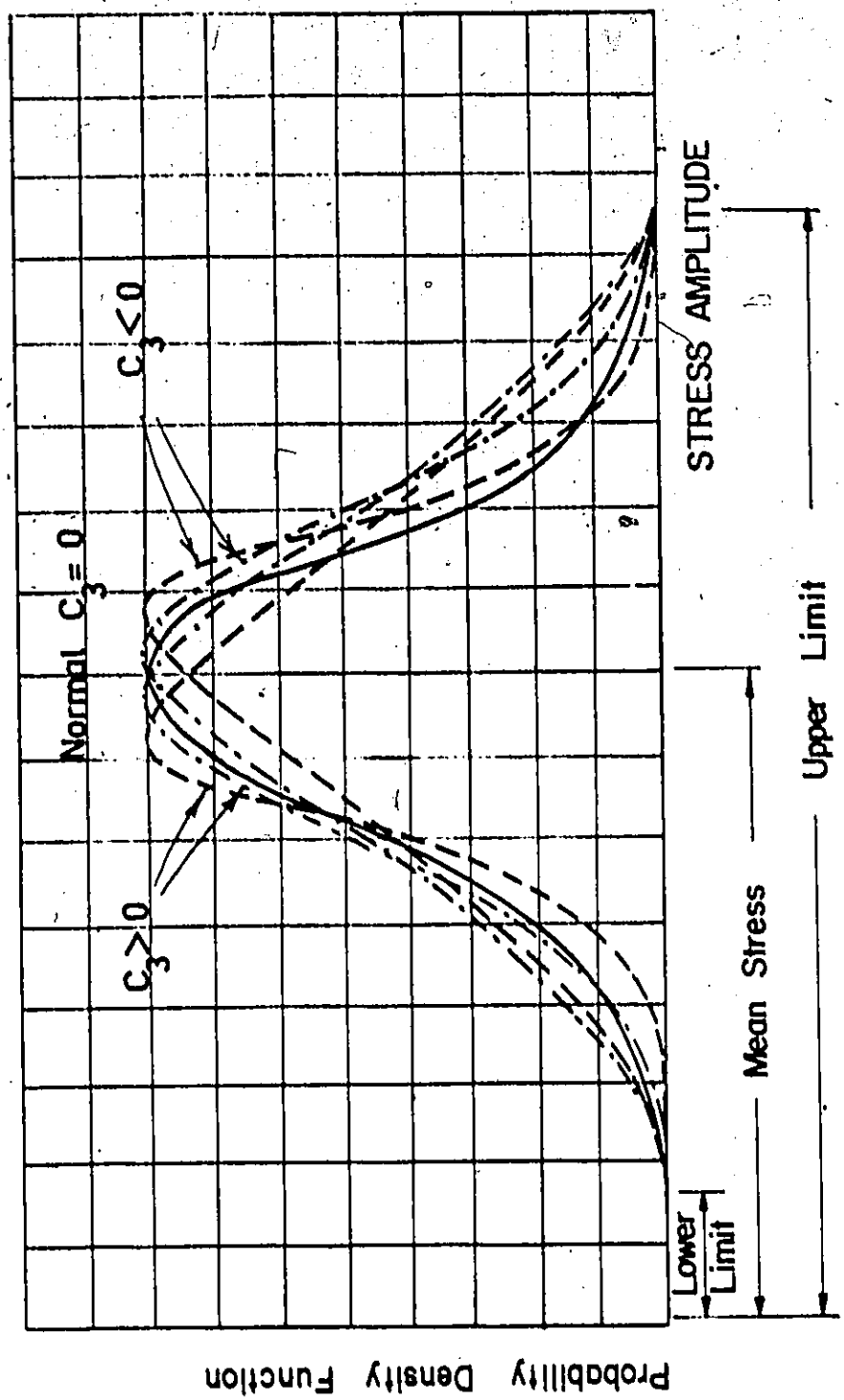

Figure 5.17 Schematic Representation of the Stress Distributions Used to Test the Shape Effect of the Load PDF.

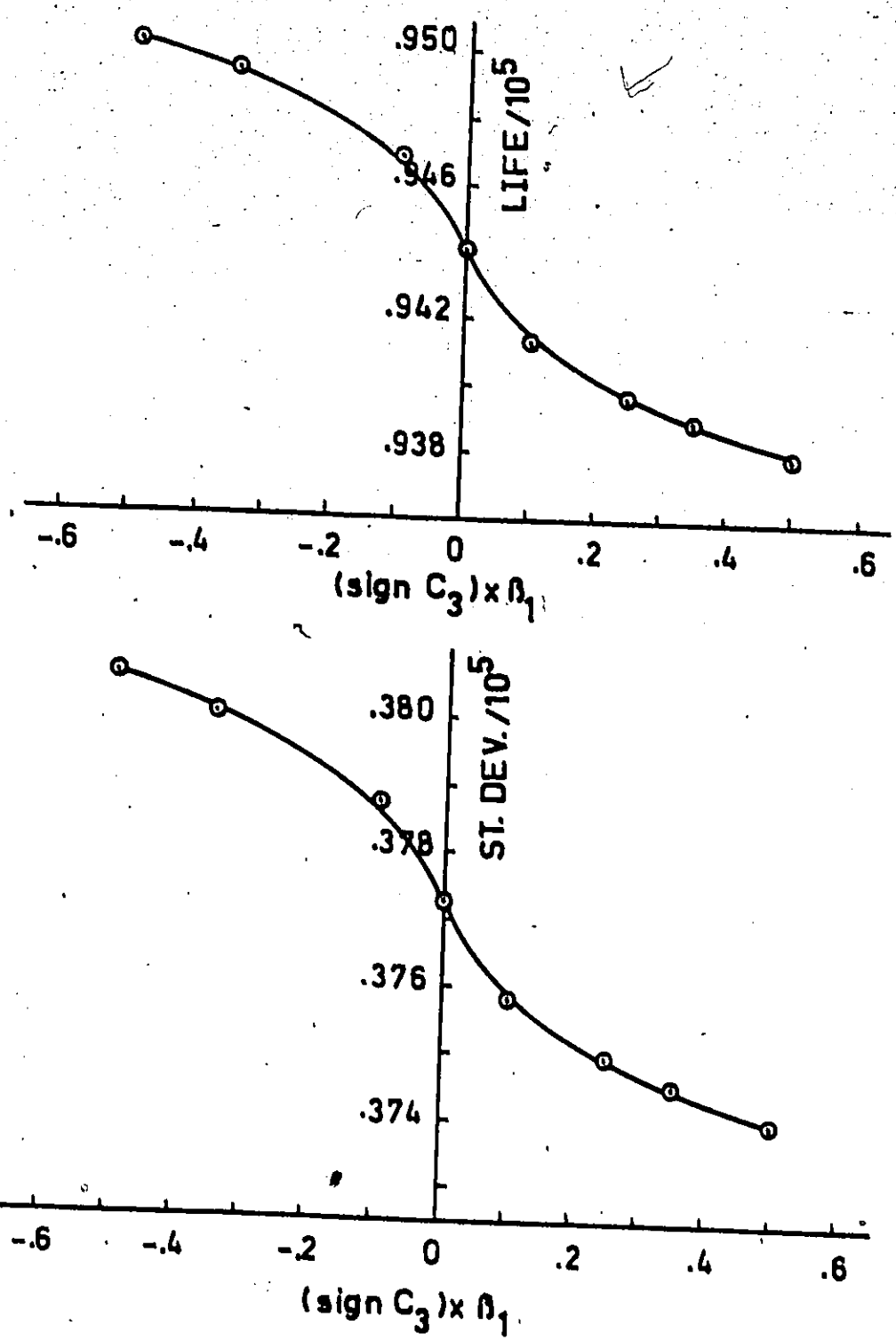

Figure 5.18 Effect of the Coefficient of Skewness of the Input PDF on the Fatigue Life and Its Standard Deviation.

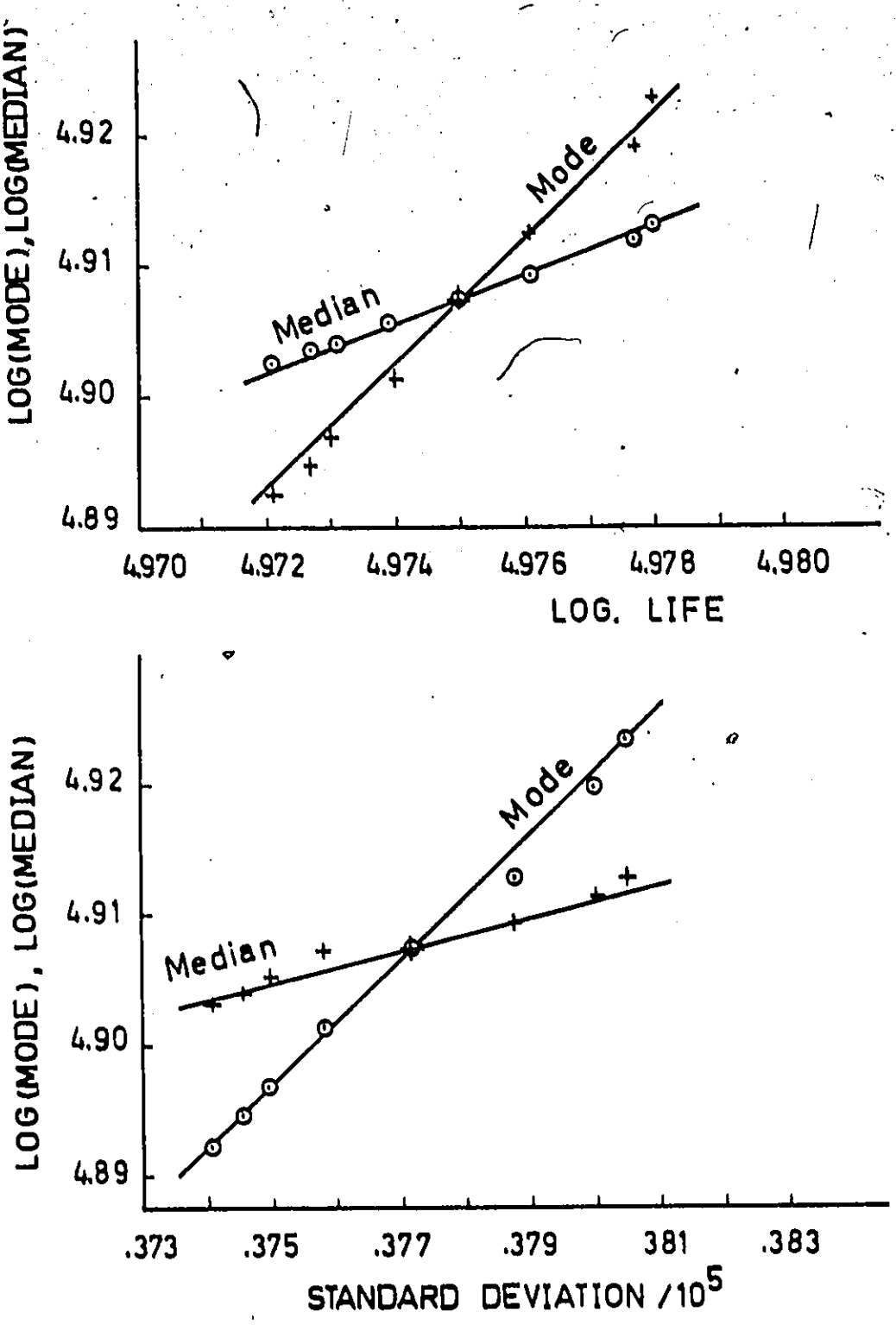

Figure 5.19 Plots of Both the Mode and Median Stresses vs. the Fatigue Life and its Standard Deviation.

skewness, β_1, is non-linearly correlated with the predicted mean life and the standard deviation. However, a linear correlation between both the mode and median stresses with the predicted fatigue life and its standard deviation is shown to exist. It is noticed that changes in the shape of the load probability density function affects the scatter of the fatigue life more than it affects its mean value. The effect, however, is generally small. This is partially due to the fact that the change of the shape of the load probability density function was made small to simulate the small deviation from the Gaussian shape, which is usually encountered in the actual load-time histories. For example a change of 3.47% of the mode stress produces a change of 2.1% in the standard deviation of the fatigue life and only 0.66% change in its mean. These results agree with previous findings of other investigators [87].

In view of these results, random load tests with a Gaussian loading and constant power spectrum seem acceptable for load distributions with small deviations from normality. However, the actual probability density function should be used if measurements revealed significant deviations from normality.

This advantage of using the simulation model to study the effect of the shape of the load distribution over the complicated, and rather crude, analogous electronic equipment for shaping the density function is evident.

CHAPTER 6

CONCLUSIONS AND RECOMMENDATIONS FOR FUTURE RESEARCH

6.1 Concluding Remarks

Design engineers always face the problem of selecting the optimum shape and material of different components. Such decisions involve the interplay of several factors including product performance, reliability, cost, and appearance. The mechanical reliability of load-bearing members is frequently dictated by fatigue resistance. The assurance of adequate fatigue performance requires an assessment of the ability of a particular material and configuration to resist an anticipated service load history.

Since reliability is the best available quantitative measure of the performance integrity of the designed component, it is very important to provide the basic design data, in a distribution form, to aid the designer in the formation of an engineering judgement. Estimates of the statistical characteristics of fatigue life distribution can be obtained using the technique presented in this thesis. The growing interest in probability and statistics, and the recognition of its relevance to engineering design confirm the current timeliness of this study.

The new method is intended to supplement the existing fatigue analysis procedures, not to replace them. It provides

a unique way of predicting the scatter of fatigue life using the randomness of relevant material properties.

An important advantage of this technique is that it can be programmed for digital computers. Computer-aided fatigue analysis procedures can provide a valuable analytical tool for predicting the fatigue life of components in service situations. This approach offers considerable potential for optimizing component design and material selection, with attendant savings in development costs, since design iterations can easily be performed prior to making prototype parts or full scale testing. It follows that, in addition to the results and conclusions reached in this research, one of the most important contributions is that a technique for predicting fatigue life distributions has been developed.

The method presented in this thesis provides a new way for predicting fatigue failure using Monte Carlo simulation. The randomness of material properties as well as that of the applied load can be incorporated into a stochastic model. An appropriate failure criterion is used to predict the statistical characteristics of fatigue life under constant, complex, and random amplitude cyclic loading conditions. A modified probabilistic S-N diagram is used to reflect the variability of the endurance limit and the fatigue strength coefficient.

Any damage criterion can be used with the simulated S-N diagram for each specimen. When a linear damage law is used, the analysis yields a damage criterion analogous

to Miner's rule but with a random cycle ratio. The proposed method is used to analytically predict the characteristics of the cycle ratio distribution. Good agreement with available experimental results is obtained. This result is of particular importance since no assumption regarding the fatigue failure mechanism is made. The predicted cycle ratio distributions are noticeably skewed to the right for the sinusoidal and random loading. For random loads, the mean cycle ratio its maximum value and standard deviation are higher, respectively, than those for sinusoidal loads.

The assumption of no damage accumulation below the lower limit of the endurance stress, suggested by the probabilistic behaviour of the endurance limit, is made. The lower limit of the endurance stress closely approximates the cyclic yield stress, below which there is no plastic strain component, and consequently no damage accumulation. The use of this assumption has an important significance and substantially improved the accuracy of the prediction.

The predicted life distributions and their statistical characteristics are found to be in good agreement with those obtained from the experimental results available from the literature for constant amplitude loading of SAE 4340 steel. This indicates that the proposed technique and the underlying assumptions and hypotheses are adequate. For all the cases studied the model predicted life distributions which are continuous, unimodal, and slightly skewed to the right; a result borne out by previous evidence.

Experiments were conducted to further assess the validity of the proposed method for different loading conditions and materials. SAE 1008 steel specimens were tested in bending fatigue under constant, block, and narrow band random loading. The comparison between the predictions and experimental results shows that the suggested model is successful in predicting fatigue life and its scatter for all the considered cases. The predictions were always conservative estimates of the experimental values. While these results are very positive and suggest that the method should be equally applicable to other load histories and materials which exhibit an endurance limit, the validity can be verified experimentally.

Using an electromagnetic shaker together with a noise generator to load the specimens is shown to be a useful and efficient way of fatigue testing. The inertia effects of the moving parts of the electromagnetic shaker are negligible, which allows a good response to the output of the filtered random process generator. This system is superior to the electro-hydraulic test machines since it allows higher testing frequencies with obvious savings in time and cost. Between 30 to 45 specimens were tested for each loading program which provides good confidence in the statistical conclusions drawn. A flat power spectral density was achieved over the frequency range of interest, by optimizing the dynamic characteristics of the specimen-shaker assembly.

The analytical model was used to study the effect of

some important factors on the randomness of fatigue life. This study indicates that the large scatter exhibited in fatigue tests is mostly explained by the scatter in the material properties itself. Only a small amount of this scatter is explained by the scatter in the applied load. This result is borne out by experimental observation of previous researchers in this area.

It has been shown that the mean value of fatigue life decreases slightly as a result of increasing the variance of the applied load. The results obtained in this study also confirm many conclusions which appear in the cited references, that the scatter in fatigue life under random loading is less than that under sinusoidal constant amplitude loading.

It was found that the randomness of the fatigue strength coefficient does not significantly affect the scatter of the predicted fatigue life or its estimated mean value. On the other hand, the variance of the endurance limit has a pronounced effect on the variability of the fatigue life. Most of the scatter of fatigue life is explained by the scatter of the endurance limit. Its effect on the estimated mean is also appreciable. A 50 percent reduction in the variance of the endurance limit results in about 5 percent reduction in the mean fatigue life.

The effect of the shape of the probability density function of the applied load was investigated using the analytical model. It was found that changes in the shape of

the probability density function affect the scatter of fatigue life more than its mean value. It is interesting to note that this effect is small for small deviations from the normal distribution, which is in agreement with previous findings reported in the literature. An instance of a situation where such knowledge is important is when the designer is dealing with loads having a probability density function (PDF) which deviates slightly from normality. In such cases it is reasonable to assume a Gaussian PDF for the input loads. This is only true for small deviations from normality. However, the shape of the PDF merits more attention since a large range of shapes are possible between the Gaussian bell-shape and the uniform rectangular shape.

Recognizing that the local stress-strain behaviour of the critical location governs the fatigue failure of structural components, the actual experimental cyclic stress-strain relation was always used in the prediction. The stabilized cyclic stress-strain curve was considered deterministic in the present analysis. It is believed that the scatter of this curve is not significant.

It is believed that the proposed method is an easy, fast and effective design tool to generate fatigue life distributions under different loading conditions, and to study the effect of different factors on these distributions. Its potential lies in the fact that very little experimental data is needed for the analysis.

Conventional design for fatigue methods have performed

well in the past. However, with a rational approach that includes probabilistic considerations together with statistical tools, considerable improvement in design is possible.

6.2 Scope for Future Investigations

Despite the many investigations that have been carried out; studies of the basic fatigue mechanism, involving engineering data, and final components testing, will continue to attract the attention of many investigators. As a result of this research a number of problems and areas for further studies are identified. Some of the problems worth investigating are:

(i) The applicability of the present model to additional load histories such as wide-band or multi-peaked random loading, non-stationary random loads, and multi-axial stresses, needs to be confirmed experimentally.

(ii) The variability of the stabilized cyclic stress-strain curve should be investigated experimentally. Refinement of the present model to include the effect of this factor is possible, if it is found that the scatter is significant.

(iii) The type of load probability density function has a recognized influence on the distribution of fatigue life. This influence was investigated analytically in this study. Experimental investigations of this

effect using analogous electronic equipment was also reported in the literature. It is, however, recognized that the latter approach for density function shaping is rather crude. Refined shaping is possible if a digital computer is used on-line with the testing equipment. These new methods of testing will need to be developed.

(iv) The simulation technique could be extended to include generation of random samples with a prescribed correlation pattern, for loads which exhibit a pronounced correlation between its successive peaks.

(v) Overstressing and understressing effects could be included in the model by revising the mean value of endurance limit to be used.

(vi) The accurate determination of the S-N curve for the different materials used in engineering applications will facilitate the extension of the new method to these materials.

The problems mentioned above are only a few of the many interesting probabilistic aspects of metal fatigue which will likely continue to challenge research workers for a long time.

REFERENCES

1. Poncelet, Mechanique Industrielle, 2nd ed., 1939.

2. Rankine, W. J. M. "On the Causes of the Unexpected Breakage of the Journals of Railway Axles; and On the Means of Preventing Such Accidents by Observing the Law of Continuity in their Construction", Proc. ICE 2, 1943, 105-108.

3. McConnell, J. E. "On Railway Axles", Proc. I.Mech.E., 1847-1849, 13-21.

4. Wöhler, A. Zeitschrift fur Bauwesen 8, 1858, 641-652, 10, 1860; 583-616, 16, 1866, 67-84, 20, 1870, 73-106.

5. Bauschinger, J. Mitt. Mech. Tech. Lab., 25, Technischen Hochschule, Munich, 1897.

6. Foppl, A. Mitt. Mech. Tech. Lab., 31, Technischen Hochschule, Munich, 1909.

7. Gerber, W. "Bestimmung der Zulossigne Spannugen in Eisen Constructionen", Z. Bay. Arch. Ing. Ver. 6, 1874, p. 101.

8. Goodman, J. Mechanics Applied to Engineering, Longmans, Green and Co., London, 1899.

9. Basquin, O. H. "The Exponential Law of Endurance Tests", Proc. ASTM 10, 1910, 625-630.

10. Manson, S. S. "Fatigue: A Complex Subject - Some Simple Approximations", Experimental Mechanics J., Vol. 5., July 1965, 193-226.

11. Swanson, S. S. "Random Load Fatigue Testing: A State of the Art Survey", Materials Research and Standards, MTRSA, Vol. 8, No. 4, April 1968, 10-44.

12. Sines, G. and Waisman, J. L., (Editors) Metal Fatigue, McGraw-Hill, N.Y., U.S.A., 1959.

13. Burka, J. J., Reed, N. L., and Weiss, V., (Editors) Fatigue - An Interdisciplinary Approach, Syracuse University Press, U.S.A., 1964.

14. "Fatigue Crack Propagation", ASTM STP No. 415, U.S.A., 1967.

15. Yokobori, T. Strength, Fracture and Fatigue of Materials, P. Noordhoff/Groningen/The Netherlands, 1965.

16. Heller, R. A., (Editor) "Probabilistic Aspects of Fatigue", ASTM STP 511, 1972.

17. Osgood, C. C., Fatigue Design, Wiley-Interscience, 1970.

18. Schijve, J. "The Analysis of Random Load-Time Histories with Relation to Fatigue Tests and Life Calculations", Fatigue of Aircraft Structures, Pergamon Press, London, 1963, 115-150.

19. Martin, J. F., Topper, T. H., and Sinclair, G. M. "Computer Based Simulation of Cyclic Stress-Strain Behaviour", Materials Research and Standards, Vol. 11, No. 2, February 1971.

20. Dowling, N. E. "Fatigue Life and Inelastic Strain Response Under Complex Histories for an Alloy Steel", J. of Testing and Evaluation, JTEVA, Vol. 1, No. 4, 1973, 271-287.

21. Dowling, N. E. "Fatigue Failure Predictions for Complicated Stress-Strain Histories", J. of Materials, JMLSA, Vol. 7, No. 1, March 1972, 71-87.

22. Manson, S. S. "Behaviour of Materials Under Conditions of Thermal Stress", Heat Transfer Symposium, Univ. of Mich. Eng. Research Institute, 1953, 9-75.

23. Coffin, L. F. "A Study of the Effects of Cycle Thermal Stresses on a Ductile Metal", Trans. ASME, 76, 1954, 931-950.

24. Topper, T. H., Wetzel, R. M., and Morrow, J. "Neuber's Rule Applied to Fatigue of Notched Specimens", J. of Materials, JMLSA, Vol. 4, No. 1, March 1969, 200-209.

25. Morrow, J., Wetzel, R. M., and Topper, T. H. "Laboratory Simulation of Structural Fatigue Behaviour, Effects of Environment and Complex Load History on Fatigue Life", ASTM STP 462, 1970, 74-91.

26. Koibuchi, K. and Kotani, S. "The Role of Cyclic Stress-Strain Behaviour on Fatigue Damage Under Varying Load", Cyclic Stress-Strain Behaviour - Analysis, Experimentation, and Failure Prediction, ASTM STP 519, 1973, 229-245.

27. Landgraf, R. W. "Comulative Fatigue Damage Under Complex Strain Histories", ASTM STP 519, 1973, 213-288.

28. Neuber, H. "Theory of Stress Concentration for Shear Strained Prismatical Bodies with Arbitrary Non-Linear Stress-Strain Law", J. Appl. Mech., December 1961, 544-550.

29. Wei, R. P. "Fracture Mechanics Approach to Fatigue Analysis in Design", Design Engineering Conference and Show, Philadelphia, Pa., 1973, April 9-12.

30. Palmgren, A. "Die Lebensdauer von Kugellagern", ZVDI, Vol. 68, No. 14, 1924, p. 339.

31. Miner, M. A. "Cumulative Damage in Fatigue", Journal of Applied Mechanics, Trans. ASME, Vol. 67, 1945, A-159.

32. Corten, H. T., and Dolan, T. J. "Cumulative Fatigue Damage", Int. Conf. on Fatigue of Metals, Vol I, Brit. Inst. of Mech. Engrs., London, 1956.

33. Kowalewski, J., "On the Relation Between Fatigue Lives Under Random Loading and Under Corresponding Program Loading", Full-Scale Fatigue Testing of Aircraft Structures (ICAF-AGARD Symposium at Amstordam, 1959), ed. by Plantema and Schijve, Pergamon Press, N.Y., 1961.

34. Freudenthal, A. M. and Gumbel, E. J. "Physical and Statistical Aspects of Fatigue", Advances in Appl. Mech., Vol. 4, 1956, 117-158.

35. Sinclair, G. M. and Dolan, T. J. "Effect of Stress Amplitude on Statistical Variability in Fatigue Life of 755-T6 Aluminum Alloy", Trans. ASME, Vol. 75, July 1953, 867-872.

36. Weibull, W. "A Statistical Distribution Function of Wide Applicability", Trans. ASME, J. Appl. Mech. Section, Vol. 73, 1954, 293-297.

37. Weibull, W. SAAB Aircraft Tech. Notes TN 30, 1954.

38. Heller, R. A., editor "Probabilistic Aspects of Fatigue", ASTM STP 511, 1971.

39. Ford, D. G. "Fatigue Scatter Factors for Lives with Known Variances", Aeronautical Research Labs., Australia, Note ARL/SM.368.

40. Freudenthal, A. M. and Heller, R. A. "Accumulation of Fatigue Damage", Proc. Columbia and International Conference on Fatigue in Aircraft Structures, New York, 1956, 146-177.

41. Buck, A. "Fatigue Resistance of Materials and Metal Structural Parts", Proc. of an International Conference on Fatigue held in Warsaw, Pergamon Press, 1964.

42. Forsyth, P. J. E. The Physical Basis of Metal Fatigue, Blackie and Son Limited, 1969.

43. Dolan, T. J., Lazan, B. T. and Horger, O. J. A Series of Educational Lectures on Fatigue presented to ASM, 1953.

44. Weibull, W. Fatigue Testing and Analysis of Results, Pergamon Press, 1961.

45. Freudenthal, A. M. and Gumble, E. J., "On the Statistical Interpretation of Fatigue Tests", Proc. Royal Soc., London, Series A., Vol. 216, 1953, 309-331.

46. Marin, J. Mechanical Behaviour of Engineering Materials, Prentice-Hall, 1962.

47. Kececioglu, D., Smith, R. E., and Plested, E. A. "Distributions of Cycles-to-Failure in Simple Fatigue and the Associated Reliabilities", 8th Reliability and Maintainability Conf., July 7-9, 1969, 357-374.

48. Kececioglu, D., and Haugen, E. B. "Fatigue Reliability Design Data for Dynamic and Rotary Machinery", ASME Space Technology and Heat Transfer Conference, Los Angeles, California, June 21-24, 1970. Also ASME Paper No. 70-Av/SpT-36.

49. Haugen, E. B. "Statistical Definition of Fatigue Behaviour of Strength of Low Alloy Steels", Proceedings of the 1971 International Conference on Mechanical Science, Vol. II, Japan, 1972, 299-311.

50. Kececioglu, D. et al. "Generation of Finite Life Distributional Goodman Diagrams for Reliability Prediction", NASA CR-120813, August 1971.

51. Hanke, M. E., and Bussa, S. L. "Estimation of Life Using Stress Distribution Parameters", SAE Automotive Engineering Congress, Detroit, Mich., Jan. 12-16, 1970.

52. Kececioglu, D. and Broome, H. "Probabilistic-Graphical and Phenomenlogical Analysis of Combined Bending-Torsion Fatigue Reliability Data", NASA-CR-72839, 1969.

53. Brinbaum, Z. W., and Saunders, S. C. "A Probabilistic Interpretation of Miner's Rule", SIAM J. Appl. Math., Vol. 16, No. 3, May 1968, 637-652.

54. Saunders, S. C. "A Probabilistic Interpretation of Miner's Rule II", SIAM J. Appl. Math., Vol. 19, No. 1, July 1970, 251-265.

55. Sweet, A. L., and Kozin, F. "Investigation of a Random Cumulative Damage Theory", J. of Materials JMLSA, Vol. 3, No. 4, Dec. 1968, 802-823.

56. Kogaev, V. P. "Simulation of Metal Fatigue by the Monte Carlo Method", Zavodskaya Laboratoriya, Vol. 34, No. 7, July 1968, 828-832.

57. Haugen, E. B. Probabilistic Approaches to Design, John Wiley and Sons, Inc., 1968.

58. Siddall, J. N. Analytical Decision-Making in Engineering Design, Prentice-Hall Inc., 1972.

59. Saunders, S. C. "On the Probabilistic Determination of Scatter Factors Using Miner's Rule in Fatigue-Life Studies", ASTM STP 511, 185-203.

60. "Manual on Low Cycle Fatigue", ASTM STP 465.

61. Ransom, J. T. and Mehl, R. F., ASTM STP 137, 1953, p. 3.

62. Ransom, J. T. ASTM STP 121, 1953, p. 867.

63. "Fatigue Design Handbook", A Special Technical Publication of ASTM.

64. Shigley, J. E., Mechanical Engineering Design, 2nd edition, McGraw-Hill, 1972.

65. Ineson, E., Clayton-Cave, J. and Taylor, R. J. "Variation in Fatigue Properties Over Individual Case of Steels", Iron and Steel Institute, Vol. 184, 1956, p. 179.

66. Libertiny, G. Z. "The Problem of Life Prediction of Stamped Structural Parts Subjected to Cyclic Loads", ASME Paper 74-WA/DE-18.

67. Dieter, G. E. Mechanical Metallurgy, McGraw-Hill, Chapter 9, 1961.

68. Manson, S. S. Thermal Stress and Low Cycle Fatigue, McGraw Hill, U.S.A., 1966.

69. Krishnasamy, S. "Beams Under Cyclic Alternating Deflections", Ph.D Thesis, Dept. of Civil Engg., University of Waterloo, Waterloo, Ontario, Canada, December 1966.

70. Jhansale, H. R., Topper, T. H. "Cyclic Deformation and Fatigue Behaviour of Axial and Flexural Members - a Method of Simulation and Correlation", Tech. Note No. 4, June 1971, Solid Mechanics Division, University of Waterloo, Waterloo, Ontario, Canada.

71. Raske, D. T. and Morrow, Jo Dean "Mechanics of Material in Low Cycle Fatigue Testing", Manual on Low Cycle Fatigue Testing, ASTM STP 465, American Society for-Testing and Materials, 1969, 1-25.

72. Endo, T. and Morrow, Jo Dean "Cyclic Stress-Strain and Fatigue Behaviour of Representative Aircraft Metals", J. of Materials, JMLSA, Vol. 4, No. 1, March 1969, 159-175.

73. Morrow, J. "Cyclic Plastic Strain-Energy and Fatigue of Metals", Internal Friction, Damping and Cyclic Plasticity, ASTM STP 378, July 1965, p. 45.

74. Morrow, Jo Dean "Low-Cycle Fatigue Behaviour of Quenched and Tempered SAE 1045 Steel", T & A. M. Report No. 277, Department of Theoretical and Applied Mechanics, University of Illinois, April 1965.

75. Dixon, W. J., and Massy, F. J. Introduction to Statistical Analysis, McGraw-Hill, 1957, 324-326.

76. "Manual on Fatigue Testing", ASTM STP No. 91, prepared by Committee E-9 on Fatigue, 1949.

77. Feltner, C. E., and Mitchell, M. R. "Basic Research on the Cyclic Deformation and Fracture Behaviour of Materials", Manual on Low Cycle Fatigue Testing, ASTM STP 465, 1969, 27-66.

78. Kececioglu, D., Chester, L. B., and Dodge, T. M. "Combined Bending-Torsion Fatigue Reliability of AISI 4340 Steel Shafting with K_t = 2.34", ASME Paper No. 74-WA/DE-12.

79. "Decimak", Designer's Stochastic Simulation Subroutines, Part 1, The Maximum Logarithmic Entropy Subroutines, Department of Mechanical Eng., McMaster University, Canada, ME/73/DSN/REP1.

80. Siddall, J. N. and Diab, Y. "The Use In Probabilistic Design of Probability Curves Generated by Maximizing the Shannon Entropy Function Constrained by Moments", Trans. ASME J. Eng. for Industry, Vol. 97, Ser. B., No. 3, Aug. 1975, 843-850.

81. Saunders, S. C. "On the Probabilistic Determination of Scatter Factors Using Miner's Rule in Fatigue-Life Studies", ASTM STP 511, 185-203.

82. Smith, C. R. "A Method for Estimating the Fatigue Life of 7075-T6 Aluminum Alloy Aircraft Structures", Aeronautical Structures Laboratory, Report No. NAEC-ASL-1096, December 1965.

83. Rice, J. R., Beer, F. P., and Paris, P. C. "On the Prediction of Some Random Loading Characteristics Relevant to Fatigue", Acoustical Fatigue in Aerospace Structures, edited by W. J. Trapp and D. M. Forney, Jr., Syracuse University Press, 1965, 121-144.

84. Schijve, J. "Fatigue Life and Crack Propagation Under Random and Programmed Load Sequences", NLRL Report MP219, Amsterdam.

85. Bendat, J. S., and Piersol, A. G. Random Data: Analysis and Measurement Procedures, Wiley-Interscience, 1971.

86. Sjöstrom, S. "On Random Load Analysis" KTH Report No. 181, Transactions of the Royal Institute of Technology, Stockholm, Sweden, 1961.

87. Strating, J. "Fatigue and Stochastic Loadings" Ph.D Thesis, Department of Civil Engineering, Delft University of Technology, 1972.

88. Madayag, A. F. Metal Fatigue: Theory and Design, Wiley, New York, 1969.

89. Feltner, C. E., and Morrow, J. D. "Microplastic Strain Hysteresis Energy as a Criterion for Fatigue Fracture", J. of Basic Engineering, Trans. of ASME, Vol. 83, Ser D, 1961, 15-22.

90. Martin, D. E., "An Energy Criterion for Low-Cycle Fatigue", J. of Basic Engineering, Trans. of ASME, Vol. 83, Ser. D, 1961, 565-571.

91. Halford, G. R. "The Energy Required for Fatigue", Journal of Materials, Vol. 1, No. 1, March 1966, 3-18.

92. Pimbley, W. T., and Ku, T. C. "Design for Fatigue Based on Energy Concept", ASME Paper No 68-DE-17, 1968.

93. Bastenair, E. "Fatigue Scatter by Statistical and Physical Approaches", Fatigue of Aircraft Structures, Proc. of the Symposium held in Paris, 16th-18th May, 1961, Pergamon Press, 1963.

94. Ford, D. G., Graff, D. G., and Payne, A. O. "Some Statistical Aspects of Fatigue Life Variations", Fatigue of Aircraft Structures, Proceedings of the Symposium held in Paris, 16th-18th May, 1961, Pergamon Press, 1963.

95. Itagaki, H. and Shinozuka, M. ASTM STP 511, 1971, 168-184.

96. Pestel, E. C., and Leckie, F. A. Matrix Methods in Elastomechanics, McGraw-Hill, 1963.

97. Apodaca, D. R., and Louvier, J. G. "Static and Fatigue Properties of Aluminum and Magnesium Premium Quality Castings, ASM Rept. No. W6-6.3, Amer. Soc. Metals, Metals Park, Ohio, 1963.

98. Swanson, S. R. "An Investigation of the Fatigue of Aluminum Alloy Due to Random Loading", UTIA Report 84, February 1963.

99. Head, A. K., and Hooke, F. H. "Random Noise Fatigue Testing", Proc. Int. Conf. on Fatigue of Metals (London & New York), Inst. of Mech. Eng. & ASME, September 1956, 301-303.

100. Fuller, J. R. "Research on Techniques of Establishing Random Type Fatigue Curves for Broad Band Sonic Loading", ASD TDR 62-501, U.S.A.F., October 1962. (Also SAE Paper 671c, April 1963).

101. Schijve, J. and Jacobs, F. A. "Program-Fatigue Tests on Notched Light Alloy Specimens of 2024 and 7075 Material", Tech. Report M 2070, National Aeronautical Research Institute, Amsterdam, 1960.

APPENDIX A

EVALUATION OF FATIGUE ENDURANCE LIMIT DISTRIBUTION USING THE STAIRCASE METHOD

A.1 Long Life Tests

The object of the long-life tests is to determine a number of percentage points of the distribution of the fatigue strength at a preassigned cycle life. These tests differ from the routine tests in that the observed values of fatigue life are not used directly, only the fraction that failed (or survived) at different stress levels being used.

The long-life tests may be classified into a constant-amplitude test, which is called the "response" test, and the "increasing-amplitude" test. In this appendix we will only be concerned with the response test which can be conducted according to two different methods. The first, using the "Probit method", is designed with predetermined stress levels and numbers of specimens at each stress level; the second, using the "staircase method", is a sequential test, the choice of stress level is determined by the preceding result.

The primary purpose of this type of test is to determine the distribution of fatigue endurance limit ($N = \infty$), approximated by the fatigue strength at a sufficiently high cycle life. These methods have the merit of not requiring any assumptions of doubtful reliability.

It is to be noted that the observed percentage points

of the strength distribution measured by this method are independent of each other, and accordingly the method of least squares can be applied, contrary to the case when these points are estimated by means of order statistics. The only difference between the two methods used in the response tests consists in the distribution of specimens among the stress levels, in the probit method being spread out and in the staircase method more concentrated.

A.2 The Staircase Method

The procedure of the staircase method is as follows: the first test is started at a stress level which is equal to an estimated mean value of the fatigue strength. If a failure occurs prior to the preassigned cycle life, the next specimen is tested at a lower level; if the specimen does not fail within the preassigned number of cycles, the next test is run at a higher level. The intervals between the stress levels should be approximately equal to the standard deviation, but this is not a strict condition, the interval should not, however, be larger than twice the standard deviation. The test continues in this way, the stress level of each succeeding test being raised or lowered depending on the preceding result.

This procedure results in the testing being concentrated mainly on three stress levels, centered on the mean level. For this reason, this method is more efficient than the probit method with regard to the determination of the mean value resulting in a reduction in the number of specimens

of about forty percent.

A disadvantage of this, as of all, sequential methods is that only one specimen can be tested at a time. If more than 30 specimens are needed, the time required for the test will be rather long. A modification may then be introduced, whereby the total number of specimens is split into subgroups of equal size. Each group may then be tested simultaneously and independently of each other. The method is called the modified staircase test [75, 76].

A.3 Evaluation of Data from Staircase Method

The analysis of data from staircase tests is quite simple and also reliable on the condition that the distribution is normal and the interval between the stress levels is approximately equal to the standard deviation of the distribution.

The mean value, S_e, and the standard deviation, σ_e, are estimated by using only the failures or only the survivals, depending on which has the smaller total. The stress levels, S, which are equally spaced with an interval equal to d are given coded scores i, where i = 0 for the lowest stress level S_o.

Suppose that the total of failures is less than the total of survivals. Denote by n_i the number of failures at the coded stress level i and by $\sum_i n_i$ the total of failures. Two quantities A and B are defined as

$$A = \sum_i i\, n_i \qquad (A.1)$$

and

$$B = \sum_i i^2 n_i \qquad (A.2)$$

The estimate of the mean is then

$$\hat{S}_e = S_o + d\,(A/\sum_i n_i \pm \tfrac{1}{2}) \qquad (A.3)$$

where $+\frac{1}{2}$ is used if runouts are less frequent and $-\frac{1}{2}$ if failures are less frequent. The estimate of the standard deviation is

$$\hat{\sigma}_e = 1.620\, d\, \left(\frac{B \sum_i n_i - A^2}{(\sum_i n_i)^2} + 0.029\right) \qquad (A.4)$$

The estimate $\hat{\sigma}_e$ is quite accurate when $(B \sum_i n_i - A^2)/(\sum_i n_i)^2$ is larger than 0.3; otherwise the formula cannot be used.

A.4 Analysis of Data for SAE 1008 Steel and Determination of the Endurance Limit Distribution

The analysis is based on the survivals (fewer events)

S_o = 18,980 psi

d = 1,265 psi

STRESS (psi)	i	n_i	$i\,n_i$	$i^2\,n_i$
S_4 = 24,[illegible]	4	0	0	0
S_3 = 22,[illegible]	3	1	3	9
S_2 = 21,500	2	9	18	36
S_1 = 20,245	1	6	6	6
S_o = 18,980	0	1	0	0
Totals		N = 17	A = 27	B = 51

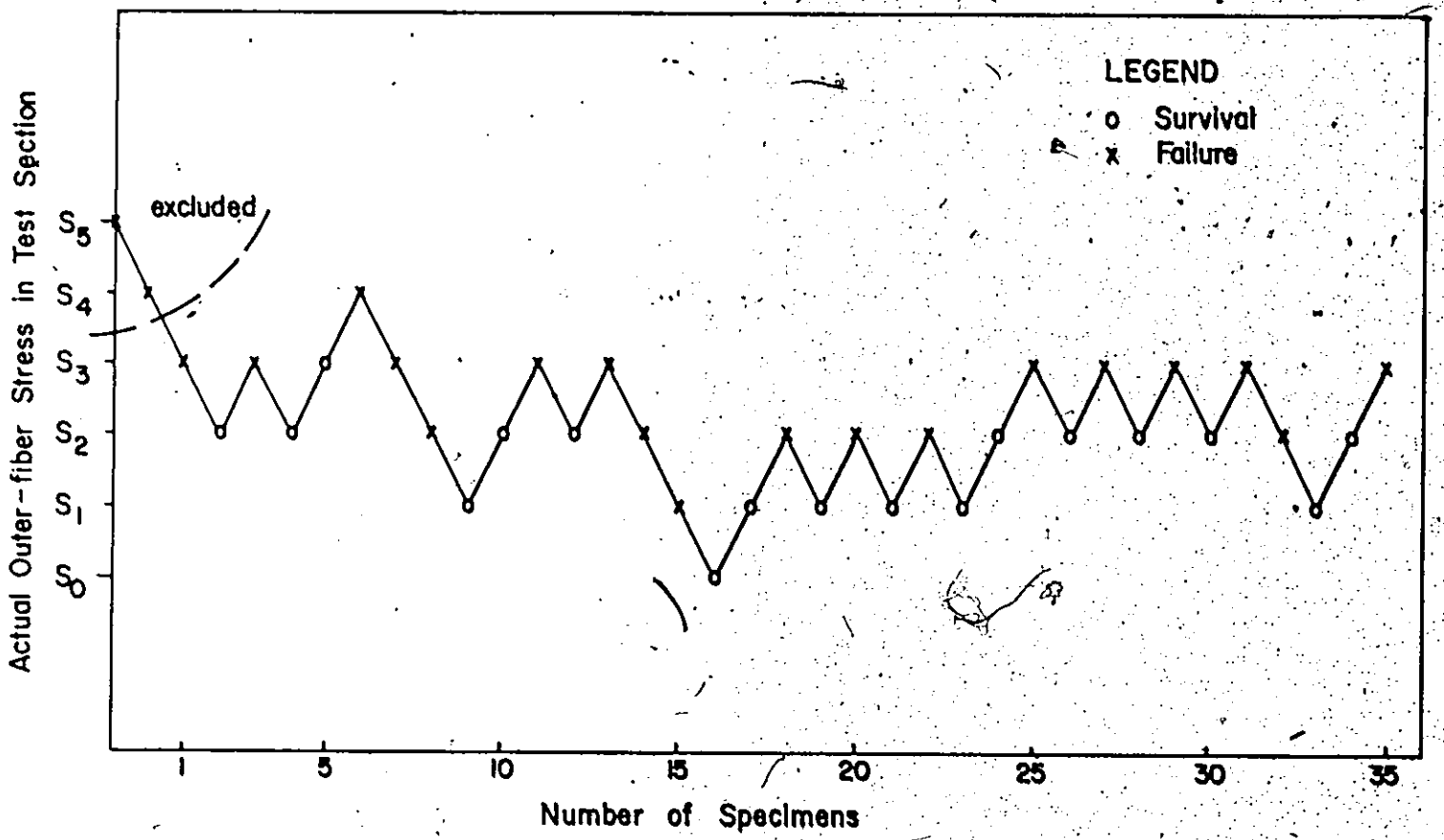

Figure A.1 Experimental Results of the Staircase Test to Determine the Distribution of the Endurance Limit of SAE 1008 Steel.

$$\frac{NB - A^2}{N^2} = 0.478 > 0.3$$

Hence the empirical formula (A.3) can accurately be used for estimating the mean and the standard deviation.

$$\text{Mean} = \hat{S}_e = S_o + d\,(A/N + \tfrac{1}{2})$$

$$= 21621.62 \text{ psi}$$

$$\text{Standard deviation } \hat{\sigma}_e = 1.620\,(d)\,[\frac{BN-A^2}{N^2} + .029]$$

$$= 1038.995 \text{ psi}$$

$$\text{Coefficient of variation} = \frac{\hat{\sigma}_e}{\hat{S}_e} = 0.048$$

Hence the fatigue endurance limit distribution has the following characteristics

Mean ($\hat{S}_e$)	= 21,622 psi
Standard deviation ($\hat{\sigma}_e$)	= 1,039 psi
Coefficient of variation	= 0.048

APPENDIX B

NUMERICAL CONTROL PROGRAM FOR CUTTING BENDING FATIGUE SPECIMENS

The Numerical Control program used to control the TOS-FA4V knee-type milling machine for cutting the bending fatigue specimens is described in this Appendix.

The NC programming comprises the collection of all data required to produce the specimen, the calculation of the tool path along which the machine operations will be performed and the arrangement of the data in a standard format. In the NC program each horizontal line comprises a "block" of information called a data block. It contains the required data for transferring the cutting tool from one point to another point, including all machining instructions that should be executed during this motion.

The NC program is given in Table B.1, where:

n - sequential number of the block

g - preparatory function, consisting of 2 digits

x,y,z,i,j,k - dimension words

f - feed-rate code

m - miscellaneous functions.

A detailed description of these words is given below:

1. Sequence Number, n

Each block of the tape has a sequential number - the

TABLE B.1

N/C DATA PROGRAM USED TO MANUFACTURE THE BENDING FATIGUE SPECIMENS

N	G	X	Y	Z	I	J	K	F	M
001	00	+00000	+00000	+00000	00000	00000	00000	0000	00
002	01	+00000	+00000	+00000	00000	00000	00000	3000	00
003	18	+00000	+00000	+00000	00000	00000	00000	3000	03
004	01	+00000	+00000	-06000	00000	00000	00000	0060	00
005	01	+00000	+00000	+06000	00000	00000	00000	1500	00
006	17	+16875	+00000	+00000	00000	00000	00000	3000	00
007	18	+00000	+00000	-06000	00000	00000	00000	0060	00
008	01	+00000	+00000	+06000	00000	00000	00000	1500	00
009	01	+00000	+00000	+02500	00000	00000	00000	1500	03
010	17	-16875	+00000	+00000	00000	00000	00000	2000	06
011	18	+00000	+00000	-04700	00000	00000	00000	0100	03
012	01	+00000	+00000	+04700	00000	00000	00000	1500	00
013	17	+16875	+00000	+00000	00000	00000	00000	2000	00
014	18	+00000	+00000	-04700	00000	00000	00000	0100	00
015	01	+00000	+00000	+04700	00000	00000	00000	1500	00
016	17	+05050	-06250	+00000	00000	00000	00000	2000	06
017	18	+00000	+00000	-02500	00000	00000	00000	0700	00
018	17	-13175	+00000	+00000	00000	00000	00000	0300	00
019	01	-15050	+00000	+00000	00000	00000	00000	0300	00
020	17	+00000	-02000	+00000	00000	00000	00000	0700	00
021	18	+00000	+00000	-02200	00000	00000	00000	0700	00
022	17	+00000	+02000	+00000	00000	00000	00000	0100	00
023	17	+15050	+00000	+00000	00000	00000	00000	0300	00
024	01	+13175	+00000	+00000	00000	00000	00000	0300	00
025	18	+00000	+00000	+04700	00000	00000	00000	0900	00
026	17	+00000	+14500	+00000	00000	00000	00000	2000	00
027	18	+00000	+00000	-02500	00000	00000	00000	1000	00
028	17	+00000	-02000	+00000	00000	00000	00000	0100	00
029	17	-13175	+00000	+00000	00000	00000	00000	0200	00
030	17	-15050	+00000	+00000	00000	00000	00000	0200	00
031	17	+00000	+02000	+00000	00000	00000	00000	1000	00
032	18	+00000	+00000	-02200	00000	00000	00000	1000	00
033	17	+00000	-02000	+00000	00000	00000	00000	0100	00
034	17	+15050	+00000	+00000	00000	00000	00000	0200	00
035	01	+13175	+00000	+00000	00000	00000	00000	0200	00
036	01	-13175	+00000	+00000	00000	00000	00000	1000	00
037	18	+00000	+00000	+02000	00000	00000	00000	1500	00
038	17	+00000	-01250	+00000	00000	00000	00000	0050	00
039	17	-15050	+00000	+00000	00000	00000	00000	0100	00
040	17	+00000	+02000	+00000	00000	00000	00000	1000	00

Continued Table B.1

041	18	+00000	+00000	-02000	00000	00000	00000	1000	00
042	17	+00000	-02000	+00000	00000	00000	00000	0100	00
043	17	+15050	+00000	+00000	00000	00000	00000	0100	00
044	17	+00000	+01250	+00000	00000	00000	00000	0100	00
045	17	-15050	-01250	+00000	00000	00000	00000	2000	00
046	18	+00000	+00000	+04700	00000	00000	00000	1500	00
047	17	+00000	-12000	+00000	00000	00000	00000	2000	00
048	18	+00000	+00000	-02500	00000	00000	00000	1000	00
049	17	+00000	+02000	+00000	00000	00000	00000	0100	00
050	17	+15050	+00000	+00000	00000	00000	00000	0100	00
051	17	+00000	-02000	+00000	00000	00000	00000	1000	00
052	18	+00000	+00000	-02200	00000	00000	00000	1000	00
053	17	+00000	+02000	+00000	00000	00000	00000	0100	00
054	17	-15050	+00000	+00000	00000	00000	00000	0100	00
055	17	+15050	-01300	+00000	00000	00000	00000	1000	00
056	18	+00000	+00000	+03000	00000	00000	00000	1500	00
057	17	+00000	+04085	+00000	00000	00000	00000	0050	00
058	17	-03750	+00000	+00000	00000	00000	00000	0100	00
059	17	+00000	-02000	+00000	00000	00000	00000	0100	00
060	17	+00000	+02410	+00000	00000	00000	00000	0100	00
061	17	+03750	-00410	+00000	00000	00000	00000	0100	00
062	17	+00000	-04085	+00000	00000	00000	00000	1000	00
063	18	+00000	+00000	-01500	00000	00000	00000	1500	00
064	17	+00000	+04085	+00000	00000	00000	00000	0100	00
065	17	-03750	+00000	+00000	00000	00000	00000	0100	00
066	17	+00000	-02000	+00000	00000	00000	00000	0100	00
067	17	+00000	+02410	+00000	00000	00000	00000	0100	00
068	17	+03750	-00410	+00000	00000	00000	00000	0100	00
069	17	+00000	-04085	+00000	00000	00000	00000	1000	00
070	18	+00000	+00000	-01500	00000	00000	00000	1500	00
071	17	+00000	+04085	+00000	00000	00000	00000	0100	00
072	17	-03750	+00000	+00000	00000	00000	00000	0100	00
073	17	+00000	-02000	+00000	00000	00000	00000	0100	00
074	17	+00000	+02410	+00000	00000	00000	00000	0100	00
075	17	+03750	-00410	+00000	00000	00000	00000	0100	00
076	18	+00000	+00000	+04700	00000	00000	00000	1500	00
077	17	+00000	+08515	+00000	00000	00000	00000	2000	00
078	18	+00000	+00000	-01700	00000	00000	00000	0060	00
079	17	+00000	-04085	+00000	00000	00000	00000	0050	00
080	17	-03750	+00000	+00000	00000	00000	00000	0100	00
081	17	+00000	+02000	+00000	00000	00000	00000	0100	00
082	17	+00000	-02410	+00000	00000	00000	00000	0100	00
083	17	+03750	+00410	+00000	00000	00000	00000	0100	00
084	17	+00000	+04085	+00000	00000	00000	00000	1000	00
085	18	+00000	+00000	-01500	00000	00000	00000	0060	00

Continued Table B.1

086	17	+00000	-04085	+00000	00000	00000	00000	0100	00
087	17	-03750	+00000	+00000	00000	00000	00000	0100	00
088	17	+00000	+02000	+00000	00000	00000	00000	0100	00
089	17	+00000	-02410	+00000	00000	00000	00000	0100	00
090	17	+03750	+00410	+00000	00000	00000	00000	0100	00
091	17	+00000	+04085	+00000	00000	00000	00000	1000	00
092	18	+00000	+00000	-01500	00000	00000	00000	0060	00
093	17	+00000	-04085	+00000	00000	00000	00000	0100	00
094	17	-03750	+00000	+00000	00000	00000	00000	0100	00
095	17	+00000	+02000	+00000	00000	00000	00000	0100	00
096	17	+00000	-02410	+00000	00000	00000	00000	0100	00
097	17	+03750	+00410	+00000	00000	00000	00000	0100	00
098	18	+00000	+00000	+04700	00000	00000	00000	1500	00
099	17	+13125	-08465	+00000	00000	00000	00000	2000	00
100	18	+00000	+00000	-00750	00000	00000	00000	0060	00
101	17	+00000	+12500	+00000	00000	00000	00000	0100	00
102	17	-26875	+00000	+00000	00000	00000	00000	2000	00
103	17	+00000	-12500	+00000	00000	00000	00000	0100	00
104	18	+00000	+00000	+01000	00000	00000	00000	1500	00
105	17	+05000	+06250	+00000	00000	00000	00000	2000	30

sequence number word, which is the first in the block.

2. Preparatory Function, g

The preparatory function prepares the N/C program to be ready to perform a specific mode of operation. Notice that since the code g oo indicates a point-to-point operation , a (g) function must be programmed in every single block. A point-to-point operation is allowed only in the X-Y plane. Some examples of these preparatory functions are as follows:

g 00 Point-to-Point, Positioning

g 01 Linear interpolation

g 02 Circular interpolation arc CW

g 03 Circular interpolation arc CCW

g 17 XY plane selection

g 18 XZ plane selection

g 19 YZ plane selection

3. Dimension Words

Dimension words in the system are classified as follows:

(i) x,y,z Distance dimension words for X ,Y ,Z axis motion lengths.

(ii) i,j,k Circular dimension words. They determine the distance of the arc starting point to the arc center in directions parallel to X,Y,Z respectively

4. Feed Function, f

Use of the f word is necessary only in a contouring operation.

The feed-rate word will range from 1 to 3000, and is equivalent to the required feed-rate in in/min. multiplied by 100.

5. Miscellaneous Function, m

The miscellaneous function pertains to auxiliary information such as spindle command and other functions which are explained below:

m 03 Start spindle rotation in a clock-wise direction.

m 06 Execute the change of a tool.

m 30 Indicates completion of the workpiece. It stops spindle and feed after completion of all instructions in the block. It includes rewinding of tape to the end of record character, thus ready for next workpiece (when RUN pushbutton is pressed).

APPENDIX C

TABLES OF EXPERIMENTAL DATA, ANALYTICAL PREDICTIONS, AND COMPUTER OUTPUTS

TABLE C.1 RESULTS OF TENSILE TESTS OF SAE 1008 STEEL

Spec. No.	Initial Cross-Sectional Area, A_o (in^2)	Lower Yield Load (lb)	Maximum Load (lb)	Fracture Load (lb)	% Elongation (2" gauge length)	Cross-Sectional Area at Fracture, A_f (in^2)
1	.0418	1550	2065	1550	15.25	.0160
2	.0420	1550	2055	1585	19.5	.0152
3	.0419	1560	2040	1500	17.75	.0161
4	.0418	1525	2030	1550	21.	.0145
5	.0421	1560	2050	1500	20.	.0149
6	.0421	1535	2035	1580	17.5	.0146
7	.0423	1520	2040	1550	18.75	.0156
8	.0422	1565	2060	1550	18.75	.0149
9	.0418	1510	2020	1545	18.	.0150
10	.0424	1555	2060	1525	16.75	.0147
11	.0418	1550	2005	1535	19.5	.0153
12	.0415	1695	2110	1600	18.5	.0141
13	.0422	1625	2080	1600	18.25	.0152
14	.0419	1545	2035	1500	18.25	.0154
15	.0415	1565	2035	1570	18.75	.0148
16	.0410	1655	2060	1600	19.25	.0140
17	.0412	1685	2100	1620	19.25	.0151
18	.0420	1560	2020	1550	13.75	.0152
19	.0418	1525	2070	1600	20.	.0152

Table C.1 (Continued)

Spec. No.	Initial Cross-Sectional Area, A_o (in^2)	Lower Yield Load (lb)	Maximum Load (lb)	Fracture Load (lb)	% Elongation (2" gauge length)	Cross-Sectional Area at Fracture A_f (in^2)
20	.0424	1545	2055	1600	18.25	.0155
21	.0419	1565	2060	1600	20.75	.0150
22	.0410	1675	2105	1615	19.75	.0155
23	.0418	1610	2040	1575	17.5	.0152
24	.0416	1665	2075	1525	19.75	.0148
25	.0422	1535	2055	1550	18.75	.0154
26	.0419	1545	2050	1550	18.75	.0144
27	.0420	1565	2060	1660	15.	.0153
28	.0419	1510	2015	1550	17.75	.0143
29	.0422	1540	2050	1570	16.5	.0155
30	.0419	1570	2045	1590	21.75	.0147
31	.0425	1535	2080	1645	18.25	.0151
32	.0420	1565	2050	1590	18.5	.0148
33	.0415	1600	2060	1585	19.5	.0141
34	.0420	1585	2070	1595	18.25	.0147
35	.0410	1765	2125	1600	16.25	.0144
36	.0420	1520	2025	1470	20.	.0144
37	.0419	1570	2070	1570	18.75	.0139
38	.0416	1600	2050	1550	19.5	.0151
39	.0424	1515	2050	1425	19.25	.0139
40	.0416	1485	2000	1525	16.25	.0143

Table C.1 (Continued)

Spec. No.	Initial Cross-Sectional Area, A_o (in^2)	Lower Yield Load (lb)	Maximum Load (lb)	Fracture Load (lb)	% Elongation (2" gauge length)	Cross-Sectional Area at Fracture a_f (in^2)
41	.0413	1560	2045	1565	12.75	.0139
42	.0422	1550	2045	1595	19.5	.0149
43	.0423	1575	2060	1475	19.75	.0147
44	.0418	1550	2015	1550	18.75	.0145
45	.0421	1560	2060	1600	17.	.0151
46	.0422	1535	2055	1600	18.75	.0139
47	.0417	1610	2045	1580	18.	.0147
48	.0419	1625	2070	1525	17.75	.0140
49	.0420	1585	2055	1545	14.25	.0154
50	.0419	1600	2060	1585	18.75	.0150
51	.0410	1685	2085	1580	19.	.0138
52	.0411	1660	2070	1590	18.75	.0142

TABLE C.2 RESULTS OF AXIAL FATIGUE TESTS OF SAE 1008 STEEL (LOADING PARALLEL TO DIRECTION OF ROLLING)

Type of Test	Spec. No.	Initial Cross-Sectional Area, A_o (in^2)	$\pm \frac{\Delta\varepsilon_t}{2}$	$\pm \frac{\Delta\varepsilon_p}{2}$	$\pm \frac{\Delta\varepsilon_e}{2}$	$\frac{\Delta S}{2}$ (ksi)	Cycles-to-Failure
Incremental-Step Test	1	.00853	±.4				
	2	.00854	±.5				
Fully-Reversed Strain Control	3	.00860	±.5	.382	.118	34.3	3,830
	4	.00850	±.3	.197	.103	30.9	15,500
	5	.00806	±.5	.398	.102	30.4	2,840
	6	.00821	±.15	.093	.057	17.1	89,090
	7	.00860	±.08	.019	.061	18.3	1,511,210
	8	.00857	±.3	.199	.101	30.3	15,820
	9	.00806	±.15	.091	.059	17.7	100,290
	10	.00867	±.08	.016	.064	19.3	811,350

TABLE C.3 RESULTS OF THE STAIRCASE TEST TO DETERMINE THE DISTRIBUTION OF THE FATIGUE ENDURANCE LIMIT

Signal: Sinusoidal constant amplitude
Frequency: 50 Hertz
Life Limit: $6. \times 10^6$ cycles

Spec. No.	Stress Level	Time-to-Failure (Seconds)	Cycles-to-Failure
1	S_5	12,961.94	6.48097×10^5
2	S_4	15,257.30	7.62865×10^5
3	S_3	19,821.42	9.91071×10^5
4	S_2		$>6. \times 10^6$*
5	S_3	28,537.82	1.426891×10^6
6	S_2		$>6. \times 10^6$*
7	S_3		$>6. \times 10^6$*
8	S_4	16,899.52	8.44976×10^5
9	S_3	19,171.88	9.58594×10^5
10	S_2	65,318.88	3.265944×10^6
11	S_1		$>6. \times 10^6$*
12	S_2		$>6. \times 10^6$*
13	S_3	23,155.50	1.157775×10^6
14	S_2		$>6. \times 10^6$*
15	S_3	53,576.94	2.678847×10^6
16	S_2	98,071.32	4.903566×10^6
17	S_1	95,879.26	4.793963×10^6
18	S_0		$>6. \times 10^6$*

TABLE C.3 (Continued)

Spec. No.	Stress Level	Time-to-Failure (Seconds)	Cycles-to-Failure
19	S_1		>6. x 10^6*
20	S_2	81,916.28	4.095814 x 10^6
21	S_1		>6. x 10^6*
22	S_2	73,697.66	3.684,883 x 10^6
23	S_1		>6. x 10^6*
24	S_2	55,322.28	2.766114 x 10^6
25	S_1		>6. x 10^6*
26	S_2		>6. x 10^6*
27	S_3	18,320.58	9.16029 x 10^5
28	S_2		>6. x 10^6*
29	S_3	43,138.42	2.156921 x 10^6
30	S_2		>6. x 10^6*
31	S_3	68,775.84	3,438792 x 10^6
32	S_2		>6. x 10^6*
33	S_3	19,250.76	9.62538 x 10^5
34	S_2	6,165.26	3.08263 x 10^5
35	S_1		>6. x 10^6*
36	S_2		>6. x 10^6*
37	S_3	38,417.54	1.920877 x 10^6

* Run out

TABLE C.4 EXPERIMENTAL DATA OF THE SINUSOIDAL BENDING FATIGUE TESTS (Frequency = 50 Hertz) FOR SAE 1008 STEEL

Specimen Number	Time-to-Failure (Seconds)	Specimen Number	Time-to-Failure (Seconds)
1	15,092.58	19	10,225.31
2	6,544.36	20	10,567.41
3	14,056.12	21	15,352.63
4	9,733.92	22	14,447.36
5	5,314.26	23	7,784.76
6	15,532.92	24	9,054.70
7	5,283.29	25	1,616.82
8	6,849.27	26	11,247.92
9	8,286.10	27	8,639.43
10	9,671.53	28	11,852.68
11	5,918.69	29	12,093.48
12	21,338.37	30	7,300.62
13	18,056.07		
14	6,517.70		
15	13,327.01		
16	26,914.17		
17	8,075.80		
18	4,560.80		

TABLE C.5 STATISTICAL CHARACTERISTICS OF THE EXPERMENTAL AND PREDICTED LIFE DISTRIBUTIONS OF SAE 1008 STEEL UNDER CONSTANT AMPLITUDE SINUSOIDAL LOADING.

CENTRAL MOMENTS

EXPERIMENTAL DISTRIBUTION

LOGARITHM N

M1 =	.567387880163E+01
M2 =	.538554064769E-01
M3 =	-.109286772607E-01
M4 =	.146622941194E-01
MIN =	.490763167708E+01
MAX =	.612695099588E+01

LIFE N

M1 =	.535443466667E+06
M2 =	.685933954177E+11
M3 =	.193996143342E+17
M4 =	.204256633776E+23
MIN =	.808410000000E+05
MAX =	.134570850000E+07

PREDICTED DISTRIBUTION

LOGARITHM N

M1 =	.564166439802CE+01
M2 =	.390567201[illegible]73E-01
M3 =	.241319525[illegible]19E-03
M4 =	.43[illegible]0[illegible]4503243[illegible]-02
MIN =	.506633432441E+01
MAX =	.626189692820E+01

LIFE N

M1 =	.486075634861E+06
M2 =	.540307914220E+11
M3 =	.175768737[illegible]87E+17
M4 =	.172213755545E+23
MIN =	.116502253077E+06
MAX =	.1[illegible]276664017[illegible]+07

THE CYCLE RATIO DISTRIBUTION

M1 =	.111340209E04E+01
M2 =	.283469966847E+00
M3 =	.210784140215E+00
M4 =	.474[illegible]97[illegible]02E+00
MIN =	.266859400779E+00
MAX =	.418644230391E+01

TABLE C.5 Continued

		STANDARDIZED MEASURES OF SKEWNESS AND PEAKEDNESS	
		(B1)	(B2)
EXPERIMENT	LOGARITHM N	.76462E+00	.50553E+01
	LIFE N	.11068E+01	.43412E+01
PREDICTION	LOGARITHM N	.97746E-03	.28521E+01
	LIFE N	.19498E+01	.58991E+01
CYCLE RATIO		.19498E+01	.58991E+01

TABLE C.5 Continued

THE MATHEMATICAL MODEL OF THE MAXIMUM ENTROPY PROBABILITY DISTRIBUTION AS THE FORM

$$Y=EXP(Z(1)+Z(2)*X+....+....+Z(I+1)*X**I+...+..+Z(N+1)*X**N)$$

WHERE X IS THE VARIABLE
Y IS THE CORRESPONDING PROBABILITY DENSITY FUNCTION
Z(I) ARE CONSTANTS EQUALS TO

EXPERIMEN					
(N	-.190088820E+02	.097817396E-04	-.893459410E-10	.765073365E-16	-.229027209E-22
log(N	.180856199E+05	-.128576781E+05	.341352462E+04	-.401124719E+03	.176050390E+02
PREDICTION					
(N	-.173283734E+02	.268721664E-04	-.543456902E-10	.389186300E-16	-.980177822E-23
log(N	-.391679065E+03	.386743575E+03	-.121148508E+02	-.349169835E-01	.185428085E-02
(C	-.433943985E+01	.117242565E+02	-.103503170E+02	.323527874E+01	-.355654029E+00

TABLE C.6 EXPERIMENTAL DATA OF THE HI-LO BENDING FATIGUE TESTS (Frequency = 50 Hertz) FOR SAE 1008 STEEL

Specimen Number	Time-to-Failure (Seconds)	Specimen Number	Time-to-Failure (Seconds)
1	10,712.47	19	5,827.09
2	7,392.02	20	8,468.30
3	5,090.00	21	6,667.01
4	4,210.99	22	26,305.51
5	5,381.86	23	9,732.35
6	4,183.37	24	6,657.07
7	8,632.20	25	6,158.79
8	4,434.24	26	2,911.86
9	7,109.84	27	5,547.29
10	11,677.25	28	5,154.31
11	3,271.24	29	3,736.31
12	4,779.45	30	15,206.44
13	8,672.66		
14	8,588.64		
15	6,010.70		
16	780.14		
17	3,293.68		
18	11,653.52		

TABLE C.7 STATISTICAL CHARACTERISTICS OF THE EXPERIMENTAL AND PREDICTED LIFE DISTRIBUTIONS OF SAE 1008 STEEL UNDER HI-LO BLOCK LOADING.

CENTRAL MOMENTS

EXPERIMENTAL DISTRIBUTION

LOGARITHM N

M1 =	.548626576073E+01
M2 =	.704432536486E-01
M3 =	-.140112867819E-01
M4 =	.290574365661E-01
MIN =	.459114255072E+01
MAX =	.611901656537E+01

LIFE N

M1 =	.363744333333E+06
M2 =	.540716708794E+11
M3 =	.290079520336E+17
M4 =	.290032490040E+23
MIN =	.390070000000E+05
MAX =	.131927500000E+07

PREDICTED DISTRIBUTION

LOGARITHM N

M1 =	.542745420321E+01
M2 =	.872341346537E-01
M3 =	-.597195593479E-02
M4 =	.196168076856E-01
MIN =	.466497362584E+01
MAX =	.621763386290E+01

LIFE N

M1 =	.332305931118E+06
M2 =	.494582649824E+11
M3 =	.164903217964E+17
M4 =	.152042654145E+23
MIN =	.451828504595E+05
MAX =	.164298600000E+07

THE CYCLE RATIO DISTRIBUTION

M1 =	.118299351854E+01
M2 =	.624676996268E+00
M3 =	.740612516387E+00
M4 =	.242548386629E+01
MIN =	.160576478745E+00
MAX =	.583904982248E+01

TABLE C.7 Continued

STANDARDIZED MEASURES OF SKEWNESS AND PEAKEDNESS

		(B1)	(B2)
EXPERIMENT	LOGARITHM N	.56161E+00	.58557E+01
	LIFE N	.53211E+01	.99199E+01
PREDICTION	LOGARITHM N	.53717E-01	.25778E+01
	LIFE N	.22502E+01	.62157E+01
CYCLE RATIO		.22502E+01	.62157E+01

TABLE C.7 Continued

RESULTS FOR SUBROUTINE MEP

THE MATHEMATICAL MODEL OF THE MAXIMUM ENTROPY PROBABILITY DISTRIBUTION AS THE FORM

Y=EXP(Z(1)+Z(2)*X+....+....+Z(I+1)*X**I+...+..+Z(N+1)*X**N)

WHERE X IS THE VARIABLE
Y IS THE CORRESPONDING PROBABILITY DENSITY FUNCTION
Z(I) ARE CONSTANTS EQUALS TO

EXPERIMENT

(N)	-.148873816E+02	.120594691E-04	-.121002687E-10	-.246381112E-16	.208747034E-22
log(N)	-.212757116E+03	.772009660E+02	-.683958877E+01	-.406613221E-01	.243606789E-02

PREDICTION

(N)	-.166472431E+02	.426372269E-04	-.144494816E-09	.168755858E-15	-.655767544E-22
log(N)	.331328087E+03	-.220248971E+03	.484995973E+02	-.374598618E+01	.398464306E-01
(C)	-.108678902E+01	.203041614E+01	-.187450054E+01	.422046923E+00	-.328317317E-01

TABLE C.8 EXPERIMENTAL DATA OF THE LO-HI-LO BENDING FATIGUE TESTS (Frequency = 50 Hertz)

Specimen Number	Time-to-Failure (Seconds)	Specimen Number	Time-to-Failure (Seconds)
1	2,542.31	19	3,490.96
2	5,369.87	20	7,075.82
3	25,910.97	21	5,043.75
4	7,032.65	22	12,371.52
5	7,022.14	23	7,501.37
6	10,290.59	24	4,419.22
7	4,681.82	25	5,676.78
8	7,212.13	26	5,437.46
9	3,094.24	27	12,838.88
10	6,495.65	28	6,145.72
11	9,161.01	29	1,219.13
12	3,467.61	30	8,943.53
13	6,339.35		
14	8,436.30		
15	7,800.43		
16	11,338.08		
17	18,173.74		
18	3,952.15		

TABLE C.9 STATISTICAL CHARACTERISTICS OF THE EXPERIMENTAL AND PREDICTED LIFE DISTRIBUTIONS OF SAE 1008 STEEL UNDER LO-HI-LO BLOCK LOADING.

CENTRAL MOMENTS

EXPERIMENTAL DISTRIBUTION

LOGARITHM N

M1 =	.550737324672E+01
M2 =	.654440760075E-01
M3 =	-.450737582611E-02
M4 =	.173069582635E-01
MIN =	.475502002273E+01
MAX =	.611245367582E+01

LIFE N

M1 =	.380886333333E+06
M2 =	.584909227195E+11
M3 =	.285016771688E+17
M4 =	.270355531371E+23
MIN =	.609565000000E+05
MAX =	.129554850000E+07

PREDICTED DISTRIBUTION

LOGARITHM N

M1 =	.549358417343E+01
M2 =	.435364058221E-01
M3 =	.623153610982E-02
M4 =	.521835633379E-02
MIN =	.506633432441E+01
MAX =	.621563386283E+01

LIFE N

M1 =	.353809345779E+06
M2 =	.412759043163E+11
M3 =	.169046127848E+17
M4 =	.131414998527 7E+23
MIN =	.116582253077E+06
MAX =	.164298600000E+07

THE CYCLE RATIO DISTRIBUTION

M1 =	.125773800666 7E+01
M2 =	.521319252229E+00
M3 =	.718406289337E+00
M4 =	.209697771128E+01
MIN =	.414040326665E+00
MAX =	.593904982248E+01

TABLE C.9 Continued

		STANDARDIZED MEASURES OF SKEWNESS AND PEAKEDNESS	
		(B1)	(B2)
EXPERIMENT	LOGARITHM N	.72483E-01	.40395E+01
	LIFE N	.40595E+01	.79024E+01
PREDICTION	LOGARITHM N	.47058E+00	.27531E+01
	LIFE N	.36427E+01	.77159E+01
CYCLE RATIO		.36427E+01	.77159E+01

TABLE C.9 Continued

RESULTS FOR SUBROUTINE MEP

THE MATHEMATICAL MODEL OF THE MAXIMUM ENTROPY PROBABILITY DISTRIBUTION AS THE FORM

Y=EXP(Z(1)+Z(2)*X+....+....+Z(I+1)*X**I+...+..+Z(N+1)*X**N)

WHERE X IS THE VARIABLE
Y IS THE CORRESPONDING PROBABILITY DENSITY FUNCTION
Z(I) ARE CONSTANTS EQUALS TO

EXPERIMENT

(N)	-.153041340E+02	.178675487E-04	-.366981601E-10	.126825961E-16	.432781181E-23
log(N)	-.227763309E+03	.807022305E+02	-.646282259E+01	-.175868983E+00	.995622380E-02

PREDICTION

(N)	-.147984612E+02	.203191459E-04	-.619492277E-10	.591163098E-16	-.189410976E-22
log(N)	.531428095E+04	-.400018331E+04	.111838952E+04	-.137700549E+03	.630114552E+01
(C)	-.224041727E+01	.568911084E+01	-.488138985E+01	.130971801E+01	-.117990243E+00

TABLE C.10 EXPERIMENTAL DATA OF THE NARROW BAND RANDOM BENDING FATIGUE TESTS

Central frequency = 48 Hertz, Band width = 10 Hertz

Spec. No.	Time-to-Failure (seconds)	Spec. No.	Time-to-Failure (seconds)	Spec. No.	Time-to-Failure (seconds)
1	13,843.23	19	8,979.34	37	18,360.12
2	18,789.77	20	28,718.61	38	11.860.92
3	12,997.11	21	17,075.82	39	18,566.94
4	17,425.46	22	13,437.98	40	19,836.37
5	18,024.48	23	16,400.42	41	25,029.23
6	8,668.93	24	11,942.25	42	9,276.33
7	9,146.34	25	17,842.71	43	15,449.90
8	8,301.55	26	13,982.10	44	8,006.85
9	27,275.62	27	16,568.38	45	8,845.89
10	15,098.69	28	17,158.22		
11	13,316.59	29	6,934.71		
12	8,167.77	30	11,420.47		
13	10,354.95	31	12,201.77		
14	13,027.82	32	8,745.50		
15	11,021.24	33	8,151.76		
16	9,322.91	34	16,519.02		
17	13,434.80	35	15,170.31		
18	29,047.11	36	14,613.29		

TABLE C.11 STATISTICAL CHARACTERISTICS OF THE INPUT PEAK STRESS DISTRIBUTIONS AND RESULTS OF x^2 GOODNESS-OF-FIT TESTS.

RAYLEIGH DISTRIBUTION OF THE APPLIED STRESS PEAKS

STANDARD DEVIATION =	.1165000080E+05	P.S.I.
MAXIMUM PEAK STRESS =	.3644563579E+05	P.S.I.
MINIMUM PEAK STRESS =	0.	P.S.I.

RANDOM LOADING PROGRAM (MAXIMUM ENTROPY METHOD)

THE MATHEMATICAL MODEL OF THE MAXIMUM ENTROPY PROBABILITY DISTRIBUTION OF THE PEAK STRESS HAS THE FORM

$$P = EXP(Z(1) + Z(2)*X + Z(3)*X**2 + Z(4)*X**3 + Z(5)*X**4)$$

WHERE

X IS THE PEAK STRESS
P IS THE CORRESPONDING PROBABILITY DENSITY FUNCTION
Z(I) ARE CONSTANTS EQUAL TO

-.12729176E+02 .69290425E-03 -.55380040E-07

.17334268E-11 -.22294300E-16

MINIMUM STRESS =	0.	P.S.I.
MAXIMUM STRESS =	.3644563579E+05	P.S.I.

WEIBULL DISTRIBUTION OF THE APPLIED STRESS PEAKS

SCALE FACTOR =	.1699912061E+05
SHAPE FACTOR =	.1996788999E+01
MEAN STRESS =	.1451037926E+05
RMS STRESS =	.1613467341E+05
MINIMUM STRESS =	0.
MAXIMUM STRESS =	.3644563579E+05

TABLE C.11 Continued

Extreme Value Distribution of Peak Stress

$f(x) = A \exp(-y).\exp[-\exp(-y)]$

where

$$y = A\,(x-\bar{x})/\sigma_x + B$$

$\bar{x}$ = mean value of x

σ_x = standard deviation of x

A = 1.25965

B = 0.57552

Results of χ^2 Goodness-of-Fit Test

Distribution	Calculated χ^2	Tabulated $\chi^2_{(\alpha=5\%)}$
Rayleigh	1.2316	$\chi^2_{37-1-1} = 1.4229$
Maximum Entropy	1.3222	$\chi^2_{37-4-1} = 1.4436$
Weibull	1.9203	$\chi^2_{37-2-1} = 1.4229$
Extreme Value	2.7433	$\chi^2_{37-2-1} = 1.4229$

TABLE C.12 STATISTICAL CHARACTERISTICS OF THE EXPERIMENTAL AND PREDICTED LIFE DISTRIBUTIONS OF SAE 1008 STEEL UNDER NARROW BAND RANDOM LOADING.

CENTRAL MOMENTS

EXPERIMENTAL DISTRIBUTION

LOGARITHM N

M1 =	.581134496830E+01
M2 =	.243183307387E-01
M3 =	.775302486410E-03
M4 =	.142420806399E-02
MIN =	.552226954157E+01
MAX =	.614434416675E+01

LIFE N

M1 =	.691583552000E+06
M2 =	.676976979811E+11
M3 =	.178557109404E+17
M4 =	.172520285081E+23
MIN=	.332866080000E+06
MAX=	.139426128000E+07

EXPERIMENT STANDARDIZED MEASURES OF SKEWNESS AND PEAKEDNESS

	(B1)	(B2)
LOGARITHM N	.41905E-01	.24083E+01
LIFE N	.10276E+01	.37644E+01

Y=EXP(Z(1)+Z(2)*X+....+....+Z(I+1)*X**I+...+..+Z(N+1)*X**N)

Z(I)

N

-.251905103E+02 .574653995E-04 -.958444403E-10

.648553806E-16 -.159461854E-22

LOG N

.120113911E+04 -.124[illegible]414E+04 .403255535E+03

.532505335E+02 .249341480E+01

TABLE C.12 Continued

PREDICTED DISTRIBUTION

RAYLEIGH INPUT

LOGARITHM N

		β_1	β_2
M1 =	.57805971649 6E+01		
M2 =	.26623216925 8E-01		
M3 =	.10990648275 8E-03		
M4 =	.19940427929 7E-02	.64013E-03	.28133E+01
MIN=	.23057551720 4E+01		
MAX=	.62812954806 8E+01		

LIFE N

		β_1	β_2
M1 =	.64756458360 6E+06		
M2 =	.63117750276 9E+11		
M3 =	.17442187421 6E+17		
M4 =	.18771520705 1E+23	.12099E+01	.47119E+01
MIN=	.20218730483 9E+06		
MAX=	.19111531064 4E+07		

THE CYCLE RATIO DISTRIBUTION

		β_1	β_2
M1 =	.15669875344 9E+01		
M2 =	.36955[illegible]724 8E+00		
M3 =	.24710713184 5E+00		
M4 =	.64749508127 1E+00	.12099E+01	.47119E+01
MIN =	.48923398245 6E+00		
MAX =	.46244163114 7E+01		

Y=EXP(Z(1)+Z(2)*X+....+....+Z(I+1)*X**I+...+..+Z(N+1)*X**N)

	Z(I)				
(N	-.22447085 8E+02	.452801507E-04	-.746992554E-10	.484574335E-16	-.113771218E-22
log(N	-.60082503 9E+03	.206754853E+03	-.173392847E+02	-.102292521E+00	.509915783E-02
(C	-.75959626 5E+01	.139143874E+02	-.890763767E+01	.217701296E+01	-.193826787E+00

TABLE 3.12 Continued

MAXIMUM ENTROPY INPUT

PREDICTED DISTRIBUTION

	β_1	β_2
LOGARITHM N		
M1 = .3856252859935E+01		
M2 = .2797888622055E-01		
M3 = .2223669249395E-03	.68366E-03	.28131E+01
M4 = .2221052077775E-02		
MIN= .3795081855655E+01		
MAX= .3799701490355E+01		
LIFE N		
M1 = .3158267641055E+06		
M2 = .9944250527735E+11		
M3 = .3543276538545E+17	.12766E+01	.48135E+01
M4 = .1760111863515E+23		
MIN= .3296117911245E+06		
MAX= .2398668042375E+07		

THE CYCLE RATIO DISTRIBUTION

M1 = .3915392245915E+01		
M2 = .5822407082795E+00		
M3 = .1019834276565E+00	.12766E+01	.48135E+01
M4 = .1631784985625E+01		
MIN = .3797885431355E+00		
MAX = .3804055962495E+01		

Y=EXP(Z(1)+Z(2)*X+.....+Z(I+1)*X**I+...+..+Z(N+1)*X**N)

	Z(I)				
(N	-.2174832085+02	.0319785445-04	-.443333774E-10	.230464130E-16	-.432703245E-23
LOG(N	-.5688213575+03	.3997044295+03	-.165181746E+02	-.933268034E-01	.459157388E-02
((	-.7313020525+01	.2078050785+02	-.565273493E+01	.112494260E+01	-.812778411E-01

TABLE C.12 Continued

PREDICTED DISTRIBUTION

WEIBULL INPUT

β_1 β_2

LOGARITHM N

M1 = .66F72929C241E+01
M2 = .6901731982350E-01
M3 = .1101C8A11554E-03
M4 = .1891932477515E-02
MIN= .3189181596365E+01
MAX= .6152018165987E+01

.69676E-03 .28134E+01

LIFE N

M1 = .3668843496 1E+06
M2 = .3464978168 9E+11
M3 = .3005052037775E+16
M4 = .2602507198EC5E+22
MIN= .1345900170896E+06
MAX= .1419116879925E+07

.11797E+01 .46667E+01

THE CYCLE RATIO DISTRIBUTION

M1 = .1773891061 5E+01
M2 = .3128674269 5E+00
M3 = .9924234319 0E-01
M4 = .4920561408775E+00
MIN = .1740615249685E+00
MAX = .4338364756 0E+01

.11797E+01 .46667E+01

Y=EXP(Z(1)+Z(2)*X+....+Z(I+1)*X**I+...+..+Z(N+1)*X**N)

Z(I)

(N -.2277024475E+02 .6460594205E-04 -.143007075E-09 .125212389E-15 -.397100903E-22

log(N -.5912339435E+03 .2079436625E+03 -.178358465E+02 -.104300504E+00 .531904381E-02

-.7512782165E+01 .1932595075E+02 -.165391165E+02 .543380124E+01 -.651686155E+00

TABLE 13 EFFECT OF CHANGING THE STANDARD DEVIATION OF THE ENDURANCE LIMIT (σ_e) AT STRESS LEVEL OF 89,000 PSI ON THE PREDICTED LIFE DISTRIBUTION OF SAE 4340 STEEL.

$(\frac{\sigma^*_e}{\sigma_e})$ [1]	(σ^*/σ') [2]		(μ^*/μ') [3]	
	Log Life	Life	Log Life	Life
0.9	0.88279	0.88333	1.0	0.98697
0.8	0.768904	0.77223	0.99978	0.97546
0.7	0.659735	0.66590	0.99978	0.96541
0.6	0.55482	0.56369	0.99978	0.95679
0.5	0.453214	0.46484	0.99957	0.94957

1 Ratio of reduced to the experimental standard deviation of the endurance limit distribution

2 Ratio of new predicted standard deviation of fatigue life to that originally predicted using the experimental standard deviation of the endurance limit.

3 Ratio of new predicted mean fatigue life to that originally predicted using the experimental standard deviation of the endurance limit

TABLE 14 EFFECT OF CHANGING THE STANDARD DEVIATION OF THE FATIGUE STRENGTH COEFFICIENT (σ_f) AT STRESS LEVEL OF 89,000 PSI ON THE PREDICTED LIFE DISTRIBUTION OF SAE 4340 STEEL

σ_f^*/σ_f	σ^*/σ' [1]		μ^*/μ' [1]	
	Log Life	Life	Log Life	Life
0.9	1.0	0.99995	1.0	1.0
0.8	1.0189	1.0181	0.99788	1.0003
0.7	1.0189	1.0181	0.99788	1.0003
0.6	1.0189	1.0181	0.99788	1.00031
0.5	1.0189	1.0181	0.99788	1.00031
0.25	1.01937	1.0181	0.99809	1.00031
0.1	1.02268	1.0228	0.99894	1.0014
0.0	1.02032	1.0274	1.0	1.0025

[1] (μ') and (σ') are the mean and standard deviation of the predicted life distribution due to a sinusoidal stress of amplitude 89,000 psi, using the experimental value of σ_f and σ_e.

(μ^*) and (σ^*) are the mean and standard deviation predicted under the same conditions, using new values σ_f^* as the standard deviation of the fatigue strength coefficient.

TABLE C.15 EFFECT OF CHANGING THE VARIANCE OF A RANDOM STRESS S ~ N (101,000, σ) FOR SAE 4340 STEEL

Percentage σ/S_{mean}	μ_ℓ/μ'*		σ_e/σ'*	
	Life	Log (Life)	Life	Log (Life)
0.5	.9968	.9973	.9901	.9880
1.0	.9951	.9950	.9881	.9797
3.0	.9776	.9787	.9668	.9649
5.0	.9441	.9451	.9266	.9262
10.0	.80796	.8104	.7668	.7638

* (μ') and (σ') are the mean and standard deviation of the predicted life distribution due to a sinusoidal stress of amplitude 101,000 psi as given in Table 2.1.

TABLE C.16 EFFECT OF CHANGING THE VARIANCE OF A RANDOM STRESS $S \sim N(68{,}000, \sigma)$ FOR SAE 4340 STEEL.

Percentage σ/S_{mean}	μ_ℓ/μ'^*		σ_e/σ'^*	
	Normal	Log (Life)	Normal	Log (Life)
0.5	1.002	1.006	1.002	.994
1.0	1.0005	1.004	1.0002	.992
3.0	.982	.986	.979	.971
5.0	.9635	.952	.937	.930
10.0	.8042	.8124	.773	.7684

* (μ') and (σ') are the mean and standard deviation of the predicted life distribution due to a sinusoidal stress of amplitude 68,000 psi as given in Table 2.1.